DIRECT AND MULTISTEP CONVERSION OF LIGNIN TO BIOFUELS

A Dissertation
Presented to
The Academic Faculty

by

Matyas Kosa

In Partial Fulfillment
of the Requirements for the Degree
Doctor of Phiosophy in the
School of Chemistry and Biochemistry

Georgia Institute of Technology
December, 2012

DIRECT AND MULTISTEP CONVERSION OF LIGNIN TO BIOFUELS

Approved by:

Dr. Arhur J. Ragauskas, Advisor
School of Chemistry and Biochemistry
Georgia Institute of Technology

Dr. Sheldon W. May
School of Chemistry and Biochemisty
Georgia Institute of Technology

Dr. Yulin Deng
School of Chemical and Biomolecular Engineering
Georgia Institute of Technology

Dr. Preet Singh
School of Materials Science and Engineerng
Georgia Institute of Technology

Dr. Nicholas V. Hud
School of Chemistry and Biochemistry
Georgia Institute of Technology

Date Approved: August 28, 2012

ACKNOWLEDGEMENTS

First of all the author would like to express his gratitude to Dr. Arthur J. Ragauskas for his guidance, encouragement, advice, and mentorship throughout the work that led to this dissertation. The highest acknowledgements are due to thesis committee members: Dr. Yulin Deng, Dr. Nicholas Hud, Dr. Sheldon May, Dr. Preet Singh, and Dr. Nils Kröger (even in his absence) in the author's committee, for their insightful comments and support from the initial to the final level of this project. The author is also grateful to his co-workers at Georgia Tech, especially Dr. Marcus Foston, Dr. Leslie Gelbaum, Dr. David Bostwick, Dr. Fang Huang, Dr. Bassem Hallac, Dr. Yang Li, Dr. Poulomi Sannigrahi, Dr. Yunqiao Pu, Dr. Mate Nagy, Shaobo Pan, Rajalaxmi Dash, Tyrone Wells and Jung Seokwon.

The author would like to also acknowledge the financial support from the Paper Science and Engineering Fellowship program at the Institute of Paper Science and Technology.

TABLE OF CONTENTS

LIST OF TABLES

LIST OF FIGURES

LIST OF SYMBOLS AND ABBREVIATIONS

4-HBA	4-hydroxybenzoic acid
ACC	Ac-CoA carboxylase
Ac-CoA	acetyl coenzyme A
ACP	acyl carrier protein
Ara	arabinose
ASL	acid soluble lignin
CAT	catechol
CBP	consolidated bioprocessing
CMD	carboxymuconate decarboxylase
CMLE	carboxymuconate lactonizing enzyme
CP/MAS	cross polarization/magic angle spinning
DA	diterpenoic acid
DAG	diacylglycerol
DAME	diterpenoic acid methyl ester
DGAT	diacylglycerol acyl-transferase
DH	dehydratase
DP	degree of polymerization
ELH	enol lactone hydrolase
EOL	ethanol organosolv lignin
ER	enoyl reductase
FA	fatty acid
FAME	fatty acid methyl ester

FAS	fatty acid synthase
G	guaiacyl
Gal	galactose
GalA	galacturonic acid
GEN	gentisate
GK	glycerol kinase
Glc	glucose
GlcA	glucuronic acid
GPC	gel permeation chromatography
H	p-coumaryl lignin monomer
HE Kraft	high extractive content Kraft
HPAEC	high performance anion exchange chromatography
HPLC	high performance liquid chromatography
HSQC	heteronuclear single quantum coherence
HW	hardwood
KR	keto-reductase
KS	keto-synthase
LCC	lignin carbohydrate complex
Man	mannose
MAT	malonyl-CoA transacylase
M_n	number average molar mass distribution
M_w	weight average molar mass distribution
P	peta
P3,4O	protocatechuate 3,4-dioxygenase
PAP	phosphatidate phosphatase

PCA	protocatechuic acid
PD	polydispersity
PPO	pure plant oil
R. opacus	*Rhodococcus opacus*
Rha	rhamnose
S	syringyl
SSF	simultaneous saccharification and fermentation
SW	softwood
SyrA	syringic acid
TAG	triacylglycerol
TCA	tri-carboxylic acid cycle
TH	thiolase
TR	transferase
VanA	vanillic acid
WVO	waste vegetable oil
Xyl	xylose

SUMMARY

Lignin is the second most abundant biopolymer on Earth, right after cellulose, with a highly complex chemical structure that hinders its possible utilizations. As a consequence, it is mostly burned as an inexpensive resource, generating green electricity or heat that in turn can be used for the deconstruction of biomass itself. Applications that utilize lignin in different manners are of great interest, due to its inexpensive nature and promising return in case an efficient conversion process is discovered with possibly a high value end-product. The integrated biorefinery concept formulates that all biomass components should be used to their maximal potential to minimize emissions and generate a renewable biopolymer-based industry.

Present work is based on a more modest notion of converting lignin into different biofuels that have only a few, however important, advantages over lignin as a direct energy source. Pyrolysis, for instance, results a bio-oil that has a higher (in some cases 20 times) energy density than the starting lignin. Another possibility is bioconversion, through oleaginous microorganisms that can live off lignin as a sole carbon source, producing biodiesel precursor lipids. This latter path is more ambitious by aiming for the simplification of lignin's structure, through intermediate materials that have a uniform structure, facilitating various applications. These mentioned lignin modification methods represent the core of this dissertation.

The first part of current work (Chapter 4) details the analysis of lignin from a relatively new lignin isolation process called LignoBoost. It is obtained from the pulp and paper industry as a residual product of Kraft pulping, via CO_2 precipitation of lignin from black liquor (BL). This method is environment friendly (CO_2 is consumed), results a

good quality lignin (detailed below), eliminates the main bottleneck of the Kraft cycle (recovery boiler capacity), and yet leaves enough lignin within the "weak" BL to recover pulping chemicals and generate energy for the pulp mill. Pyrolysis directly converts this lignin into biofuel with several advantageous properties.

The second part of this dissertation (Chapters 5-6) seeks proof for the theory that lignin degradation and lipid accumulation metabolic pathways can be interconnected to gain lipids while utilizing lignin. First, to prove the core concept, pure model compounds, such as vanillic acid, are used in nitrogen-limited fermentations with Gram-positive *Rhodococcus opacus* species, DSM 1069 and PD630. Subsequently, the same strains are used to evaluate lignin to lipid bioconversion, starting with ethanol organosolv and Kraft lignin. This conversion is a first step in a multistep process towards biodiesel production, which includes transesterification, after lipids are extracted from the cells.

CHAPTER 1

INTRODUCTION

"The efficient conversion of the lignin component in biomass into value added products." A short, simple statement expressing a goal so difficult to reach that overall convincing solutions have eluded biomass researchers for the longest time. Most importantly, feasible utilization of this complex macromolecule can decide the fate of future biorefineries that in turn can secure energy independence, create employment opportunities and ease the persistent environmental problems [1-5].

Dwindling fossil fuel resources together with increasing demand and modern society's justifiable concern for the condition of our environment, as a legacy to future generations, has attracted scientists towards renewable resources, which can provide sustainable solutions to replace these conventional fuels [4]. Lignocellulosic biomass, namely plant materials, is a promising resource for fuels and materials considering their ability to keep the carbon balance in neutral by repetitively reducing CO_2 into useful organic matter. Some plant materials however, are grown on agriculturally valuable land, consequently, lignocellulosic biomass resources for biofuel and biomaterial production have to fit important criteria such as land-use and lack of alternative consumption [2-4, 6]. The latter property by itself describes low digestibility, caused by the recalcitrant nature of biopolymers building up lignocellulosic plant materials, disabling facile degradation and conversion for different applications. Consequently, a considerable knowledge of plant cell wall composition has been accumulated over the past decades in the literature that is constantly expanding [2, 6].

Over 90 % of the plant cell wall is composed of polysaccharides and lignin, while other materials such as different extractives and inorganic elements are present as well, with contributions depending on the plant source [2]. Research focuses on main elements: hemicellulose, cellulose (polysaccharides) and lignin, materials that are present in a large enough quantity for industrial scale applications [4]. Cellulose is a polymer of cellobiose that is built up from two β-D-glucose units via a 1-4 bond (Figure 1.1), and it is the most abundant contributor of plant cell walls. Hemicelluloses or "hemis" are also sugar polymers of mainly glucose, galactose, mannose, xylose, arabinose and glucuronic acid. The sugar monomers in hemis are connected with a variety of bonds to each other and they can be acetylated at different positions. In general their structure will highly depend on the plant source (Figure 1.1) [2, 6].

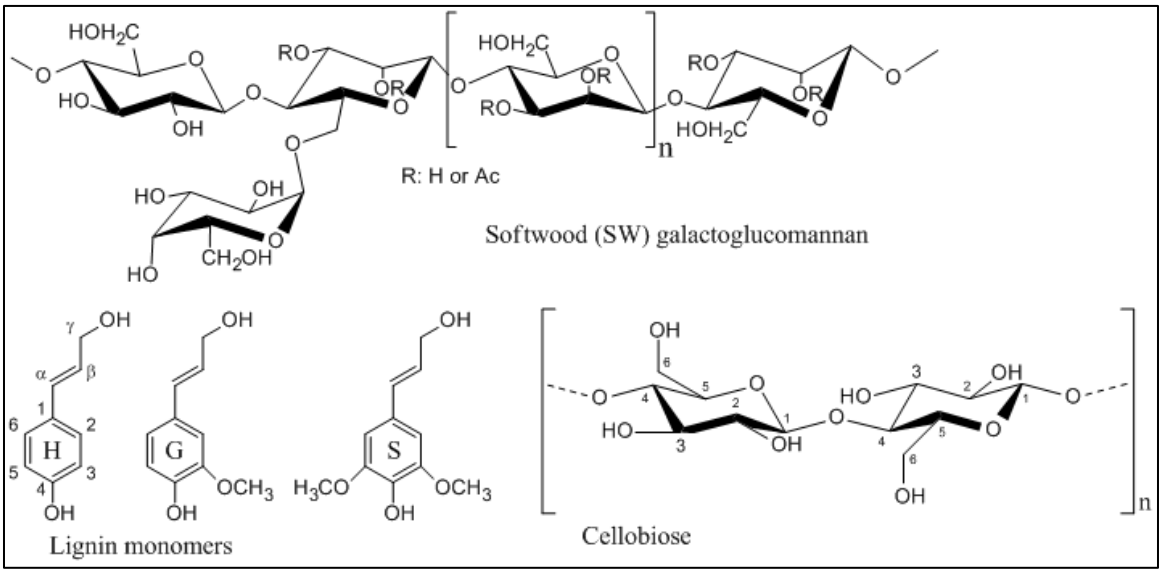

Figure 1.1. Plant cell wall chemical components, typical softwood hemicellulose on top, lignin building blocks in bottom left, and cellulose monomer cellobiose in bottom right

Lignin is a polyaromatic, three-dimensional macromolecule synthesized from an array of phenylpropanoid units via radical coupling. The three main building blocks are coumaryl (H), coniferyl (G) and synapyl (S) alcohols. Lignin as a result of their polymerization is a complex non-uniform structure that further varies depending on plant source (Figure 1.1). All these variations and non-uniformities make hemis and lignin less attractive for conversion, while cellulose's uniform structure and the ease to turn its monomers to ethanol made it the most well studied and widely utilized polymer of all cell wall materials [2, 6].

Although cellulosic ethanol is considered to be a second-generation biofuel from all perspectives, its production is still too expensive to consider it feasible as a standalone product [1, 7, 8]. Furthermore the pulp and paper industry also use mainly the cellulose part of biomass while other components are underutilized. Accordingly, utilizing all parts of the cell wall at their highest possible value can possibly increase feasibility in both current and future industries. The integrated biorefinery concept aims to address all these issues through adaptive design and depending on resource and primary products, such as ethanol or paper, enable autonomic economy for industries interested in biomass conversion and reforming [3]. To this date as mentioned earlier, conversion and valorization of lignin proved to be the most problematic part in both traditional (e.g. pulp and paper) and intensely researched future applications (e.g. second generation bioethanol) [2, 3, 9, 10]. The literature review, chapter two, of this dissertation aims to depict our current knowledge on environmental concerns, plant biomass components with emphasis on lignin, and sustainable solutions based on this renewable resource. That

section also details and justifies our methods of interest with emphasis on already present advantages obtained from the literature.

There are two distinct branches of methods, thermo-chemical and bioconversion, that have the most attention in current literature as promising lignin valorization techniques. Thermo-chemical conversion includes gasification to gain syngas then Fischer-Tropsch reformation into different small molecules, such as methanol or dimethyl-ether. This process needs a rather large capital investment and works at high temperatures and pressures, while on the other hand pyrolysis applies less extreme reaction conditions and requires less capital. For these reasons this latter thermo-chemical process gained considerable interest and currently it is used to upgrade lignin from different sources [2]. Lignin can be precipitated from the caustic pulping liquors of the paper industry by lowering the pH, and when CO_2 is used to recover lignin the process is called LignoBoost. The LignoBoost process was successfully tested on both lab and pilot plant scales and chapter 4 of this dissertation details the chemical analysis of lignin from this process, and also, results from pyrolysis experiments are compared to lignin gained by mineral acid precipitation from the same pulping liquor [9, 10].

Some bacterial species are also capable of aerobic bioconversion of lignin-like aromatic compounds, through the β-ketoadipate pathway [11]. Coincidentally, some of these bacteria belong to the actinomycetes [11, 12] group that has also been shown to accumulate lipids [13]. The Gram positive species of soil dwelling *Rhodococcus* is of particular interest. Initial work proved that *R. opacus* DSM 1069 can grow on coniferyl alcohol and other lignin model compounds as sole carbon sources (Eggeling and Sahm 1980). Later, different *Rhodococci* were shown to be oleaginous [13]. *R. opacus* PD630

was intensely investigated for its high (sometimes over 80 % [13]), lipid accumulation that exceeds the limit of oleaginicity at 20 % [14]. This strain was also grown on aromatic compounds, such as phenylacetic acid, and proved to be oleaginous (Alvarez et al. 1996), however, it was yet to be tested with lignin model compounds and lignin itself [2, 15]. Chapter 5 of this dissertation shows how the two above mentioned *R. opacus* strains grow and accumulate lipids on lignin model compounds, such as vanillic acid, while chapter 6 examines growth on different lignin sources.

The major objectives set in this dissertation are summarized as follows:

- Examine different lignin resources, such as pulping liquor precipitates, to determine chemical and physical properties for possible fuel utilizations
- Pyrolysis properties of lignin originating from pulping liquor
- Investigate the bioconversion of lignin by bacterial hosts
- Employ β-ketoadipate pathway using oleaginous bacteria in lignin to lipid bioconversion
- Analyze pure, lignin model compound conversion
- Test lignin from different sources, such as pulping liquor precipitates and biomass pretreatment residues, with the same bacteria
- Evaluate bioconversion efficiencies and pathways

CHAPTER 2

LITERATURE REVIEW

2.1 Problem statement

The most well recognized scientific journals have spent countless pages to examine alternatives to conventional fuels, and these papers all emphasize three points in close interaction: dwindling petroleum resources, increasing energy demand and prices, and concomitantly global warming from combustion of these resources [3, 4, 16-19] . There are very recent, great reviews and reports on how humanity depletes fossil fuel resources while rising average global temperature (e.g. ~1 °C in the last 30 years in the northern temperate region [19]) due to net CO_2 emissions [4, 6, 19], that reached between ~105-130 P g C/year (peta g carbon per year) [20]. On the other hand nationally sponsored research, such as the revisit of the billion ton report [7], proves that there is enough, otherwise unexploited, biomass to replace a considerable amount of fossil fuels [3, 4, 7, 21, 22]. As an example, the United States alone has approximately 1.3 billion dry ton residual biomass potential per year that can be directed to biofuels production, which is enough to address approximately one-third of its current demand for transportation fuels in an environmentally compatible manner [3, 7, 9]. Furthermore, even in a pessimistic scenario by 2020 the price of conventional (cane) bioethanol should be almost equal to the price of petroleum gasoline, while cellulosic ethanol should reach this point by 2050 (2030 by the optimistic scenario) [21]. Even though the U. S. energy legislation (from 2007) mandates over 10 million gallons of advanced cellulosic biofuel production per year for 2020, the industry, unfortunately, has fallen behind proposed

targets [23]. In the future though, plant biomass based biorefineries hand-in-hand with mainly solar, geothermal and wind power should at one point completely replace conventional energy sources [3, 4, 21, 23-26]. As biofuel research reaches new heights and production comes closer to feasibility, "ecopolitical" processes will be increasingly important in which proven advances in research intertwine with societal interests, e.g. biofuels for employment [27], or decisions over subsidies for biofuels [18]. Most importantly, the biorefinery concept provides an unambiguously closed cycle from both environmental (neutral carbon cycle) and economics perspectives (domestic biomass, conversion and utilization) [4].

Positive developments have to be emphasized as well though, e.g. society's general belief that global warming is present and is mainly caused by human activities resulting in excessive CO_2 release. After the 2011 fall ACS meeting, the editor-in-chief of C&EN wrote a very emotional and well opinionated editorial on why we can, at this point, and should ignore people, including scientists, who deny global warming [28].

The "problem", as it appears in the title of this section, has changed in recent years. Scientists have made their point and it is agreed upon that serious changes must be implemented in our attitude towards the environment, even if society's deeply rooted habits are at stake. Accordingly, the "gain society's attention" problem turned into a "how to implement changes without risking living standards" issue, with obstacles greater than ever before. Researchers still face major hurdles in biomass conversion and its supporting and residual effects. This can be visualized by difficulties currently present in for example cellulosic ethanol production via enzymatic hydrolysis and fermentation (Table 2.1).

Table 2.1. Obstacles in cellulosic ethanol production

Issue	Possible solution	Reference
Logistics	Optimization of biomass transport and biofuel redistribution based on feedstock density, moisture content, mode of transportation available etc. In case of bioconversion the optimal predicted facility size would produce ~1500 MLGE (million liter gasoline equivalent) annually, transported via trucks or rail. This is much higher than the proposed 50-70 ML/y (million liters per year) facilities. Consequently, significant scale up needs to be implemented.	[29]
Recalcitrance	Understanding recalcitrance through cell wall topochemistry by developing analytical techniques. Lowering biomass recalcitrance by genetic engineering e.g. manipulating the expression of lignin biosynthesis genes like the downregulation of CCR (Cinnamoyl-CoA oxidoreductase) will lower lignin content by ~50%.	[2]
Pretreatment	Optimizing pretreatment conditions (severity) to specific biomass, e.g. pine and other recalcitrant softwoods require dilute acid pretreatment (DAP), to reach optimal properties (e.g. solid digestibility, lignin recovery and concentration of toxic compounds etc.). However, DAP is one of the most expensive technique and money is an important factor considering that pretreatment takes up 18-20% of the total cost (more than any other single step).	[2, 30, 31]
Hydrolysis	Currently, after pretreatment, to get optimal sugar recovery around 15 FPU/g (filter paper unit per g cellulose) cellulase is needed. This costs about $0.85/gal ethanol, and the goal is to reach $0.1/gal. Accordingly significant increase in enzyme activity and /or enzyme production cost decrease is needed. To address this, gene transfer technologies are applied to obtain glycosyl hydrolase overexpression and high volume, cheap production. Also, additives like surfactants (Tween 20) can enhance hydrolysis at low cost.	[2, 31, 32]
Fermentation	Work with novel, genetically manipulated strains that can digest both C5 and C6 sugars into ethanol with high efficiency. Preferably at elevated temperatures where enzymatic hydrolysis is more efficient as well. Simultaneous saccharification and fermentation (SSF) was applied in the recent past to enhance productivity.	[2, 32]

Table 2.1 continued		
Fermentation cont.	In this scenario glucose was immediately consumed by the cell, consequently cellulose product inhibition was avoided. Currently, separate hydrolysis is used because the modern glycosyl hydrolases are much more efficient at elevated temperatures that microbes cannot tolerate. Consolidated bioprocessing (CBP) also has to be mentioned against the fact that hitherto it hasn't delivered the expected results.	
Recovery	Ethanol is traditionally recovered by distillation; however as an example, primary process economic analysis of in situ fermentation-pervaporation sytem showed 75 % decrease in fermentation cost.	[32]
Scale up	A 30-50 fold scale up will be needed to reach full potential from demo scale; this will require significant engineering work. Furthermore, the global biomass production will need to grow 15-20 times (in case of woodchips and bales) to reach the 50 % reduction in GHG (greenhouse gas) emissions by 2050, that will prove to be yet another logistic issue.	[17, 31, 33]

All the above ideas aim to overcome hurdles with cellulosic ethanol; however, there are multiple other first-, second- and third-generation biofuels, e.g. corn ethanol, cellulosic biodiesel and algae biodiesel being pursued also [4, 8, 15, 34]. Moreover, currently operating and highly productive industries, such as paper mills produce significant amounts of residual products, like lignin rich pulping (black) liquor (currently, 45 million dry tons annually in the U. S. alone [7]), that could/should be utilized further, in the form of biofuels for example. These resources have to be connected with the right technologies to increase their value in a possibly integrated process to maximize efficiency and profitability. Different plant biomass resources contain various amounts of structural components that can be utilized as summarized in Table 2.2 [35, 36].

Table 2.2. Composition of structural components in assorted biomasses, analyzed extractives free

Wood Species	Cellulose (%)	Lignin (%)	Hemicelluloses (%)
Softwoods			
Picea glauca	41	27	31
Pinus strobes	41	29	27
Tsuga canadensis	41	33	23
Norway spruce	46	28	25
Loblolly pine	39	31	25
Hardwoods			
Eucalyptus globulus	45	19	35
Populus tremuloides	48	21	27
Agricultural residues			
Corn stover	40	25	17
Wheat straw	30	50	20
Switchgrass	45	30	12

A concept called the integrated biorefinery connects biomass productivity and processing to obtain a range of fuels, power and chemicals while utilizing all components to maximize sustainability and economic pay off. It seeks to develop a "carbohydrate-lignin economy" that will become the primary resource for energy and materials. Within this proposed sustainable economy lignin is probably the weakest link, due to its non-uniform and resource dependent nature. As a consequence lignin is produced in large excess by the pulp and paper industry and future biorefineries have to deal with the same problem. Accordingly, lignin valorization is quite possibly the only route to facilitate the autonomic economy of a biorefinery, furthermore it would considerably increase the profitability of paper mills [2-5, 9, 10, 15].

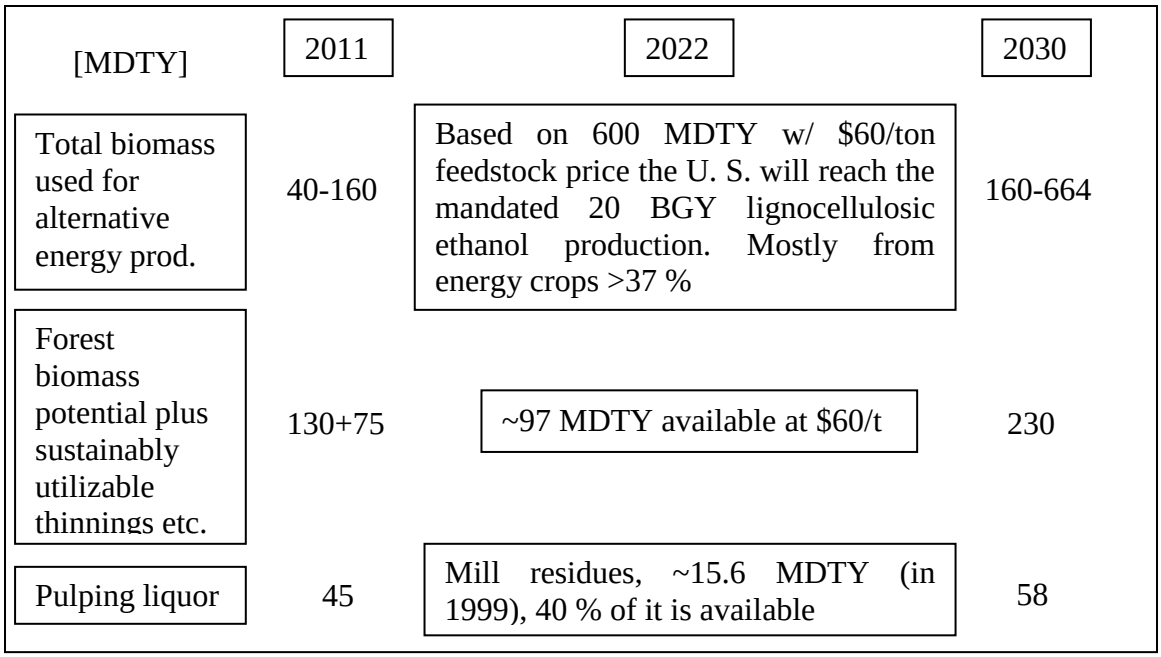

Figure 2.1. Annual biomass and lignin production and availability in the U. S. MDTY- million dry tons per year; BGY- billion gallons per year [7]

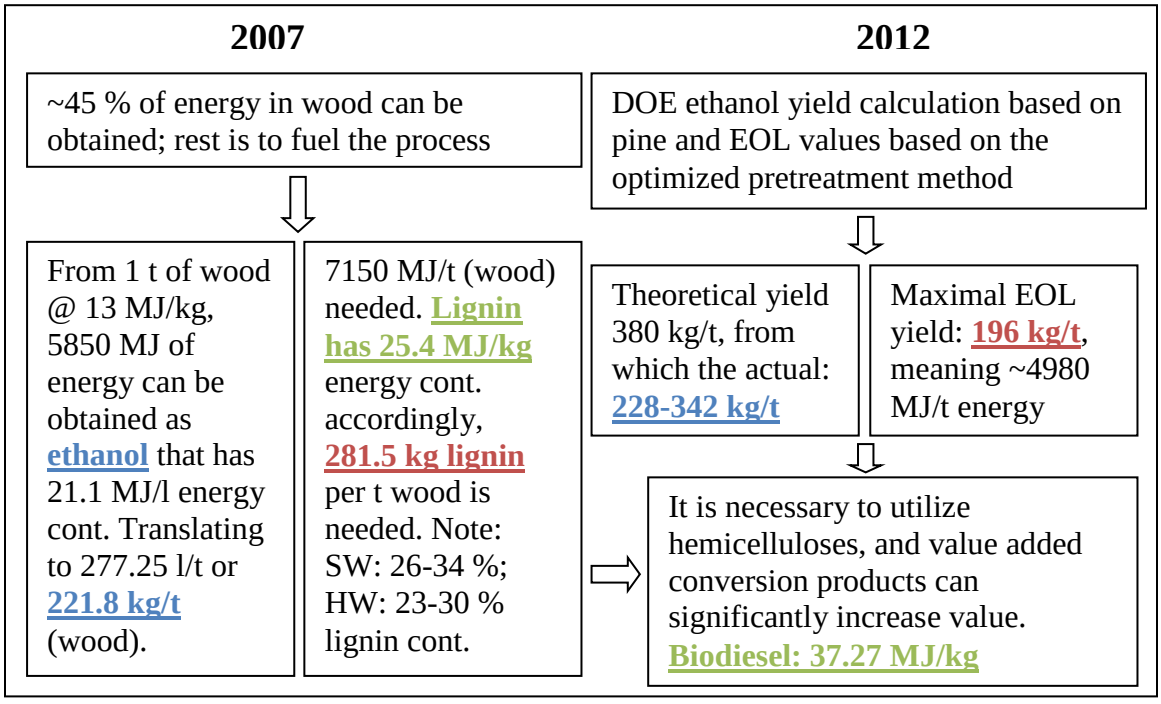

Figure 2.2. Converting wood to ethanol, energy balance and need for value added products. DOE- Department of Energy, MJ- mega joule, EOL- ethanol organosolv lignin [2, 7, 29, 31, 37-40].

Figures 2.1 and 2.2 show the biomass and lignin potential present in the U. S. and also indicate that cellulosic ethanol production has serious energy needs [29, 31]. When using the optimized ethanol organosolv pretreatment, it can also be calculated that for every ton of ethanol produced ~694.5 kg lignin (EOL) can also be gained [37, 39]. All this lignin, not mentioning the considerable amount (Figure 2.1) of lignin from pulping liquors, can be feedstock for alternative materials and fuels [1, 4, 5, 9, 10] possibly enhancing the profitability of a future biorefinery.

In brief, a common issue facing all current and future biomass conversion processes is the obstacle created by the intricate, recalcitrant structure of lignin. Consequently, it is vitally important to understand biomass composition, especially our current knowledge of lignin, and then utilization technologies can be proposed and evaluated. This dissertation addresses the lignin conversion problem, by examining possibilities via pyrolysis (applied on CO_2 precipitated LignoBoost lignin) to produce bio-oils and aerobic bioconversion using oleaginous microbes to produce lipids, as biodiesel precursors.

2.2 Current and proposed lignin based liquid biofuels

Lignin based materials and fuels are gaining more and more interest in the last few decades [1, 5] which is not surprising considering its availability (Figure 2.1). Currently available and possible future lignin resources, like Kraft and EOL, are discussed in detail in section 2.4. Briefly, monolignol units (Figure 1.1) through radical coupling (Figure 2.9) form this polyaromatic highly recalcitrant biopolymer with a structure detailed on Figure 2.10. Liquid biofuels, based on lignin, were in the focus of

the work presented in this dissertation, as shown on Figure 2.3, and first, pyrolysis oil as well as biodiesel properties are briefly summarized below.

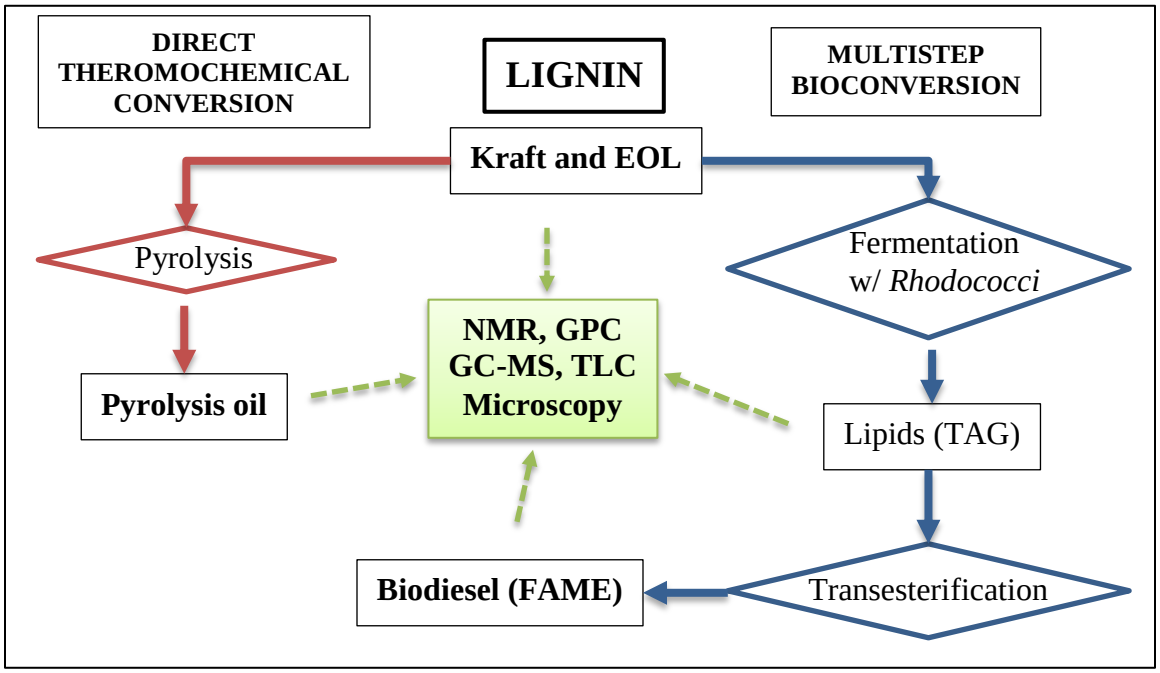

Figure 2.3. Flowchart of lignin to biofuel conversion routes, and analytical techniques applied in the work presented in this dissertation.

2.2.1 Pyrolysis oils

Lignin, just like whole biomass, can be pyrolyzed into char, gas and oil with latter being a potential alternative liquid fuel source [2, 9, 41-46]. Applied pyrolysis temperatures are usually between 400-700 °C, this is where oil yields are optimal under constant N_2 flow to exclude O_2 [42]. Non-catalyzed lignin pyrolysis usually yields two types of liquid phases: one "light" phase containing mainly water with minor amounts of catechols, methanol and acetic acid, and a "heavy" phase containing a mixture of low molecular weight (M_w ~300) aromatic compounds with some aliphatic side-chains [9, 42]. In general only the above "heavy" phase is considered as pyrolysis oil, and it mainly

contains: cathecols, phenols, guaiacols, anisole, toluene, xylols and other lignin related aromatic dimers and monomers, as collected on Figure 2.4 [9, 42, 44, 45, 47, 48].

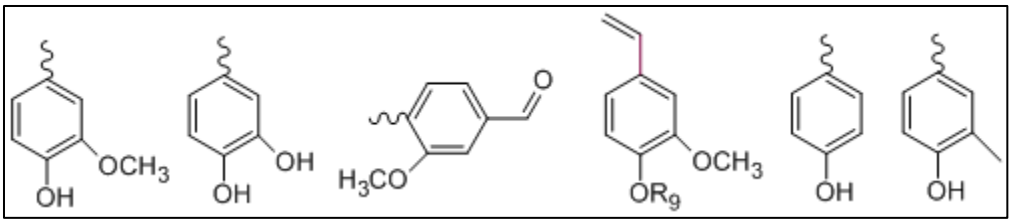

Figure 2.4. Main lignin based pyrolysis oil components

By looking at Figure 2.4 the first thing that comes to mind is that the mixture of these compounds doesn't represent anything like gasoline. Gasoline is a transparent liquid, obtained from crude oil via distillation in oil-refineries and it's bulk consist of 4-12 carbon chain length aliphatic alkanes, and its main physicochemical properties are listed in Table 2.3, in comparison to pyrolysis oil and biodiesel [49-52]. Pyrolysis oil has higher moisture content, viscosity and lower heating value, yet it is still the most feasible way to convert lignin into transportation fuel [9, 42-45, 47, 48]. Accordingly, since the early 2000's multiple companies have operated demo plants with 10-50 t/d output, with different lignins/biomass as feedstocks, in both Europe and the Americas [43]. All in all, pyrolysis is a promising way to convert the energy in lignin into a transportation fuel. Section 2.4.5 gives more detail on lignin thermo-chemical conversion, with more detail on pyrolysis and the properties of the obtained oil, while Chapter 4 goes into great detail on Kraft and LignoBoost lignin derived pyrolysis oil properties.

Table 2.3. Physicochemical properties of various pyrolysis oils and biodiesels compared to gasoline. n.p.- non published

Fuel source	Gasoline	Pine pyrolysis oil	Poplar pyrolysis oil	Rapeseed biodiesel	Soybean biodiesel
O/C ratio	0.011	0.655	0.570	0.14-0.16	0.14-0.16
H/C ratio	0.14	0.12	0.11	0.15-0.17	0.15-0.17
Viscosity [mm^2/s]	2.6	44	11	4.53	4.0-4.3
Density [kg/m^3]	800	1210	n.p.	900	900
Moisture [%]	0	13-14	14-15	n.p.	n.p.
Heating value [GJ/t]	42-44	17-20	18-21	37.3-39.9	39.7-40.1

2.2.2 Biodiesel

Biodiesel is the monoalkyl-ester of vegetable oils or animal "fats" [51], and in general it is obtained from lipids [i.e. triacylglycerols (TAG)], that can be oils (liquid at RT) or fats (solid at RT), via catalyzed transesterification with methanol, ethanol or other short chain alcohols [53]. TAGs can come from different sources, with the most prevalent ones being pure plant oils (PPO), waste vegetable oils (WVO) and animal fats [54]. Select TAGs are listed in Table 2.4, including their fatty acid (FA) composition that defines their physicochemical properties [51, 54, 55], such as viscosity or heating value (Table 2.3), as well as their cetane number (CN) as detailed below (Table 2.5) [51]. Transesterification catalysts can be enzymes, like lipases, bases and acids with latter's catalytic mechanism shown on Figure 2.5 [53].

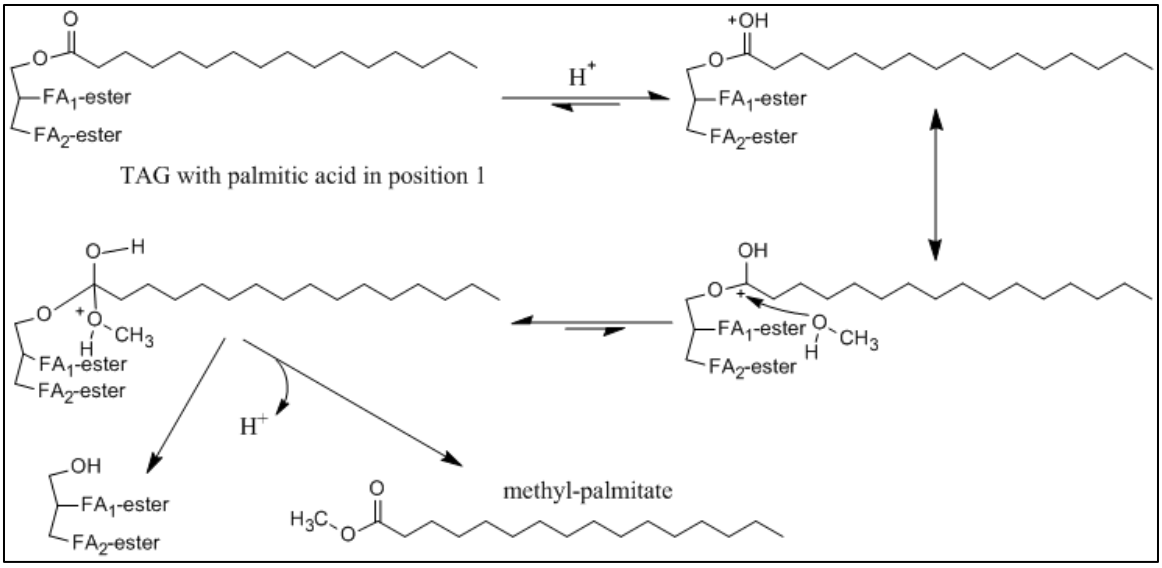

Figure 2.5. Acid catalyzed transesterification of triacylglycerols (TAG) to biodiesel e.g. methyl-palmitate, FA- fatty acid

Table 2.4. Fatty acid (FA) composition of pure plant oils (PPO), waste vegetable oils (WVO) and animal fats. FAs are listed in the top row indicated with carbon chain length, and number of unsaturations

PPO	**14:0**	**16:0**	**18:0**	**18:1**	**18:2**	**18:3**	**20:0**	**22:1**
Soybean	trace	6-10	2-5	20-30	50-60	5-11		
Rapeseed		2-6	4-6	18-26	49-57	10-11		
Palm		40-47	3-6	36-44	6-12			
Peanut		6-14	2-6	36-67	13-43			
WVO								
Yellow grease	1.3	17.3	12.4	54.7	8.0	0.7	0.3	0.5
Animal fat								
Chicken	0-1	26-33	7-10	32-36	16-21	0-1	1-2	0-1
Lard	1-2	28-30	12-18	40-50	7-13	0-1		

Fatty acid methyl esters or FAMEs can be directly blended into diesel fuel, with ratios typically 5 and 20 % designated as B5 and B20 respectively, and used in light or heavy duty diesel vehicles without modification [56]. Most of the oil feedstock originates from plant seeds, such as rapeseed or soybean (PPO, Table 2.4), however, there are examples for animal fat use as well as used restaurant cooking oil transesterification (WVO, Table 2.4) [53, 57, 58]. In 2008 the global biodiesel production was 12.2 MT with 7.7 MT

produced in Europe, including Germany as the largest scale producer with 2.8 MT [58]. In the U. S. the Environmental Protection Agency (EPA) monitors all biodiesel production and ensures that it meets the standards of ASTM (American Society for Testing and Materials) since 2001. Production, consumption and net export of biodiesel approximately doubled from year to year between 2004-2007, then reached maxima in 2008 with production close to 700 MG [57]. Since then however, this trend is steadily decreasing, in 2010 the production was only a bit above 300 MG, probably in part due to the economic crisis as well as the redeployment of governmental resources more towards algae based biofuels that doesn't need agriculturally valuable land for growth [57]. Hopefully these numbers will increase again, especially with initiatives like DOE's "clean cities program" in which last year multiple metro areas increased biodiesel in their communal/maintenance machinery (e.g. in New York) [56].

Table 2.5. Cetane number (CN) and melting point of various fatty acid methyl esters (FAME) that are the most abundant in biodiesel

FAME	Melting point [°C]	CN
14:0	18.5	66.2
16:0	30	85.9
18:0	39	101
18:1	-19.5	56-59
18:2	-35	38

Multiple properties of biodiesel, like density, viscosity, melting point, heating value (or heat capacity, Tables 2.3-4), cloud point and cetane number (CN, Table 2.5), must meet certain specifications to enable blending into diesel, as an example CN must be a minimum of 47 to meet biodiesel specifications [51, 53, 55, 58-60]. Cetane number (CN) is an indicator of diesel fuel quality and it correlates to ignition delay (ID) in the

engine, briefly the time delay between fuel injection and the onset of ignition [51]. CNs for typical FAs originating from TAG sources specifically used for biodiesel production are listed in Table 2.5 [51] While rapeseed (a.k.a. canola) and soybean oil based ethyl and methyl esters (REE, RME, SEE, SME) have similar densities (800-900 kg/m3), their viscosity is significantly higher 4.0-4.5 mm^2/s than diesel's 2.5-3 [51, 58]. This is one of the main reasons for transesterification, considering the really high viscosity of seed oils 30-40 mm^2/s, moreover, it explains the need for blending. Another similarity is the heating value with RME and SME having only ~10 % less than diesel that has ~45 MJ/kg. On the other hand the above mentioned CN will always be 10-20 % higher for biodiesel (50-60) indicating a shorter ID, accordingly, blending is inevitable if changes in engine design are to be avoided [58]. As a consequence, there are FAMEs that will be better in biodiesel blends than others, like palmitic, stearic, oleic, linoleic and linolenic acids, as investigated by the National Center for Agricultural Utilization Research (Dept. of Agriculture, Peoria, IL) [51, 55, 59, 60].

In summary, TAG's are produced by animals, plants and algae, with the latter two producing lipids by utilizing only sunlight, water and CO_2, through sugar synthesis (photosynthesis) and subsequent metabolic conversion [15, 34, 59-62]. Consequently, lipid synthesis is closely linked to sugars as substrates, however, there are some heterotrophic microbes that can degrade lignin, and it has also been proven that some of them can be oleaginous (produce >20% of their cell mass in lipids) [13-15, 63]. Attempting simultaneously using these microorganisms for lignin degradation and oil production can be a feasible way to convert lignin, just like pyrolysis, however, before introducing these thermochemical and bioconversion routes the detailed composition of

plant cell wall (biomass) has to be reviewed, especially considering the heterogeneous nature (Section 2.4).

2.3 Biomass composition

The National Renewable Energy Laboratory (NREL) defines biomass as "Any plant-derived organic matter. Biomass available for energy on a sustainable basis includes herbaceous and woody energy crops, agricultural food and feed crops, agricultural crop wastes and residues, wood wastes and residues, aquatic plants, and other waste materials including some municipal wastes. Biomass is a very heterogeneous and chemically complex renewable resource." [64] In this dissertation biomass is always obtained from wood, in particular loblolly pine (*Pinus taeda*), a type of softwood (SW).

Wood is a natural three-dimensional bio-composite composed of cellulose, hemicellulose and lignin (>90 %), with minor amounts of inorganics and extractives. Wood generally is classified into two groups: coniferous wood or softwood (SW), obtained from gymnosperm trees, and hardwood (HW), obtained from angiosperm trees. The major biopolymers of wood cell walls are sugar-based polymers (i.e., cellulose and hemicellulose, 65-75 %) and lignin (18-35 %) [65]. On a dry-weight basis, wood typically has an elemental composition of about 49 % carbon, 6 % hydrogen, and 44 % oxygen [66]. The cell types and chemical compositions vary between hardwood and softwood as well as among species. In general, softwood species have a comparable cellulose content (40-44 %), higher lignin (26-34 %), and lower hemicellulose content (20-32 %) as compared to hardwood species (cellulose 40-44 %, lignin 23-30 %, hemicellulose 15-35 %, detailed in Table 2.2) [65, 66].

The cell wall in wood is a complicated and dynamic structure, consisting of three anatomical regions: the middle lamella, the primary wall, and the secondary wall. The latter unit, contributing up to ~89 % of the mass of mature trees, is made up three layers: the outer (S1), the middle (S2), and the inner (S3) layers (Figure 2.6) [65, 67]. Cell walls are typically deposited by layers upon synthesis, with the primary cell wall formed during cell growth as the first wall laid down in dividing and growing plant cells, and the secondary cell wall deposited when cell growth has ceased [68]. The middle lamella is the layer between two neighboring cells (Figure 2.6) [69]. The thickness of each layer and its constituents vary in different cell types, tissues and wood species. The ultrastructure of cell wall is generally considered to be comprised of long cellulose microfibrils held together by hemicellulose and lignins, as shown on Figure 2.6 [67, 69]. Recently developed analytical methods, such as atomic force microscopy (AFM) and single molecule methods, have advanced our knowledge about the ultra-structure of plant cell walls. For example, using advanced AFM techniques Ding et al. proposed a model of plant cell wall cellulose elementary fibril that consists of 36 β-1,-4 glucan chain, with hemicellulose particles interacting with the surface of the chain to form a ribbon-like bundle of microfibril [70].

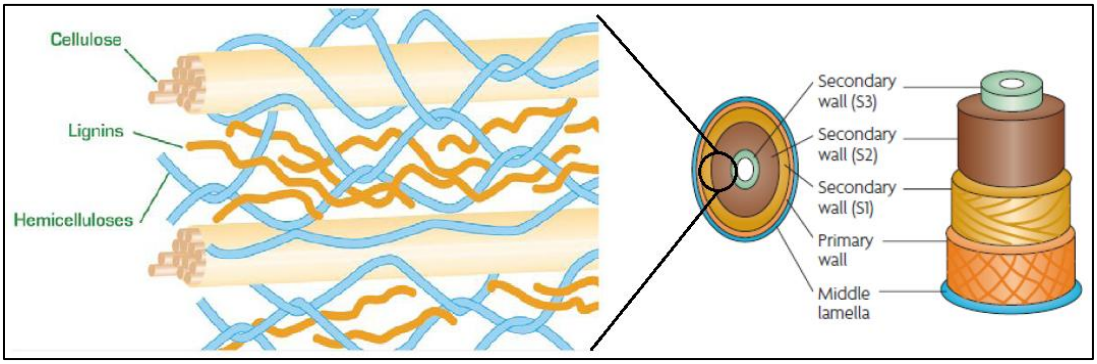

Figure 2.6. The schematic structure of wood cell wall, including the layering of primary and secondary cell walls that contain cellulose, hemicellulose and lignin as shown on the enlarged scheme on the left hand-side [67, 69].

2.3.1 Cellulose

Cellulose is a linear homopolymer of (1→4)-β-D-glucopyranosyl units with a varying degree of polymerization (DP_v) typically in a range of 1000-5500 (Figures 1.1 and 2.7) [71]. DP_v can be obtained by different methods, such as viscometry or gel permeation chromatography (GPC), furthermore, the resulting values can be interpreted differently, such as weight (DP_w), number (DP_n) and viscosity average (DP_v)'s. These are all related to glucose, as the basis of the polymer (not cellobiose) and DP_v's of assorted plant celluloses have been recently reviewed, as summarized in Table 2.6 [71].

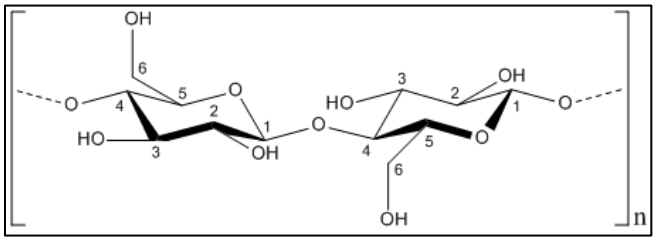

Figure 2.7. β-D-glucopyranosyl-(1-4)-β-D-glucopyranoside, the cellobiose building block of cellulose polymer

Table 2.6. Viscosity average degree of polymerization of various plant celluloses

Plant origin	**Cellulose DP_v**
Beech	4050
Red maple	4450
Jack pine	5000
White spruce	4000
Southern pine	1450
Wheat straw	1045
Bagasse	925

The cellulose chain has a strong tendency to form intra- and inter-molecular hydrogen bonds connecting the hydroxyl groups on these linear glucan chains, enhancing stiffness and promoting cellulose aggregation. Using X-ray and solid state NMR two crystal types were detected in native biomass: Iα and Iβ, with average cellulose degree of crystallinity of ~50–70 % in wood [71-74]. With the advancement of NMR analytical techniques, especially the cross-polarization magic angle spinning solid state (CP/MAS) ^{13}C NMR, further details were revealed about crystallinity [75-78]. As a result it was shown, that native cellulose in plants is a composite of three crystalline allomorphs: cellulose Iα, cellulose Iβ (above mentioned), and *para*-crystalline cellulose; and two noncrystalline forms: amorphous cellulose at accessible and inaccessible fibril surfaces [76-78]. Cellulose Iα has a one chain triclinic unit cell and it is the dominant form in bacterial and algal cellulose, whereas cellulose Iβ with a monoclinic two-chain unit cell, is dominant in higher plants, such as wood [75-78]. *para*-Crystalline cellulose is the form that is less ordered than cellulose Iα and cellulose Iβ but more ordered than amorphous cellulose [75-78]. Accessible fibril surfaces are those in contact with water, while the inaccessible fibril surfaces are fibril-fibril contact surfaces and surfaces resulting from distortions in the fibril interior [75-78]. Table 2.7 lists the cellulose crystallinity and ultrastructure of various biomasses as determined by CP/MAS ^{13}C NMR [75].

Table 2.7. Crystallinity and ultrastructure of different celluloses, determined by CP/MAS ^{13}C NMR

Plant origin	Crystallinity (%)	Iα	Iα+β	para-crystalline	Iβ	Accessible fibril surfaces	Inaccessible fibril surfaces
Hybrid poplar	63	5.0	14.2	31.1	19.8	10.2	18.3
Loblolly pine	63	0.1	30.7	24.8	6.9	33.1	15.6
Alamo switchgrass	44	2.3	8.8	27.3	4.5	5.7	51.3

Though crystallinity has been widely studied in wood cellulose ultrastructure during the last three decades, recent evidence has suggested that the microfibrils/nanofibrils of cellulose in higher plants including wood poses a helical twist in their native state, which is not consistent with the assumptions of the symmetry of the crystal structures under crystallographic analysis. Atalla et al. therefore proposed to use the term "aggregate" to indicate the highly ordered cellulose fibrils [79]. Cellulose crystallinity is important because it is widely accepted that reduced cellulose crystallinity can facilitate enzymatic deconstruction [2].

2.3.2 Hemicelluloses

After cellulose, the other major polysaccharide obtained from wood is hemicellulose. Unlike cellulose, hemicelluloses have a much lower DP (i.e., generally 100-200, as listed in Table 2.8) [80, 81], frequently have side chain groups and are essentially amorphous [3, 82]. The major hemicelluloses in softwoods are galactoglucomannans and arabinoglucuronoxylan, while in hardwood the predominant hemicellulose is glucuronoxylan (Figure 2.8). HW glucuronoxylan and SW arabinoglucuronoxylan both have a backbone of (1-4)-linked β-D-xylopyranosyl units but

exhibit differences in branching and substitution patterns. In HW, the xylan polymer is usually acetylated at C_2- and C_3- positions (i.e., ~3.5–7 acetyl groups/10 xylose) and is also branched with small amounts of (1→2)-linked pyranoid 4-O-methyl-α-D-glucuronic acid units. On the other hand in SW the xylan polymer is not acetylated, but branched with (1→2)-linked pyranoid 4-O-methyl-α-D-glucuronic acid and (1→3)-linked α-L-arabinofuranosyl units, with a typical arabinose: uronic acid: xylose ratio of ~1: 2: 8. Galactoglucomannan is comprised of (1→4)-linked β-D-glucopyranosyl and D-mannopyranosyl units that are partially acetylated at the C_2- and C_3- positions. Galactoglucomannan is more important than arabinoglucuronoxylan in SW, contributing 15–20 % of the dry wood mass [2]. The sugar monomer composition of different hemicelluloses originating from SW and HW are listed in Table 2.9 [80, 81].

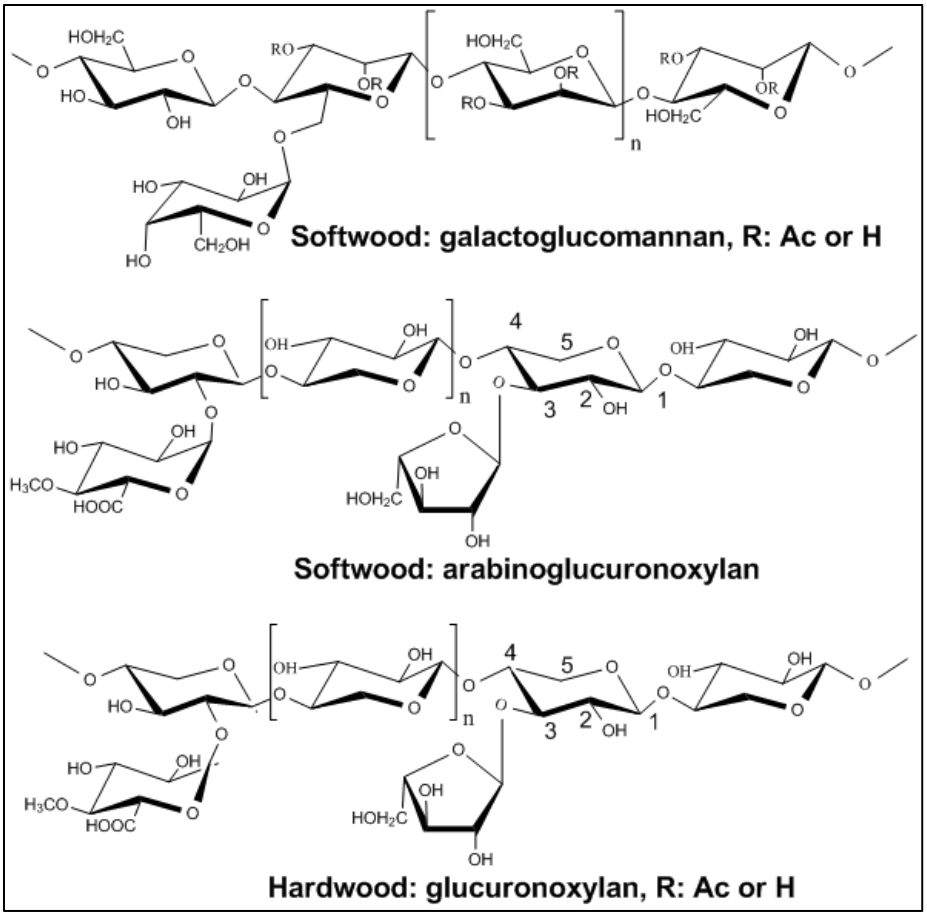

Figure 2.8. Softwood (SW) and hardwood (HW) hemicellulose chemical structures

Table 2.8. Composition and DP of hemicelluloses in two typical wood species, SW and HW respectively

Wood	Species	Hemicellulose	Amount (% of wood)	DP
SW	Loblolly pine	Galactoglucomannan	15-20	100
		Arabinoglucuronoxylan	7-10	100
HW	Birch	Glucuronoxylan	15-30	200
		Glucomannan	2-5	200

Table 2.9. Relative distribution of hemicellulose sugars in typical SW and HW species

Wood Species	Ara	Xyl	Gal	Glc	Man	Rha	GlcA	GalA	4-O-MeGlcA	Total [%]
SW										
Picea abies	0.16	0.65	0.23	0.36	**1.00**	0.03	0.04	0.18	0.10	24.8
Pinus banksiana	0.20	0.61	0.23	0.41	**1.00**	0.02	0.06	0.15	0.12	28.0
HW										
Populus tremuloides	0.03	**1.00**	0.04	0.11	0.07	0.03	0.01	0.12	0.13	29.0

2.3.3 Lignin

Of the three major biopolymers that constitute wood, lignin is chemically different from the other macromolecular polymers. This biopolymer is an amorphous polyphenolic polymer that is synthesized by enzymatic (laccase or peroxidase) dehydrogenative polymerization of 4-hydroxyphenyl propanoid units (Figure 2.9). The biosynthesis of lignin is generally considered to stem from the polymerization of three types of phenylpropane units as monolignols: coniferyl (G), sinapyl (S), and *p*-coumaryl (H) alcohol (Figure 2.9) [83-85].

SW lignin is composed mainly of coniferyl (G) alcohol units and minor amounts of *p*-hydroxyphenyl (H) units, while HW lignin is generally composed of G and sinapyl (S) alcohol units, with minor amounts of (H). Although the structure of lignin is usually regarded as irregular and highly heterogeneous with no regular extended repeating unit structures observed, recent studies on biosynthesis of lignin by altering the expression of individual genes of phenylpropanoid and monolignol biosynthetic pathways in poplar (HW) have suggested a partially linear structure of lignin [86, 87]. While the exact structure of lignin is unknown, the most common interunit linkages in

softwood/hardwood lignin have been identified (Figure 2.10) with the improvements in methods for identifying lignin degradation products and advancements in spectroscopic techniques [3, 88]. Many of these advances have been spurred by the use of advanced NMR (Nuclear Magnetic Resonance) techniques supported by lignin model compound synthesis. For example, in the early 1990's the detection of dibenzodioxocin in SW at a level of ~10-15 % initiated a flurry of research efforts that has led to several new sub-unit structures to be detected [2, 89-91]. Lignin inter-unit linkage proportions in SW and HW are detailed in Table 2.10, while Table 2.11 summarizes some of the average lignin molecular weights [54, 88, 92].

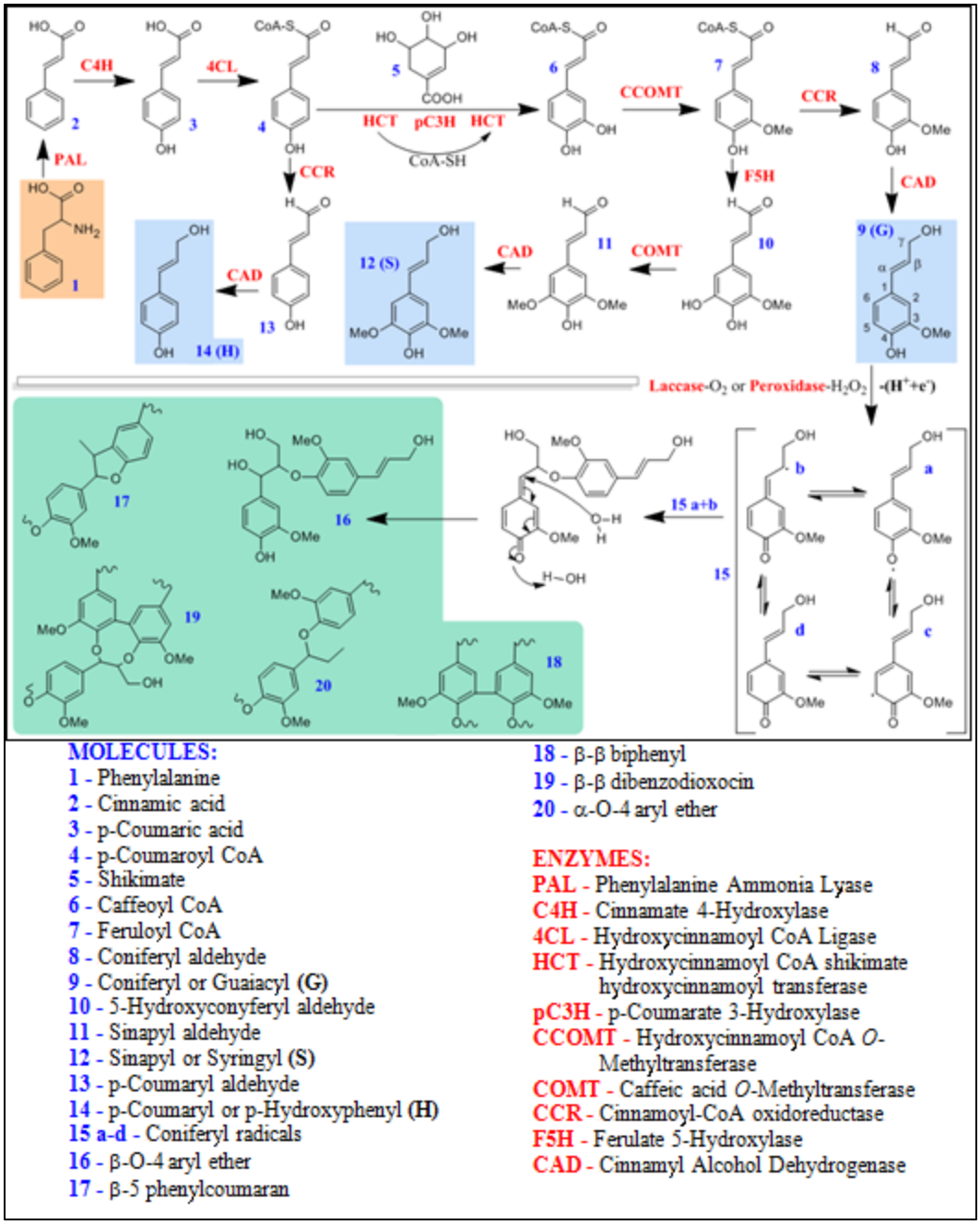

Figure 2.9. Lignin monomer (S, G, H) biosynthesis as well as polymerization as catalyzed by cell wall peroxidases and laccases, including a simplified –OH substitution and rearrangement.

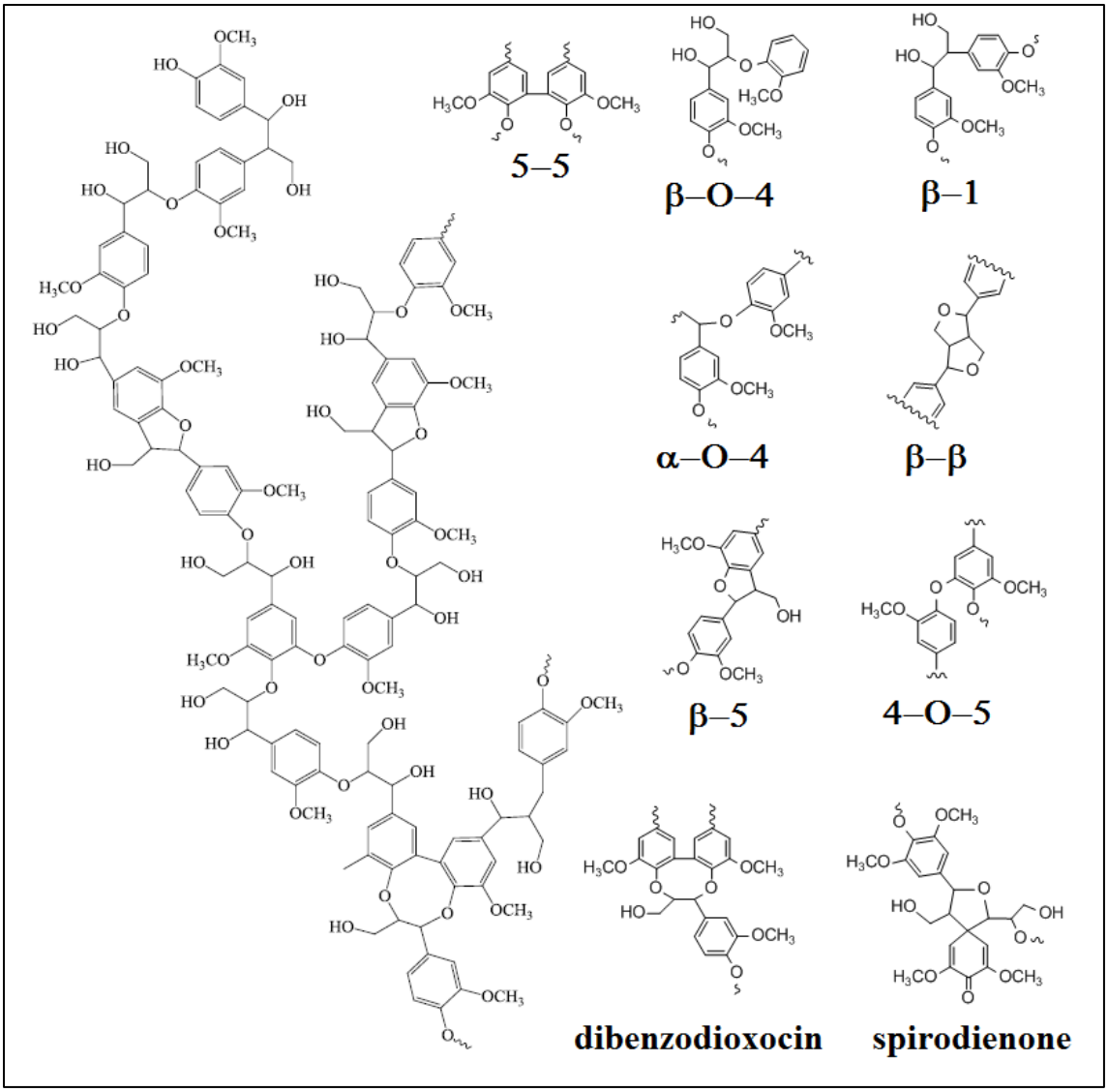

Figure 2.10. Lignin inter-unit linkages and an illustrative example structure of native SW lignin on the left hand-side

Table 2.10. Lignin inter-unit linkage type distribution averaged for softwood, and measured for spruce (SW) and eucalyptus (HW), occurrence in 100 aromatic units; n.p.- non published

Linkage type	Softwood	Spruce	*Eucalyptus grandis*
β-O-4	45-50	45	61
α-O-4	6-8	16	n.p.
β-β	3	2	3
β-5	9-12	9	3
5-5	18-25	24-27	3
β-1	7-10	1	2
4-O-5	4-8	n.d.	9
Dibenzodioxocin	n.p.	7	n.p.

Table 2.11. Number and weight average molecular weights and polydispersity (PD) of different lignins obtained via various extractions from biomass, such as milled wood (MWL) process, pulping and ethanol organosolv (EOL) pretreatment

Biomass origin	Lignin extraction	M_w	M_n	PD
Mixed SW	Kraft lignin	9735	2755	3.5
Bagasse	Soda pulping	8481	2684	3.2
Mixed HW	Sulfite pulping	4317	2173	2.0
Mixed HW	Organosolv	3959	511	7.7
Loblolly pine	MWL	13500	7590	1.8
	EOL	2440	1191	1.7

2.3.4 Lignin carbohydrate complexes (LCC)

Sugar components in hemicellulose can take part in the formation of lignin-carbohydrate complexes (LCC) by covalent linkages between lignin and carbohydrates, mostly at the α and γ positions on monolignols' propanoid sidechains [93, 94]. Despite significant analytical efforts directed at characterizing LCC's, they remain poorly defined and their biosynthetic pathways need further investigation. Recently research efforts using two-dimensional NMR ^{13}C-^{1}H correlation techniques such as HMBC/HMQC have identified the ester/ether linkages of LCC [95, 96]. For example, in the lignin-carbohydrate ester linkages in loblolly pine, an uronic acid residue was observed to attach to the γ–position of lignin side chain [95]. These signals were further investigated and are accounted for in this work as well (Chapter 6 and Appendix D) referring to the latest results from the literature [93-96].

2.3.5 Extractives

Wood, especially softwoods and tropical hardwoods contain significant amounts of extractives that can be classified by both the solvent they are extracted with or by

chemical compound groups, as summarized in Table 2.12 together with ash and structural components [36]. In general, everything other than poly-carbohydrates and lignin is considered an extractive, accordingly, there are inorganic and organic compounds present and further classification is depicted on Figure 2.11 [97].

Table 2.12. Structural biopolymer and extractive contents in select wood species, based on oven dried weight (ODW) in weight percentage

Wood species	Lignin [%]	Cellulose [%]	Hemi. [%]	Extractives[%]	Ash [%]
SW					
Western white pine	25.4	42.3	7.9	***8.3***	0.3
White spruce	27.8	42.1	12.1	***2.3***	n.p.
Norway spruce	26.9	42.3	11.0	***0.9***	0.3
Loblolly pine	28.1	43.3	12.6	***3.8***	0.4
Jack pine	28.3	45.2	11.3	***4.0***	1.3
HW					
Yellow birch	21.2	49.4	21.4	***2.6***	1.7-2.9
Red maple	22.8	44.5	17.1	***2.5***	5.2
Yellow poplar	25.3	33.5	20.1	***3.6***	2.8
Quaking aspen	18.2	50.2	17.5	***2.4***	4.0

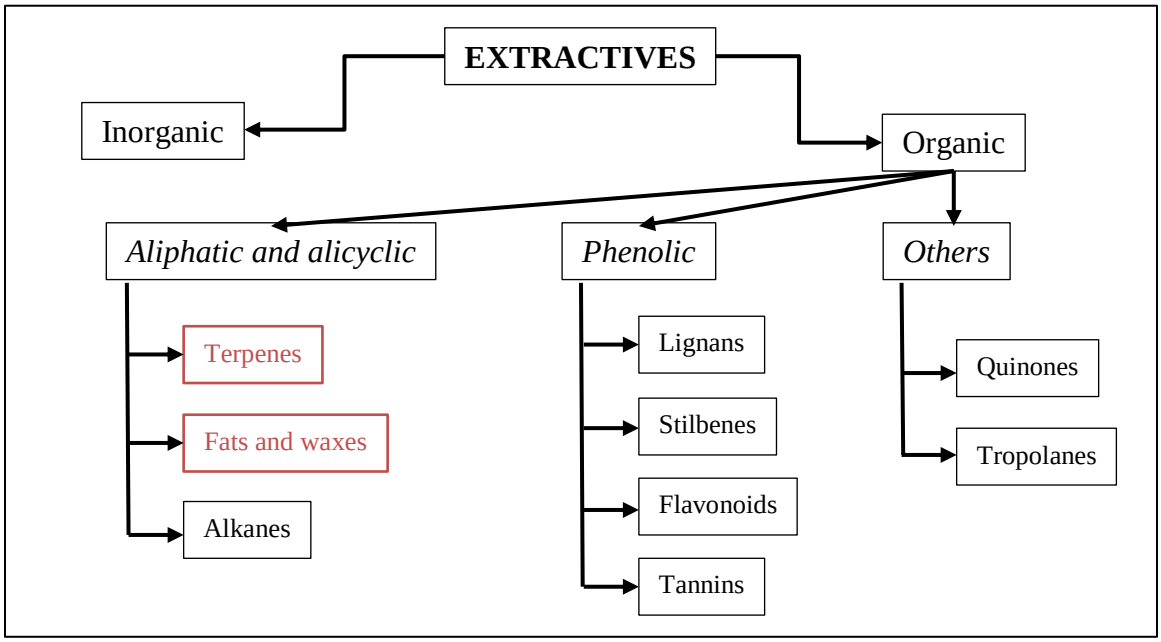

Figure 2.11 Extractives in wood by chemical classification. Terpenes and fats are highlighted because Kraft lignin contains them after extraction and purification from black liquor (BL) to various extents.

Inorganics can be measured by ash content that is usually between 0.3-1.5 % for both HW and SW. The most abundant elements are: Ca, K, Mg and P with approximately 1000-1500, 200-400, 100-200 and 40-60 mg/kg wood. Other elements usually present below 100 ppm are F, Na, Si, S, Al, Mn, Fe, Zn, B and Ba [98]. Organic extractives can be present in much higher amounts, especially in SW, as an example loblolly pine (*Pinus taeda*) contains ~2-3 % resin acids [97]. Here the focus is on SW with emphasis on pine that represents all samples used in this work. Overall, SW contain 1-8 % extractives (Table 2.12) most of which are resin acids, a mixture of diterpenes, originating from the resin canals [97]. Wood resins, separated by lipophilic (organic solvent) extraction, are a collection of oleoresins –that contain a volatile (monoterpenes) and a non-volatile (fatty acids and diterpenes) portion- and parenchyma resin (triterpenes and steroids), with the exception of phenolic substances [97].

Following Figure 2.11, aliphatic and alicyclic components contain terpenes (and terpenoids), fats, waxes and alkanes. The first two will be discussed in more detail in the following sections (2.3.5.1-2), because of their presence in Kraft lignin separated from SW black liquor [97, 99, 100].

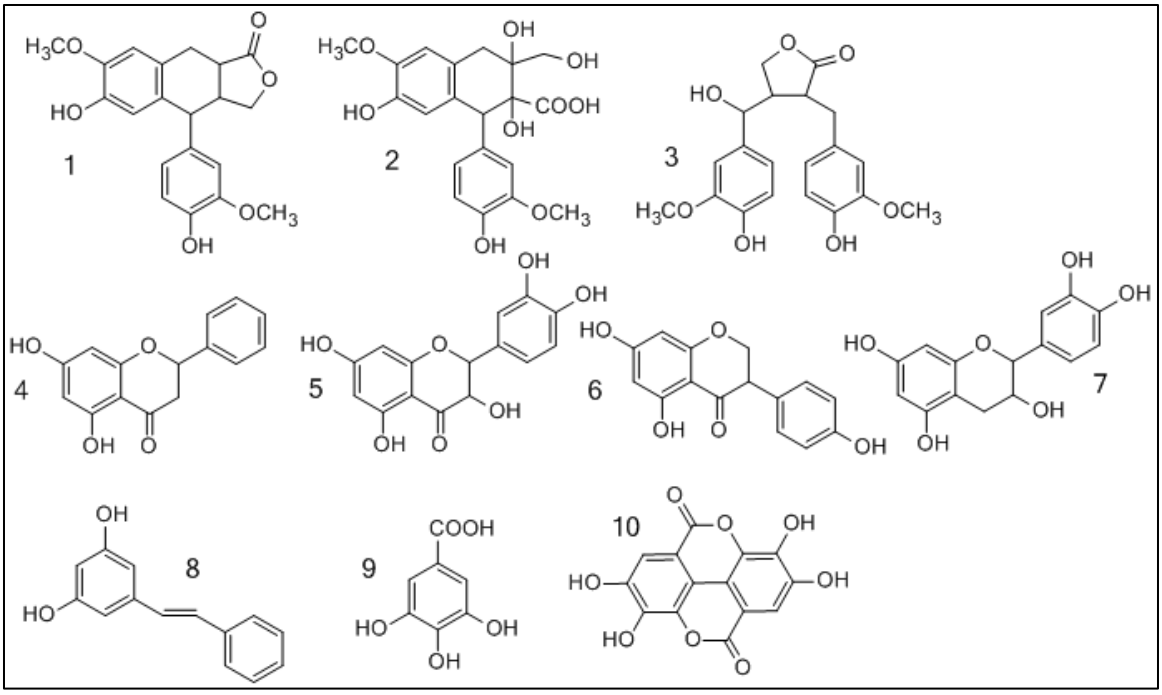

Figure 2.12. Lignans 1-3: conidendrin, plicatic acid and hydroxymatairesinol; 4-7 flavonoids: chrysin, taxifolin, genistein and catechin; stilbenes e.g. 8: pinosylvin; hydrolysable tannin monomers 9-10: gallic and ellagic acids.

Phenolic extractives (Figure 2.12 and 2.13) include lignans, stilbenes, flavonoids and tannins. Lignans are β–β linked monolignol units that differ in aromatic ring substitution (3, 4 and 5), nature of side chain and other linkage(s) between rings as shown on Figure 2.12. In neolignans the connection between the phenyl-propanoid units doesn't occur between β carbons. Lignans have medicinal (antitumor and antiviral) and food preservative commercial applications [97]. Stilbenes are derivatives of 1,2-diphenylethene, e.g. pinosylvin (Figure 2.12). Their concentration is low in wood, but they can form during Kraft pulping, for example, from β-5 phenylcoumaran (Figure 2.10) lignin units via reverse aldol addition (formic acid release) [96, 97, 101, 102]. Stilbenes can be useful anti-microbial agents as well as active agents in herbal medicine [97]. Flavonoids have a tricyclic (Figure 2.12) carbon skeleton, and they are used in

commercial dyes, food colorings and pharmaceuticals. Moreover, high flavonoid content diets have proven health benefits [97]. Tannins can be further classified into hydrolysable and non-hydrolysable tannins, with the former found rarely in wood, except for some hardwoods such as oak or eucalyptus. Hydrolysable tannins are polymers of gallic and ellagic acids (Figure 2.12) esterified to a core molecule that is often glucose or catechin (flavonoid). These compounds are utilized in the adhesives industry. Non-hydrolysable tannins are polymers of flavonoids, typically 3-8 units, and they are similarly underrepresented in SW compared to HW. They have a wide array of commercial uses, such as the manufacture and preservation of fishing nets, plastic and adhesive production and protection of metals [97]. Quinones and tropolanes are only present in negligible amounts in wood, however, special quinones such as anthraquinone can occur in mold and large fungi and it can be utilized as a pulping catalyst [97].

2.3.5.1 Terpenes (terpenoids), diterpenoids

Terpenes are built from isoprene units and in general cyclic molecules formed from 2 isoprenes per cycle. Accordingly, there are mono-(2), sesqui-(3), di-(4) and tri-(6)-terpenes. Steroids also belong to this family of compounds; they are triterpenoids with sterane structure. Terpenoids differ from terpenes by an oxygen-containing functional group that is completely missing from neutral terpenes. Furthermore, acidic terpenoids are saponifiable, because their carboxylic group can form a conjugated base and salt bridge with e.g. Na^+ under alkali conditions (e.g. Kraft pulping) [97]. Figure 2.13 summarizes the main terpenoids with emphasis on diterpenoids that were found to be present in Kraft lignin [97, 99, 100].

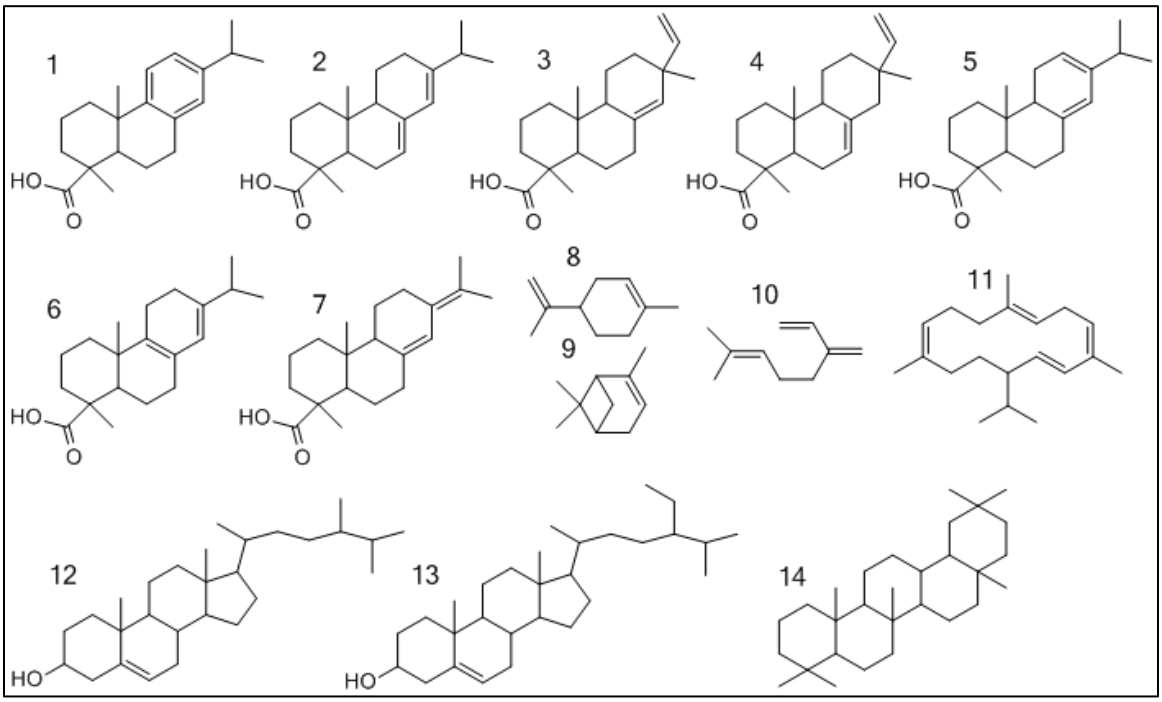

Figure 2.13. Terpenes and terpenoids, with emphasis on rosin forming diterpenoids (acids). Diterpenoids 1-7: dehydroabietic, abietic, pimaric, isopimaric, levopimaric, palustric and neoabietic. Monoterpene examples 8-10: limonene, α-pinene and mircene; neutral diterpene e.g. 10: thunbergene. Steroidal triterpenoids e.g. 12-13: campesterol and sitosterol; and neutral-nonsteroidal triterpene e.g. 14: oleanane.

Monoterpenes are present in ~0.3 % in pine wood, mostly as the volatile portion of oleoresin (resin canal) called turpentine and their uses involve insecticides, fragrances, flavor chemicals and pine oil. Nonsteroidal triterpenyl alcohols and steroids are usually present in very low (<1 %) amounts and are generally ester bonded to glycerol. Latter are highly valuable pharmaceutical precursors as well as components of cosmetics and food additives [97].

Resin acid diterpenoids (Figure 2.13) are the main constituents of rosin, the non-volatile fraction of oleoresin (canal resin), that seal injuries of the tree after volatile turpentine evaporate. These resin acids represent ~2-3 % of softwood and their

composition in e.g. loblolly pine (*Pinus taeda*) is listed in Table 2.13 [97, 103, 104]. They can be utilized for paper sizing, adhesive systems and components in printing ink and paints, however they also cause "pitching" of the paper (holes, discoloration) and are proven to be toxic for fish living close to paper mill effluents, and consequently their removal is of great interest [97, 103, 104].

2.3.5.2 Fatty acids (lipids, waxes)

Pine and wood in general also contain fatty acids (FA) in forms of triacylglycerols (TAG or aka lipids), waxes (esterified to long chain alcohols) and as free acids. The overall FA content of SW usually varies around 0.5-2 % (including all forms) and the most abundant FAs in pine are summarized in Table 2.13, while Figure 2.14 shows all FAs found in pine [97, 104]. These FA esters (TAGs, waxes) are also saponifiable and during alkaline pulping they are cleaved by the hydroxide ion into carboxylate salts and alcohol. This requires additional alkaline during pulping and causes foaming issues during the Kraft process, while extracted FAs are useful in biodiesel, soap and detergent as well as rubber manufacturing (softening agents) [97, 104].

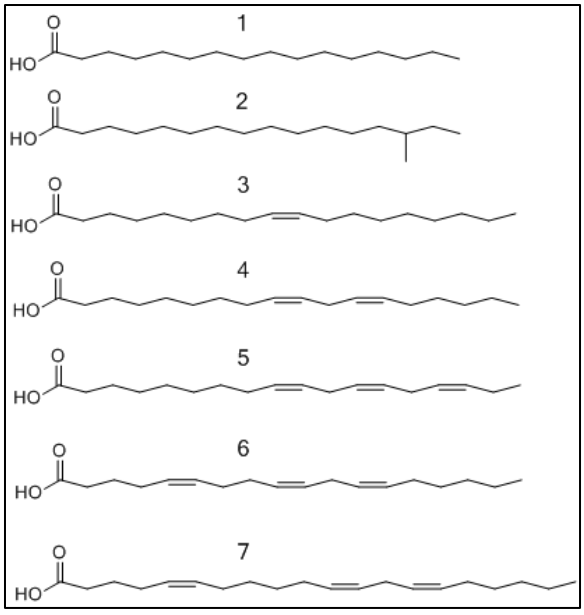

Figure 2.14 The main fatty acids found in pine wood: 1. Palmitic, 2. 14-methylhexadecanoic, 3. Oleic, 4. Linoleic, 5. Linolenic, 6. Pinoleic and 7. 5,11,14-eicosatrienoic acids.

Table 2.13. Non-volatile extractives in pine wood

Composition of non-volatile pine extractives			
Diterpenoic (resin, DA) acids		**Fatty (FA) acids**	
Content in wood [%]	2.0-3.0		0.5-2.0
Components based on total DA or FA [%]			
Pimaric	8.1	Linoleic	40.5
Sandaracopimaric	1.6	Oleic	35.3
Levopimaric	30.0	Pinoleic	10.6
Isopimaric	3.5	5,11,14-eicosatrienoic	4.6
Abietic	15.8	Linolenic	0.8
Dehydroabietic	14.4	Other unsaturated	4.2
Neoabietic	11.1	Palmitic	1.0
Palustric	15.1	14-Me-heptadecanoic	0.8
Other	0.4	Other saturated	1.3

2.4 Present and promising future lignin resources, their analysis, properties and pyrolysis

Previous sections summarized biomass composition and implied that future biorefineries must utilize all components of this resource at their highest values to reach feasible operation [4, 9, 73]. It was also determined that lignin is possibly the most under-

utilized of all components in woody biomass. The following sections detail the currently most abundant lignin source, namely Kraft lignin, as a possible residual product of the pulp and paper industry [9]. Furthermore, one of the most promising future lignin resources, ethanol organosolv lignin (EOL), acquired during pretreatment will also be examined [39]. Moreover, the analytical methods applied to evaluate the properties of these lignin sources will be accounted for. The following sections also include a brief summary of lignin thermochemical conversions, such as pyrolysis, to show alternative utilization possibilities. In brief, this section concentrates on the most abundant lignin substrates available for conversion including pyrolysis, as shown on Figure 2.3.a, while section 2.5 covers the possible microbial conversion pathways and justifies the selection of strains used in this work.

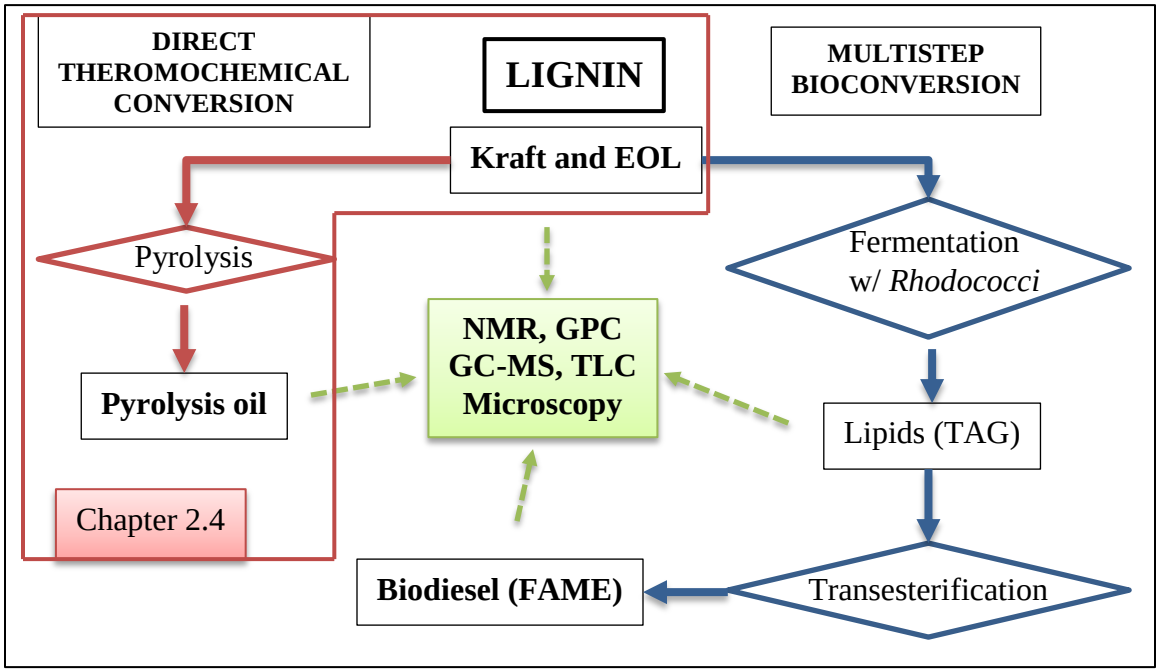

Figure 2.3.a. The introduction of present and possible future lignin resources and their thermochemical conversion

2.4.1 Lignin from the pulp and paper industry

As mentioned in earlier sections the pulp and paper industry has probably the highest quantity of underutilized lignin in the form of black liquor (BL), with worldwide production reaching 50 million tons [5, 10]. Paper production begins with the liberation of cellulose fibers from the secondary cell wall matrix (Figures 2.6 and 2.15), with a process known as pulping [88, 105]. Pulping takes place in the digester (Figure 2.15) and it can involve physical and chemical treatments, while the most common is thermo-chemical pulping that results in solids (containing cellulose fibers with some residual lignin and hemicelluloses), as well as a liquid phase called black liquor (BL), rich in lignin [88, 105]. The digester is operating around 170 °C for a few hours (~2 h) and the most common chemicals used in pulping are NaSH and NaOH. When these chemicals are applied the process is called Kraft pulping and it is the most widely practiced pulping process globally and in the U.S. [88, 105]. These highly valuable pulping chemicals are retained in the BL and they need to be recycled for economic efficiency. The process in which these chemicals are regenerated is called the Kraft-recovery cycle and a simplified version is shown on Figure 2.15.

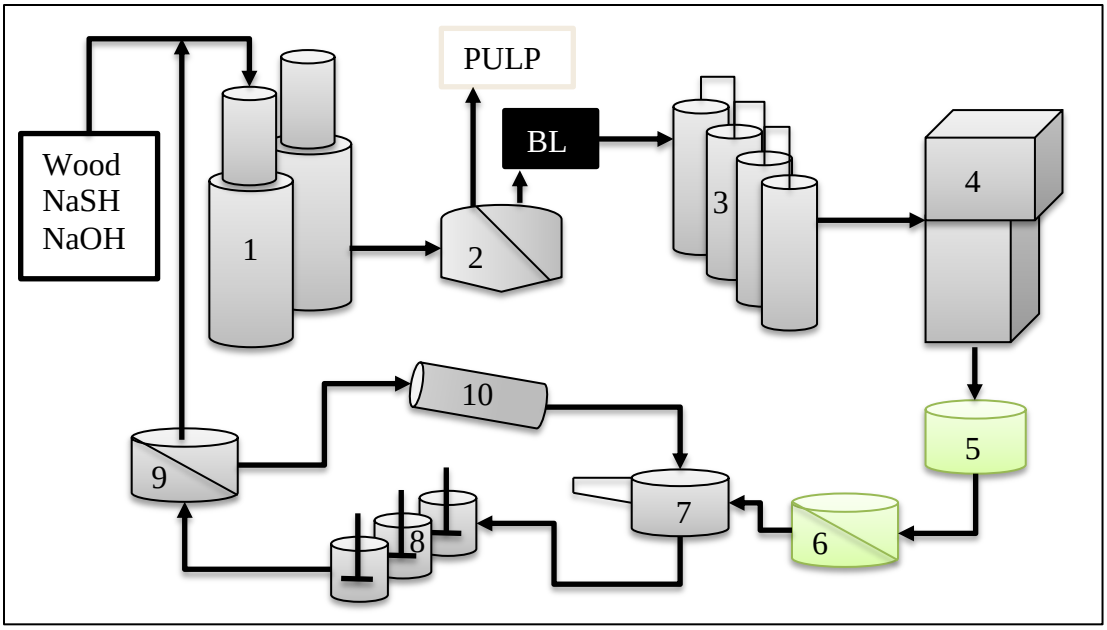

Figure 2.15. The Kraft process starts with wood chips suspended in white liquor (NaOH and NaSH) then fed to the digesters 1. Pulp is separated from BL by the brown stock washer 2. BL is concentrated in the multiple effect evaporators 3 and then burned in the recovery boiler 4. Salts are re-dissolved in the smelt dissolver 5 and green liquor is clarified 6. CaO is added to the slaker 7 and further dissolved in the causticizers 8, where NaOH is regained. White liquor is clarified in 9 then feeds back to 1, while lime is regenerated through heating in the kiln 10.

Pulping releases lignin that is soluble in caustic BL, while the residual lignin still in the fibers will go through various stages of bleaching until the desired brightness is reached (Figure 2.15) [88, 106]. BL is concentrated by a series of evaporators (Figure 2.15) then fed to the recovery boiler, where it is burned and the pulping chemicals are regained. This step is the mass flow bottleneck of the Kraft-cycle considering the mass balance, 70 % of approximately 30 % (lignin cont.) of the starting biomass has to be burned in the most expensive and delicate equipment of the whole process. As a consequence most paper mills run below capacity to enable as much recovery as possible, and use the energy obtained from the burning of excess lignin [9, 10, 88, 107-113]. Alkali is consumed during pulping and the leftover is converted to carbonate in the recovery boiler, this and

other salts formed are re-dissolved resulting in green liquor (Figure 2.15, equation 1). The recovery of alkali proceeds as following:

$2NaOH + CO_2 \longrightarrow Na_2CO_3 + H_2O$ recovery furnace (1)

$CaO + H_2O \longrightarrow Ca(OH)_2$ slaker, causticizers (2)

$Na_2CO_3 + Ca(OH)_2 \longrightarrow 2NaOH + CaCO_3$ causticizers (3)

$CaCO_3 \longrightarrow CaO + CO_2$ lime kiln (4)

White liquor (Figure 2.15), containing NaOH and Na_2S, is subsequently re-fed into the digesters to minimize extra chemical needs ("make-up chemicals") [99]. Reactions of lignin with alkali and sulfide are detailed in the following section, as they determine the structure of Kraft lignin obtained from BL.

2.4.1.1 Kraft lignin

Lignin has to be burned to regain valuable pulping chemicals as mentioned in the previous section. However, there is a considerable effort in turning Kraft lignin into value added materials and fuels to further valorize the pulping process [1, 4, 5, 9, 10, 73]. Investigating promising lignin conversion into value added materials or chemicals (including fuels) starts with the evaluation of its structure that is determined by its biosynthesis (Section 2.3.3, Figure 2.9), environmental factors [2-4, 73] and reactions during Kraft pulping [88, 99, 105]. These latter reactions are governed by the alkaline pulping chemicals (OH^-, SH^-) attacking the lignin structure, followed by internal nucleophilic reactions from neighboring hydroxyls (Figure 2.16) [88, 105]. In case free hydroxyls (on side-chain) or free phenols are present, alkaline pulping chemicals can act as Bronsted bases initiating internal rearrangements that result in quinone methides and epoxides, which are in turn prone to external nucleophilic attack (Figure 2.16) [88, 105].

β-5 and β-O-4 structures (Figure 2.10) can undergo reverse aldol reaction during Kraft pulping, in case γ-OH is present, resulting stilbene and enol-ether (Figure 2.16) structures respectively, that are recalcitrant to pulping [88, 101, 105, 114]. These structures are in fact observed in Kraft lignin next to other recalcitrant linkages, namely: 4-O-5, 5-5 and β-β (pinoresinol), while highly abundant (>45 % SW, Table 2.11) native lignin linkages, e.g. β-O-4 will be degraded, as observed by multiple research groups [10, 96, 101, 102, 115], and quantified cumulatively (Aliphatic C-OR) in Table 2.14 [116].

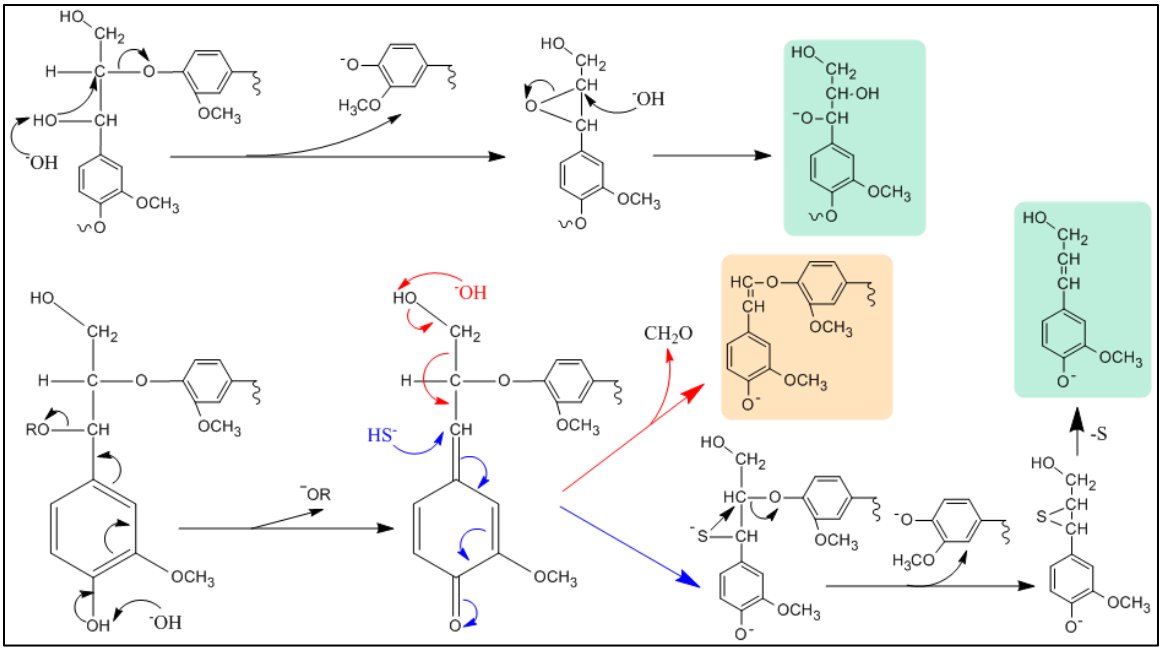

Figure 2.16. Kraft pulping reactions resulting in lignin breakdown and some recalcitrant enol-ethers (orange background)

Consequently, Kraft lignin contains, in general, much smaller amount of ether linkages than native lignin (Table 2.14), C-C linkages are more prevalent and has lower degree of polymerization (Table 2.11), while it will retains some sulfur (1-4 %) from NaSH, Na_2S pulping chemicals [10, 88, 96, 101, 102, 105]. Lignin structure, however, is highly dependent on source biomass and environmental conditions as well; consequently,

accentuated attention must be paid for detailed analysis when working with it. All lignin substrates must be analyzed by e.g. NMR for chemical structure and GPC for polymerization both before and after modifications (thermo-chemical or biological) to follow changes as closely as possible. NMR and GPC analysis are detailed in Chapter 3.

Table 2.14. Number of functional groups per 100 carbon atoms in spruce milled wood lignin (MWL) and in the residual and dissolved lignins after a Kraft cook (to kappa# 30.5)

Type of carbon	Native lignin (MWL)	Residual lignin	Dissolved lignin
Carbonyl	0.8	n.p.	0.3
Carboxyl	n.p.	2.1	1.5
Aromatic, olefinic	39.0	54	39.0
Aliphatic C-OR	23.6	9.5	10.1
Methoxyl	11.2	9.1	8.9
Aliphatic	4.9	10.4	16.0

2.4.1.2 CO_2 precipitated lignin

Decreasing the load on the recovery furnace by extracting some of the lignin from BL and selling it for converting into higher value materials should be a great opportunity. Precipitating Kraft lignin from BL requires low pH, however mineral acids are quite expensive and would require some kind of recycle in case another low value side-product is to be avoided. Carbon dioxide can also lower the pH efficiently by forming carbonate and "fixing" OH^-, according to equations below [112, 117], and at the same time this is a green solution [107-113, 117-125].

$$CO_2 + OH^- \longleftrightarrow HCO_3^- \quad (5)$$

$$CO_2 + H_2O \longleftrightarrow HCO_3^- + H^+ \quad (6)$$

$$HCO_3^- + OH^- \longleftrightarrow CO_3^{2-} + H_2O \quad (7)$$

$$CO_2 + 2OH^- \longleftrightarrow CO_3^{2-} + H_2O \quad (8)$$

Reaction (6) is normally negligible at pH>10 when determining the rate of absorption of CO_2. The rate of reaching CO_2: bicarbonate equilibrium (5) is relatively slow, while (7) occurs instantaneously. Consequently, the overall reaction can be summarized by equation (8) that lowers alkalinity and enables lignin precipitation, as the pH falls below 11-10, the pK_a of free phenolic groups [112, 117].

The CO_2 precipitation method was under intense research from the mid 1980's and detailed description of the process can be found in the literature [118, 124, 125]. It was later optimized and patented by Chalmers University and Innventia AB researchers as the "LignoBoost" process, and Figure 15 shows its flowchart [124, 125] connected to the Kraft cycle (Figure 2.17). CO_2 precipitated BL lignin has some advantages over H_2SO_4 precipitation –the two most appropriate precipitations for the Kraft cycle- namely, it doesn't disrupt the chemical balance by excess sulfur and the resulting lignin is easier to filter [120]. Optimal precipitation pH was first defined as 8.5 to minimize the CO_2 per unit lignin load [120], then this was further decreased to 7.7 for optimal filtration and lignin product properties [117]. Optimal BL solids contents were defined to be 27-35 % depending on wood species, 27-30 % for pine as an example, for precipitation conditions [117, 118].

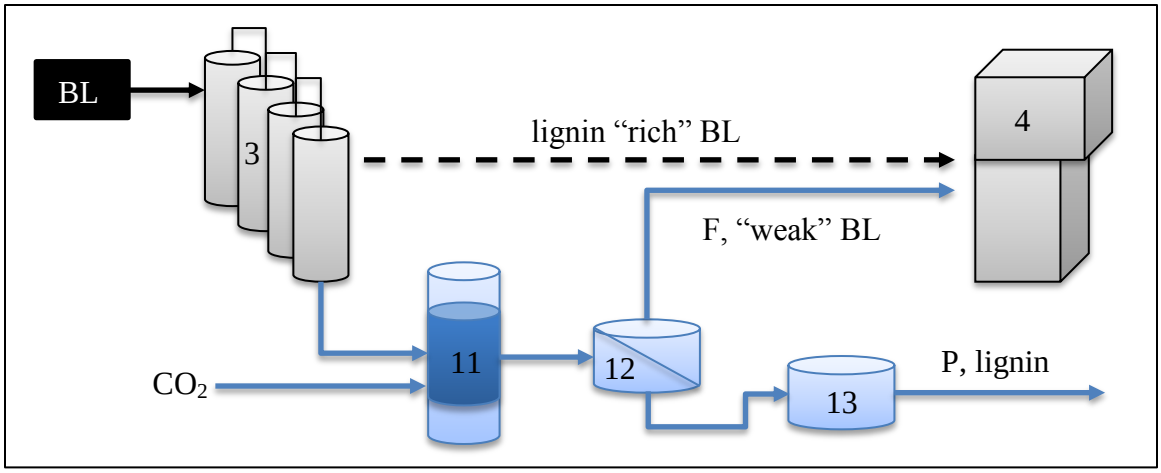

Figure 2.17. The separation of LignoBoost (CO_2 precipitated) lignin from BL, connected to the Kraft cycle. Instead of burning all concentrated BL it is precipitated by pressurized CO_2 in a pressure vessel: 11 then separated: 12 into a low lignin content filtrate: F, that is recycled to the recovery furnace (4); and a precipitate: P. Fraction P is further washed: 13 to obtain the final lignin product.

Sulfur (~3 %) and sodium (<0.5 %) contents of the exported lignin have to be minimal to avoid corrosion issues and to recover the maximal amount of valuable pulping chemicals, these issues are all taken into account in the final pH of precipitation, as well as boiling point elevation and viscosity decrease of the “weak” BL (LignoBoost filtrate) [107, 112, 117, 120-122, 124, 125]. The main issue however, was that the precipitated lignin had to be further purified, by washing, to obtain a pure product, and this step had a large energy demand, because of filter fouling [108, 120]. After multiple trials the best way to avoid fouling was to re-slurry the precipitate before washing in low pH (<3) sulfuric acid, and changing the wash water pH as well to below 3. This way large ion-strength and pH gradients are avoided during washing steps and lignin is kept physically suspended, instead of being partially dissolved, resulting in lower filtration resistance and easier filtration. Increased temperature can also enhance filtration by lowering viscosity 2-5 times as temperature increases from 20 to 80 °C [108-110, 112, 117, 123-125].

Some of the above optimization was done in pilot scale enabling feasibility calculations and even more efficient large scale trials [9, 10, 108-110, 112, 117, 121, 123, 124]. In one of the earliest calculations an ~8 % pulp increase in pulp production could be achieved due to the higher throughput through the recovery boiler, as well as complete replacement of all lime kiln fuel by recovered lignin. Furthermore 21 % of lignin was assumed to be sold as high value chemicals resulting in a four year investment return at industrial scale (700 average dry ton per day, ADt/d) [120]. In 2006 Olsson et al. concluded that electricity and lignin price ratio can be a good indicator of LignoBoost feasibility, they showed that if this ratio is below 1.9 then lignin separation was preferable. Between 1.9-2.3 enhanced energy production was approximately the same as if lignin was sold, while above 2.3 extra energy brought more profit in a techno-economic comparison of model mills [111]. The same year Wising et al. compared model mills to a reference mill concluding that optimally 37 % of all lignin should be exported and if lignin price is above 12 $/MWh (12 dollars per mega Watt hour produced, if lignin is burned), i.e. more expensive (valuable) than bark, than lignin export is profitable. They also concluded, that CO_2 price can be eliminated almost completely by using lime kiln flue gas (mainly CO_2), and so the profitability limit decreases to 9 $/MWh [113]. Another study in 2009 examined a 16 % pulp production increase in an existing Portuguese eucalyptus mill, where the authors compared the investment into a new higher capacity recovery boiler in comparison of the installment of the LignoBoost units. They came to the conclusion that unless electricity price goes above 80 Euros/MWh, and the exported lignin can reach 88 kg/ADt, lignin precipitation and export is preferable [119]. Finally, after decades of optimization and pilot plant operations the company Metso is now

developing and already marketing their industrial scale LignoBoost “units” that canbe seen on their website [126]. According to chemical structure it can be assumed that LignoBoost lignin will be the more hydrophobic part of lignin with possibly higher DP that precipitates as pH is decreasing. This work puts CO_2 precipitated lignin samples to compositional and pyrolysis tests in Chapter 4.

2.4.2 Lignin from biomass pretreatment

Consolidated bioprocessing (CBP) by definition makes cellulose degrading enzyme loads obsolete; however, until its full potential is reached, pretreatment of biomass before enzymatic hydrolysis is inevitable [2, 4, 30, 127-129]. The role of pretreatment in biomass to biofuel (e.g. ethanol) conversion is very important, because it decreases hemicellulose and lignin content leaving cellulose more accessible [30, 130-133]. During various pretreatments lignin separates from cellulose to different extents (depending on pretreatment method), similarly to pulping [30, 130, 132, 133]. The structure and DP of both residual and separated lignin will depend on the applied pretreatment, and although the primary goal of pretreatment is not a remarkably pure lignin product, ethanol organosolv pretreatment gives just that [30, 39, 115, 133, 134]. Accordingly, the following sections discuss pretreatments in general, however, a separate section is dedicated to ethanol organosolv pretreatment and the resulting lignin (EOL).

2.4.2.1 Pretreatments

Depending on the pretreatment parameters, several properties of biomass are altered including the resulting biomass constituents, cellulose crystallinity, lignin/hemicellulose structure, lignin-carbohydrate complexes, degree of polymerization,

fiber and pore size [30, 130, 133]. Each of these changes will impact the recalcitrance of pretreated biomass and need to be optimized. Optimization of key operational factors such as temperature, residence time and pH, enable good digestibility of the resulting polysaccharides; low sugar degradation; minimal generation of toxic by-products, and fermentation compatibility. Furthermore, key factors are also cost optimizing considerations including reasonable chip size, low operating temperatures/pressures, minimal use of chemical additives as well as efficient lignin recovery [30, 130]. As to be expected, these factors change according to pretreatment applied and substrate utilized.

The primary comparison method of pretreatments, especially steam explosion, is the severity factor (R_0) that describes the severity of the pretreatment as a function of time (t, min) and temperature (T, °C), equation 9 [130].

$$\log(R_0) = log\left[t \cdot exp\left(\frac{T-T_{REF}}{14.75}\right)\right] \qquad T_{REF} = 100\ °C \qquad (9)$$

Under acidic conditions combined severity can be also calculated, from (10) [130].

$$(CS) = \log(R_0) - pH \qquad (10)$$

Although severity is a good rough comparison between pretreatments the goal of increasing cellulose reactivity towards enzymatic depolymerization is not reached under similar severity conditions. Accordingly, pretreatment has to be evaluated from the substrates', optimal yield of sugars and energy efficiency point of views [30, 130, 133]. Briefly, all substrates will have preferred pretreatment methods, and the most efficient ones are summarized in Table 2.15 [30, 130, 133].

Table 2.15. Comparison of different pretreatment methods

Pretreatment type	Steam explosion	Dilute acid (DAP)	Ammonia fiber explosion (AFEX)	Organosolv (e.g. ethanol)
Advantages	Lignin transformation and hemicellulose solubilization, cost effective. Better yields in two stages.	High glucose yield, less formation of inhibitors and corrosion than concentrated acid.	Increase in accessible surface area, low formation of inhibitors.	Both lignin and hemicelluloses are degraded. Relatively pure lignin can be extracted.
Disadvantages	Generation of toxic compounds, partial hemicellulose degradation.	Generation of degradation products.	Not efficient for high lignin content feed-stocks, high cost of ammonia.	High cost, solvent needs to be drained and recycled. Difficult hemicellulose recovery.
Biomass	HW and agricultural residues. Not SW, low acetylation.	Favorable industrial application, wide range of biomass.	Agricultural residues and herbaceous crops, less effective on woody biomass.	Optimized for almost all woody biomasses.
Increase in accessible surface area	high	high	high	high
Cellulose decrystallization	-	-	high	none
Hemicellulose solubilization	high	high	medium	high
Lignin removal	medium	medium	high	high
Generation of toxic compounds	high	high	low	medium
Lignin structure alteration	high	high	high	high

Table 2.15 clearly shows why DAP and organosolv pretreatments are favorable in the case of SW, such as pine, is the feed-stock for bioethanol production. Furthermore, in this work the emphasis is on lignin conversion and organosolv pretreatment provides

relatively high purity lignin, that have been utilized already in adhesives and in biodegradable polymers [133]. Accordingly, the next section is dedicated to the ethanol organosolv process yielding a reactive cellulose, and lignin which is widely utilized.

2.4.2.1.1 Ethanol organosolv pretreatment, and lignin obtained

In general organosolv pretreatment has been shown to be successful with multiple solvents, e.g. methanol, ethanol, acetone or ethylene-glycol, however, it was optimized for pine pretreatment using ethanol [30, 39]. Accordingly, due to preference for pine in this work, the ethanol organosolv process was chosen to obtain ethanol organosolv lignin (EOL). In fact the exact conditions for the optimized pretreatment were identified earlier in the literature, namely 10 % solids (ODW) content, 65 % ethanol, 1.1 % sulfuric acid (based on wood), 170 °C and 1 h treatment time [39]. The reactor used in the mentioned publication was specialized, consequently, the lignin yields were as high as ~19 %, based on starting wood ODW [39]. The chemistry of ethanol organosolv treatment was studied in detail and Figure 2.18 shows the main reactions [135]. Acid catalyzed ether hydrolysis is one of the primary reactions that begins with the protonation of the ether itself, followed by its cleavage (and release of alcohol) and the formation of a benzyl carbocation, which is subsequently attacked by a nucleophile, like water, to form the other alcohol after proton “recovery” (Figure 2.18) [135]. Consequently, only a catalytic amount of acid is needed, furthermore, it is also noteworthy that although enol-ethers form (Figure 2.18) [101, 135] the acidic reaction conditions enable their cleavage (Figure 2.18) that was not possible in e.g. alkaline Kraft pulping (Figure 2.16) [101, 135].

NMR analysis of loblolly pine EOL showed that aromatic C-C bonds increase significantly, in case of C-5 carbon 5 times, while the number of aromatic C-H bonds all decrease (C-6, C-5 and C-2), suggesting a more substituted lignin than native lignin, as illustrated in Table 2.16 [115]. The same pine EOL also had a lower weight and number average molecular weight, by more than 50 %, compared to native lignin [115]. Further results on EOL analysis are detailed in Chapter 6 where it was used as a substrate for biological conversion.

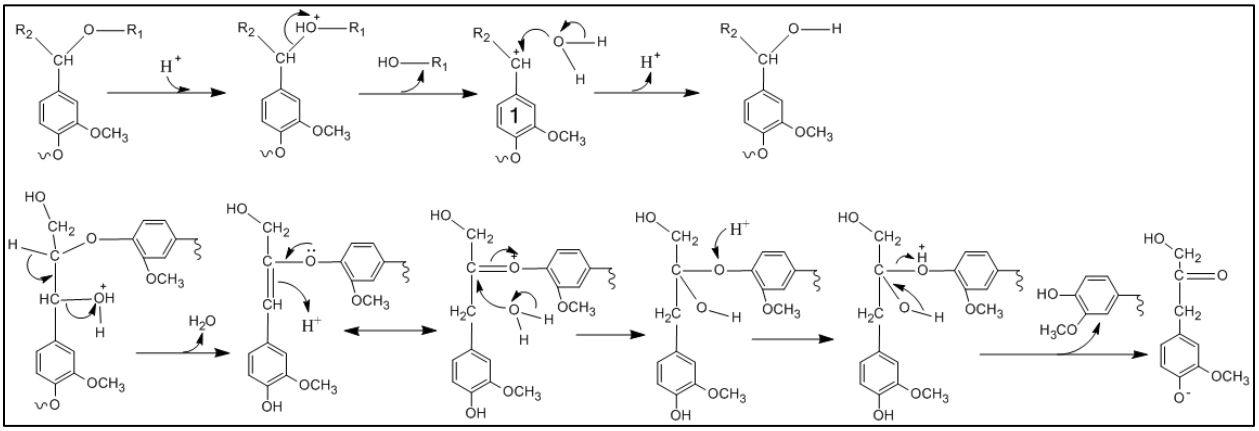

Figure 2.18. Ethanol organosolv pretreatment reactions including cleavage resulting benzyl carbocation (1) intermediate (top row); and cleavage initiated by α-OH protonation and proceeding through enol-ether intermediate (bottom row)

Table 2.16. Effect of ethanol organosolv pretreatment on loblolly pine lignin, followed by ^{13}C NMR

Functionality	Number of carbons/aromatic ring	
	Native lignin	EOL
Unconjugated COOH	n.p.	0.3
Conjugated COOH	n.p.	0.1
C-3, C-4 aromatic C-O	2.0	2.1
C-1, aromatic C-C	1.4	1.6
C-5, aromatic C-C	0.1	0.5
C-6, aromatic C-H	0.8	0.7
C-5, aromatic C-H	0.8	0.6
C-2, aromatic C-H	1.0	0.7
Aliphatic C-O, Cβ in β-O-4, Cα in β-5 and β-β	0.5	0.4
Aliphatic C-O, Cα in β-O-4	0.5	0.6
Aliphatic C-OR	0.2	0.3
Aliphatic C-O, Cγ in β-O-4	0.6	0.3
Methoxyl OCH_3	1.0	0.9
Cβ in β-β and β-5	0.2	0.1

2.4.3 Lignin analysis

As shown in previous sections lignin's structure depends on multiple conditions, such as environmental effects during growth and separation process [2, 3], concomitantly, before proceeding to the introduction of thermochemical conversion processes (Figure 2.3.a), lignin analytical techniques are briefly reviewed. Lignin analysis was "traditionally" used to follow pulp residual lignin contents; accordingly, these measurements were developed more, to exactly show total lignin contents in the fiber than to follow lignin structural changes [99, 100, 136]. Nevertheless, these early analytical methods fully separate –or at least apply specific reactants for- lignin from sugar polymers in the analyzed samples [99, 100, 136]. Kappa number for example measures the amount of potassium permanganate solution consumed by lignin in the pulp, resulting in a representative number describing the residual lignin amount [100, 136, 137]. Another method is the Klason lignin analysis that employs acid to hydrolyze

and solubilize all sugars which are separated from lignin by filtration [100, 136, 138]. This technique had been implemented in biomass research, it was further developed to involve acid insoluble (Klason, AISL), acid soluble (ASL) lignin and carbohydrate content determinations, and subsequently it was standardized by NREL [138]. The standard method is widely used in this work as well for example for the comparison of lignin contents before and after pretreatment or for residual sugar content measurements in purified lignin (Kraft, EOL etc.). To utilize this method correctly, first the biomass sample has to be extracted, in case of wood (pine in present work), with toluene: ethanol (2: 1) solvent mixture [115, 134, 138]. Then sugars are digested with a two-step (concentrated then dilute) H_2SO_4 treatment, and all solubilized sugars are filtered out, leaving Klason lignin behind. Sugars are analyzed by HPLC, while ASL is determined by UV-Vis spectrometry at 205 nm, according to the rearranged Beer's law (11) [138].

$$ASL\left[\frac{g}{l}\right] = \frac{A - A_{H_2O}}{\varepsilon \cdot l} \cdot D \qquad (11)$$

In equation (11) ASL is calculated in g/l and to obtain this value the absorbance at 205 nm is needed as well as the absorbance of background (usually distilled water). ε is the absorption coefficient of lignin [110 l/g·cm]; l is the optical path length through the sample [cm], while D is the dilution factor. ε = 110 is a median value for different woody resource lignin, standardized by TAPPI [100, 136, 138, 139]. The absorption wavelength was optimized to minimize hydroxymethyl furfural (HMF) and furfural signal overlaps with lignin [139], however, in this work the mentioned compounds are not present. This standardized lignin-sugar method (after extraction) accounts for all biomass components as shown in equation (12) and most importantly quantifies lignin vs. carbohydrate contents [138].

BIOMASS = Carbohydrates (HPLC) + Lignin (Klason, ASL) + Extractives (12)

This basic weight distribution analysis has to be accompanied by more sophisticated spectroscopic methods to get insight into lignin structural changes during treatments, as detailed in the following section.

2.4.3.1 Spectroscopic analysis of lignin

Fourier Transform Infra-Red (FT-IR) and Nuclear Magnetic Resonance (NMR) spectroscopic analyses are the most widely applied techniques for lignin structure evaluation in the literature, as well as Mass Spectrometry (MS), especially in connection with pyrolysis (Pyr-MS) [2, 9, 42, 100, 136]. MS and FT-IR are not applied in this work, however, their usefulness is proven by recent research on lignin structure [140-144]. NMR, on the other hand, is probably the most important tool in lignin analysis (not just in this study); it gives detailed information on the structure as a whole without degradation. This is important because during extraction from the cell wall matrix the structure of lignin is inevitably disrupted, consequently, further degradation has to be avoided as much as possible [100, 145-151]. There is a multitude of NMR techniques that were developed throughout the years for more and more detailed analysis (not just lignin); classification can be based on excited isotope (e.g. ^{13}C or ^{31}P); nature of sample, e.g. solution or solid-state, and single- or hetero-nuclear (multidimensional) resonance and so on [2, 100, 145, 149, 152]. The present work employed ^{1}H, ^{13}C, ^{31}P and HSQC (Heteronuclear Single Quantum Coherence) NMR measurements to gain detailed insights into lignin structural changes during pyrolysis and bioconversion with oleaginous

bacteria. Accordingly, the following sections concisely describe these NMR techniques with recent advances that were taken into account here.

2.4.3.1.1 Proton (^{1}H), Carbon (^{13}C) and (^{31}P) NMR

Proton NMR enables the differentiation between at least carboxylic, carbonyl, phenolic, aromatic and olefin/vinyl, methoxy and aliphatic functionalities [9, 10, 146-148, 151, 153-158]. The assignment regions change slightly, depending on source for example, such as various lignins (Kraft, EOL) or pyrolysis oils, as well as solven type, temperature applied and sample concentration used. Aliphatic protons show a rather good separation on the proton NMR spectra, however, by most papers their respective region is either ignored or only mentioned as one region [147, 148, 151, 153]. A noteworthy advancement of this field, is the recent (and not so recent) work on asphaltite, oil-shale pyrolysis and experimental model compounds reveal enough information on this region, that it can be subcategorized into 3 classes depending on their position from the aromatic ring (α, β, γ…) and saturation of the carbon moiety (CH, CH_2, CH_3) [9, 146, 155-158].

Carbon NMR has multiple advantages compared to proton NMR, including better resolution, and only a few disadvantages, such as reduced isotope sensitivity and extended time delays needed to obtain quantitative spectral data [146, 159]. The majority of these pros and cons are considered and constant improvement can be observed following the literature, most importantly in the area of enhancing carbon NMR quantification. Carbon NMR of Kraft lignin was reported as early as 1987, using DEPT (Distortionless Enhancement by Polarization Transfer) to separately evaluate CH, CH_2, CH_3 and –from their combination- quaternary spectra. These spectra were assigned to

functionalities resulting the ability to compare different Kraft lignins [160]. As more and more model compound work was done increasingly advanced chemical shift/structure tables for lignin were developed [146-148, 150, 151]. Lignin inter-unit linkages (Figure 2.10) have specific chemical shifts, almost all of them however, overlap with at least 1-2 others. To overcome this problem Capanema et al. developed a method, in which the same lignin sample was tested both in native and in acetylated state. The change in chemical shifts, due to acetylation, enabled to calculate the amounts of given inter-unit linkages –by differentiation between integrals- in comparison to all bonds present. An equation system was built to calculate and compare all linkages in good detail [145]. This latter technique combined with integration methods, widely used in the literature, proved to be one of the most efficient tools for lignin analysis, next to pyrolysis-MS for example [9, 10, 42, 115, 141, 143-151, 153, 158, 160-167].

Phosphorous NMR is an excellent tool to analyze the hydroxyl functionalities in lignin quantitatively, through derivatization with ^{31}P containing TMDP (2-chloro-4,4,5,5-tetramethyl-1,3,2-dioxaphospholane), also known as phosphitylation, as shown on Figure 2.19 [9, 10, 42, 46, 115, 152, 154, 168-172]. Quantitative analysis of phosphitylated lignin by ^{31}P NMR yields a limited number of signals, such as aliphatic, phenolic and acidic hydroxyls in general. However, model compound work, made it possible to assign multiple sub-regions in the phenolic region [9, 46, 169, 170, 173]. As another advancement of the field, the internal standard (IS) used for these experiments was initially cyclohexanol but has now been changed to N-hydroxy-5-norbornene-2,3-dicarboximide (NHND), because the cyclohexanol was overlapping with aliphatic-OH signals [9, 46, 152, 172].

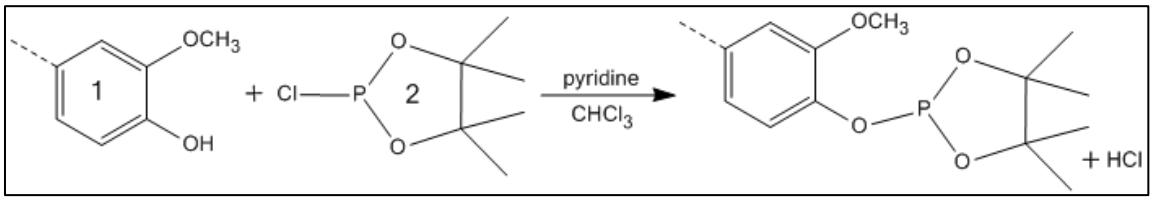

Figure 2.19. Phosphitylation of lignin-phenolic hydroxyls (1) with TMDP (2)

2.4.3.1.2 HSQC NMR

Lignin analysis using multidimensional NMR techniques such as Heteronuclear Single Quantum Coherence (HSQC) have a significant advantage allowing the resolution of otherwise overlapping resonances in either ^{1}H or ^{13}C spectra axis. In HSQC, two polarization transfer delay periods are used to transfer magnetization between ^{1}H and ^{13}C nuclei, and the spectrum is obtained with the optimized $^{1}J_{CH}$-coupling of 145 Hz [174]. As a result the spectrum gives information about the correlation between ^{1}H and ^{13}C atoms via one bond coupling (directly bonded carbons and hydrogens) [96, 101, 174]. This 2D technique enables the separation of signals heavily overlapped in 1D spectra, that is due to the complex structure of lignin [96, 101, 102, 174]. Signal intensity errors arise however from multiple sources when applying this technique, namely: coupling constant deviations, effects of resonance offset, ^{1}H T_1 relaxation effects, proton and carbon nuclei T_2 relaxation effects and proton homonuclear coupling effects. T_1 differences can be suppressed by setting the relaxation delay to at least 5 times the longest T_1 [175] that is practiced in present work. Cross signal intensity (HSQC peaks) depends on $^{1}J_{CH}$ value and T_2 relaxation, values that will be "distance" (Hz, ppm) dependent from the pulse frequency [142]. In accordance, only relative signal intensities can only be compared within given regions, such as aromatic, lignin inter-unit linkage

and aliphatic, that contain peaks corresponding to chemically analogous C-H pairs, with similar $^{1}J_{CH}$ values [142]. Although even this criterion is fulfilled in all recent research, evaluation of HSQC spectra is only semi-quantitative, due to all the effects described. Concisely, HSQC is a high resolution tool for analyzing lignin, showing functionalities and inter-unit linkages well separated, compared to overlapping 1D spectrum, however, it is only semi-quantitative [96, 101, 102, 142, 145, 174-176]. Whole biomass itself is more frequently being characterized by HSQC [177, 178], along with milled wood (MWL) and other extracted lignin samples [95, 140-145, 162, 165, 174, 176, 178-180]. Examples include Kraft and technical lignin [96, 101, 102], EOL [162, 180], sugars [177], lignin carbohydrate complexes (LCC) [93, 94], pyrolysis oil [48] and even extractives [181-186].

After briefly reviewing the analytical tools whole biomass and lignin thermochemical conversions can now be introduced.

2.4.4 Thermochemical conversion of biomass (including lignin) to biofuels

2.4.4.1 Thermochemical conversion techniques, biomass pyrolysis

Section 2.2.1 briefly mentioned pyrolysis as one of the most promising current thermochemical conversion methods to valorize residual lignin streams. The elemental composition of lignin, cellulose and hemicelluloses show that a key conversion issue is efficient depolymerization and deoxgenation of these biopolymers yielding a liquid fuel with a lower oxygen content resulting in higher heating values, hence, better fuel quality properties [3]. Thermochemical conversions, such as gasification and pyrolysis, address this issue by applying heat and pressure to varying degrees. Gasification applies

significantly higher temperatures (875-1275 K, [187]) and produces a syngas (i.e., CO, CO_2, H_2, CH_4 etc.) that can be catalytically converted into an array of fuels including methanol, dimethyl ether, ethanol, and short chain alkanes [188].

Compared to gasification, pyrolysis generates a wide array of products, possibly in the hundreds; containing aromatic compounds (e.g. catechols, phenols, etc) as well as low molecular weight acids, ethers, and alcohols. The latter route requires less capital investment than gasification and is attracting the interest of researchers and industry worldwide [50]. Pyrolysis reactors use inert atmosphere and yield approximately >50 % bio-oil along with a char, with reactor temperatures varying typically from 673 – 873 K. The latter product is frequently viewed as a thermal resource for pyrolysis and as a possible resource for bio-char in land reclamation efforts. Bio-oils traditionally suffer from high viscosity values and oxygen content, lower heating values, corrosiveness and a tendency to polymerize and age during storage. Practical fuel applications of pyrolysis oils necessitate that these unfavorable properties be removed prior to their utilization as a green diesel or gasoline equivalent. Traditionally this is done by hydrogenation, however, recent research is pursuing catalytic systems that can either improve the products from pyrolysis and/or can be used downstream for refining bio-oils [50, 189].

To have good char: liquid: gas ratio, temperature, heating rate and residence time have to be optimized [50, 188, 190-192]. The changes occurring in whole biomass during pyrolysis are briefly reviewed As temperature increases between 395-475 K pre-pyrolysis reactions occur such as moisture loss, hemicellulose breakdown, as well as free radicals appear, CO and CO_2 form together with carbonyl and carboxyl groups. Subsequently, the second stage of solid decomposition, also called main pyrolysis, proceed fast due to

exothermic reactions, causing woody biomass temperature to rise from 525 to 625 K, resulting in the formation of pyrolysis products: bio-oil and char. In the third step the char slowly decomposes forming carbon rich solids, and gas [190, 191]. Beyond 700 °C secondary pyrolysis reactions occur as well, increasing char and gas quantities, due to heterogeneous (multi-phase) autocatalytic reactions between char and gas. These reactions are more prominent in whole woody biomass, where pyrolytically exothermic cellulose is overrepresented compared to endothermic lignin [190, 191, 193]. Hemicellulose and cellulose decompose over a very narrow temperature range compared to lignin, as shown in Table 2.17, with increasing decomposition temperatures [190, 191, 193].

Table 2.17. Decomposition temperature ranges for biomass components during pyrolysis

Wood component	Decomposition T range [K]
Hemicellulose	470-530
Cellulose	510-620
Lignin	550-770

Hemicelluloses have a lower softening point and higher moisture content compared to lignin, and they react more readily during heating then cellulose, due to xylan being the least thermally stable component. Xylan degradation yields eight main products: water, methanol, formic, propionic and acetic acids, hydroxy-1-proanone, hydroxy-1-butanone and 2-furfulaldehyde [191]. Where water and furfural are formed by dehydration, acetic acid comes from the elimination of acetyl groups, while formic acid and methanol form from the carboxylic and methoxyl groups of uronic acids present [191]. Cellulose pyrolysis proceeds through the mechanism described by the Broid-

Shafizadeh model, as shown on Figure 2.20. Destructive reactions start below 325 K causing a significant drop in DP, followed by gradual decomposition and charring in parallel with rapid volatilization accompanied by levoglucosan formation [191]. Table 2.18 summarizes cellulose pyrolysis reactions at different temperature ranges [191, 192, 194], while Figure 2.21 is showing levoglucosan and hydroxymethyl-furfural (HMF) formation through radical intermediates according to the latest research [195, 196]. Further degradation of levoglucosan, furfurals and other intermediate pyrolysis products is intensely researched [195-201], however it is not detailed here.

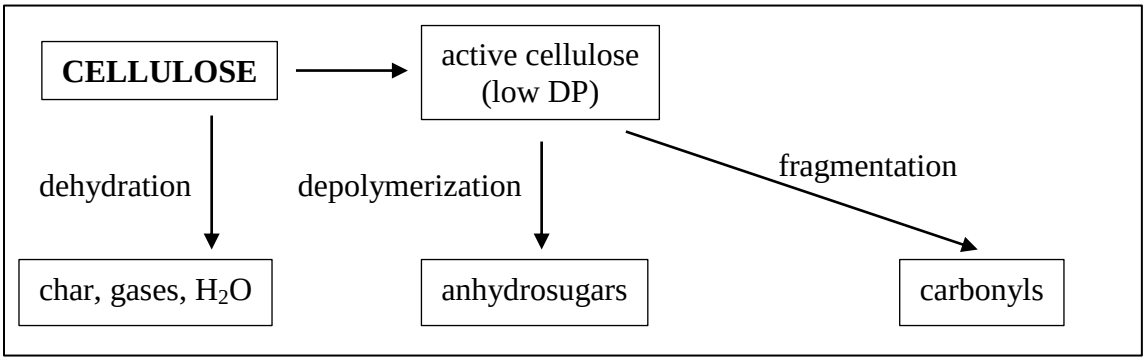

Figure 2.20. The main cellulose pyrolysis degradation routes, as described by the Broid-Shafizadeh model

Table 2.18. Reactions of cellulose at different temperatures during pyrolysis

Condition	Process	Products
Below 575 K	Free radical formation, elimination of water, depolymerization	Carbonyl, carboxyl, CO, CO_2, char
575-725 K	Breaking of glycosidic linkages of polysaccharide by substitution	Tar fraction: levoglucosan, anhydrides, oligosaccharides
>725 K	Dehydration, rearrangement and fission of sugar units	Carbonyls, like acetaldehyde
>775 K	All above processes	Mixture of above cpds.
Condensation	Cleavage and condensation of unsaturated products, char formation	Highly active char, with trapped free radicals

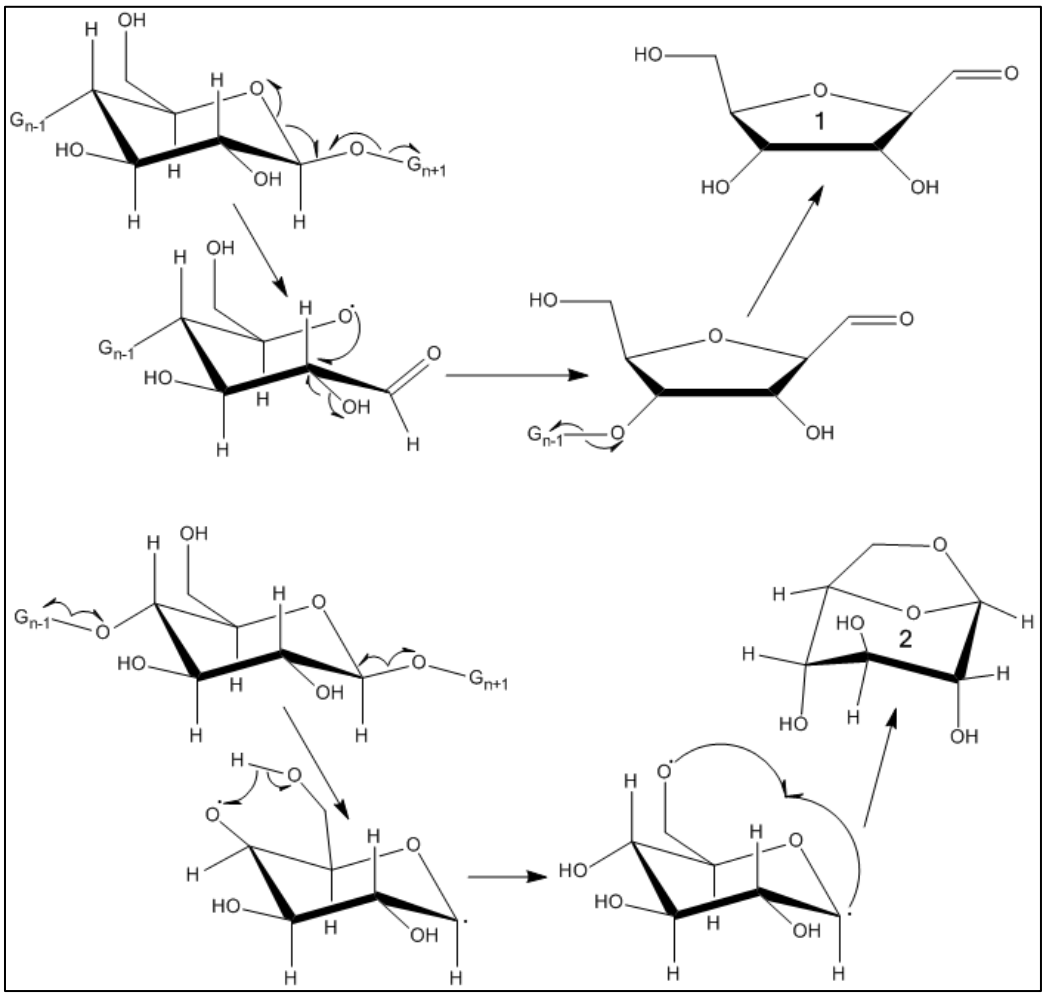

Figure 2.21. Formation of carbonyls (e.g. aldehyde), like hydroxymethyl furfural (HMF, 1); and anhydrosugars, like levoglucosan (2) through radical intermediates, during pyrolysis.

Whole biomass pyrolysis results in a bio-oil, with yields between 20-70 % of total pyrolysis products, that contains mostly anhydrosugars, short chain (1-3 carbon backbone) aldehydes, acids and alcohols (~70-80 %), with some furfurals, lignin degradation products (cathhecols, guaiacols etc.) and other compounds (~20-30 %) [50, 192]. The three main disadvantages of whole biomass bio-oils compared to diesel, is their significantly higher (20-30 % compared to <1 %) water content, viscosity (25-30 times)

and acidity (pH 2.5-3 compared to neutral), not mentioning the aging issues such as viscosity increase, phase separation and gum deposition [50, 192].

2.4.4.2 Lignin Pyrolysis

The rough formulae of biomass components can be written as $CH_{1.67}O_{0.83}$, $CH_{1.64}O_{0.78}$ and $CH_{1.1}O_{0.35}$, for cellulose, hemicellulose and lignin respectively [194]. Consequently, pyrolysis of lignin should result in products with lower oxygen content, giving it superior properties compared to whole biomass. First dehydration reactions occur around 473 K, while also, between 423-573 K cleavages of α- and β-aryl-alkyl ether linkages happen. At approximately 570 K aliphatic side-chains start splitting off from the aromatic ring, and subsequently at temperatures between 643 and 673 K carbon-carbon inter-unit linkages break [191]. The rate of heating for lignin pyrolysis has multiple effects defining the ratio of final product phases as well as their chemical composition; accordingly, optimal conditions have been intensely studied [42, 202]. Pyrolysis-GC-MS and NMR studies were conducted to analyze the chemical structure and composition of lignin based pyrolysis oils [9, 42, 48, 153, 163, 164, 202, 203]. These studies have shown that lignin based pyrolysis oils are mainly consist of substituted phenols, with guaiacol, cathecols and xylols as most abundant compounds, as shown on Figure 2.4 in Section 2.2.1 [50]. The reactions occurring during lignin pyrolysis have been studied sporadically over the last three decades by various research groups using model compounds or lignin itself [9, 42, 163, 164, 204-216]. Research studies have used α-O-4, β-O-4, β-1, β-5 and 5-5 model compounds, containing these linkages with different substitutions, such as hydroxyl, alkyl or methoxyl, and as a result, some

pyrolytic pathways were predicted [9, 42, 163, 164, 204-206, 209-212, 214, 216]. These pathways are supported by the results of product analysis, and the most abundant reaction types are shown on Figures 2.22 and 2.23 [9, 42, 163, 164, 204-206, 209-212, 214, 216], showing cleavages, rearrangements and condensations. It has also been revealed that during pyrolysis, when free phenolic and α-OH are present, quinone methide formation will precede radical formation [209-212, 216]. Furthermore, highly stable aromatic enol-ether units, that form during pyrolysis will cleave into keto- and guaiacol related compounds, due to the external energy provided [191]. Conversely, β-5 linkages can form an even more stable conjugated bond between aromatics that can withstand pyrolysis [214] as well as 5-5 bonds, that are also recalcitrant at pyrolysis conditions [209]. Finally, as a result of pyrolysis, lignin weight average molar mass usually decreases to 1-300 g/mol as measured by GPC giving a highly viscous (Table 2.3), water immiscible dark oil [9, 42, 50, 164, 194].

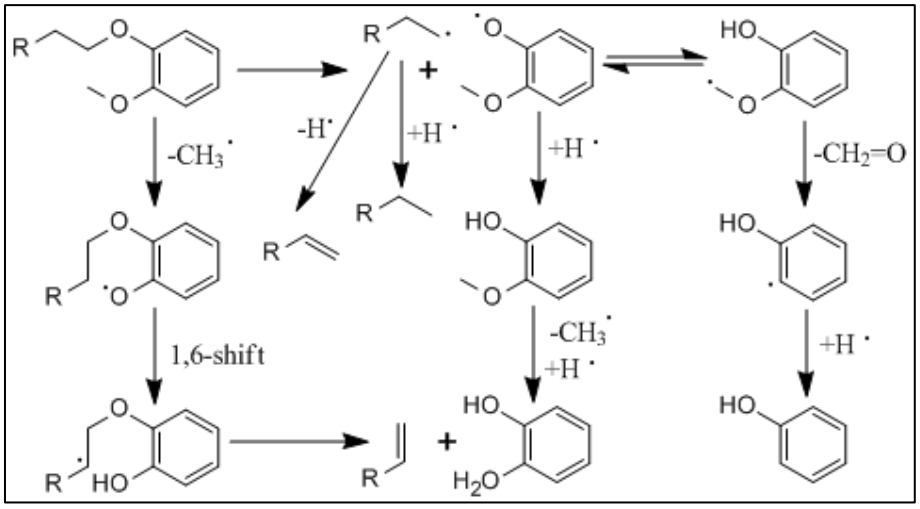

Figure 2.22. The proposed ether degradation pathways in lignin, during pyrolysis; predictions are based on model compound work

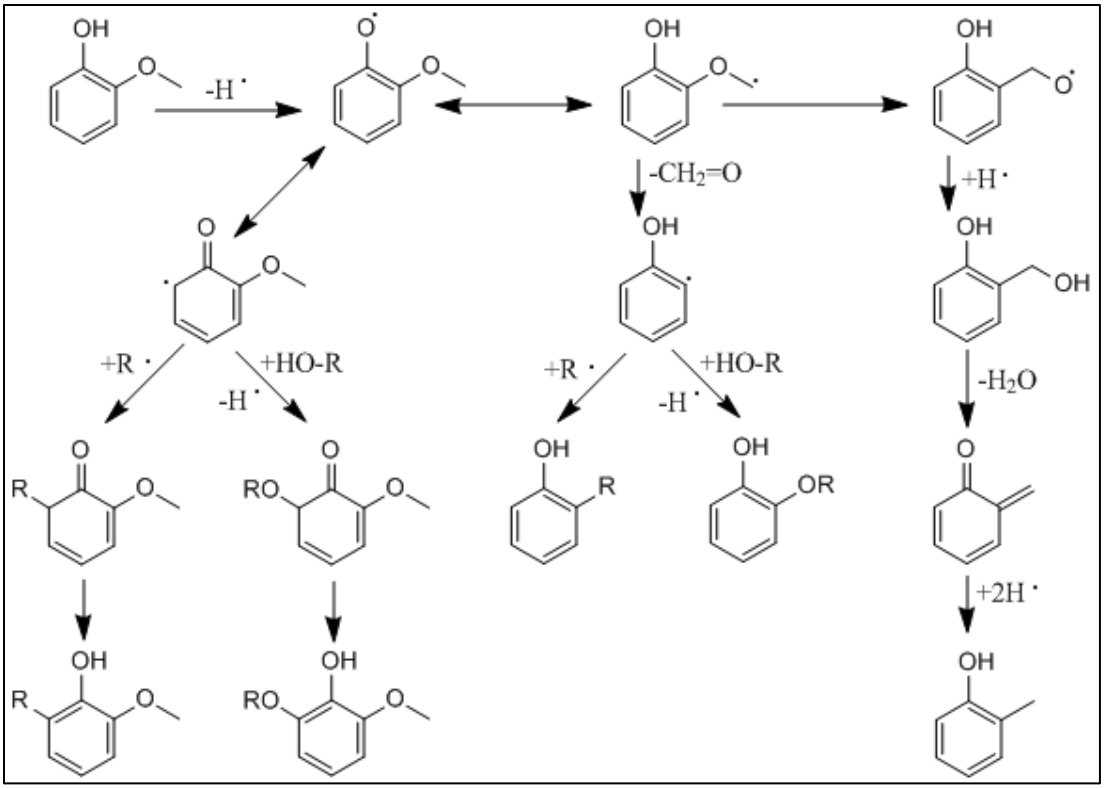

Figure 2.23. The reformation of C-O and C-C bonds during lignin pyrolysis

In summary, pyrolysis converts lignin directly to pyrolysis oil that can serve as a liquid biofuel. While another, theoretically possible conversion route, is the multistep bioconversion of lignin through fermentation with oleaginous microbes, as shown on Figure 2.3.b. This multistep process first aims to generate lipids, while utilizing only lignin as carbon and energy source, that can be further transesterified into biodiesel.

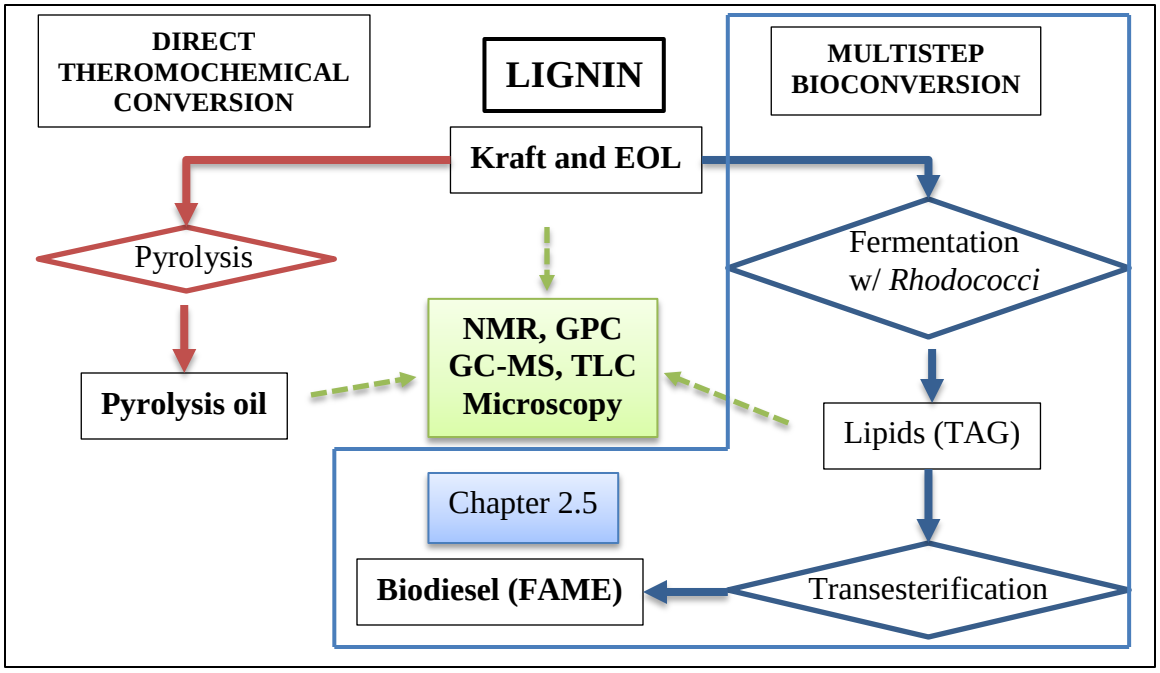

Figure 2.3.b. The introduction of bacterial lignin degradation and lipid accumulation pathway(s)

2.5 Lignin bioconversion

Until recently, lignin bioconversion was almost completely restricted to fungal degradation, using mostly white-rot fungi derived enzymes, like laccase, to biologically pulp or bleach biomass while liberating cellulose [15, 217, 218]. The abundance of lignin however, generated interest in revisiting bacterial lignin degraders and their "product profile" with hopes that these microorganisms can possibly yield a commercially relevant process, lacking the practical challenges faced by fungi [15, 63, 219-222]. Bacterial species are indeed capable of aerobic digestion of lignin resembling aromatic compounds, through the β-ketoadipate, and similar intra- and extra-diol pathways [11, 12, 63, 219-222]. Coincidentally, some of these bacteria belong to the actinomycetes [11, 12, 15, 63, 219] group that has also been shown to accumulate lipids. The Gram positive species of

soil dwelling *Rhodococcus* is of particular interest, because of its high lipid build-up capacity [13]. Recently, a few authors have reviewed the current knowledge on bacterial lignin degradation enzymes, their genetic background and control [219, 222], concluding that fungal pathways are superior in lignin degradation efficiency, however, some bacteria have all the tools for complete lignin degradation. Enzymes involved in the process were analyzed kinetically, as well as amino acid sequences were uploaded into bioinformatics databases and comparison showed that actinomycetes do contain lignin and aromatic compound degrading enzymes [219, 222]. Connecting the traits of lignin degradation to oleagenecity was the primary target of this work.

Bacterial lignin degradation proceeds in three major steps, according to our knowledge in this area (Figure 2.24). First lignin is de-polymerized via prokaryotic lignin active enzymes, like laccases, lignin- and manganese-peroxidases and others into monomeric and oligomeric aromatic units [219, 222]. The second step begins with a myriad of different compounds that are funneled into aromatic ortho-diols or a para-diol with a carboxylic acid neighboring one of the hydroxyls. Resulting compounds resembling protocatechuic acid (PCA), catechol (CAT) and gentisate (GTA) are further processed in the third step of lignin degradation using ring cleaving (intra- and etra-diol) dioxygenases leading to tricarboxylic acid (TCA) cycle intermediates, such as succinyl- and acetyl-CoA [11, 219, 222]. These intermediates can later undergo anabolic processes such as fatty acid, then lipid synthesis [15, 63]. Accordingly, the following, most important steps of lignin to lipid bioconversion are (Figure 2.24):

1. De-polymerization of lignin: degradation to decrease DP and molecular weight to oligomeric and preferably monomeric units

2. Funneling: pathways that convert a multitude of different oligomers and monomers into the three main substrates of aerobic, aromatic compound degrading routes, namely: protocatechuate, cathecol and gentisate
3. Conversion of these substrates into tricarboxylic acid (TCA) cycle intermediates, through e.g. the β-ketoadipate pathway
4. Anabolic processes starting with Ac-CoA and resulting in "value-added" products, such as lipids
5. Lipid transesterification to biodiesel (Figure 2.5) is the last step, however, it is done posterior to bioconversion, separately. Although, it is noteworthy that direct biodiesel biosynthesis has been successfully conducted [223, 224].

Section 2.5 of this chapter summarizes the knowledge accumulated, mostly recently, on the above 5 steps in bacterial hosts.

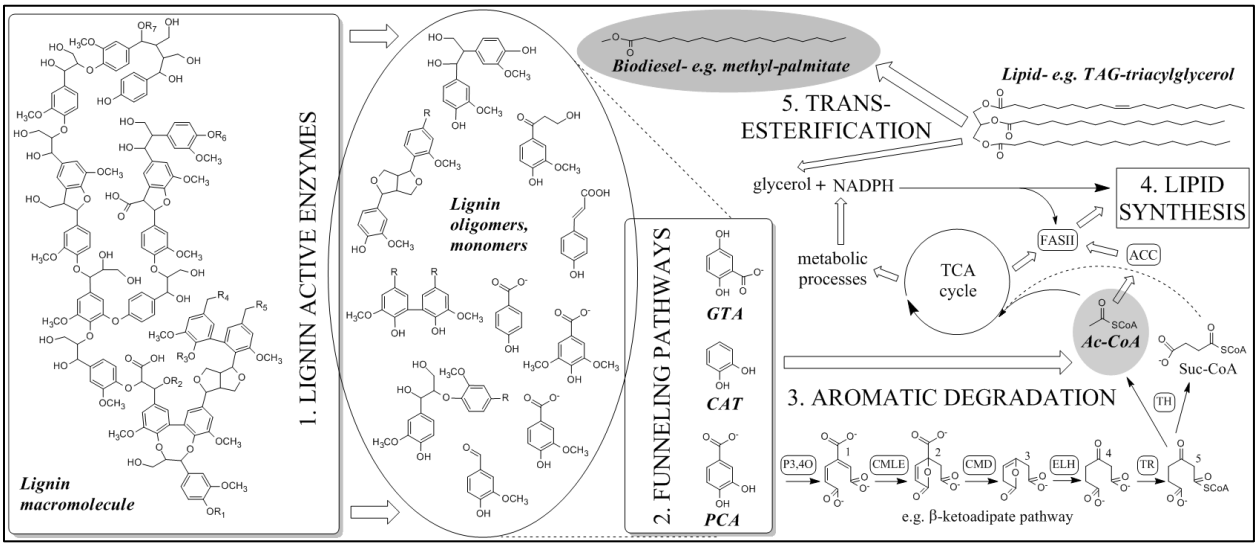

Figure 2.24. Proposed bacterial lignin degradation connected with lipid synthesis. From left to right; first lignin active enzymes (degradation is not necessarily primary function) break up the macromolecule into fragments; then, in the second step, these fragments are funneled into archetypal dioxygenase substrates for the cleavage of aromatic rings. Dioxygenases have a strong preference for specific ring hydroxylation and carboxylation, however, as proven in the literature, they can degrade aromatic dimers as

well as monomers in the third step. Previous results showed that *R. opacus* strains digest lignin model compounds, such as vanillic (VanA) and 4-hydroxybenzoic (4-HBA) acids, through protocatechuate (PCA) and the β-ketoadipate pathway (lower right side) into succinyl- (Suc-CoA) and acetyl-CoA (Ac-CoA). Latter (and maybe both) compound is the starting material for the fourth step, namely lipid anabolism and the resulting oils can be transesterified into biodiesel in step five (upper right side).
Enzymes in rounded rectangles are: P3,4O, protocatechuate 3,4-dioxygenase; CMLE, β-carboxy-*cis*-*cis*-muconate lactonizing enzyme; CMD, γ-carboxymuconolactone decarboxylase, ELH, enol-lactone hydrolase; TR, β-ketoadipate:succinyl-CoA transferase; TH, β-ketoadipyl-CoA thiolase; ACC, acetyl-CoA carboxylase and FASII, bacterial fatty acid synthase. While numbered compounds are: (1) β-carboxymuconate; (2) γ-carboxymuconolactone; (3) β-ketoadipate enol-lactone; (4) β-ketoadipyl-CoA; (5) β-ketoadipate [15, 219].

2.5.1 Aerobic lignin degradation pathways

The title emphasizes "aerobic", because although anaerobic conversion is possible, through the "biological" Birch reduction, resulting in low oxidation level products, its efficiency is too low to consider any application [221]. The aerobic pathways on the other hand seem feasible as long as 1. sufficient number of funneling routes are present to provide specific substrates for aromatic ring opening. 2. Lignin metabolic intermediates can be converted into valuable products, such as lipids.

Lignin degradation, as shown on Fig. 2.24, is initiated by "lignin active enzymes", like lignin peroxidase (LiP), manganese peroxidase (MnP) or laccase, that are not mentioned as lignin degraders on purpose. Fungi and bacteria use a wide variety of enzymes to utilize lignin that usually oxidize the phenolic groups of the macromolecule into different radicals (e.g. phenoxy) [219-222, 225-228]. These radicals are highly instable intermediates that are predestined for intra- or intermolecular rearrangements and radical couplings to reach stability. Depending on microorganism species and enzyme(s)

used, the strategies of oxidation will differ. The main examples in fungi are subject of intense research, like laccases [225, 229-232], manganese- [227], lignin- and versatile-peroxidases [226] as well as some other enzymes [228]. On the other hand, bacterial lignin active enzymes only gained attention recently due to the lack of significant breakthroughs in industrial applicability of fungal enzymes [63, 219, 220, 222]. Most importantly though, independently of origin, lignin active enzymes don't only degrade lignin they can polymerize it as well. Accordingly, lignin breakdown will be a stochastic process with kinetic rates depending on lignin and enzyme sources, as well as on the consumption of the product low molecular weight lignin oligomers and monomers [219].

2.5.2 Bacterial lignin depolymerization including oligomer and monomer funneling pathways to archetypal aromatic degradation substrates

Fungal degradation pathways, utilize high redox potential coenzymes (like heme) resulting in 10-100 times higher degradation rate compared to the best bacterial degraders [233]. This lower efficiency in bacteria support the theory that bacteria only mineralize lignin oligomers and monomers "leftover" by fungal degraders [222]. Recently though, more evidence have been found that bacteria have unique enzymes that are specialized for lignin depolymerization, in species like *Streptomyces*, *Rhodococcus*, *Nocardia*, *Sphingomonas*, *Pseudomonas* and *Thermobifida* [219]. Most of these enzymes proved to be extracellular peroxidases, in some cases peroxide depedent, however, it seems that all lignin degraders come from the same few classes, namely actinomycetes, α- and γ-proteobacteria [219]. Bugg and colleagues have recently developed two novel techniques for the evaluation of bacterial lignin degrading enzymes and discovered a dyp-type peroxidase in *R. jostii* RHA1, from the class of actinobacteria [219, 220, 233, 234].

Furthermore, this same research group has analyzed the newly discovered enzyme's product spectra based on a β-O-4 lignin model compound as feed-stock. They concluded that DypB, produced by *R. Jostii* RHA1, is an iron dependent dyp-type peroxidase that is further enhanced by the presence of manganese. Guaiacol and vanillin were the main products, based on a phenolic-β-O-4 substrate dimer, that supports an α–β cleaving route as shown on Figure 2.25 [219, 233, 234].

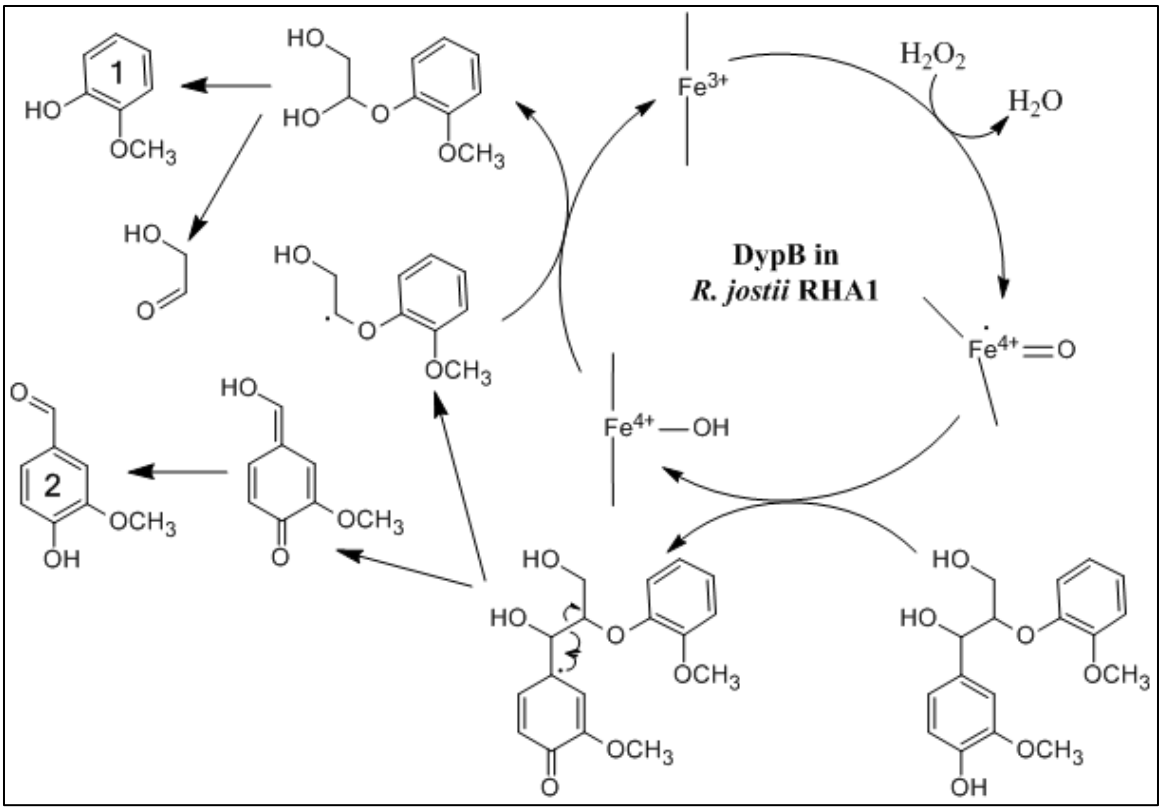

Figure 2.25. Degradation of a lignin model dimer by DypB enzyme from *R. jostii* RHA1, as hypothesized from the detected cleavage products: guaiacol (1) and vanillin (2) [234]

Both fungal and bacterial lignin active enzymes had been shown to catalyze polymerization and depolymerization simultaneously, resulting in an equilibrium product spectra [219, 221, 222, 226, 228]. Consequently, to push these reactions towards depolymerization, lignin oligomers and monomers have to be withdrawn from the system

by uptake and digestion. Bacterial breakdown of these different depolymerization products have drawn considerable attention recently. As a consequence some genetic mapping, as well as theoretical and model compound enzymatic metabolism results has become available. These catabolic routes converge –"funnel"- into archetypal aromatic degradation starting compounds, such as CAT, PCA and GTA (Figure 2.24) that are further degraded into TCA cycle intermediates as detailed in the next section [219, 221, 222, 226, 228].

Depolymerized lignin is further degraded by bacteria, however, it has only been studied in a very few cases, consequently, all pathways reported herein are deduced from breakdown results overwhelmingly obtained from *Sphingomonas paucimobilis* SYK-6, *Rhodococcus jostii* RHA1 and some other *Pseudomonas*, *Acinetobacter* and *Streptomyces* studies [219, 221, 222]. Moreover, in some cases fungal breakdown is mentioned, for two reasons; one, there can be similar, yet undefined, enzymes in bacteria based on recently identified product profile and phylogenetic research [219, 221, 222]; and two, although the initial enzyme mechanism may be completely different, in case the intermediates are radicals, the outcome of the cleavage can be similar, due to radical stabilization on the same atoms (e.g. $C_{1,3,5}$ in aromatic ring and C_{β} [105, 106]).

2.5.2.1 β-aryl ether degradation

β-aryl ethers are the most abundant linkages in lignin (Table 2.10) and breakdown studies usually start with them [219, 222]. In *S. paucimobilis* SYK-6 the α-hydroxyl is first oxidized to a ketone catalyzed by a NAD-dependent dehydrogenase LigD, Figure 2.26. Subsequently, LigEFG β-etherase (glutathione S-transferases: GST) enzymes utilize glutathione in a reductive ether cleavage to gain an α-keto-phenylpropanoid, that

has been shown as a breakdown product in case other bacteria, such as *Pseudomonas putida* or *R. jostii* RHA1, were used (Figure2.26). The most abundant final products are vanillic acid and acetovanillone that are hypothetically obtained via β-oxidation (analogous to fatty acid break down) and decarboxylation (CO_2 release), from the α-keto-phenylpropanoid, respectively (Figure 2.26) [219, 222, 233].

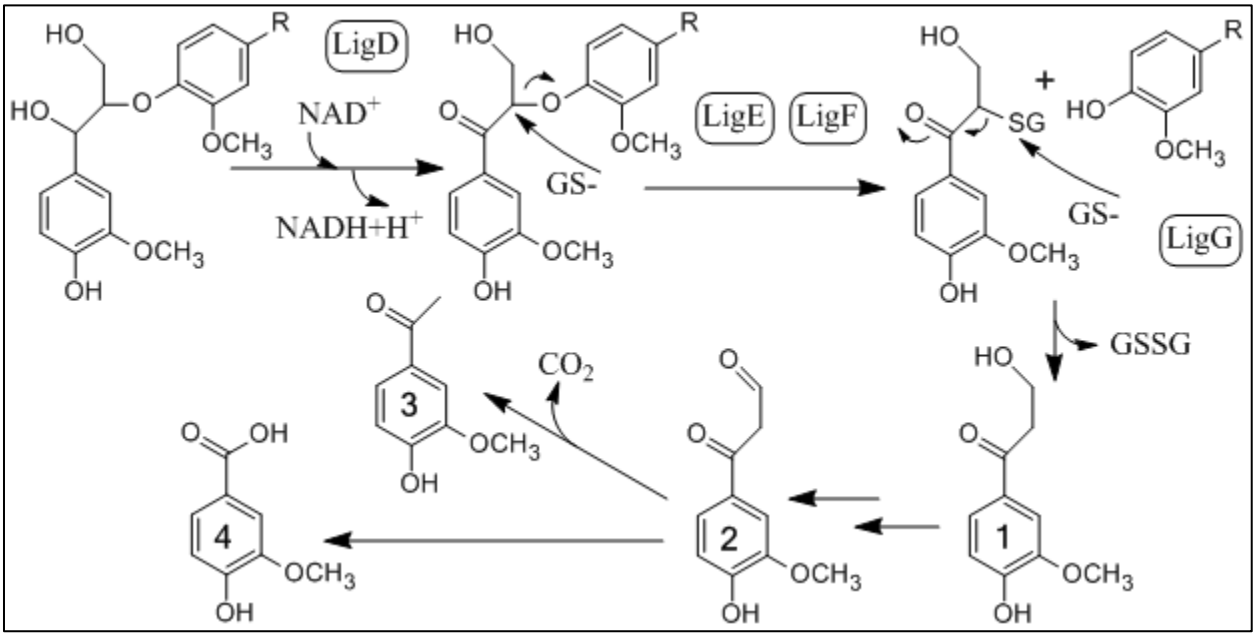

Figure 2.26. β-O-4 reductive cleavage in bacteria, including glutathione (GS), with α-keto-phenylpropanoid (1) intermediate. 1 is further degraded, through most likely a β-oxidation (2), to either vanillic acid (4) or through decarboxylation to acetovanillone (3) [219, 222]

The above reductive mechanism is unusual for two reasons, one, lignin is usually degraded oxidatively, as has been shown in fungi, and two, it does not proceed through radical intermediates [219, 222]. This defines the final products and eliminates the chance of re-polymerization, unlike radical mechanism. The final products are (Figure 2.26) vanillic and syringic acids (latter if HW lignin is used) that are only a "demethylation" step away from being aromatic ring cleavage substrates for dioxygenases [222].

2.5.2.2 Demethylation

Vanillate and syringate O-demethylation proceeds through multiple pathways as found in different species, resulting protocatechuic acid (PCA) and 3-O-methylgallate (3MGA) respectively. The two major aerobic, aromatic demethylase systems follow different mechanisms [219, 222]. One, called vanillate demethylase is composed of two parts VanA and VanB, catalyzing oxidation and reduction cooperatively; while the other one specific to *S. paucimobilis* SYK-6 is a tetrahydrofolate dependent aromatic O-demethylase [219, 222]. This latter system is usually found in anaerobic microorganisms, consequently the only similarity is the use of tetrahydrofolate as a methyl-receiver molecule, as well as oxidizing platform to release formic acid while recovering the reduced coenzyme (Figure 2.27) [222]. Vanillate is transformed to PCA by LigM and DesZ enzymes in SYK-6, while syringate can only be modified by DesZ to 3MGA, however, 3MGA to gallate demethylation will be catalyzed by LigM, while in all cases the methyl group is transferred to H_4folate (Figure 2.27) [222]. The conenzyme is subsequently reduced via 5,10-methylene-H_4folate reductase (MetF) then converted to the aldehyde form, and finally formic acid is released by a putative 10-formyl-H_4folate synthetase (LigH), recovering H_4folate (Figure 2.27) [222].

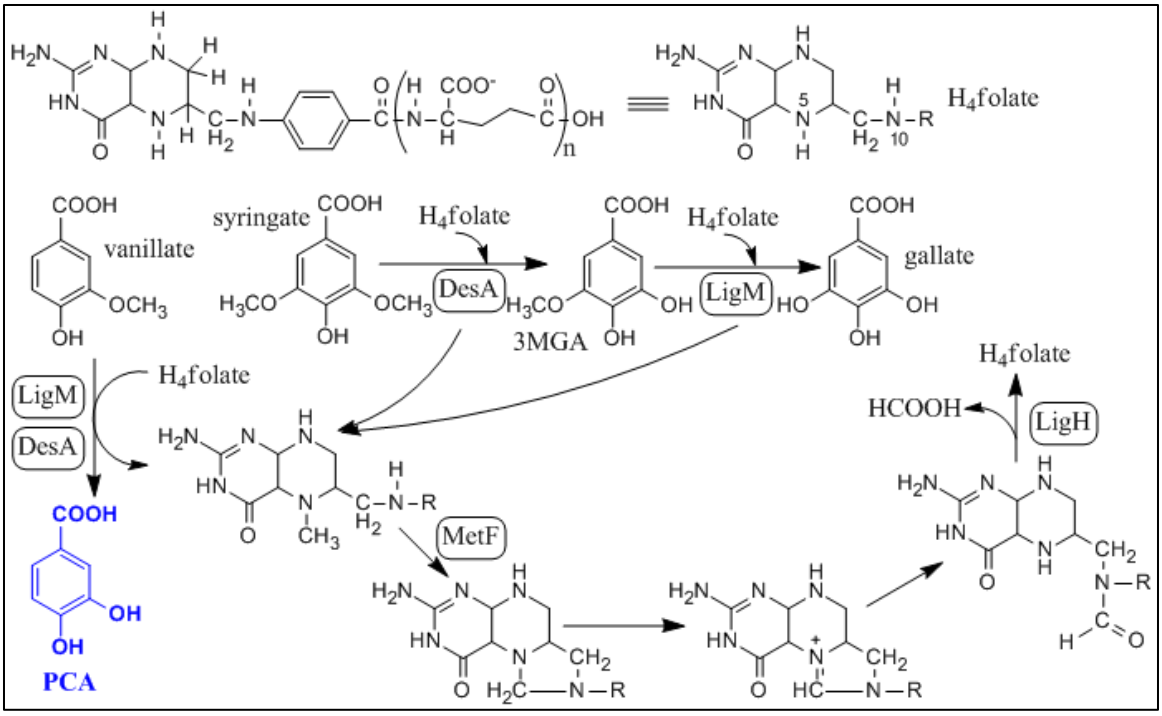

Figure 2.27. Vanillate and syringate O-demethylation in *S. paucimobilis* SYK-6, resulting gallate and β-ketoadipate pathway starting substrate protocatechuic acid (PCA); tetrahydrofolate coenzyme shown in top part, n=1-6 [222].

Vanillate demethylase (VanA/B), found in bacteria like *Pseudomonas*, *Acinetobacter* and *Rhodococcus*, uses hydroxylation and spontaneous splitting of formaldehyde to eliminate the methyl group. This is achieved by the Rieske-type oxygenase (VanA) part simultaneously acting with the $NADH+H^+$ or $FADH_2$ (reduced nicotine- or flavin-adenine dinucleotide coenzymes) containing reductase (VanB) part (Figure 2.28) [219, 222, 235-238]. It is noteworthy that p-coumaryl (H, Figures 1.1 and 2.9) lignin can be degraded to 4-hydroxybenzoic acid (4-HBA) through similar pathways as mentioned above. This compound cannot be directly degraded by dioxygenases, consequently 4-HBA is converted to PCA by Rieske-type hydroxylation as well, as hypothesized from results with actinomycetes, such as *Rhodococcus* [236].

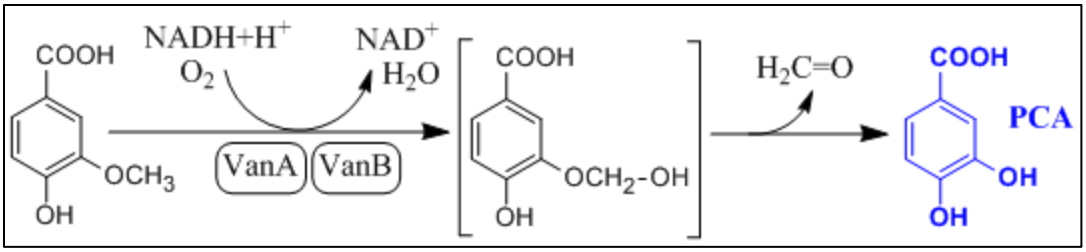

Figure 2.28. Hydroxylation of vanillic acid to a spontaneously degrading hemiacetal that releases formaldehyde to form PCA, as governed by VanA/B vanillate demethylase enzyme [219, 236]

2.5.2.3 Biphenyl degradation

Biphenyl degradation has been widely studied, due to the fact that this structure resembles highly toxic environmental pollutants like chlorinated biphenyls, and multiple soil bacteria, such as *Pseudomonas* species, can degrade it. It is also degraded by *S. paucimobilis* SYK-6 via the same mechanism, oxidation to 2,3-dihydroxybiphenyl followed by meta-cleavage [11, 219, 222], Figure 2.29. Meta-cleavage refers to the opening of the aromatic ring right next to the hydroxyls, between carbons 4 and 5, and it is also known as extradiol cleavage (Figure 2.33) [11]. Actinomycetes species contain intradiol (ortho-, between carbons 3-4, Figure 2.33) cleaving dioxygenases, unlike SYK-6 and the above species, possibly explaining their decreased ability in lignin degradation [219]. In lignin biphenyl linkage is quite abundant (SW, 18-25 %, Table 2.10) and it consists of two guaiacols (vanillates in model compounds) connected between the 5 positions (hence the name 5-5), depicted on Figures 2.9 and 2.29 [99, 100]. Degradation in bacteria begins with the demethylation of one of the methoxyl-groups resulting 2,2',3-trihydroxy-3'-methoxy-5,5'-dicarboxybiphenyl (OH-DDVA), catalyzed by LigX a non-heme iron dependent demethylase (Figure 2.29) [219, 222]. In the following step the ring is opened by LigZ, an extradiol- (protocatechuate-4,5-) dioxygenase (meta-cleavage) with a subsequent C-C bond hydrolysis by LigY to form 5-carboxyvanillic and 4-

carboxy-2-hydroxypentadienoic acids. 5-carboxyvanillate is further decarboxylated by the non-oxidative aromatic acid decarboxylase LigW enzyme into vanillic acid (Figure 2.29), that can be converted to PCA through previously introduced pathways (Figures 2.27-8) [219, 222]. The other intermediate of ring fission, 4-carboxy-2-hydroxypentadienoic acid is converted to 4-hydroxy-4methyl-2-oxoglutarate by a hydratase enzyme, and latter compound is further degraded to acetyl-CoA by an aldolase (Figure 2.29) [219, 222].

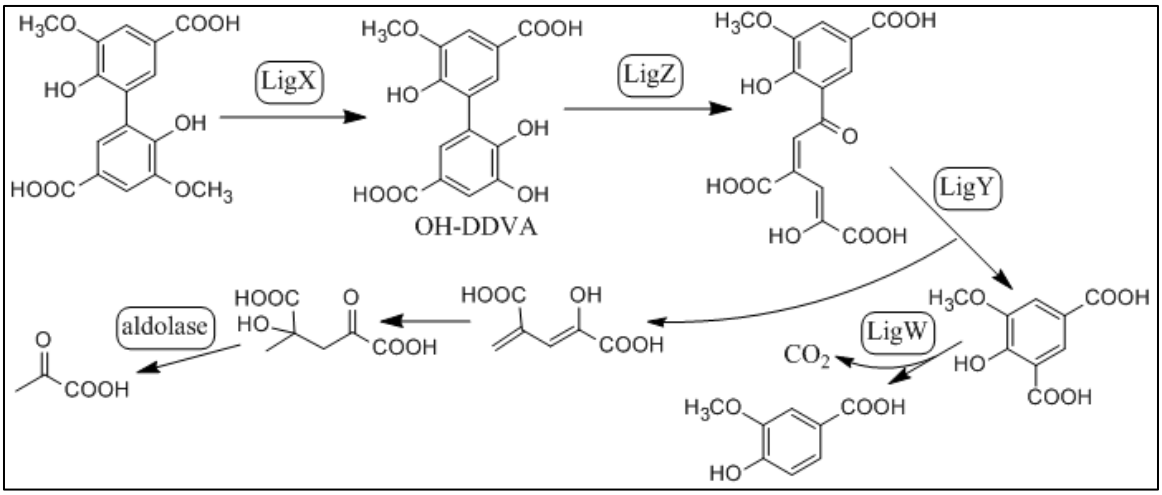

Figure 2.29. Biphenyl degradation through meta-cleavage and hydrolysis in bacteria [219, 222]

2.5.2.4 Diarylpropane degradation

Diarylpropane refers to β-1 linkage in lignin (Figures 2.9 and 2.30), that is cleaved via an α-β radical mechanism in fungi resulting in aromatic aldehydes. Bacteria on the other hand, including *Pseudomonas*, employ an enzyme that catalyzes the elimination of water and formaldehyde to form stilbene (just like β-5 under Kraft pulping conditions, reverse aldol [101]) as shown on Figure 2.30 [219]. Lignostilbene is then processed by a non-heme iron dependent (carotenoid cleavage) dioxygenase, oxidatively

into two vanillins [219, 239] that are substrates to vanillate dehydrogenase, LigV in *S. paucimobilis* SYK-6. Latter forming vanillic acid (Figure 2.30) that can be converted to PCA through previously introduced pathways (Figures 2.27-8) [219, 222].

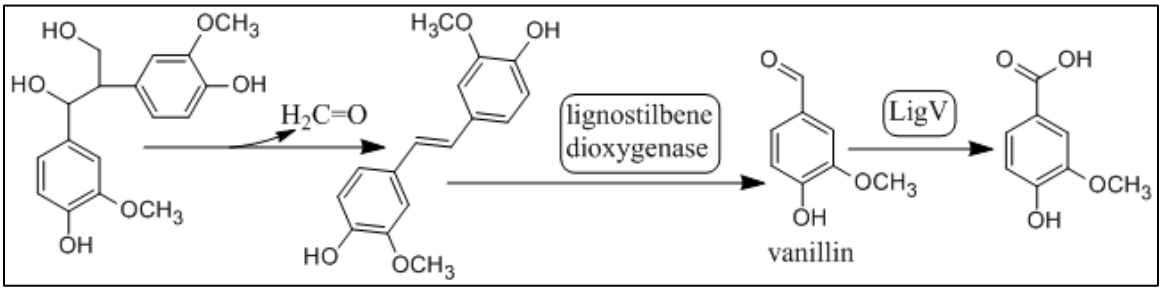

Figure 2.30. Diarylpropane degradation through lignostilbene, as catalyzed by stilbene dioxygenase [219, 222]

2.5.2.5 Degradation of phenylcoumarane, pinoresinol and ferulate

Fungi have multiple strategies to degrade β-5 (phenylcoumarane) and β-β (pinoresinol), resulting vanillic acid and acetovanillone. On the other hand, although degradation of these linkages had been observed with bacterial preparations, the mechanisms involved remain elusive. It is hypothesized that both pathways begin with the α-hydroxylation of the phenylpropanoid structure that induces the spontaneous ring opening between the α-carbon and the β-oxygen of the connected aromatic ring, resulting a benzylic-ketone [219]. Subsequent reduction of this ketone would result in the diarylpropane structure that can be degraded through the stilbene intermediate as shown earlier (Figure 2.30) [219]. This theoretical pathway is shown on Figure 2.31, with phenylcoumarane as starting substrate [219].

Ferulic acid is a part of lignin that is usually attached to hemicellulose via ester linkages (at γ-position for example) that are degraded by both bacterial and fungal

esterases, liberating ferulate, which is further degraded via two distinct pathways in bacteria. *S. paucimobilis* SYK-6, for example, utilizes feruloyl-CoA synthetase (FerA), followed by feruloyl-CoA hydratase/lyase (FerB) to convert ferulate to feruloyl-CoA then vanillin respectively (Figure 2.32). A pathway used by multiple bacteria, such as *Pseudomonas* and *Amycolatopsis*. While on the other hand *Bacillus*, *Lactobacillus* and *Enterobacter* use ferulic acid decarboxylase to convert into vinylphenol that can be further reduced to ethylphenol (Figure 2.32) [219].

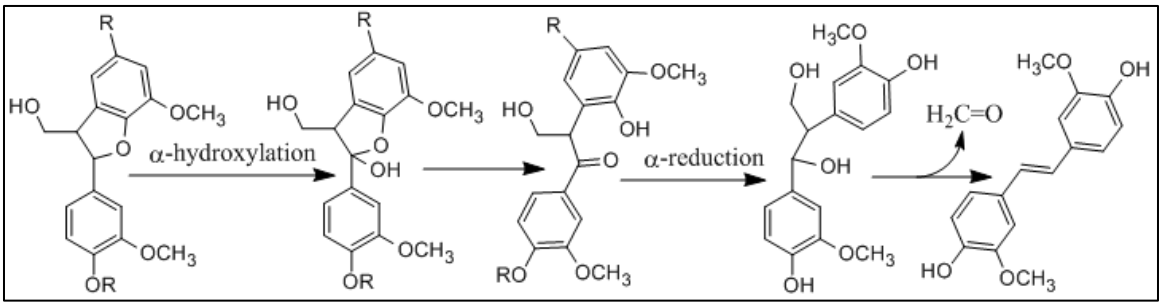

Figure 2.31. The hypothetical pathway for phenylcoumaran catabolism (also pinoresinol) in bacteria, based on degradation products; the resulting stilbene can further degrade as shown on Figure 2.30 [219, 222]

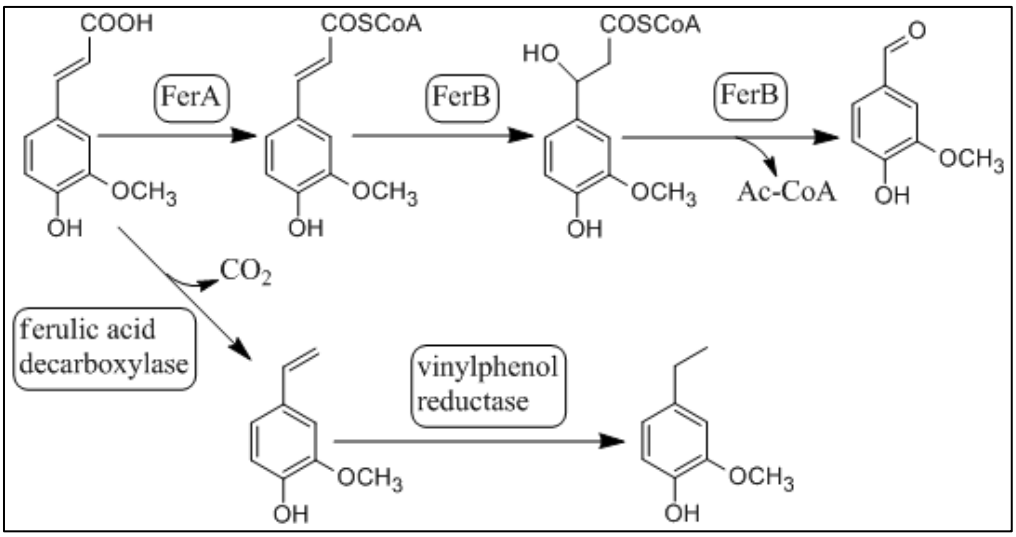

Figure 2.32. Ferulate degradation in two different bacterial groups producing vanillate (*Sphingomonas*, *Pseudomonas* etc.) or ethylguaiacol (*Bacillus*, *Enterobacter* etc.) [219, 222]

2.5.3 Aromatic compound degradation

The previous sections (2.5.1-2) concentrated on lignin degradation and oligomer funneling to protocatechuate (PCA), one of the archetypal substrates of aromatic ring opening enzymes called dioxygenases (Figure 2.24). Bacteria contain dioxygenases species specifically, in fact, the presence of different aromatic degradation pathways can be used as identification tools for given strains [11]. Moreover, recent bioinformatics research based on the enzymes' amino acid sequences revealed that only a few classes of bacteria contain these dioxygenases, namely α-, β-, γ-proteobacteria and actinobaceria [219]. The species can be further classified based on the cleavage mechanism of their respective dioxygenases. Some will cleave the aromatic ring adjacent to the catechol (neighboring hydroxyls) functionality using 4,5-protocatechuate dioxygenases (4,5-PCD), while others cut between the hydroxyls (3,4-PCD same as P3,4O shown on Figure 2.26), moreover some strains will contain both pathways [11, 219]. The use of 4,5-PCD results in extradiol or meta-cleavage (also mentioned in biphenyl degradation, section 2.5.2.3) and it is utilized mostly by proteobacteria (e.g. *Sphingomonas*, *Burkholderia*). Consequently, P3,4O will lead to intradiol (or ortho-) cleavage defining the whole following pathway till β-ketoadipate, and further to succinyl and acetyl-CoA (Figure 2.33). Accordingly, the β-ketoadipate pathway is only defining aromatic degradation in strains, like *Rhodococcus*, which degrade PCA through intradiol cleavage. Other bacteria use different archetypal intermediates such as gentisate or catechol (Figure 2.24), in addition there are various intra- and extradiol cleavage types, not mentioning strains that have enzymes for multiple pathways [11, 219, 222]. In conclusion, the β-ketoadipate

pathway is only a narrow region within all the possible bacterialaromatic degradation routes, however, it is the sole catabolism employed by *Rhodococci*, the chosen species of this work. Figure 2.33 summarizes the funneling steps leading to PCA, illustrates both intra- and extra-diol cleavages, as well as concisely describes steps after ring opening considering pathways initiated by both 3,4- a 4,5-dioxygenases. These catabolic routes result tricarboxylic-acid cycle (TCA) intermediates, as depicted on Figure 2.33, most importantly acetyl-CoA (Ac-CoA) the fundamental building block of fatty acid (FA) and later lipid synthesis [11, 219, 222]. Following parts of this section detail the current knowledge on the β-ketoadipate pathway enzymes (and intermediates), utilized during lignin digestion by the chosen *Rhodococcus* strains, as briefly depicted on Figure 2.34.

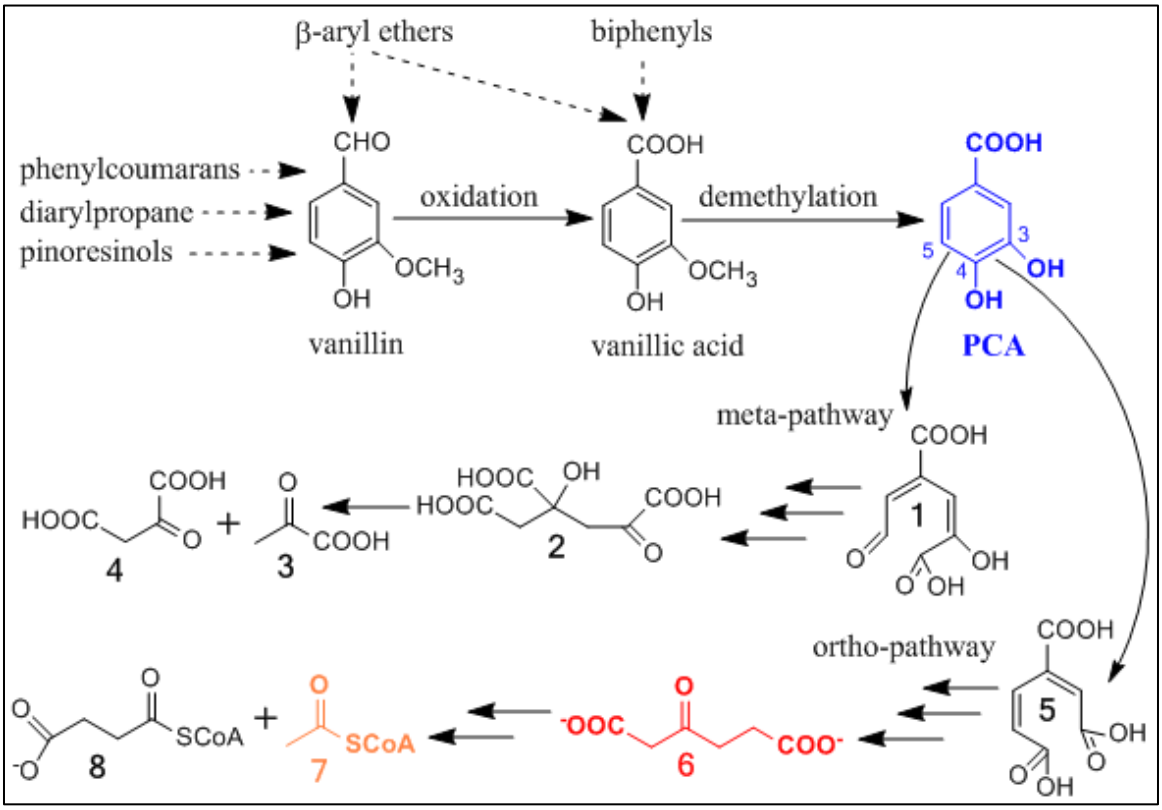

Figure 2.33. Lignin oligomers converging to PCA that is subject to different ring opening reactions and further degradation defined by bacterial species, e.g. ortho- and meta-pathways. (1) 4-carboxy-2-hydroxymuconate-6-

semialdehyde; (2) 4-carboxy-4-hydroxy-2-oxoadipate subsequently cleaved by an aldolase to pyruvate (3) and oxaloacetate (4). (5) β-carboxymuconate; (6) β-ketoadipate cleaved to acetyl- and succinyl-CoA by thiolase [11, 219]

2.5.3.1 The β-ketoadipate pathway

Figure 2.34 shows the theoretical pathway of protocatechuate (PCA) conversion into succinyl- (8) and acetyl-CoA (7) by *R. opacus* strains as hypothesized from the literature of other species' enzymatic activities [11, 63, 240-248]. First protocatechuate 3,4-dioxygenase (P3,4O) ruptures the aromatic ring by using a non-heme Fe^{3+} complex to coordinate molecular oxygen incorporation, as investigated in *Acinetobacter* strain ADP1 [248] and *Pseudomonas putida* [246], creating β-carboxymuconate (5). The second step, as predicted from the literature, is an *anti*-1,2-addition-elimination reaction catalyzed by carboxymuconate lactonizing enzyme (CMLE) to form γ-carboxymuconolactone (9) as researched in *P. putida* [247] and *Agrobacterium radiobacter* S2 [243]. At this point, as hypothesized, γ-carboxymuconolactone decarboxylase (CMD) activity results an enol-lactone (10) product that is further converted to β-ketoadipate (6) by enol-lactone hydrolase (ELH), with former enzyme's reaction mechanism investigated in *Acinetobacter calcoaceticus* and *P. putida* [241], while latter reaction was predicted in *Burkholderia xenovorans* LB 400 [240]. It is important to emphasize, that although the β-ketoadipate pathway is highly conserved these last two steps are most likely merged in *R. opacus* 1CP under one enzyme's activity [242]. It can also be predicted from literature that in the final steps β-ketoadipate (6) is possibly converted into β-ketoadipyl- (11) then succinyl- (8) and acetyl-CoA (7) by transferase (TR) and thiolase (TH) activities

respectively [11]. Subsequently, the anabolic action of acetyl-CoA carboxylase (ACC), fatty acid synthase II (FASII) and other metabolic processes can result lipids as shown on Figure 2.24 [15, 63].

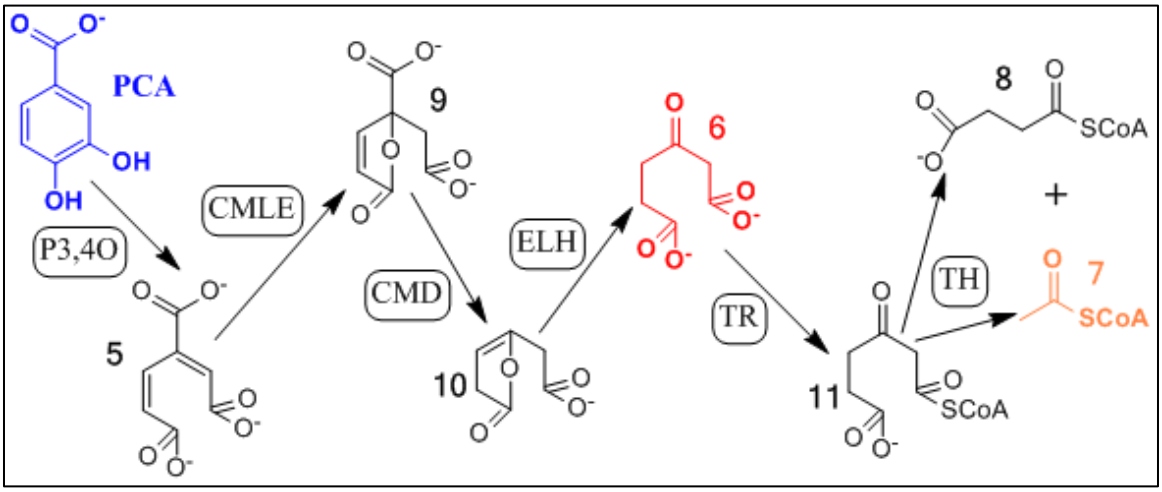

Figure 2.34 The β-ketoadipate (6) pathway, including (5) β-carboxymuconate; (9) γ-carboxymuconolactone; (10) β-ketoadipate enol-lactone; (11) β-ketoadipyl-CoA; (7) acetyl-CoA and (8) succinyl-CoA. Enzymes in rounded rectangles are: P3,4O, protocatechuate 3,4-dioxygenase; CMLE, β-carboxy-*cis*-*cis*-muconate lactonizing enzyme; CMD, γ-carboxymuconolactone decarboxylase, ELH, enol-lactone hydrolase; TR, β-ketoadipate:succinyl-CoA transferase and TH, β-ketoadipyl-CoA thiolase [11, 219]

PCA degradation begins with an intradiol cleavage catalyzed by P3,4O (Figure 2.34), a non-heme iron dependent enzyme, that exhibits true dioxygenase stoichiometry, both oxygen atoms from molecular oxygen are incorporated in the product β-carboxymuconate [244]. It has been shown that intradiol dioxygenases usually contain ferric ion (Fe^{3+}) in their active site (extradiol dioxygenases contain Fe^{2+}) that predetermines the cleavage mechanism [244-246, 248]. Although the overall reaction is exotermic, dioxygenases have to overcome major hurdles, like the stability of the aromatic ring and as a consequence the stabilization of its opened form until the oxidation

is completed. The catalytic Fe^{3+} is stabilized by two histidines and two tyrosines in the active site between the 2 subunits (α, β) of P3,4O, and the enzyme exhibits high substrate specificity. The carboxyl group at position 1 ensures rapid turnover, while the lack of charged substituent at position 4 completely inhibits activity [244-246, 248]. The proposed mechanism begins with PCA binding to the active site of P3,4O replacing two hydroxyls, with one belonging to a tyrosine the other to the active site itself, consequently, water is released and the substrate is stabilized by Fe^{3+} (Figure 2.35). The enzyme chelates PCA asymmetrically, resulting a shorter bond between Fe^{3+} and C_4-O than the other Fe-O bond, giving a slight anionic nature to PCA at C_4 position that induces a direct electrophilic attack from molecular oxygen positioned in a binding cleft proximal to the active site. Then the O_2 also coordinates into the active site creating an iron-akylperoxo intermediate (PCA_a). Subsequently, rearrangement and oxygen bond cleavage results a cyclic-anhydride (PCA_b) and an iron-oxide, with latter acting as a nucleophile in the final ring cleavage step. Next the previously protonated tyrosine residue reattaches to the active site and another water molecule releases β-carboxymuconate while the enzyme returns to resting state (Figure 2.35) [244-246, 248].

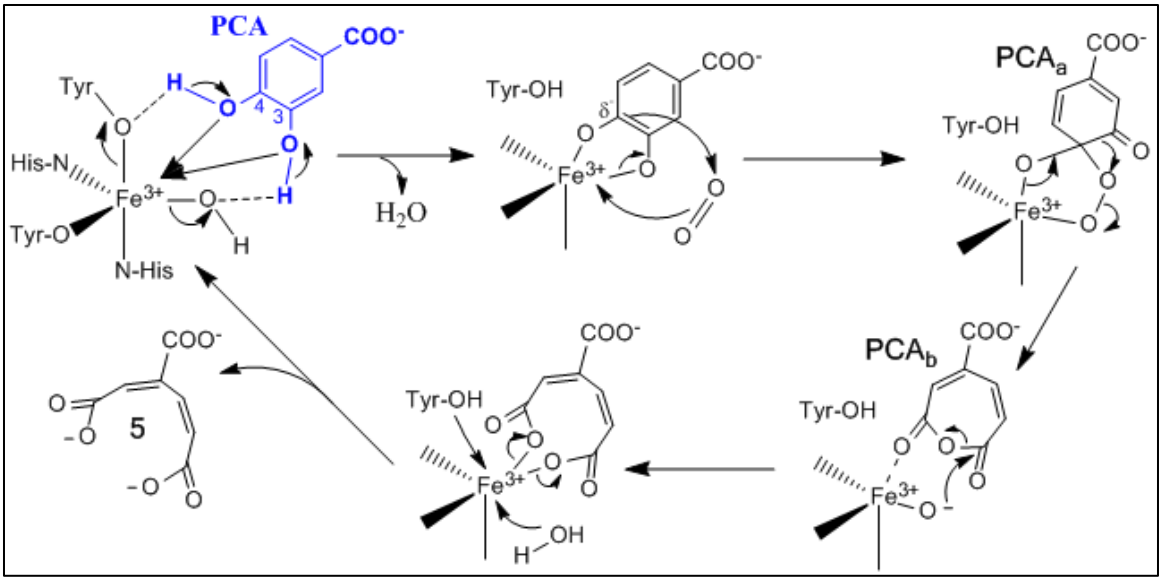

Figure 2.35. Conversion of PCA to β-carboxymuconate via iron-akylperoxo (PCA_a) and cyclic-anhydride (PCA_b) intermediates, catalyzed by the intradiol dioxygenase P3,4O [245, 246, 248]

The second step in the β-ketoadipate pathway is the cyclization of β-carboxy-cis,cis-muconate (5) into a 4-carboxy-(S)-muconolactone (9), catalyzed by carboxy-muconate lactonizing enzyme (CMLE, Figures 2.34, 2.36). The reaction doesn't need catalyrtic metal ions and it is most likely an anti-1,2-addition-elimination process. The cycloisomerization proceeds through an aci-carboxylate (5_a) intermediate catalyzed by a general base, illustrated on Figure 2.36 [243, 247].

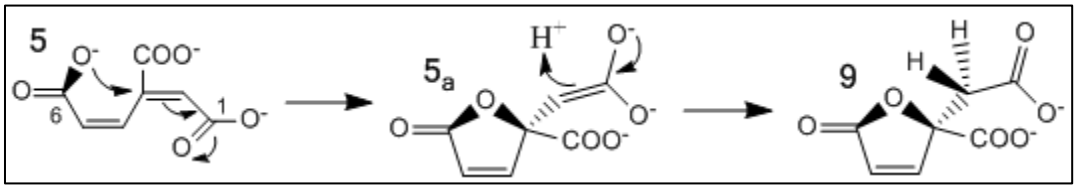

Figure 2.36. Cycloisomerization of β- carboxymuconate (5) through an aci-carboxylate (5a) to carboxy-muconolactone (9), catalyzed by CMLE [241]

Carboxy-muconolactone (9) is a highly unstable intermediate that is converted to β-ketoadipate enol-lactone (10) by γ-carboxymuconolactone decarboxylase (CMD) that also acts as a muconolactone isomerase (Figures 2.34, 2.37). Decarboxylation is almost spontaneous, while isomerization is directed by a basic side-chain protonating at the C_5 position (Figure 2.37) [240, 241, 249]. Figure 2.37 also briefly illustrates enol lactone (10) hydrolysis to β-ketoadipate (6) by enol lactone hydrolase (ELH), however, there is proof that the activity of latter two enzymes are integrated in *R. opacus* (Figures 2.34, 2.37) [240, 242]. In the last two steps, as mentioned above, β-ketoadipate (6) is converted to β-ketoadipyl-CoA (11) by a transferase (TR), then a thiolase (TH) introduces another CoA-SH liberating the final products succinyl- (8) and acetyl-CoA (7, Figure 2.34) [11]. Ac-CoA (7) is the absolute final product of lignin degradation, while it is also the fundamental substrate that the bacteria will use to build up all necessary compounds for survival and even growth, when utilizing lignin as a sole carbon source. It is also the fundamental building block of fatty acid and lipid synthesis, which is detailed in the next section.

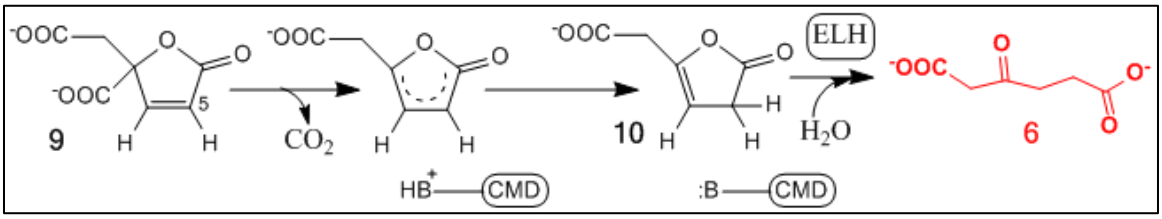

Figure 2.37 The formation of β-ketoadipate from carboxy-muconolactone [11]

2.5.4 Fatty acid and lipid biosynthesis in bacteria

Fatty acid (FA) synthesis, starting form Ac-CoA, is the first step of lipid accumulation (Figure 2.38) [250-254]. Following steps include phospholipid (PL) and

triacylglycerol (TAG) (also known as "neutral lipid") synthesis resulting in membrane and reserve lipid accumulation respectively (Figure 2.38) [250-256]. Conversion of these lipids into FA short-chain alcohol esters is the final step in biodiesel production (Figure 2.4). Table 2.19 lists all enzymes involved in both bacterial FA and TAG biosynthesis, accordingly the following text and figures will only contain the abbreviations.

Table 2.19. Bacterial enzymes of FA and TAG synthesis; [a]*E. coli* Gram-negative bacteria model; [b]*B. subtilis* Gram-positive bacteria model organism enzymes; [c]Oleaginous *R. opacus* DGAT enzyme genes [15]

Abbreviation	Enzyme name	Example gene product[a]
	FA synthesis	
ACC	Acetyl-CoA carboxylase	AccABCD
ACP	Acyl carrier protein	AcpP
DH	β-Hydroxyacyl-ACP dehydratase	FabZ, FabA[a] FabL, FabK[b]
ER	Enoyl-ACP reductase	FabI
KR	β-Ketoacyl-ACP reductase	FabG
KS	β-Ketoacyl-ACP synthase	FabB (KSI) FabF (KSII) FabH (KSIII)
MAT	Malonyl-CoA:ACP transacylase	FabD
TAG synthesis, also acyl-ACP modification in Gram-positive bacteria[b]		
G3PAT	Acyl-ACP:G3P acyltransferase	PlsB[a] PlsX, PlsY[b]
AG3PAT	Acyl-ACP:1-acyl-G3P acyltransferase	PlsC
DGAT	Acyl-CoA:DAG acyltransferase	Atf1, Atf2[c]
GK	Glycerol kinase	
PAP	Phosphatidate phosphatase	PgpB

In prokaryotes, the fatty acid synthase FASII (eukaryotic system is FASI and it is an enzyme complex) is composed of individual enzymes. Acetyl-CoA is always the basis for FA biosynthesis and is the substrate of KS (β-ketoacyl-ACP synthase) [250, 253]. Subsequently FASII catalyses KS, β-ketoacyl-ACP reductase (KR), β-hydroxyacyl-ACP

dehydratase (DH) and enoyl-ACP reductase (ER) (Table 7) steps in a repetitive manner, usually until palmitoyl-ACP (C-16) forms after seven cycles (Figure 2.38) [250, 253]. The resulting acyl-ACP is used differently by various bacterial species. Almost all bacteria use PlsX first to form acyl-phosphate from acyl-ACP then it is transferred onto glycerol-3-phosphate (G3P, position-1) by PlsY. *E.coli* on the other hand, only uses PlsB acyltransferase to load an acyl group directly onto G3P from acyl-ACP (Figure 2.38, Table 2.19) [250-254]. Subsequently, acyl-CoA-1-acyl-G3P acyltransferase (AG3PAT, PlsC) loads the second acyl group, followed by the action of phosphatidate phosphatase (PAP) that dephosphorylates phosphatidic acid (PA) to form diacylglycerol (DAG). DAG can be further acylated by acyl-CoA:DAG acyltransferase (DGAT) to form TAG (Figure 2.38; Table 2.19) [15].

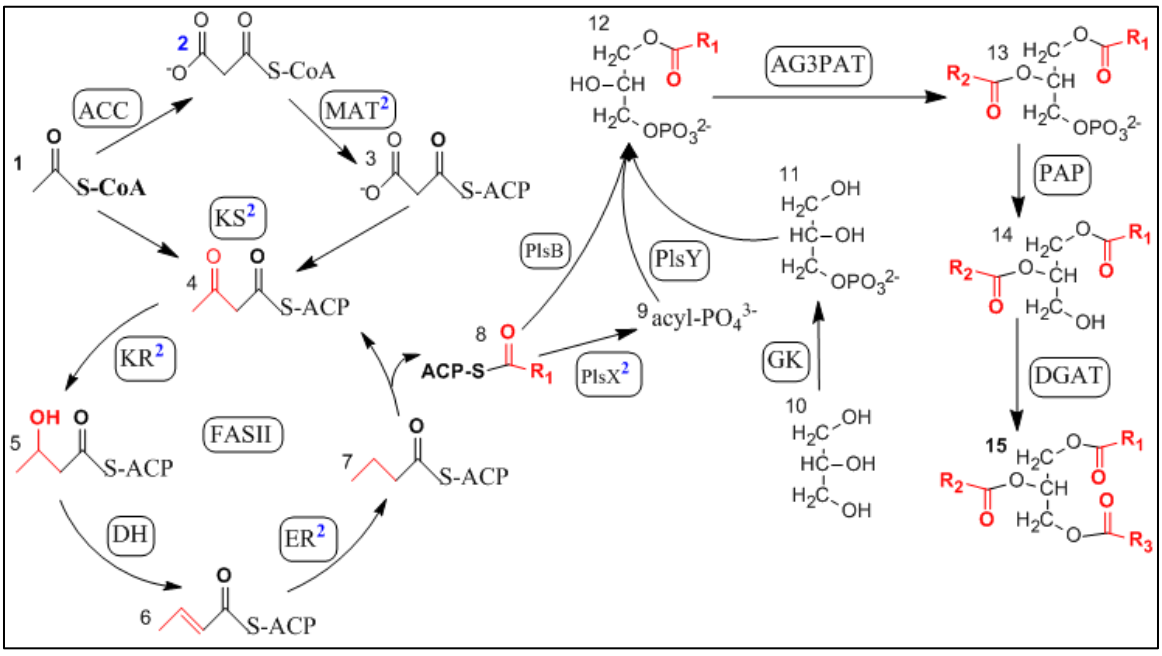

Figure 2.38. TAG biosynthesis in bacteria, full names for enzymes in rounded rectangles are located in Table 2.19, and newly incorporated atoms are shown in red. FA synthesis starts with acetyl-CoA (1) (compound 7 on Figure 2.34, the final result of lignin biodegradation) and ends with acyl-ACP (8). Malonyl-CoA (2) appears with a superscript blue number, which

also appears on enzymes regulated by FapR. 2 is the effector of FapR, a transcriptional regulator in Gram-positive bacteria. Molecules: (3) malonyl-ACP; (4) acetoacetyl-ACP; (5) β-hydroxybutyryl-ACP; (6) β-trans-butenoyl-ACP; (7) butyryl-ACP; (9) acyl phosphate; (10) glycerol; (11) glycerol-3-phosphate (G3P); (12) 1-acyl-G3P; (13) phosphatidic acid; (14) diacylglycerol (DAG) and (15) triacylglycerol (TAG) [15].

Bacteria generally accumulate polyhydroxyalkanoates (PHAs), mainly polyhydroxy butyrate (PHB), for energy storage; TAGs are only produced by select strains [13]. Acetyl-CoA carboxylase (ACC) initially catalyzes the formation of malonyl-CoA from acetyl-CoA (Figure 2.38) [20-21]. Malonyl-CoA:ACP transacylase (MAT) loads malonyl-CoA onto ACP (Table 2.19), which will transfer the growing acyl groups between FA elongation stages [253]. *Escherichia coli* is a model organism for FASII and it is suitable for genetic engineering [224], while the genus *Acinetobacter* is the only Gram-negative oleaginous group identified and studied to date [13, 256]. Conversely, elevated lipid accumulation is well-studied and highly efficient in the Gram-positive group of *Actinomycetes* [13, 256]. For these reasons, when describing pathways for FA synthesis, the basis is usually *E. coli* FASII; however, understanding the differences between Gram-positive and Gram-negative bacteria is of great importance (Figure 2.38; Table 2.19). FASII cycle proceeds according to Figure 48; to balance chain initiation with growth and utilization KSIII, ER and KR are under negative feedback control by long-chain acyl-ACPs (LCA-ACPs). LCA-ACPs directly control reductase activities; consequently, FASII will be biased to "catalyze forward" if these products are withdrawn from the system by any conversion, including PL or TAG synthesis (Figure 2.38). KSI and KSII are responsible for the elongation of the growing acyl-ACP chain (Table 2.19). FabA isomerizes *cis*-2-decenoyl-ACP into *trans*-3-decenoyl-ACP, and the latter is

elongated by FabB, resulting in unsaturation [253]. Lipid synthesis then proceeds according to Gram class (Figure 48). Under balanced growth, palmitic acid (PA) in *E. coli* is channeled to PL and other non-reserve lipid synthesis; while in oleaginous species under nutrient limitation, PA will be converted into DAG by PAP, then into TAG by DGAT, forming lipid particles (Figure 2.38) [13, 250, 256].

2.5.4.1 Regulation of lipid biosynthesis

Many Gram-positive bacteria, like *Bacillus subtilis*, coordinate FA biosynthesis with the FapR repressor that downregulates transcription for biosynthetic pathway enzymes (e.g. MAT, KSIII, KR and ER) as well as for the first steps in phospholipid biosynthesis, like PlsX (Figure 2.38). FapR also regulates its own gene, *fapR*, and its effector is malonyl-CoA – a product of ACC whose activity depends on LCA-ACP. When malonyl-CoA (#2 molecule on Figure 2.38) attaches to FapR, it induces a conformation change that results in the release of all controlled operators; concomitantly, all biosynthetic genes are transcribed (bold, blue 2 in superscripts show the produts of FapR regulated genes on Figure 2.38) and acyl-ACP levels increase. The acyl-ACPs are consumed by PlsX to produce acyl phosphates, which are used for PL synthesis. In conclusion, ACC through malonyl-CoA production controls FA biosynthesis, while ACC itself is under growth rate and autoregulatory control [252, 254]. It is noteworthy that the transcriptional regulators of desaturating enzymes in both *E. coli* (FadR and FabR) and *B.subtilis* (DesR) have been studied recently, thereby opening the possibility to "genetically optimize" FA desaturation for subsequent biodiesel production and application [252, 254].

2.5.4.2 Examples of lipid accumulation, and its enhancement

Oleaginous species under growth-restricted conditions are capable of producing large quantities of TAG owing to their high DGAT activity (Figure 48). *Rhodococcus opacus* PD630 and *Gordonia sp* DG were grown solely on carob and orange wastes producing TAGs up to 59.27 mg L^{-1} d^{-1} and 14.45 mg L^{-1} d^{-1}, respectively [257]. Focusing on enzymes involved in lipid body formation [13, 255, 256], it has been shown that WS/DGAT enzyme (wax ester synthase/acyl-CoA:diacylglycerol acyltransferase) is responsible for the accumulation of TAG in *Acinetobacter baylyi* ADP1 and that it has low substrate specificity. *atfA* encoding WS/DGAT has become a key component in engineering heterologous *E. coli* strains for direct biodiesel production [223, 224, 258]. In 2006, the first microbial biodiesel ("microdiesel")-producing recombinant *E. coli* was created by cloning pyruvate decarboxylase (*pdc*) and alcohol dehydrogenase (*adhB*) genes from *Zymomonas mobilis* and *atfA* from *A. baylyi* ADP1 [223]. The resulting microdiesel strain is able to produce up to 1.28 g L^{-1} FAEEs (Fatty Acid Ethyl Ester), although only when sodium oleate is present in the media. The authors emphasized, however, that oleaginous species might be more suitable for this purpose because they can direct FAs more efficiently towards esterification [223]. *R. opacus* PD630 has also been researched since the mid-1990s because of its ability to accumulate over 80% of its cell dry weight (CDW) in TAGs [13]. Recently, two highly efficient *atfA* homologous genes *atf1* and *atf2* were identified in *R. opacus* PD630 [259] and a gene transfer system has been established for *R. opacus-E.coli* exchange [260]; however, *R. opacus* cannot ferment alcohol. Lu and colleagues have recently attempted to maximize FA production in *E. coli* by knocking out the *fadD* gene (codes first enzyme in β-oxidation pathway);

heterologously expressing a plant thioesterase to increase the abundance of shorter chain FAs; overexpressing ACC; and releasing feedback inhibition by LCA-ACPs through overexpressing an endogenous thioesterase. This recombinant *E.coli* strain reached a FA production rate of 0.11 g L^{-1} h^{-1} under fed-batch conditions while living exclusively on glycerol [258]. In a recent study *adhB*, *pdc* and *atfA* genes were introduced to *E. coli* for ethanol production *in situ* and two xylanase genes, *xyn10B* and *xs*a, have also been cloned to enable hemicellulose utilization [224]. When xylan was added, the strain produced threefold more FAEEs than when only glucose was present, representing the first example of direct biodiesel production [224].

In brief summary, Chapter 1 introduced the hypothesis that *Rhodococcus* species are capable of both lignin degradation and lipid accumulation, while Chapter 2, especially sections 2.5.2-4, collected and presented all supporting information found in the literature to date. Consequently, Chapters 5-6 will focus on model compound and direct lignin bioconversion by the selected *Rhodococci*, to evaluate possible lipid production.

CHAPTER 3

EXPERIMENTAL SECTION

3.1 Materials, chemicals and microorganisms

3.1.1 Chemicals

All chemicals were purchases either from Sigma-Aldrich (St. Louis, MO, USA) or VWR (West Chester, PA, USA), and used as received. All gases were purchased from Airgas (Radnor Township, PA, USA).

3.1.2 Materials

3.1.2.1 Loblolly pine

A 15-year old loblolly pine tree (*Pinus taeda*) was acquired from a University of Georgia plot in Baldwin County, GA and used for all studies in this report. The tree was 45-50 feet high and was visually free of disease and compression wood. The wood was manually debarked, chipped and refined with a Wiley mill through a 0.05" screen. The refined wood had 10.34 % moisture content, samples were stored below 0 ^{o}C prior to use.

3.1.2.2 EOL

Ethanol organosolv lignin was obtained according to a literature procedure optimized for mountain pine beetle killed lodgepole pine (*Pinus contorta*) [39], however, the feedstock was loblolly pine.

3.1.2.3 Kraft lignin, black liquor (BL)

Kraft lignin was always obtained through acidification and purification of BL, following the same literature method [148], however, the extra steps of dilution (100x) in pH 12 water, 2 h stirring and re-precipitation at pH 3 were employed subsequently, to remove residual dioxane. Latter purification solvent is needed to remove EDTA that is previously used for metal removal. ^{13}C NMR experiments proved that all these steps are required to gain pure lignin. Consequently, this extended purification method was used for the two different BL sources utilized in present work. The work in Chapter 4 utilizes a BL obtained from Chalmers University of Technology (Göteborg, Sweden), together with CO_2 precipitated lignins (P 9.5,10.5), and filtrates (F9.5, 10.5). While the work detailed in Chapter 6 employed a BL obtained from a U. S. paper company (Cedar Springs, US). The differences between the Kraft lignin obtained are detailed in respective chapters.

3.1.3 Microorganisms

Rhodococcus opacus DSM 1069 and PD630 (DSMZ 44193) strains were purchased from the German Collection of Microorganisms and Cell Cultures (DSMZ).

3.1.4 Fermentation media

Two types of media were used during shake flask fermentations in case of both strains; a full media and a minimal media with adjusted carbon and nitrogen source concentrations. Full media were prepared according to DSMZ recommendations; DSMZ 65 for strain DSM 1069 and DSMZ 535 for PD630. Minimal media for DSM 1069 contained: 0.40 g KH_2PO_4, 1.60 g K_2HPO_4, 0.20 g $MgSO_4x7H_2O$, 0.015 g $FeCl_3$, 0.5 mg $MnSO_4xH_2O$, 1.0 mg $CuSO_4x5H_2O$, 1.0 mg $ZnSO_4x7H_2O$, 0.5 mg $CaCl_2$, 0.1 mg KCl and 0.5 mg H_3BO_3 per liter distilled water [261]. In case of PD630: 9.00 g

$Na_2HPO_4x12H_2O$, 1.50 g KH_2PO_4, 0.20 g $MgSO_4x7H_2O$, 1.2 mg $FeNH_4$-citrate, 20 mg $CaCl_2$, 2 ml Hoagland solution (Sigma, H2395) and 0.50 g $NaHCO_3$ per liter distilled water [262]. Added to minimal media were nitrogen [DSM 1069: NH_4NO_3 [261]; PD630: NH_4Cl [262]] and carbon [glucose, 4-hydroxybenzoic (4-HBA), vanillic (VanA) acids and different lignin] sources, according to adaptation or lipid accumulation conditions (nitrogen 0.05-0.1 w/v%, carbon 0.2-1.0 w/v%). The pH was set to 7 in all cases then the media was sterile filtered before use.

3.2. Experimental procedures

3.2.1 Ethanol-Toluene extraction of wood

Extractions had been conducted in a 2:1 toluene: ethanol solvent mixture for 48 h at the consistency of 2.5 w/V% based on ODW sawdust. Before extraction the loblolly pine chips were milled to sawdust until passed through a 5 mm mesh.

3.2.2 Ethanol organosolv pretreatment of extracted wood

Ethanol organosolv pretreatment was conducted following the method of Pan et al. [39], briefly, 170°C for 1 h in 65 % EtOH as solvent, with 1.1 % concentrated (>97 %) H_2SO_4 as catalyst, based on ODW extracted loblolly pine sawdust at 7 w/V% final consistency, in a 1 gal pressure reactor (Parr Instruments, Moline, IL). Lignin (EOL) was recovered from the separated pretreatment liquor by four times dilution with distilled water and subsequent filtration through Whatman No.1 filter paper.

3.2.3 Kraft lignin purification from BL

BL samples were diluted in distilled water to 5 % solids content. Next EDTA-$2Na^+$ was added to the aqueous solution (in 5.00 g/l concentration) to facilitate metal-ion removal and the pH was adjusted to a value of 6 with aqueous sulfuric acid (2 M) and stirred for 1 h. Subsequently, the pH was further lowered to a value of 3. The resulting samples were frozen (-20 °C) over night, thawed and filtered through medium sintered glass funnel at 0 °C. Retentates were dissolved in pH 3 aqueous sulfuric acid solution up to 5 % and the filtration process was repeated three times for effective salt removal. Retentates were air dried, extracted with pentane to remove free sulfur and extractives (48 h, 5 % consistency) and dissolved in dioxane:water (9:1) solution (1 g/l). Subsequently, residual impurities were removed by filtration through medium sintered glass funnel, and then the solvent was removed under reduced pressure [148]. Dioxane was then removed as detailed in section 3.1.2.3. The resulting solid provided purified lignin samples which were stored in a freeze dried form at (-20°C) until further use. In addition, filtrates of acid precipitated LignoBoost lignin samples (salt fraction) were collected and salts were gravimetrically determined.

3.2.4 Lignin pyrolysis

Pyrolysis of lignin samples (P9.5, P10.5 and APBL) were conducted in a quartz pyrolysis tube heated with a split-tube furnace. Typically, a sample of lignin powder (~ 3.00 g) was placed in a quartz sample boat that was then positioned in the center of a pyrolysis tube. The furnace was preheated to 500 °C, and residence time was 30 min. The pyrolysis tube was flushed with nitrogen gas and the flow rate was adjusted to a value of 500 ml/min. The outflow from pyrolysis was passed through two condensers, which were immersed in liquid N_2. Upon completion of pyrolysis the reaction tube was removed from

the furnace and allowed to cool to room temperature under constant N_2 flow. The condensers were then removed from liquid nitrogen. The pyrolysis char and pyrolysis oil were collected for subsequent chemical analysis. In general, the liquid products contained two immiscible phases referred to as "heavy" and "light". The light liquid phase was acquired by decantation and the heavy liquid phase was recovered by washing the reactor with acetone followed by evaporation under reduced pressure. Char yields were determined gravimetrically and gas formation was calculated by mass difference.

3.2.5 Oxygen delignification (O_2-delig)

Oxygen delignification conditions were: 3.00 g lignin dissolved in 100 ml DI water, containing 1.5 % NaOH, and the mixture was heated to 80 °C for 1 h in a Parr reactor with 100 psi O_2 pressure. The resulting O_2-delig lignin was soluble at neutral pH and was recovered by acidification (pH 3) and filtration.

3.2.6 Ultrasonication combined with peroxide bleaching

Optimal conditions were found to be: 2 w/V% ODW lignin, 1 w/V% H_2O_2, pH set to 12 with NaOH, 40% amplitude, with tapered microtip at 500 Watts, 5 min residence time, and the temperature was kept below 40 °C with water bath (starting T= 18 °C). The resulting ultrasonicated- lignin was the substrate for the fermentations, since it was completely water soluble at pH 7 in the minimal media. The optimal conditions were defined by minimal peroxide use and shorter reaction time to reach water solubility at neutral pH. The experiments used for optimization, and the molecular weights of the resulting lignin are found in Appendix A.

3.2.7 Low molecular weight Kraft lignin separation

Low molecular weight Kraft lignin, was separated from Kraft lignin by pH change, and it is referred to as low M_w Kraft. Briefly, Kraft lignin was dissolved in distilled water at pH 12.0 (set by 2 M NaOH) then pH was decreased accurately till 4.5 (with 2 M H_2SO_4) and the precipitated higher molecular weight part was separated by filtration through a fine sintered glass funnel. The filtrate pH was then adjusted to 3.0 and in the second separation step low M_w Kraft was filtered from solution. pH 4.5 was designated as a good separation point by previous Kraft separation experiments at multiple pH's, as detailed in Appendix B.

3.2.8 Fermentations

In all cases cells (R. opacus PD630 or DSM 1069) were first inoculated into aerobic shaker tubes with 10.00 ml full media, and when the absorbance at 600 nm (OD) reached ~0.6 (after 10 h in general) cells were centrifuged and washed twice with minimal media. Cells were then re-suspended in 10.00 ml minimal media and 0.10-1.50 ml was inoculated into the larger flasks.

Subsequently, in case of model compound experiments (e.g. vanillic acid) adaptation proceeded in minimal media containing 0.1 w/v% nitrogen source and, conclusively from preliminary growth experiments, 0.5 w/v% of the given carbon source. After reaching approximately OD ~1.0 while shaking at 150 rpm and 30 °C, the cells were collected by centrifugation, washed then suspended in lipid accumulation media containing only 0.05w/v% nitrogen source. Samples were acquired in every 12 h for at least 5 days.

With lignin, fermentations were monitored directly, without adaptation, on a daily basis, except for Kraft lignin as detailed in Chapter 6 (low M_w Kraft adaptation). Furthermore bench-top scale fermentation was conducted in a New Brunswick Scientific (Enfield, CT) BioFlo 110 3 l reactor with 2 l loading, at 0.35 w/V% Kraft lignin consistency, using R. opacus DSM 1069 and 0.1 w/V% nitrogen source. Dissolved oxygen (DO) levels were kept constant, ~80 % saturation, by coupling DO measurement to stirring control. Neutral media soluble lignin samples (*us*-EOL, Low M_w Kraft and O_2-Kraft) were filter sterilized prior to fermentation, while insoluble samples were dissolved in high pH (12.0) media, sterile filtered, than pH was readjusted by sterile acid (0.2 M H_2SO_4).

3.3 Analytical procedures

3.3.1 Wood analysis, including carbohydrate, lignin and ash contents

The carbohydrate profile and lignin content were measured as previously described in literature [138]. The untreated and pretreated wood (0.175 g dry weight) was hydrolyzed with 72 % sulfuric acid for 1 h, diluted to 3 % sulfuric acid with water, and then autoclaved at 121 °C for 1 h. Subsequently, the samples were filtered, and the residue was dried and weighed to give the Klason lignin content. The acid-soluble lignin in the filtrate was measured from the absorbance at 205 nm, and the carbohydrates were quantified using high performance anion exchange chromatography with pulsed amperometric detection (HPAEC-PAD). The system used was Dionex ICS-3000 ion chromatography with CarboPactm PA-1 column. The column was set at 23 ºC and eluent A was 100% DI water (18 MΩ-cm) and the eluent B was 200 mM NaOH. The flow rate

was 0.3 ml/min. The ash content was measured by heating the samples at 525 °C in a furnace.

3.3.2 Lignin structural and polymerization properties

3.3.2.1 NMR experiments

All NMR spectral data were recorded with a 400 MHz DMX Bruker spectrometer (Billerica, MA, USA) at room temperature. Spectra were acquired using inverse gated decoupling pulse sequence and 90° pulse. Proton and phosphorous experiment were quantitative, while carbon and HSQC runs were semi-quantitative.

Samples (~100 mg) for ^{13}C NMR runs were dissolved in DMSO-d_6 and spectra were acquired from 6144 scans with 220 ppm sweep width and 5 s pulse delay, and the solvent peak at 39.51 ppm was used for calibration. ^{13}C NMR T_1 times were estimated for all resonances in a representative sample by saturation recovery to optimize the recycle delay and maintain the quantitative nature of the experiment. In spectra analysis integration values of given peaks were compared to the sum area of all peaks, resulting mol % units; or relative to the aromatic region (C-C and C-H signals), resulting "per-aromatic ring" values.

For ^{1}H NMR, the samples were prepared under inert (N_2) atmosphere by dissolving ~25 mg of given heavy oil in 0.7 mL DMSO-d_6 containing 4 mg/ml pentafluorobenzaldehyde (PFB) as internal standard. Spectra were acquired with 16 transients using a 15 ppm sweep width, 10 s pulse delay and calibrated to 2.54 ppm, the DMSO-d_6 peak. Integral values were converted to mmol/g by comparison to PFB.

Samples for ^{31}P NMR analysis (~20 mg) were dissolved in a solution of (1.6:1 v/v) pyridine/$CDCl_3$, containing 3.6 mg/ml chromium acetylacetonate (relaxation agent) and 4 mg/ml endo-N-hydroxy-5-norbornene-2,3-dicarboximide (NHND) as internal standard. Then 2-chloro-4,4,5,5-tetramethyl-1,3,2-dioxaphospholane (TMDP) was added to derivatize hydroxyls. Spectra were acquired from 200 scans with 200 ppm sweep width, 25 s pulse delay and were calibrated to the internal standard peak at 151.9 ppm. Water content analyses were done according to a recently published method.

Conditions for the HSQC analysis were as follows: 13 ppm spectra width in F2 (^{1}H) dimension with 1024 data points (95.9 ms acquisition time), 210 ppm spectra width in F1 (^{13}C) dimension with 256 data points (6.1 ms acquisition time); a 3 s pulse delay; a $^{1}J_{C\text{-}H}$ of 145 Hz; and 32 scans. The central solvent peak (δ_C 39.5 ppm; δ_H 2.5 ppm) was used for chemical shifts calibration. Spectra processing used a typical squared sine apodization in F2 and F1. NMR data were processed using the TopSpin 2.1 software (Bruker BioSpin).

3.3.2.2 GPC (Gel Permeation Chromatography, synonym to SEC- Size Exclusion Chrom.)

Lignin (20 mg) was first acetylated by stirring with acetic-anhydride: pyridine 1:1 (2 ml) at room temperature for 72 hours. The solvent mixture was then removed under vacuum at 50 °C, the acetylated lignin was dissolved in chloroform (50 ml) and washed with deionised water (20 mL). The organic fraction was dried over anhydrous $MgSO_4$ and the chloroform was removed under reduced pressure. The dried acetylated lignin was solved up in tetrahydrofuran (1 mg/ml) and filtered through a 0.45 μm PTFE membrane for analysis. Only the last step was applied as preparation for “heavy-oil” pyrolysis

samples. Then they were injected into a Polymer Standards Service (PSS) Security 1200 system featuring Agilent HPLC parts including refractive index (RI) and UV detectors (270 nm). Separation was achieved on four Waters Styragel columns (HR0.5, HR2, HR4, HR6) using THF as the mobile phase (1.0 ml/min) with injection volumes of 30 µl. Data collection and processing were performed using PSS WinGPC Unity software. Molecular weights (M_n and M_w) were calibrated against a polystyrene calibration curve.

3.3.3 Cell growth, substrate loss and lipid accumulation

3.3.3.1 Growth and living cell number, including lignin separation

In case of model compound experiments, after each sampling, cells were pelleted by centrifugation (supernatants saved) and washed in physiological salt solution twice, then absorbance at 600 nm was recorded (OD) after re-suspension, or the pellets were freeze-dried and cell dry weights (CDW) were recorded to follow cell growth.

When fermenting lignin, after sampling, pH was set to 10.3 (complete solubility of lignin) and Residue-10.3 was separated through centrifugation (8000 rpm, 5 min). Residue-10.3 mainly contains cells (lignin stays in solution), accordingly after freeze drying it represents cell dry weight (CDW), however, the separation from lignin is not assumed to be complete. Subsequently, the supernatant was sterile filtered, and the pH was set to 2.0 for complete lignin separation. The separated Residue-2.0 represents lignin, however, it can contain cellular residues as well, furthermore, due to filtration loss there is a high ±5 % error to this separation. This error was calculated from over 10 different filtrations. Accordingly, lignin losses are only approximations, however, the freeze dried Residue-2.0 was analyzed by NMR for structural changes.

Living cell number was followed by serial dilution and plating (SDP) experiments that were done until 10^8 dilutions, then the results were averaged and converted to colony forming units per ml (CFU/ml). Differences between measurements in general stayed within 20 %, meaning for instance that when on one plate we saw 10 CFUs on the other plate we saw between 8 and 12 at the same dilution.

3.3.3.2 Microscopy

Separated cell suspensions were diluted and 100 μl of them were dried on objective pates, and then fixed with heat. Fixed cells were stained with Sudan B first then counterstained with Safranine O according to published method [263]. Followed by light microscopy with a Leica DMIRM microscope equipped with a digital camera and a Hamatsu ORCA-ER camera controller; pictures were taken using the Simple PCI software.

3.3.3.3 Substrate loss (model compounds)

Ammonium loss was measured semi-quantitatively by EM Quant Ammonium Test (EMD chemicals), that shows 10, 30, 100, 300 and 500 mg/l ammonium ion contents. Glucose and 4-HBA losses were followed by an Agilent 1200 series HPLC set up with a BIO-RAD organic acids analysis column (Aminex HPX-87H), with 10 mmol HNO_3 as eluent at elution rate of 0.6 ml/min, and with a refractive index detector. The same setup was used for VanA analysis except the eluents were 10 w/w% CH_3CN and 0.01 N H_2SO_4 in a half-half mixture, and a multiple wavelength detector was used at 254.16 nm (UV). In all cases external standard series were used with 0.1, 1.0, 5.0 and 10.0 mg/ml concentrations, and R^2 values were calculated to be above 0.985. Lignin was

separated according to the previous point (3.3.3.1) then freeze-dried, and kept under 0 °C until further analysis.

3.3.3.4 Whole cell methanolysis and direct FAME measurements

For transesterification (methanolysis), approximately 6-8 mg of freeze dried cells were dissolved in 1.00 ml $CHCl_3$, 0.85 ml methanol and 0.15 ml concentrated H_2SO_4, then kept at 100 °C for 140 min (obtaining fatty acid methyl esters FAME, from all lipids present). Subsequently, 0.50 ml distilled water was added and the samples were shaken vigorously for 1 min, and after phase separation the organic phase was removed, containing the FAMEs, and stored in freezer until GC measurements [264, 265].

GC-MS measurements for FAME obtained from model compound and EOL experiments (including ultrasonicated EOL), an Agilent 7890A GC system equipped with FID and a Supelco SP-2560 column, specifically designed for FAME, was used. Helium, 19.7 cm/sec, was used as carrier gas and 2 μl samples were split injected (100:1) the oven was 140 °C and kept for 5 min then ramped by 4 °C/min until 240 °C, and kept at final temperature for 15 min. A 37 compound FAME mix from Sigma (47885U) prepared in dichloromethane at 0.5, 1.0, 5.0 and 10 mg/ml concentrations were used as external standards. Accordingly, FAME contents were calculated in mg/ml and these values represent approximate total lipid contents, with a standard deviation of equal or less than 2.88 %. A 5957C Agilent MS detector was also used in EI (70 keV) mode to identify FAMEs not found in the standard mixture. These FAMEs were identified using Agilent's NIST08 library with above 93 % compound m/z spectrum similarity.

In case of Kraft lignin grown then separated and transesterified cell materials the following setup was used; Micromass (now Waters) AutoSpec M mass spectrometer with

a Hewlett-Packard (now Agilent) 5890 GC and a J&W DB-5, 30 m x 0.250 mm column with a 0.250 μm film thickness. The initial temperature of the GC oven was 30 °C, and it was held there for 1 min. The temperature was then ramped at 15 °C/min to 300 °C, and held there for 6 minutes. One μl of sample was injected with a 50:1 split, and the external standards were the same as above. Unknown peaks were identified by their mass/charge (m/z) spectra using the same agilent library as above.

3.3.3.5 Folch-extraction and thin-layer chromatography

Modified Folch extractions were carried out in some instances [266]. Briefly, approximately 50 mg lyophilized cells were suspended in 20 volumes of 2:1 (V:V) chloroform methanol mixture then incubated overnight at 37 °C with shaking. Followed by adding 20 V% sterile physiological salt solution and incubation for 2 more h, then the organic phase was separated and the solvents were removed under reduced pressure [266]. Lipids were dissolved in chloroform at 10 mg/ml concentration for TLC experiments. TLC was carried out using a 80:20:1 (V:V:V) hexane: diethyl ether: acetic acid solvent mixture and iodine vapor as visualization agent, on a silica gel 60 F_{254} (VWR) plate [264]. Standards were palmitic and stearic acids, 1-stearoyl-glycerol, 1-oleoyl-glycerol, 1,3-dimiristoyl-glycerol, 1,2-dipalmitoyl-glycerol, tripalmitoyl-glycerol and 1,3-dipalmitoyl-2-oleoyl-glycerol.

3.3.4 Error analysis

The error associated with the Dionex sugar concentration measurements were below ±1 %. For NMR measurements, multiple spectra were recorded for the same sample and errors were calculated from integral deviations. Resulting errors of: ±4.0 %

semi-quantitative ^{13}C NMR, ±2.0 % quantitative ^{1}H and ±1.8 % quantitative ^{31}P NMR. In case of the GC-MS analysis error was calculated from external standard regressions that never fell below 0.9906 (R^2).

Chapter 4

Characterization of CO_2 precipitated lignin and its pyrolysis[1]

4.1 Introduction

Continuously developing new technologies that allow for a more efficient utilization of resources including biomass is crucial in all industries for reasons like sustainability and higher profit. The pulp and paper industry is also constantly searching for alternative solutions to valorize its Kraft cycle - like the process detailed below- mainly by trying to find ways to recover lignin and sell it as a higher value material.

During chemical pulping lignin is chemically degraded and extracted from wood in aqueous environment in a pressure reactor at pH values of 13-14 and temperatures of 140-170 °C [136]. These conditions remove 85-93% of the lignin and approximately 56-71 % of the hemicelluloses [73, 136]. The approach when NaSH is used in the cooking process along with caustic to delignify wood is referred to as Kraft pulping. In the United States alone the pulp and paper industry collects and processes ~108 million tonnes of pulpwood for the production of pulp, paper and paperboard annually [73]. In turn, the paper industry produces over 50 million tons of residual lignin per year worldwide in a form of a caustic sidestream [73]. Currently, this material is burned in a low efficiency

---

[1] The manuscripts published here were accepted for publication in Green Chemistry. They are entitled as ―Characterization of CO_2 precipitated Kraft lignin to promote its utilization (2010); and –Pyrolysis oils from CO_2 precipitated Kraft lignin (2011). The other authors are Haoxi Ben, Mate Nagy and Arthur J. Ragauskas from the Institute of Paper Science and Technology and School of Chemistry and Biochemistry

1. http://pubs.rsc.org/en/content/articlelanding/2010/gc/b913602a
2. http://pubs.rsc.org/en/content/articlelanding/2011/gc/c1gc15818j

Thompson recovery furnace to recover energy and cooking chemicals. A continuing interest in this field is the desire to recover fractions of lignin from the Kraft cooking liquors for biopower, biochemical and biomaterial utilizations. Recently, a green process referred to as "LignoBoost" provides a viable separation of lignin from these cooking liquors by employing carbon-dioxide to precipitate lignin from alkaline solutions [107, 109, 110, 112, 122]. The application of this process involves acidification of the alkaline cooking liquor with CO_2, precipitation, filtration and washing, Figure 2.17 (Figure 4.1) [118, 120, 124]. Process integration and mill trials have tested this process from an engineering and economic point of view [111, 120, 122].

The lignin recovered by the LignoBoost process has been shown to be valuable green resource for biopower production [113]. This method enables lignin to be exported in the form of a solid biofuel and also gives the opportunity to transform it into materials of higher value [108, 113, 119]. Pyrolysis of lignin is a promising approach that is being investigated to upgrade this macromolecule into low-molecular weight compounds which could be used as higher value products including biofuels and aromatic chemicals [111]. This study reports on the fundamental chemical properties of pyrolysis oils generated from a softwood (SW) Kraft black liquor lignin precipitated with CO_2 at pHs 10.5 and 9.5 (P9.5 and P10.5) and compares this against H_2SO_4 precipitated black liquor at pH 3 (APBL). The chemical components of bio-oil are very complex and only about 40 % could be analyzed by GC [42, 153, 164]. In contrast, NMR has a much higher resolution and provides detailed structural information of the starting lignin [42] and pyrolysis products [111], therefore, in this study, pyrolysis oils were analyzed for elemental composition, molar weight distribution and chemical features by ^{1}H, ^{13}C and ^{31}P NMR.

Results of these experiments, together with literature data, supports lignin pyrolysis as a viable route to from biofuels from LignoBoost extracted BL lignin.

4.2 Experimental section

4.2.1 Lignin precipitation and filtration from BL

Lignin separation from a commercial Scandinavian softwood Kraft pulping liquor was accomplished following published methods [109, 123, 124]. In brief, Kraft cooking liquor (BL) was collected in a reaction vessel then treated with pressurized CO_2 (1500 kPa) [112] until the solution's pH reached 10.5 causing some of the lignin to precipitate. The suspension was subsequently separated by filtration giving a precipitate (P) and a filtrate (F) part (Figure 4.1). This process was done two separate occasions with two different final pHs: 10.5 and 9.5 resulting the following samples: P 10.5, P 9.5 (precipitates) and F 10.5, F 9.5 (filtrates). Solids were obtained from the F and BL solutions by evaporation then all samples were freeze dried and kept frozen until purification [112].

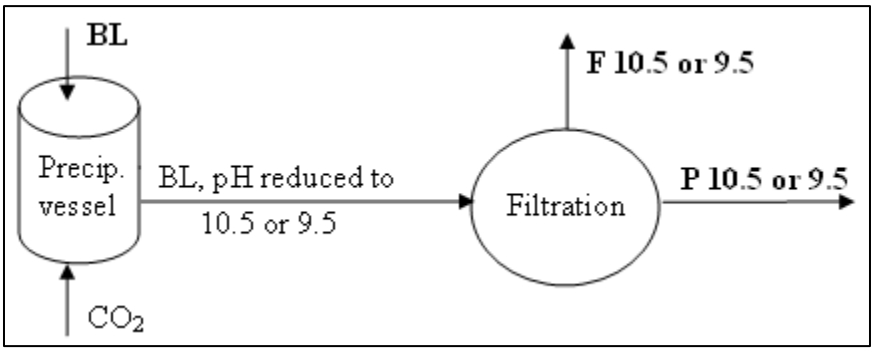

Figure 4.1. Lignin precipitation with CO_2 from black liquor, and filter separation into a filtrate (F) and a precipitate (P) fraction (Figure 2.17)

4.2.2. Sample purification before analysis

Detailed structural analysis of the lignin in the above samples (Figure 4.1) required additional purification. The initial LignoBoost samples (BL, F and P) were diluted in distilled water to 5 % solid content, then the pH was further lowered to a value of 3, facilitating lignin precipitation, as described in Chapter 3 (Appendix A). After precipitation, filtration through medium sintered glass funnel was applied to separate pure lignin (PL) from a crude solids (CS) sample. All filtrates were collected, the solvent was removed under reduced pressure and the remaining solid provided the salt fraction (SF). ^{13}C, ^{31}P, ^{1}H NMR and GPC analyses were only conducted on PL samples (Chapter 3), while all samples were analyzed for elemental composition.

4.2.3 Pyrolysis of lignin samples

Pyrolysis of all purified lignin samples (P9.5, P10.5 and APBL) were conducted in a quartz pyrolysis tube heated with a split-tube furnace. Typically, a sample of lignin powder (~ 3.00 g) was placed in a quartz sample boat that was then positioned in the centre of a pyrolysis tube. The pyrolysis tube was flushed with nitrogen gas and the flow rate was adjusted to a value of 0.5 l/min. The outflow from pyrolysis was passed through two condensers, which were immersed in liquid N_2. Upon completion of pyrolysis the reaction tube was removed from the furnace and allowed to cool to room temperature under constant N_2 flow. The condensers were then removed from liquid nitrogen. The pyrolysis char and pyrolysis oil were collected for subsequent chemical analysis. In general, the liquid products contained two immiscible phases referred to as “heavy” and “light”. The light liquid phase was acquired by decantation and the heavy liquid phase was recovered by washing the reactor with acetone followed by evaporation under

reduced pressure. Char yields were determined gravimetrically and gas formation was calculated by mass difference (Chapter 3).

4.3 Results and discussion

4.3.1 Physicochemical properties of CO_2 precipitated Kraft lignin

Recognizing the possibilities in recovering lignin from black liquor via CO_2 precipitation and washing, the detailed chemical composition and structure of the isolated lignin had become the object of interest; anticipating that structural data could facilitate future applications of this bioresource. Present section reports the characterization of LignoBoost derived lignin in terms of molecular weight profiles and functional group properties.

After purification of the unwashed samples, the lignin content of the initial LignoBoost samples could be determined. The mass balance data showed that the initial unpurified dry samples (CS) had various amounts of lignin as the following (in weight %): 25.8% in BL, 73.3% in P 9.5, 71.3% in P 10.5, 11.1% in F 9.5 and 20.0% in F 10.5. This data clearly shows that treatment of the pulping liquor with CO_2 yields a lignin rich stream and a filtrate fraction that is enriched in salts (Figure 4.2). The pH 9.5 treatment condition resulted in a better separation of lignin. Results of the elemental analysis are consistent with the mass balance data and shows that the purified lignin samples contain only organic elements up to 97.1 % (Figure 4.2).

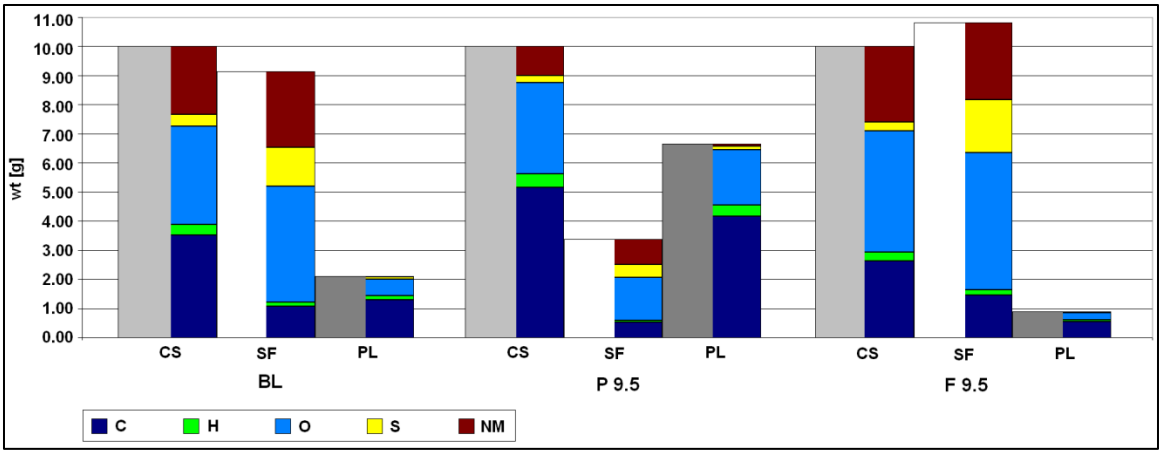

Figure 4.2. Elemental composition of LignoBoost samples (Figure 4.1) separated at pH 9.5 (crude solids- CS). Then further separated/purified into pure lignin (PL) and salt fraction (SF). C-carbon; H- hydrogen; O- oxygen; S- sulfur, and NM- not measured (e.g. cationic part of salts, Na^{+}, Ca^{2+} and Mg^{2+}).

To evaluate the primary components present in the initial LignoBoost fractions and in their purified samples, qualitative ^{1}H and ^{13}C NMR measurements were conducted (Figure 4.3) following literature methods [148, 151, 154]. Qualitative NMR data shows that during the purification step, sugars and fatty acids were removed with salts and salt-EDTA complexes from the initial LignoBoost samples and ended up in the SF. With the lignin purification method used in this study, the chemicals earlier used to bring lignin into solution can be separated from the crude samples. This allows the process chemicals to be returned to the main stream and reused, while it also produces lignin with 95-97% purity, resulting in a higher environmental and economic efficiency.

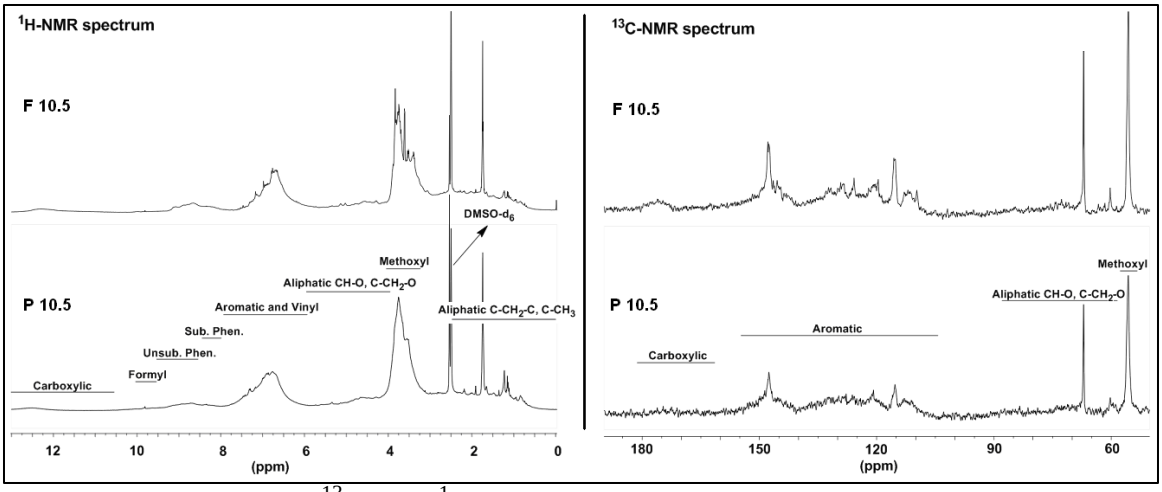

Figure 4.3. Example ^{13}C and ^{1}H NMR spectra of purified, CO_2 precipitated lignin samples (obtained by the LignoBoost process); Sub- substituted; Unsub- unsubstituted

To selectively follow the structural changes of the lignin biopolymer on the molecular level, quantitative ^{1}H NMR measurements were conducted on the purified fractions. The differences between the process fractions and the changes in the distribution of selected lignin moieties at different final pHs are shown in Table 4.1. Quantitative ^{1}H-NMR shows that the F lignin has more carboxylic and phenolic groups while P is enriched in methoxyl moieties. The hydroxyl group content of the lignin plays a crucial role in determining its solubility [136]. Selective phosphitylation of the hydroxyl groups on the lignin polymer with TMDP, followed by quantitative ^{31}P-NMR measurement provides facile monitoring of the changes in the hydroxyl content throughout the process, Table 4.2 [154].

Table 4.1. Partial hydrogen content [mol/mol %] of different lignin functional groups in the ratio of all H containing functional groups as determined by quantitative ^{1}H-NMR

Sample name	Hydrogen content of selected groups (mol/mol % relative to all H cont. groups)						
	Carboxylic acid	**Formyl**	**Phenolic**	**Aromatic, Vinyl**	**Aliphatic**	**Methoxyl**	**Aliphatic**
δ_H [ppm]	(13.50-10.50)	(10.10-9.35)	(9.35-8.00)	(8.00-6.00)	(6.00-4.05)	(4.05-3.45)	(2.25-0.00)
	-C(O)OH	-C(O)H	=HC-OH	CH=CH CH2=CH	CH-O C-CH2-O	-OCH3	C-CH2-C C-CH3
Black liquor	1.26	1.50	6.73	20.22	8.44	45.84	14.42
P 9.5	1.06	0.90	4.19	18.75	5.92	52.42	16.70
P 10.5	0.81	0.98	3.66	19.69	8.22	49.16	16.04
F 9.5	1.71	1.61	6.16	19.82	7.89	41.25	17.35
F 10.5	1.22	1.67	5.73	19.58	6.78	44.58	16.87

Table 4.2. Hydroxyl content of different LignoBoost fractions determined by quantitative ^{31}P-NMR after derivatization with TMDP

Sample name	Total –OH content (µmol/mg)	Hydroxyl content of selected groups (µmol/mg)			
		Aliphatic hydroxyl	**Condensed phenolic**	**Guaiacyl phenolic**	**Carboxylic hydroxyl**
δ_P [ppm]	(149.0-133.8)	(149.0-145.6)	(144.4-140.4)	(140.4-137.6)	(136.0-133.8)
Black liquor	6.37	1.49	1.73	2.46	0.69
P 9.5	4.30	1.11	1.14	1.47	0.59
P 10.5	3.18	0.91	0.85	1.03	0.39
F 9.5	6.74	1.27	1.80	2.55	1.11
F 10.5	5.76	1.22	1.57	2.20	0.78

The pK_a values of phenolic lignin groups fall between 9.4 and 10.8 [112] hence at pH 9.5 and 10.5 these groups get protonated consequently affecting the solubility of the polymer by determining –lowering- its charge. A polymer with a higher total hydroxyl and carboxyl content will have more sites that can stay deprotonated causing better solubility. ^{31}P-NMR results in Table 4.2 confirm the above logic by showing that both hydroxyl and carboxyl contents of F lignins are higher than their analogous P lignins'; this is also consistent with the results from ^{1}H-NMR analysis. F lignins have almost double amount of carboxylic hydroxyl groups that contribute significantly to their ability

to stay in solution despite the decreasing pH. Moreover the quantities of guaiacyl phenolic groups are also almost doubled in F lignins meaning more free hydroxyls compared to their P analogs that most likely contain etherified units in most of these positions.

Changes in the polymer structure of the lignin were followed by molecular mass distribution analysis with GPC on the purified fractions using acetylated lignin samples [107, 112, 154]. Polystyrene equivalent weight average molecular weight (M_w), number average molecular weight (M_n) and polydispersity (PD) were determined using calculation strategies from Baumberger for whole curve integration [267]. M_w/M_n gives PD that directly shows how accurate it is to evaluate a peak as one and not as a sum of multiple peaks. GPC data shows that P samples were enriched in the lower M_W fraction in the 200-300 g/mol region which represents a lignin DP of 1-2 units [73, 84, 154]. Their peaks were recognizable and easy to separate from the main peak resulted from the higher M_w lignin fractions [154, 267]. While on the contrary in case of F and BL samples, no additional peaks were recognizable in the lower M_W region and their GPC curves were integrated as one peak and as a result their respective PD's got 2-3 times larger than in case of the precipitates. These results are consistent with previous research data of Wallmo et al. [112], and table 3 shows all main peak data obtained by GPC. It is noteworthy that polydispersity of all separated lower M_w peaks fell between 1.02 and 1.12 that confirms the validity of the calculation strategy used.

Table 4.3. GPC results of LignoBoost purified lignin samples; polystyrene standards were used with M_w 1200-195000 g/mol

Sample	M_w	M_n	PD
BL	3600	800	4.44
P 10.5	2900	1700	1.73
F 10.5	2700	800	3.42
P 9.5	3000	1800	1.66
F 9.5	2100	700	2.86

In conclusion, the entering BL separates into fraction P which is enriched in lignin and into fraction F which is enriched in salts and also contains some sugars and short chain acids. It is noteworthy that lower final pH resulted in a better lignin separation. SEC data obtained on the purified P phase showed that the fraction is enriched in the ~3000 g/mol -low degree of polymerization (DP) - and in the 200-300 g/mol monomer regions. Quantitative NMR data showed that F contains almost two times the amount of carboxylic and phenolic groups causing its better solubility in water. Low DP together with low quantities of oxygen containing functional groups make both P 9.5 and P 10.5 viable starting feedstocks for future biofuel (or biomaterial) production.

4.3.2 Results of CO_2 precipitated Kraft lignin pyrolysis

4.3.2.1 Mass balance, elemental analysis and molar mass distribution

Acid (APBL) and CO_2 precipitated lignins were pyrolyzed at 500 ^oC and the resulting mass percent yields are summarized in Table 4.4. Pyrolysis resulted in the formation of char, gas and two liquid phases "heavy" and "light". CO_2 precipitated lignins yielded less gas and produced more heavy liquid phase than APBL lignin, indicating good attributes for liquid fuel production. Moreover, the aforementioned lower

density (light liquid) phase is less than that experienced with APBL. It is noteworthy that P10.5 yields slightly less char and more oil than P 9.5.

Table 4.4 Yields of pyrolysis oils, char and gas for APBL and CO_2 precipitated lignins P10.5 and P9.5 at 500 ^oC for 30 min

Sample	Yields of pyrolysis, w %			
	Gas	**Liquid, light phase**	**Liquid, heavy phase: oil**	**Char**
APBL	18.16	10.66	19.23	51.95
P9.5	12.06	5.63	31.31	51.00
P10.5	11.75	5.74	32.66	49.85

Table 4.5 Elemental analysis results of heavy oils in weight percentage, with a standard deviation of 5.58 %

Element	APBL oil	P9.5 oil	P10.5 oil
C	66.4	69.0	68.8
H	6.5	6.6	6.8
O	22.0	22.8	23.2
S	4.7	1.2	1.3

The light liquid phase contained over 80% water in all cases (confirmed by ^{31}P NMR after phosphitylation, according to a published method [46]); accordingly only the heavy liquid phase is referred to as "oil". Elemental analysis (Table 4.5) indicated that the CO_2 precipitated lignin pyrolysis oils contained higher relative percentages of carbon and oxygen, however, significantly less sulfur than APBL. The latter is attributed to the use of NaSH during pulping as well as H_2SO_4 precipitation in case of APBL, a property that makes CO_2 precipitation even more advantageous. The CO_2 precipitated lignin pyrolysis oils contained ~ 1 weight % of sulfur which is much higher than the common liquid fuels – gasoline (0.001-0.08 weight %) and diesel (0.001-0.2 weight %) [268] and lower than

the coal (~1-5 weight%) [269], therefore, further desulfurization of the pyrolysis oils should be investigated before its usage.

Table 4.6. Molecular weight distribution and polydispersity (PD) of different lignins and heavy oils

Sample	M_w, g mol^{-1}	M_n, g mol^{-1}	PD, M_w M_n^{-1}
APBL	2700	700	3.8
P 9.5	3000	1800	1.7
P 10.5	2900	1700	1.7
APBL oil	300	140	2.2
P 9.5 oil	320	160	2.1
P 10.5 oil	320	150	2.1

Number- and weight-average molecular weights (M_n and M_w), and polydispersity (PD) values of the starting lignin and product oils are presented in Table 4.6. Results indicate that both LignoBoost lignins and its pyrolysis oils have slightly larger molecular weights than APBL and its corresponding oils, although this difference is less than 10%.

4.3.2.2 NMR analysis

4.3.2.2.1 ^{13}C NMR

The chemical features of the pyrolysis oils were first investigated by ^{13}C NMR and these results are shown in Table 4 with integration regions consistent with previous reports for both lignins and pyrolysis oils [42, 115, 145-151, 160]. The typical ^{13}C NMR spectra for the heavy oils produced by the pyrolysis of APBL and CO_2 precipitated lignins are shown on Figure 4.4. Some of the main pyrolysis reaction routes based on literature [42, 163, 164, 204-216] were further confirmed by NMR results, and the proposed pathways are shown on Figure 4.5. Numbers assigned to molecules on Figure 4.5 are used in brackets in the text.

^{13}C NMR shows multiple trends including some that are specific to sources of origin, revealing unique characteristics of oils obtained from the different lignin sources [42, 115, 145-151, 160]. In the case of all starting lignins, the most significant trend is the increase in aliphatic C-C content after pyrolysis, (Table 4.7), which is accompanied mostly by decreases in aromatic C-C substitutions, aliphatic C-O bonds (e.g. ether, hydroxyl) and methoxyl contents. In particular, the P10.5 shows a remarkable ~30% decrease in aromatic C-C substitutions while gaining approximately the same amount more aliphatic C-C bonds. Accordingly, the sum aromatic carbon content (including Ar-C-O, C-C and C-H) is only around 60 % in P10.5 pyrolysis oil whereas the others are ~70%. Literature results suggest that the pyrolysis of lignin could lead to the formation of toluol, methyl-guaiacols (4), xylenes and cresols (20) (Figure 4.5) [42, 164, 204, 209-212, 214-216] which is consistent with the observed chemical shifts [e.g. methyl-anisole (b) at approximately 15 and toluol (a) at ~21 ppm] shown on Figure 4.4 [42, 164]. Consequently, CO_2 precipitated lignin pyrolysis oils will contain more methyl-guaiacol (4) and toluol aliphatic groups than APBL oil.

According to molar percentages in Table 4.7, the relative decrease in aromatic C-C substitutions is most likely not the only source for the observed increase in aliphatic carbon, especially in case of APBL and P9.5. Aliphatic C-O and methoxyl group rearrangements are also probable sources of aliphatics. These reactions are detailed in the literature [42, 204, 206, 209-212], supported by both ^{13}C and ^{1}H NMR results (Table 4.8), and are shown on Figure 4.5 (6 to 6a and 19 to 20). The decrease in methoxyl groups is most likely due to the release of methyl radicals (from 9 to 10) and 1,2-phenyl shifts [204, 206] (from 13 to 19 on Figure 4.5) [42, 163, 204, 206]. It is also noteworthy that

P10.5 lignin yields oil with more vinyl content (6) (also supported by ^{1}H NMR, Table 4.8) as well as aromatic C-O bonds, (also supported by ^{31}P NMR, Table 4.9) due, most likely, to more phenolic groups.

Table 4.7 ^{13}C NMR chemical shift assignment ranges and functionality contents of lignin and pyrolysis oils, as compared to total carbon content in mol %

Functionality	Range, ppm		Lignins and Pyrolysis oils, mol % of total carbon					
	lignins	Oils	APBL	P9.5	P10.5	APBL oil	P9.5 oil	P10.5 oil
Carbonyl C=O	215.0-162.5	215.0-166.5	0.0	4.2	3.0	0.8	1.0	1.4
Aromatic C-O	155.0-145.0	166.5-142.0	22.5	19.9	19.9	17.4	17.6	19.2
Aromatic C-C	140.0-123.0	142.0-125.0	28.6	27.8	28.4	22.2	17.0	9.2
Aromatic C-H	123.0-106.0	125.0-95.8	24.7	23.1	23.8	33.3	35.8	32.3
Aliphatic C-O	90.0-57.7	95.8-60.8	8.3	11.1	5.8	0.0	0.2	0.4
Methoxyl OCH_3	57.5-54.0	60.8-55.2	11.8	14.0	14.6	5.9	7.2	8.1
Aliphatic C-C	49.0-0.0	55.2-0.0	4.1	0.0	4.6	20.4	21.2	29.5

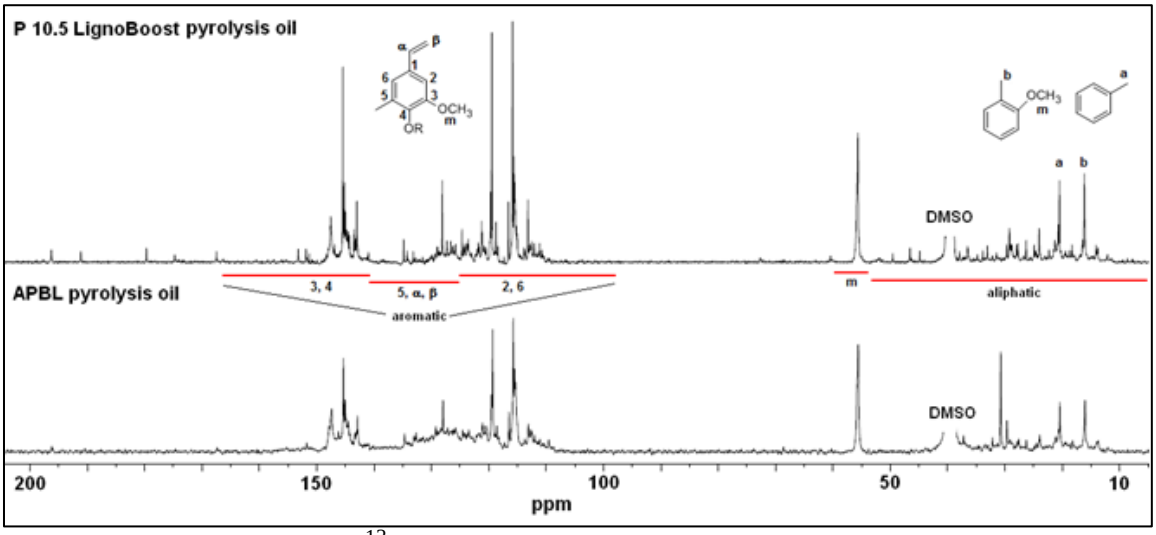

Figure 4.4. Quantitative ^{13}C NMR spectra for heavy oils produced by pyrolysis of APBL (bottom) and LignoBoost P 10.5 (top); with assignments for main regions and peaks of most abundant compounds. as compared to total carbon content in mol %

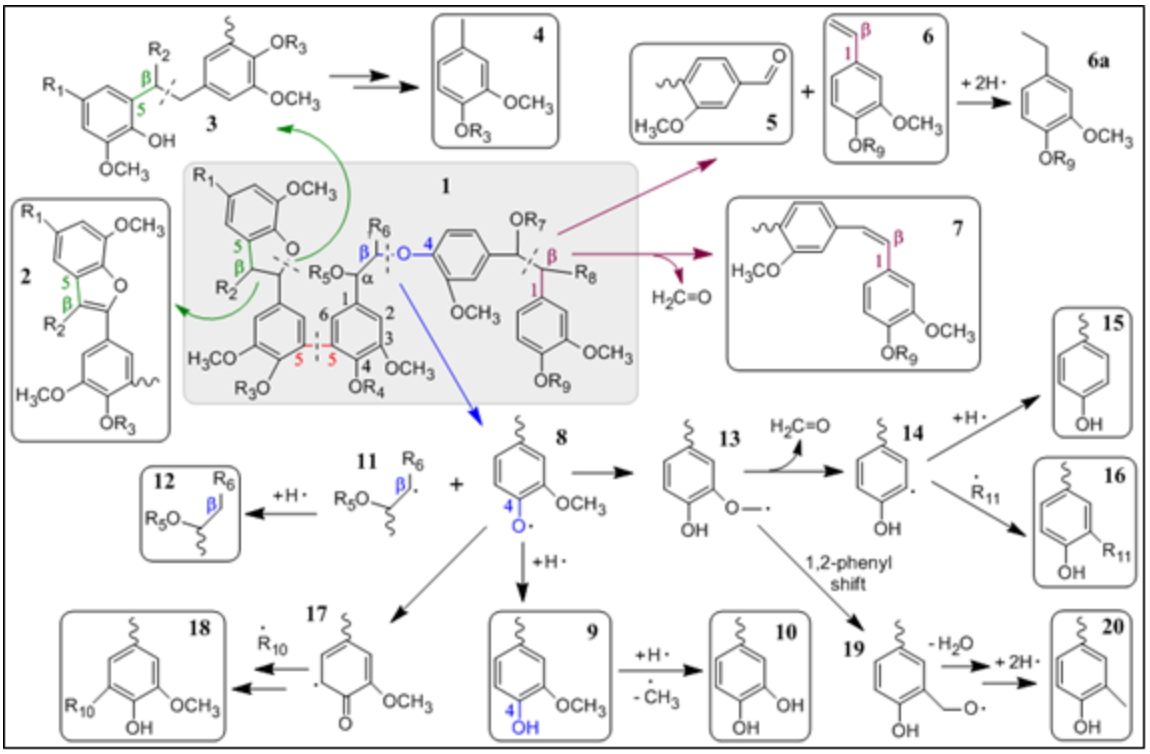

Figure 4.5. Lignin structure dependent pyrolysis reactions as predicted by literature and present NMR results, with emphasis on LignoBoost lignin pyrolysis. 1 hypothetical lignin source representing the most common bonds in LignoBoost and APBL; 2 relatively stable β-5 product in the primary decomposition step [214]; 3 α-O cleavage product; 4 methyl guaiacols; 5 aldehydes; 6 styrenes and 6a ("reduced vinyl-") ethyl-phenols; 7 stilbenes; 8 phenoxy radicals; 9 guaiacols; 10 catechols; 11, 13, 14, 17, 19 transient radicals; 12 aliphatics; 15 phenols; 16, 18 condensation products (e.g. 4-O-5 dimers); 20 cresols. Question mark shows possible 5-5 bond breakage, detailed in the ^{31}P NMR section. R_1 cinnamyl group (propanoid unit); R_2, R_6, R_8 γ carbons in cinnamyl groups; $R_{3\text{-}5}$, R_7, $R_{9\text{-}11}$ H, CH_3 or whole phenylpropanoid units/macromolecules

4.3.2.2.2 ^{1}H NMR

Proton NMR was used to gain supporting information on the aliphatic structures of pyrolysis oils (chemical shifts are consistent with literature [146-148, 151, 154-158]), it showed in all cases that the contribution of α-carbon attached hydrogens on aromatic rings, appearing at chemical shift between ~3.0-1.9 ppm [156, 157] (Table 4.8), represent

the highest proportion protons comprising the aliphatic hydrogen content (Figure 4.4 and 4.5) [156, 157]. Although ^{1}H NMR of the oils show only slight increase in aliphatic H content (Table 4.8), P10.5 represents an exception, confirming its unique nature in forming aliphatics when pyrolyzed. ^{1}H NMR also shows (Table 4.8) that there is a definite reduction in aromatic/vinyl hydrogen content after pyrolysis. It is most likely caused by the elimination of different substituents from the aromatic rings that are then replaced by hydrogens, while vinyl side-chains (from 6 to 6a, Figure 4.5) [42, 204, 206] are reduced.

Table 4.8. ^{1}H NMR chemical shift assignment ranges and functional group contributions for lignins and pyrolysis oils, oils contained between 0.2-0.78 % moisture, while the solvent itself had 0.02±0.01 %

Functionality	**Range, ppm**	**Lignin and pyrolysis oil functional group contributions, mmol/g**					
		APBL	**P9.5**	**P10.5**	**APBL oil**	**P9.5 oil**	**P10.5 oil**
Aldehyde, formyl	10.0-	1.5	0.9	0.98	0.29	0.34	0.38
Aromatic, vinyl	8.2-6.0	20.22	18.75	19.69	12.1	11.31	13.76
Methoxyl	4.2-3.0	45.84	52.42	49.16	7.36	12.57	11.23
Aliphatic	3.0-0.5	14.42	16.7	16.04	16.39	17.18	20.87

4.3.2.2.3 ^{31}P NMR

^{31}P NMR was used to precisely determine alterations in hydroxyl contents [42, 46, 115, 147, 152, 154, 164, 168, 169, 171, 172]. APBL's acidic and phenolic hydroxyl contents are higher than both CO_2 precipitated lignins'. This was attributed to the higher precipitation pH applied in latter cases which results in precipitating selectively lower hydroxyl content lignin pulping fragments. Results in Table 4.9 show some interesting trends, one of them being the increase in all non-substituted phenol contents after pyrolysis of all sources due to degradation of the macromolecules and conversion of

guaiacols (9) to catechols (10) and phenols (15), according to the literature [42, 204, 206, 209-212]. Another trend is the increase of 4-O-5 and β-5 units, particularly in CO_2 precipitated lignin pyrolysis oils, while there is a decrease in recalcitrant 5-5 bonds, that is also observed previously [42] at higher temperatures. The only literature mentioning the behaviour of 5-5 model dimers found no degradation at 400 °C [212]. A possible explanation can be the breakage of the bond between the aromatic units (Figure 4.5, red bond), however, more it is more plausible that the phenolic groups become phenoxy radicals (8) and react with other radicals to form ether bonds that ^{31}P NMR won't be able to detect (no hydroxyls present). The observed loss of methoxyl groups (by ^{13}C and ^{1}H NMR, Tables 4.7-8) is possibly due to elimination and rearrangement reactions and will contribute to catechol (10) and phenol (15) formation from guaiacols (9) (Figure 4.5) [42, 204, 206]. This is well supported by ^{31}P NMR results (Table 4.9) showing that most of the phenolic hydroxyls come from catechols (10), guaiacols (9), and p-hydroxy phenols (15). Catechols (10) are responsible for almost half of all phenolic groups, indicating that they are dominant pyrolysis products [42, 153, 164, 202, 204, 206]. CO_2 precipitated lignin derived oils have even higher catechol and *p*-hydroxy phenyl contents than APBL, but contain less guaiacols. These results indicate that guaiacol conversion towards other phenols is more efficient during CO_2 precipitated lignin pyrolysis, due possibly to substituent effects at aromatic positions 3 and 5 (Table 4.9, Figure 4.5) [204, 209-212, 214, 216]. It is noteworthy, that although the liquid light phase contains too much water for fuel applications, ^{31}P NMR [46] showed ~85-95 % water and trace amounts of methanol, ethanol, catechols and acetic acid [42, 46].

Table 4.9. ^{31}P NMR integration regions and hydroxyl contents (mmol/g) for pyrolysis oils and lignins derivatized with TMDP

Functionality		Range, ppm	Lignin and pyrolysis oil hydroxyl contents, mmol/g					
			APBL	P9.5	P10.5	APBL oil	P9.5 oil	P10.5 oil
Aliphatic OH		150.0 - 145.5	0.83	1.11	0.91	0.25	0.33	0.29
5-substituted phenolic	**β-5**	144.7 - 142.8	0.43	0.21	0.17	0.41	0.48	0.47
	4-O-5	142.8 - 141.7	0.34	0.14	0.11	0.45	0.54	0.56
	5-5	141.7 - 140.2	0.63	0.78	0.56	0.45	0.47	0.42
Non-substituted phenolic	**Guaiacyl**	140.2 - 139.0	1.49	0.64	0.47	1.56	1.34	1.32
	Catechol	139.0 - 138.2	0.12	0.83	0.56	2.82	3.08	3.16
	p-hydroxy-phenyl	138.2 - 137.3	0.14	0.00	0.00	0.87	0.97	0.98
Acid OH		136.6 - 133.6	0.75	0.59	0.39	0.36	0.48	0.5
Total phenolic		144.7-137.3	3.15	2.6	1.87	6.56	6.88	6.91
Total OH		150.0-133.6	4.73	4.3	3.17	7.17	7.69	7.7

4.4 Conclusions

Kraft-cycle derived lignins (CO_2 and acid precipitated black liquor) were pyrolyzed and the resulting oils were analyzed to obtain information on both their properties and pyrolysis behavior. These lignins contain only small amounts of α-O- and β-O-ether linkages due to degradation by pulping chemicals [88]. In accordance the major lignin inter-unit linkages are β-5, 5-5 and other minimally represented bonds e.g. β-1 (Figure 4.5) as shown in the literature and present work [42, 147, 150]. According to the literature, during pyrolysis the remaining ether linkages will be the first to degrade [204, 206, 209-212, 214, 216] starting as low as 250 °C if phenolic groups are present as well [216], together with aliphatic hydroxyl, carboxyl and aromatic-methoxyl groups (Tables 7-9 and Figure 4.5) [42, 204, 206]. Guaiacyl hydroxyls, aldehydes, toluols and styrenes are the primary cleavage products, while p-hydroxy-phenols, catechols and cresols are products of further decomposition (Figure 4.5) [42, 164, 204, 206, 209-212, 214, 216] as confirmed by NMR spectroscopy in present study. Proposed β-5 degradation

is also indicated by ^{31}P NMR, producing β-5 and methyl-guaiacol products (Figure 4.5) [214]. It is noteworthy, that different sources which proceed through multiple pathways can result in a similar product mixture (e.g. aldehydes can be products of α-O-4, β-O-4 and β-1 cleavages as well, Figure 4.5) [42, 204, 206, 209-212, 214-216]. Considering this issue, NMR results have to be used only to support theoretical reaction routes, however, they proved to be great tools in pyrolysis product analysis as well.

Pyrolysis oil yields from CO_2 precipitated lignins exceeded APBL oil yield with over 30 % and ^{13}C, ^{1}H and ^{31}P NMR experiments showed the following differences. Oils from CO_2 precipitated lignins have more aliphatic compounds and this effect is significant with P10.5 (close to 30 %). These aliphatics are methyl and ethyl substituents on aromatic compounds such as phenol or anisole. It was also observed that CO_2 precipitated lignin pyrolysis oils will have more catechols and *p*-hydroxy phenols, while APBL based oils will be richer in guaiacols indicating that rearrangement reactions are more readily occurring in former lignins during pyrolysis. Furthermore, differences between CO_2 precipitated lignin and pyrolysis oil β-5 and 4-O-5 phenol contents are more significant (4-5 times increase) than in respective APBL materials (~20 % gain). This was attributed to the higher precipitation pH applied in former cases which could selectively precipitate lignin fragments that pyrolyze easier. Above results support the applicability of CO_2 precipitated black liquor lignins for pyrolysis (high yields), as well as the utilization of the obtained oils as liquid biofuels due to their low molecular weights and advantageous changes in composition, such as increased aliphatic and low oxygen contents.

Chapter 5

Lignin model compound to lipid bioconversion with oleaginous *Rhodococci*[2]

5.1 Introduction

The gradual worldwide acceptance and responsibility for environmental issues will most likely be one of the greatest achievements of the 21st century. Response to these global problems has to be well organized and locally coordinated effort depending on the sustainable resources of the given area. Where biomass is abundant the biorefinery concept can be an ingenious and economically feasible way to meet energy, material and employment demands, given that a diverse number of high-value products can be generated from biomass [2-4]. Lignin, next to sugar polymers, is a major cell wall component with a recalcitrant, three dimensional polyaromatic structure and a chemical composition that highly depends on species, origin and soil and environmental growth conditions [2]. These properties limit lignin's potential as a valuable bioenergy and/or biomaterial resource; and while its thermochemical conversion, such as pyrolysis, has recently drawn substantial attention [2, 9, 42, 188], its bioconversion is almost exclusively restricted to fungal biopulping [270] and biobleaching [218]. On the other hand, lignin is produced in considerable quantities, for instance ~50 million tons per year by the US paper industry [10]. This lignin is of great interest, not just because it can be a

---

[2] The manuscript published here was accepted for publication in Applied Microbiology and Biotechnology. It is entitled as ―Bioconversion of lignin model compounds with oleaginous *Rhodococci* (2012). The other author is Arthur J. Ragauskas from the Institute of Paper Science and Technology and School of Chemistry and Biochemistry at Georgia Institute of Technology.

readily available feedstock, mostly by acid precipitation from pulping liquor [9, 10], but also because its large quantities in these liquors limit chemical recovery, creating a bottleneck in the Kraft cycle [10]. Moreover, different pretreatment methods, such as the ethanol organosolv process, can also provide high purity lignin as a side product of cellulosic ethanol production [30, 39].

Bacterial species are also capable of aerobic digestion of lignin resembling aromatic compounds, through the β-ketoadipate pathway [11]. Coincidentally, some of these bacteria belong to the actinomycetes [11, 12] group that has also been shown to accumulate lipids [271]. The Gram positive species of soil dwelling *Rhodococcus* is of particular interest. Initial work proved that *R. opacus* DSM 1069 can grew on coniferyl alcohol and other lignin model compounds as sole carbon sources [261]. Later, different *Rhodococci* were shown to be oleaginous [271]. *R. opacus* PD630 was intensely investigated for its high, sometimes over 80 % [264], lipid accumulation that exceeds the limit of oleaginicity at 20 % [14]. This strain was also grown on aromatic compounds, such as phenylacetic acid, and proved to be oleaginous [272], however, it was yet to be tested with lignin model compounds and lignin itself [2, 15]. The prokaryotic β-ketoadipate pathway has been well studied, however since the last major review [11]; more information has been revealed on its genetic background, regulation and enzymes, as well as practical utilizations. For instance interesting work has focused on Gram positive: *Bacillus* [273], *Corynebacterium* [274, 275], *Mycobacterium* [276], *Rhodococcus* [277] and *Streptomyces* [278]; and Gram negative species: *Acinetobacter* [279], *Agrobacterium* [280] and *Pseudomonas* [281], using this pathway for the degradation of aromatic compounds. Moreover bacterial lipid accumulation and the

origin of oleaginicity were recently investigated [15, 271], finding considerable overlaps between β-ketoadipate pathway using and oleaginous bacteria [2, 15]. Select species, namely: *Acinetobacter baylyi* [279, 282], *Rhodococcus opacus* [2, 13, 15] and *Streptomyces coelicolor* [278, 283], have gained special attention, not just as a consequence of their possible lignin to lipid bioconversion capabilities, but also because of high lipid accumulation and existing cloning techniques [15, 279, 282].

The present study investigates lipid accumulation in *R. opacus* DSM 1069 and PD630 strains when only lignin model compounds are present as carbon sources and nitrogen limiting conditions are applied to induce fat reserve build up. The hypothetical metabolic route from lignin like aromatics to neutral lipids is depicted on Figure 5.1 (part of Figure 2.24) [11, 15, 277], showing the starting materials that were used in this study: 4-hydroxybenzoic (4-HBA), vanillic (VanA) and syringic (SyrA) acids. These model compounds represent p-coumaryl (H), coniferyl (G) and sinapyl (S) alcohols as components of grass (G and H; [6]), softwood (SW: G and minor H; [2]) and hardwood (HW: G, S and minor H; [2]) lignins respectively (Capter 2, Section 2.3). Detailed analysis of substrate loss and product formation over time revealed distinct properties for the two different strains that can be harnessed in the future for specific fatty acid needs in biodiesel production or other value-added applications.

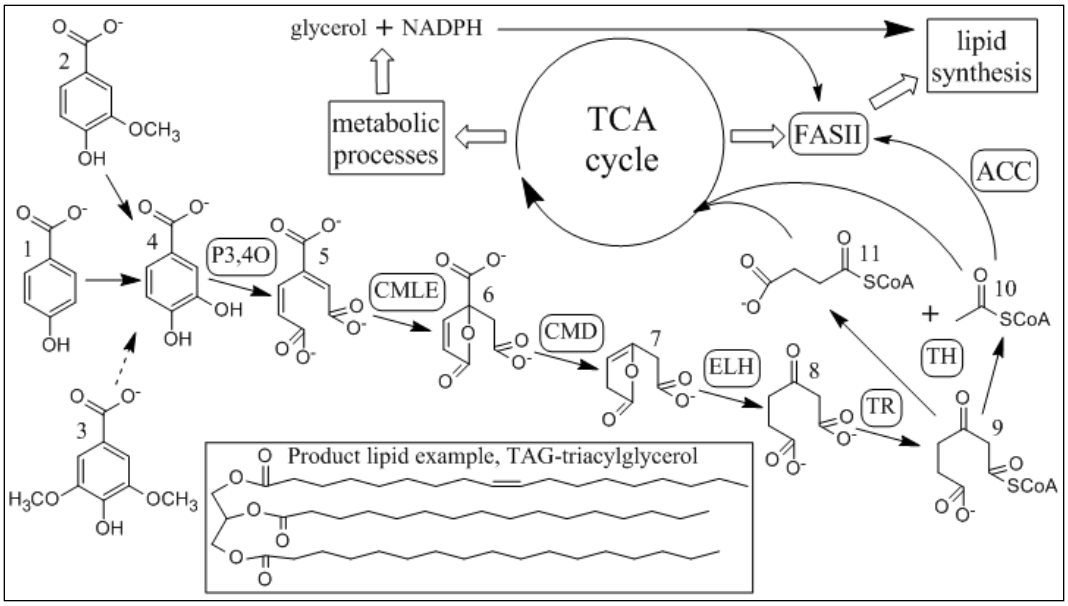

Figure 5.1. The protocatechuate (4) branch of the bacterial β-ketoadipate (8) pathway, including funneling pathways from 4-HBA (1), VanA (2) and SyrA (3). (5) β-carboxymuconate; (6) γ-carboxymuconolactone; (7) β-ketoadipate enol-lactone; (9) β-ketoadipyl-CoA; (10) acetyl-CoA and (11) succinyl-CoA. Enzymes in rounded rectangles are: P3,4O, protocatechuate 3,4-dioxygenase; CMLE, β-carboxy-*cis*-*cis*-muconate lactonizing enzyme; CMD, γ-carboxymuconolactone decarboxylase, ELH, enol-lactone hydrolase; TR, β-ketoadipate:succinyl-CoA transferase; TH, β-ketoadipyl-CoA thiolase; ACC, acetyl-CoA carboxylase and FASII, bacterial fatty acid synthase. Part of Figures 2.24 and 2.34 as well

The lower part of Figure 5.1 shows a theoretical path of lignin model compound conversion into succinyl- (11) and acetyl-CoA (10) by *R. opacus* strains as hypothesized from the literature of other species' enzymatic activities. First protocatechuate 3,4-dioxygenase (P3,4O) ruptures the aromatic ring, most likely, by using a non-heme Fe^{3+} complex to coordinate molecular oxygen incorporation, as investigated in *Acinetobacter* strain ADP1 [248] and *Pseudomonas putida* [246], creating β-carboxymuconate (5). The second step, as predicted from the literature, is an *anti*-1,2-addition-elimination reaction catalyzed by carboxymuconate lactonizing enzyme (CMLE) to form β-carboxymuconolactone (6) as researched in *P. putida* [247] and *Agrobacterium*

radiobacter S2 [243]. At this point, as hypothesized, β-carboxymuconolactone decarboxylase (CMD) activity results an enol-lactone (7) product that is further converted to β-ketoadipate (8) by enol-lactone hydrolase (ELH), with former enzyme's reaction mechanism investigated in *Acinetobacter calcoaceticus* and *P. putida* [241], while latter reaction was predicted in *Burkholderia xenovorans* LB 400 [240]. It is important to emphasize, that although the β-ketoadipate pathway is highly conserved these last two steps are most likely merged in *R. opacus* 1CP under one enzyme's activity [242]. It can also be predicted from literature that in the final steps β-ketoadipate (8) is possibly converted into β-ketoadipyl- (9) then succinyl- (11) and acetyl-CoA (10) by transferase (TR) and thiolase (TH) activities respectively [11]. Subsequently, the anabolic action of acetyl-CoA carboxylase (ACC), fatty acid synthase II (FASII) and other metabolic processes can result lipids as shown on the top of Figure 5.1 [15].

5.2 Experimental section

5.2.1 Shake tube and flask fermentations

In all cases cells were first inoculated into aerobic shaker tubes with 10.00 ml full media, and when the absorbance at 600 nm (OD) reached ~0.6 (after 10 h in general) cells were centrifuged and washed twice with minimal media. Cells were then re-suspended in 10.00 ml minimal media and 0.10-1.50 ml was inoculated into the adaptation flasks. Subsequently adaptation proceeded in minimal media containing 0.1 w/v% nitrogen source and, conclusively from preliminary growth experiments, 0.5 w/v% of the given carbon source. After reaching approximately OD ~1.0 while shaking at 150 rpm and 30 °C, the cells were collected by centrifugation, washed then suspended in lipid

accumulation media containing only 0.05 w/V% nitrogen source [264]. Samples were acquired in every 12 h for at least 5 days.

5.2.2 Analysis

5.2.2.1 Growth and living cell number

After each sampling, cells were pelleted by centrifugation (supernatants saved) and washed in physiological salt solution twice, then absorbance at 600 nm was recorded (OD) after re-suspension, or the pellets were freeze-dried and cell dry weights (CDW) were recorded to follow cell growth. To follow the living cell number, serial dilution and plating (SDP) experiments were done until 10^8 dilution, then the results were averaged and converted to colony forming units per ml (CFU/ml). Differences between measurements in general stayed within 20 %, meaning for instance that when on one plate we saw 10 CFUs on the other plate we saw between 8 and 12 at the same dilution.

5.2.2.2 Substrate loss

Ammonium loss was measured semi-quantitatively by EM Quant Ammonium Test (EMD chemicals), that shows 10, 30, 100, 300 and 500 mg/l ammonium ion contents. Glucose and 4-HBA losses were followed by an Agilent 1200 series HPLC set up with a BIO-RAD organic acids analysis column (Aminex HPX-87H), with 10 mmol HNO_3 as eluent at elution rate of 0.6 ml/min, and with a refractive index detector. The same setup was used for VanA analysis except the eluents were 10 w/w% CH_3CN and 0.01 N H_2SO_4 in a half-half mixture, and a multiple wavelength detector was used at 254.16 nm (UV). In all cases external standard series were used with 0.1, 1.0, 5.0 and 10.0 mg/ml concentrations, and R^2 values were calculated to be above 0.985.

Qualitative ^{1}H NMR analyses were conducted by adding 0.50 mL deuterated DMSO to 1.00 mL of the prepared HPLC sample, then running a proton analysis. NMR spectral data were recorded with a 400 MHz Avance Bruker spectrometer (Billerica, MA, USA) at room temperature. Spectra were acquired using 90° pulse angle, from 8 transients using 15 ppm sweep width, 2.5 s pulse delay and calibrated to 2.54 ppm, the DMSO-d_6 peak.

5.2.2.3 Lipids

5.2.2.3.1 Transesterification

Approximately 6-8 mg of freeze dried cells were dissolved in 1.00 ml $CHCl_3$, 0.85 ml methanol and 0.15 mL concentrated H_2SO_4 for transesterification at 100°C for 140 min. Subsequently, 0.50 mL distilled water was added and the samples were shaken vigorously for 1 min, and after phase separation the organic phase was removed, containing the FAMEs, and stored in freezer until GC measurements (Chapter 3).

5.2.2.3.2 GC-MS

An Agilent 7890A GC system equipped with FID and a Supelco SP-2560 column, specifically designed for FAME, was used for measurements. Helium, 19.7 cm/sec, was used as carrier gas and 2 μl samples were split injected (100:1) the oven was 140 °C and kept for 5 min then ramped by 4 °C/min until 240 °C, and kept at final temperature for 15 min. A 37 compound FAME mix from Sigma (47885U) prepared in dichloromethane at 4 and 10 mg/mL concentrations were used as external standards. Accordingly, FAME contents were calculated in mg/ml and these values represent approximate total lipid contents, with a standard deviation of equal or less than 2.88 %. A 5957C Agilent MS

detector was also used in EI (70 keV) mode to identify FAMEs not found in the standard mixture. These FAMEs were identified using Agilent's NIST08 library with above 93 % compound m/z spectrum similarity.

5.3 Results and discussion

5.3.1 Preliminary experiments

Rhodococcus opacus DSM 1069 and PD630 were both previously grown on aromatic compounds such as phenyl acetic acid, however, on most substrates their growth were poor and/or lipid accumulation was not reported [261, 264, 272, 284]. Consequently, small scale, preliminary fermentations were conducted to evaluate adaptation and growth conditions for both strains on all three substrates (4-HBA, VanA and SyrA), at different concentrations from 0.2 to 1.0 w/v%. Aerobic shaker tubes containing 10 ml minimal media with 0.1 w/v% nitrogen source and variable amounts of given carbon sources were inoculated with 0.1 ml cell suspension according to materials and methods. Subsequent growth was monitored by cell dry weight (CDW) and serial dilution and plating (SDP; living cell number) measurements with results shown in Table 5. 1.

Table 5.1. Growth of two *R. opacus* strains on substrates 4-HBA and VanA. 0.5 w/V% concentrations proved to provide the best growth. SyrA is not shown because of poor performance independent of concentration.

Strain	4-HBA at 0.5 w/v%			VanA at 0.5 w/v%		
	lag [h]	exp. growth	t [h] to OD 1.0	lag [h]	exp. growth	t [h] to OD 1.0
DSM 1069	20	$0.032e^{0.126t}$	27	32	$0.004e^{0.127t}$	44
PD 630	20	$0.141e^{0.073t}$	27	20	$0.027e^{0.110t}$	35

R. opacus PD630 performed better on VanA, however, both strains showed significant growth after an approximately 20-30 h lag (adaptation) phase. As shown in Table 1 the exponential growth phase can be best described with a growth function where OD is plotted as a function of time. In this phase the function can be described with a general equation of:

$$OD = A \cdot e^{B \cdot t} \qquad (13)$$

In equation (13) parameters A and B are strain and substrate specific constants and t represents the hours of growth in the exponential phase (after lag). Table 5.1 also shows the time needed to reach OD 1.0, which represents approximately 10^7 CFU/ml living cells in all cases (mid-exponential phase). The strains were growing less efficiently at 0.3 and 1.0 w/v% substrate concentrations (4-HBA, VanA), and they only showed measureable growth on SyrA at 0.2 w/v%. In the latter case, lag phases were at least 20 and 44 h for DSM 1069 and PD630 respectively, subsequently reaching the maximum of OD 0.2-0.25 and 10^5-10^6 CFU/ml and not growing further. Although DSM 1069, in general, adapted faster to the different lignin model compounds, PD 630 had steeper exponential growth after its longer lag phase. These experiments provided enough

information to design larger scale shake flask fermentations to investigate lipid accumulation.

5.3.2 Shake flask fermentations

Shake flask fermentation experiments were designed to support reserve lipid accumulation by separating adaptation and growth from TAG anabolism. First cells were grown in high nitrogen (0.1 w/v%) minimal media, then centrifuged, washed and transferred to low nitrogen media (0.05 w/v%) after reaching an OD of 1.0. Accordingly the C:N ratio changed from 5:1 to 10:1 between the two fermentation phases, with already significant cell concentrations. Figure 5.2 compares growth and lipid accumulation of *R. opacus* DSM 1069 and PD630 on 4-HBA and VanA after inoculation to low nitrogen media.

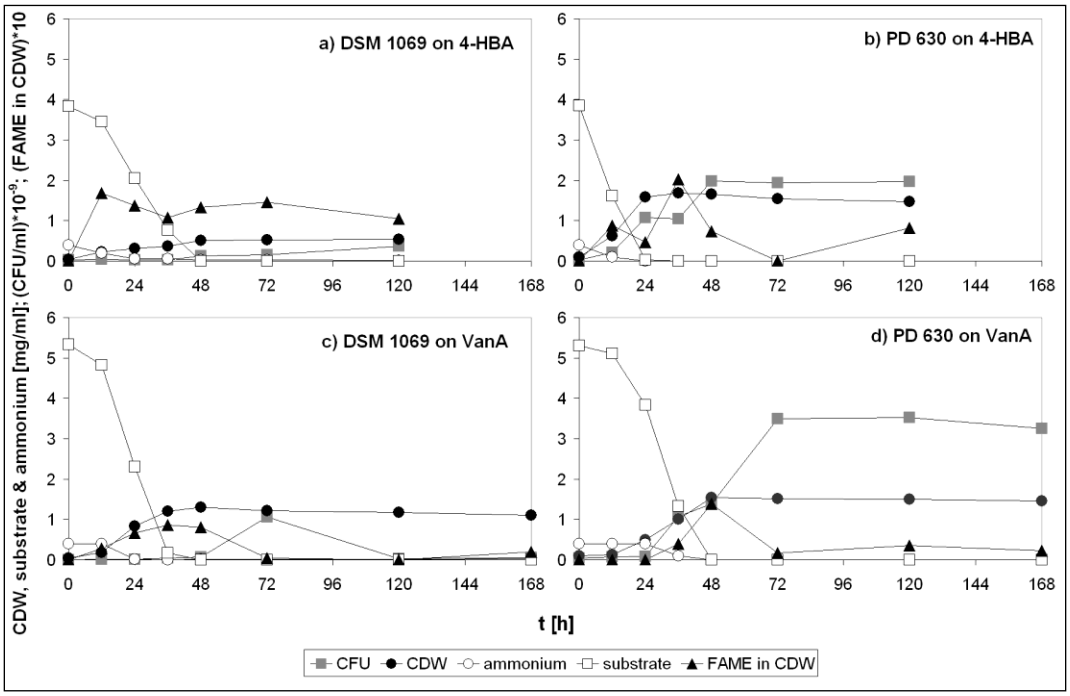

Figure 5.2. *R. opacus* DSM 1069 and PD630 growing on 0.4-0.5 w/v% 4-HBA and VanA in 0.05 w/v% nitrogen source media. CDW, carbon source and ammonium concentrations are given in mg/ml units, while living cell

numbers are shown in (CFU/ml)*10^{-9} and fatty acid methyl ester (FAME) content in (FAME [mg/ml]/CDW [mg/ml])*10 special units to allow representations on the same chart.

An interesting trend can be observed from Figure 5.2.a and c, namely the nitrogen source independence of *R. opacus* DSM 1069's lipid accumulation. This strain has never been shown to be oleaginous, however, when grown on 4-HBA it reached 16.8 % of CDW in FAME (Figure 5.2.a) generating a result that is very close to oleaginicity, after only 12 h. On the other hand, the observed ammonium concentration independence might be apparent, since the above experiments only used 0.05 w/v% nitrogen source (at C:N 10:1) and this might be below the induction limit of TAG accumulation. Conversely, *R. opacus* PD630's TAG anabolism was ammonium dependent (Figure 5.2. b and d). In all cases (Figure 5.2.a-d) lipid contents had risen first then as they fell, living cell numbers significantly increased, as observed previously with different substrates [285]. This trend can only be observed when living cell numbers are plotted against lipid (FAME) contents, and not CDW, showing that "fat cells" are considerably heavier than "lean cells" (Figure 5.2.a-d). Furthermore, all substrates were usually completely consumed after 48 h, except when PD630 was growing on 4-HBA (Figure 5.2.b), this scenario provided the only true oleaginous lipid build up by reaching 20.3 % of CDW in FAME content.

5.3.2.1 Role of pH

Another interesting observation was the parallel increase in pH and living cell number in all cases. The rising pH was detected up to 9 and above (Figure 5.3), except when DSM 1069 was growing on 4-HBA, and even in this case, living cell number rose

significantly at the very end when pH reached ~8 (Figure 5.2.a and Figure 5.3). The pH was never controlled during shake flask fermentations, accordingly all changes were due to the cells' metabolism, however, this pH increase always occurred parallel with living cell number increase in time. This effect was even more striking when DSM 1069 cell line was used, since it always reached the same living cell numbers at only higher pH's than PD630 (Figure 5.3).

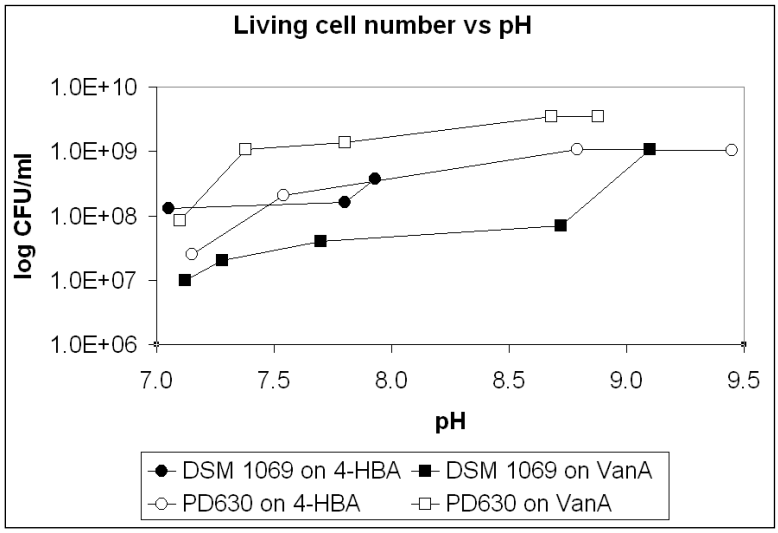

Figure 5.3. Log_{10} living cell number vs. pH diagram

The effect of pH on cell number growth cannot be easily separated and analyzed from the expected growth over time unless pH controlled experiments are conducted while living cell numbers are constantly monitored. However, when DSM 1069 was growing on 4-HBA the living cell number doubled while pH rose from 7.80 to 7.93 (Figures 5.2.a and 5.3). Moreover, growing on VanA there was a 15 times increase in living cell number while pH rose from 8.72 to 9.10 (Figures 5.2.c and 5.3). In the case when 4-HBA was used, the highest lipid accumulation showed at a decreased pH of 6.36 after 12 h (Figure 5.2.a), although lipid content was high later on at higher pH's as well. Contradicting these

results, when glucose was used without pH control cell number rose ~5 times between 48 and 72 h while pH decreased from 4.45 to 3.19. At the same time lipid contents almost parallel following cell number growth reached the maximum after 120 h at a pH of only 2.89. Even more interestingly at this point, DSM 1069 cells accumulated long chain fatty acid containing lipids, such as erucic, tricosanoic and *cis*-docosadienoic acids that were absent until 72 h. These observations imply an intricate cross dependence between substrate type and pH but not necessarily ammonium contents in case of DSM 1069, while PD630 showed ammonium dependence and reached higher pH faster. Growth rates of PD630 always exceeded DSM 1069 on every substrate and the pH of the supernatant never fell below 7.

5.3.2.2 Substrate consumption, fatty acid (FA) and lipid composition

Metabolism of all substrates was monitored by HPLC which indicated that when growing on aromatic compounds such as 4-HBA and VanA, an extra peak with the same retention time was observed after different incubation times. This peak proved to be protocatechuic acid (PCA) when examined with ^{1}H NMR. PCA is the product of the first conversion step in lignin model compound conversion (Figure 5.1; [11, 261]). This result suggests *R. opacus* DSM 1069 converts and consumes 4-HBA differently than PD630, while apparently utilizing the same strategy for VanA. According to HPLC, DSM 1069 first converts 4-HBA to PCA, while growth is constant, then after 4-HBA is fully converted PCA is still present in considerable amounts before being consumed. PD630 on the other hand follows a different strategy by which it continuously consumes both 4-HBA and PCA. As a consequence, 4-HBA and PCA are present in the fermentation broth together (PCA always in lower concentrations), and by the time 4-HBA is

converted PCA is also fully consumed. This latter strategy applies for both strains when VanA is the substrate, repeatably at 0.5 and 1.0 w/v% substrate concentrations. 4-HBA and PCA transport through the plasma membrane was shown to be mediated by PcaK protein in *Pseudomonas putida* [286], while PatDACB was investigated in phthalate uptake in *Rhodococcus* spp. RHA1 [277]. *R. opacus* funneling pathways (4-HBA->PCA and VanA->PCA, Figure 5.1.) and the membrane transport of different substrates might be the reasons why growth is enhanced at higher pH (as mentioned above). However, further investigation is needed particularly since high pH preference could be in part due to advantageous effects on other metabolic routes, variations in β-ketoadipate pathway enzymes and their regulation, furthermore differences between cell lines [11, 277, 279, 286]. Above mentioned funneling pathways converting a myriad of possible substrates, from benzene, p-cresol, toluene, naphthalene, biphenyl and lignin resembling 4-coumarate, ferulate and coniferyl alcohol, moreover, even electron donating group containing aromatics such as chlorinated phenols [11, 12, 244, 261, 272, 284] to PCA (and other dioxygenase substrates, e.g. catechol for catechol-1,2-dioxygenase) are of great importance. For the reason that P3,4O (Figure 5.1) has a high substrate specificity for PCA that will determine conversion efficiency [turnover to (5) β-carboxymuconate; [244]].

The fatty acid compositions derived from lignin model compound grown cells were investigated by simultaneous extraction and transesterification followed by gas chromatography (GC) analysis (Chapter 3). A mass spectrometer (MS) detector was used to identify any fatty acid methyl esters (FAME) that were unidentifiable by standard retention times. Four of these FAMEs were identified, namely: *trans*-hexadec-9-enoic

acid (*t*-palmitoleate, C16:1^{trans}), 10-methyl-heptadecanoic acid ($^{10\text{-me}}$C17:0), 10-methyl-octadecanoic (stearic, $^{10\text{-me}}$C18:0) acid and nonadecanoic (C19:0) acid methyl esters. *R. opacus* PD630 was previously reported to be grown on phenylacetic acid (PHA) and phenyldecane [284], and the resulting FA composition from PHA was documented [272] and used in this study as points of reference. Table 5.2 summarizes FA compositions for peak lipid productions on lignin model compounds and glucose, and is in good agreement with previous glucose and PHA results from literature [272]. Glucose grown DSM 1069 cells accumulated a significant amount (~30 %) of FAs with a chain length of C19 or above, appearing after 72 h and pH 3.19. It is noteworthy that PD630's FA composition will always contain major amounts of palmitic and oleic acids (observed earlier by Alvarez et al. [285]); however, similarly to DSM 1069, it will consume most of its FAs during growth with a slight preference for saturated fatty acids.

Further evaluation revealed that the ratio of saturated and unsaturated FAs is around 2:1 when DSM 1069 starts to grow on all substrates. This ratio then rises to 4:1 (on glucose and 4-HBA) and 3:1 (on VanA) then decreases to ~7:3 in all cases. *R. opacus* PD630's starting saturated: unsaturated FA ratio on glucose and 4-HBA is around 3:2, which changes to 1:1 and back to 2:1 during fermentation. At maximum lipid yield, occurring at 36 h, PD 630 contains a FA ratio of 1:1 when growing on 4-HBA. While when PD630 is growing on VanA, the starting ratio is ~2:1 (resembling DSM 1069) subsequently reaching 3:2 at 48 h (maximal lipid yield) then going back to ~2:1.

Table 5.2. Fatty acid (FA) composition of the two cell lines at different cultivation times (at maximum yields and productivities), np refers to non-published data. *R. opacus* DSM 1069 has a maximum productivity after 12 h on glucose, however, after 120 h the amount of "shorter" (<C18) FAs decrease and long chain acids are produced[a], namely: nonadecanoic (C19:0) 5.5 %, cis-11-eicosenoic (C20:1^{cis}) 3.4 %, heneicosanoic (C21:0) 4.5 %, cis-11,14-eicosadienoic (C20:2^{cis,cis}) 4.3 %, erucic (C22:1^{cis}) 3.5 %, tricosanoic (C23:0) 3.3 % and cis-13,16-docosadienoic (C22:2^{cis,cis}) 4.1 % acids. Data on phenylacetic acid (PHA)[b] grown cells are also shown as investigated by Alvarez and coworkers [272].[c]-cis, [tr]-trans

Strain	Carbon source	FA [%CDW]	t [h]	Relative proportion of FA [w/w%]					
				C14:0	C15:0	C16:0	C16:1[c]	C16:1[tr]	C17:0
DSM 1069	glucose	13.8	12	0.0	8.3	25.8	6.5	5.1	10.6
		17.9	120[a]	0.0	11.2	19.5	0.0	0.0	11.9
	4-HBA	16.8	12	0.0	8.6	24.2	6.0	4.0	12.8
	VanA	6.7	24	0.0	6.8	22.9	4.2	6.9	10.1
		8.7	36	0.0	8.4	32.1	7.2	4.1	10.0
PD630	glucose	19.8	12	0.0	4.3	31.1	6.4	4.5	5.7
	4-HBA	20.3	36	7.0	6.0	28.8	10.6	4.7	4.4
	VanA	14.6	48	3.3	7.6	27.9	7.7	3.7	7.6
	PHA[b]	38.0	48	3.3	23.8	27.0	4.4	np	19.8

Strain	Carbon source	FA [%CDW]	t [h]	Relative proportion of FA [w/w%]					
				[10-me]C17:0	C17:1[c]	C18:0	[10-me]C18:0	C18:1[c]	C18:2[c,c]
DSM 1069	glucose	13.8	12	0.0	6.8	9.4	9.8	12.0	5.6
		17.9	120[a]	0.0	0.0	6.9	8.7	7.2	6.1
	4-HBA	16.8	12	3.6	9.8	8.3	6.9	11.9	4.1
	VanA	6.7	24	6.2	14.5	5.2	9.2	14.1	0.0
		8.7	36	5.5	9.7	5.4	7.6	10.0	0.0
PD630	glucose	19.8	12	0.0	8.1	9.7	6.4	23.7	0.0
	4-HBA	20.3	36	0.0	9.4	5.8	7.5	15.7	0.0
	VanA	14.6	48	4.0	12.3	4.4	7.4	14.2	0.0
	PHA[b]	38.0	48	np	12.5	3.6	np	5.6	np

Although simultaneous lipid extraction, transesterification and subsequent GC analysis gave quantitative FAME contents, lipid (TAG, DAG, etc.) ratios remained unknown as well as the accuracy of this method. To address these issues a modified Folch method [266] was used to extract lipids, then these extracts were dissolved in chloroform (10 mg/ml) for thin layer chromatography (TLC, [264]). This set of experiments was only applicable to samples that contained enough freeze dried cells (~50 mg). In the present case both strains were cultivated on VanA for 48 h. Extraction showed 11.44 and 18.22

% lipid contents for DSM 1069 and PD630 at this point respectively which exceeds FAME measurement results by 25-40 %. This shows that simultaneous extraction and transesterification underestimate lipid contents, most likely due to issues like low transesterifying power when using acid catalyst [287], however, unlike the modified Folch method, the former procedure only requires small amounts of freeze dried cells. The extracted lipids were used to run TLC and results showed that VanA grown cells, in case of both strains, will mainly contain triacylglycerols (TAG), monoacylglycerols (MAG) and some free fatty acids. R_F values were consistent with previously reported values, most importantly R_F-TAG was 0.42-0.43 [284].

5.3.2.3 Yields and volumetric productivities

Cell specific (Y_{cell}, g/g), lipid specific (Y_{lipid}, g/g) yields and lipid volumetric productivities (dc_{lipid}/dt, g/l·h) were calculated for both strains growing on 0.5 w/v% substrates and maximum values are collected in Table 5.3. Glucose based productivities shown in Table 5.3 are much smaller than values reached when PD630 grows under optimized fed batch conditions, reaching 0.38 g/l·h [288]. This, over 2 magnitudes, difference in volumetric productivity is most likely due to multiple reasons such as optimal pH, temperature and dissolved oxygen levels, as well as optimized C: N ratios and perfectly timed sampling. These lignin model compound studies suggest that lignin based lipid production has real potential considering that Table 5.3 shows values that are from non-optimized fermentations and that maximal cell concentrations can reach 77.6 g/l [289] that is over 30 times higher than results presented here (Figure 5.2).

Table 5.3. Maximum cell, lipid yields and volumetric productivities shown at point of time when highest values are reached (t_{max}) after transferring from nitrogen rich adaptation media to nitrogen limited media

Strain	Carbon source	Y_{cell}		Y_{lipid}		dc_{lipid}/dt	
		t_{max} [h]	[g/g]	t_{max} [h]	[g/g]	t_{max} [h]	[g/l·h]
DSM 1069	glucose	12	0.62	12	0.06	12	0.003
	4-HBA	12	0.59	12	0.10	12	0.003
	VanA	12	0.37	24	0.02	24	0.003
PD630	glucose	12	0.51	12	0.10	12	0.003
	4-HBA	36	0.44	36	0.09	36	0.009
	VanA	12	0.67	48	0.04	48	0.005

5.4 Conclusions

Rhodococcus opacus DSM 1069 and PD630 strains were grown on 4-hydroxybenzoic acid (4-HBA) and vanillic acids (VanA) as lignin model compounds to evaluate lipid accumulation under nitrogen limiting conditions. Adaptation experiments showed that both strains can successfully grow on both substrates at multiple different concentrations, and that they can accumulate close to 20 % of their own weight in lipids in nitrogen limited shake flask fermentations. Lipid accumulation in DSM 1069 showed no nitrogen source dependence, on the other hand both strains showed pH dependence; growing faster at higher pH. This pH dependence might be due to multiple different effects, such as better conditions for substrate conversion, membrane transport or other metabolic regulatory issues [11, 277, 279, 286]. Substrate consumption and fatty acid compositions were highly carbon source and strain dependent; however, both strains first accumulated lipids, which were then utilized to increase cell number. PD630 in some instances had higher unsaturated fatty acid ratios, close to 50 %, that might be beneficial in biodiesel applications, due to lower melting points [59]. Furthermore, PD630 showed

high palmitatic and *cis*-oleic acid accumulation in all cases, while DSM 1069 fatty acid distribution allowed for more variation, especially growing on glucose at low pH. Separate lipid extraction showed that simultaneous extraction and transesterification considerably underestimated total lipid contents, however, the application of other more reliable methods requires larger scale fermentations. TLC showed that neutral (TAG) lipids contribute significantly to the total lipid content. Glucose based yields and volumetric productivities fall behind current state-of-the-art fermentations with PD630 [288, 289], showing the need for further optimization and scale-up.

On the other hand, lignin rather than lignin model compounds is the most interesting substrate. Consequently, considering that the lignin model compound to lipid bioconversion concept is now proven, the next step should be the conversion of lignin sources (e.g. coniferyl alcohol (G) rich softwood lignin instead of VanA). Kraft and biomass pretreatment residual lignins should be of primary importance, considering that the conversion of their non-uniform structures [2, 10, 290] into easy to handle compounds might significantly valorize their respective origin processes. Substrates like grass lignins (e.g. switchgrass) should also be between the first to be tested, considering their high p-hydroxy (H) aromatic contents (compared to woody biomass, [6]) resembles 4-HBA, the most efficient growth substrate in our research. Furthermore the genetic manipulation of *R. opacus* and *A. baylyi* is well established, opening possibilities for heterogeneous cloning and up-regulated expression of both lignin-degradation and lipid accumulation genes [15]. Moreover, as recently discovered *R. jostii* RHA1 has been shown to produce extracellular proteins involved in lignin degradation [234]. This discovery can be of great importance for the reason that lignin depolymerization and the

funneling of the degradation products into preferred monomers (e.g. PCA) should determine overall conversion efficiency, considering the high substrate specificity of dioxygenases (e.g. P3,4O; [11, 244]). In conclusion; efficient and economic production of value added uniform products from lignin with the above shown metabolic pathway needs considerable further research, however, one day it may enable biorefinery concept side-stream valorization.

Chapter 6

Lignin to lipid bioconversion with oleaginous *Rhodococci*

6.1 Introduction

Rising global energy demand presses the issue of sustainable resource management, not just to maintain natural reserves and a neutral carbon (CO_2) balance but also to help local economies in the long run. Where biomass is abundant the biorefinery concept can be an ingenious and economically feasible way to meet energy, material and employment demands, given that a diverse number of high-value products can be generated from biomass [3, 4]. Lignin, next to sugar polymers, is a major cell wall component with a recalcitrant, three dimensional polyaromatic structure and a chemical composition that highly depends on species, origin, soil and other environmental growth conditions (Chapter 2, Section 2.3.3) [2]. These properties limit lignin's potential as a valuable bioenergy and/or biomaterial resource; and while its thermochemical conversion, such as pyrolysis, has recently drawn substantial attention (Chapter 2, Section 2.4; [2, 42, 188]), its bioconversion is almost exclusive to fungal biopulping [270] and biobleaching [218]. Lignin is produced in considerable quantities, for instance ~50 million tons per year by the global paper industry [5]. Moreover, different pretreatment methods, such as the ethanol organosolv process (Chapter 2, Section 2.4), can also provide high purity lignin as a side product of cellulosic ethanol production [30, 39].

The abundance of this inexpensive substrate generated interest in revisiting bacterial lignin degraders and their "product profile" with hopes that these microorganisms can possibly yield a commercially relevant process, lacking the practical

challenges faced by methods developed with fungi (Bugg et al. 2011). Bacterial lignin degradation proceeds in three major steps, according to our scarce knowledge in this area (Figures 26, 43). First lignin is de-polymerized via prokaryotic lignin active enzymes, like lignin- and manganese-peroxidases into monomeric and oligomeric aromatic units (Chapter 2, Section 2.5) [220]. Bacterial lignin degradation proceeds in three major steps (Chapter 2, Section 2.5) as shown in the literature [219, 220, 222] and summarized on Figures 2.24 and 2.33. Lignin is first depolymerized by lignin active enzymes, then oligomers and monomers are funneled into archetypal substrates, such as protocatechuate (PCA) that can be degraded through the b-ketoadipate pathway for example, in the last step, to obtain acetyl-coenzyme-A (Chapter 2, Section 2.5). The Gram positive species of soil dwelling *Rhodococcus* bacteria are of particular interest, for lignin degradation, because initial work (Chapter 5) proved that both *R. opacus* DSM 1069 and PD630 can grow on lignin model compounds as sole carbon sources while accumulating lipids in oleaginous levels [63].

Present study investigates growth and lipid accumulation in *R. opacus* DSM 1069 and PD630 strains when only EOL (ethanol organosolv lignin) and Kraft lignin are present as carbon sources. The hypothetical metabolic route from SW lignin (coniferyl (G) overrepresented, [2]) to neutral lipids is depicted on Fig. 2.24 [15, 219], showing the three above mentioned steps of lignin degradation; completed with the theoretical anabolic route to lipids (step 4) and transesterification (step 5).

6.2 Experimantal section

6.2.1 Lignin preparation

Before ethanol organosolv pretreatment, loblolly pine chips were milled, extracted with toluene: ethanol solvent mixture (2:2) to eliminate extractives, then pretreatment was conducted as detailed in Chapter 3 [39]. Ashing, Klason lignin and sugar content measurements were also conducted on both the starting material (extracted wood) and the EOL product (Chapter 3) [138]. Part of the obtained EOL was ultrasonicated, as detailed in Chapter 3 (and Appendix B), to obtain samples that are soluble in neutral media, named *us*-EOL.

Kraft lignin separation was conducted according to literature method [10], until dioxane purification, then an extra step of high pH (12) water dissolution, then re-precipitation was applied to get rid of dioxane traces, as detailed in Chapter 3. Klason lignin and sugar analysis were also conducted to quantify non-lignin components. Part of pure Kraft was further separated into a low (weight and number average) molecular weight (low M_w Kraft) and a high M_w fraction by dissolving at high pH (12) and filter-separating as pH was lowered to 4.5, as detailed in Chapter 3 (and Appendix B). O_2-delignification was employed on another part of the pure Kraft lignin, as a different method for solubilization, Chapter 3.

All together 5 different lignin samples were used in fermentations, as shown in Table 6.1, including neutral media solubility that also enabled sterilization by filtration through 0.2 μm filter.

Table 6.1. Primary and secondary preparation steps and solubility of the 5 different lignin preparations used in this study

Sample name	Primary prep.	Secondary prep.	Solubility in neutral aqueous media
EOL	Ethanol organosolv pretreatment	-	No
***us*-EOL**		ultrasonication	Yes
Kraft	Purification from Kraft black liquor	-	No
low M_w Kraft		pH separation	Yes
O_2-Kraft		O_2-delignification	Yes

6.2.2 Fermentations

Shake flask fermentations were conducted at 30 °C in 500 ml baffled flasks used specifically for aerobic microbial growth experiments (sterile filter insert in cap for aeration), at 150 rpm. Consistency varied between 0.3 and 0.5 %, depending on lignin source used (Table 6.2). For preliminary experiments 45 ml centrifuge tubes were employed with specially modified aeration caps, filled with 10 ml media. Bench-top scale fermentation was also conducted with Kraft lignin at 0.35 % consistency, at 30 °C and pH control set between 7.0 and 8.0. Mixing was controlled by dissolved oxygen (DO) levels, which was set to be 80 % of the saturation value, based on air exposed probe reading (that is set as 100 %), Chapter 3. All lignin fermentations conducted are summarized in Table 6.2, including lignin types, bacteria, starting lignin concentration and experiment length; as well as indicating if a starting media was inoculated by bacteria from a previous fermentation.

Table 6.2. The list of all fermentations conducted in present work, including preliminary fermentations (10 ml). Superscript numbers after bacterial strains (e.g. DSM 1069[3]) mean that cells resulting from a given fermentation were separated, and used as inoculum in subsequent fermentation(s) (e.g. [3]DSM 1069).

Lignin type	Lignin c [mg/ml]	Volume [ml]	Length [day]	Bacteria (R. opacus)
EOL	3.0	150	7	DSM 1069 PD630
O_2-Kraft	3.0	150	9	DSM 1069 PD630
***us*-EOL**	5.0	200	9	DSM 1069
Low M_w Kraft	3.5	150	9	PD630[1] DSM 1069[3]
Kraft	3.5	150 150 2000	12 7 1	[1]PD630[2] [2]PD630 [3]DSM 1069

6.2.3 Sampling and analysis during and post-fermentation

Sampling was conducted, under sterile conditions, after every 24 h for the first 3 days, then every 2nd day until 7 to 9 days. The liquid sample pH was first set to 10.3, and then cellular material was separated by centrifugation (Residue 10.3). Subsequently, the liquid was sterile filtered, followed by lignin precipitation (pH 2.0, Residue 2.0) as, Chapter 3. In case water soluble lignin sample was used, *us*-EOL, O_2-Kraft or low M_w Kraft, cells could be readily separated by centrifugation without pH adjustment. The fresh liquid sample was subject to serial dilutions and plating (SDP) experiments to follow changes in living cell numbers, while after separation, cells were also stained and examined under light microscope, as well as their weight gain was monitored (cell dry weight- CDW, Chapter 3). Extracted, purified and freeze-dried cell material was also further extracted by the modified Folch-extraction method to obtain accumulated lipids that were analyzed by TLC; as well as GC-MS after transesterification [63] (Chapter 3).

Bacterially modified, then re-purified lignin samples were subject to ^{13}C, ^{31}P and HSQC NMR as well as GPC analysis, Chapter 3. Figure 6.1 illustrates the sequence of different analytical methods and sample preparations conducted, after fermentation broth was sampled. While Table 6.3 summarizes the abbreviations used for different analytical techniques and their purpose.

Table 6.3. Analytical techniques utilized to follow changes in lignin and strain growth during fermentation.

Analytical technique	
Abbreviation	**Full name and purpose**
SDP	Serial Dilutions and Plating; cell number changes -> calculating colony forming units (CFU), colony morphology and monitoring contaminations
OD	Optical Density; approximate cell growth
CDW	Cell Dry Weight; accurate cell growth
Microscopy	Cell shape, size monitoring (contaminations)
TLC	Thin Layer Chromatography; separation of extracted lipids
GC-MS	Gas Chromatography- Mass Spectrometry; fatty acid composition of cellular lipids
GPC	Gel Permeation Chromatograpy; lignin molar mass distribution
NMR	Nuclear Magnetic Resonance; lignin structural changes

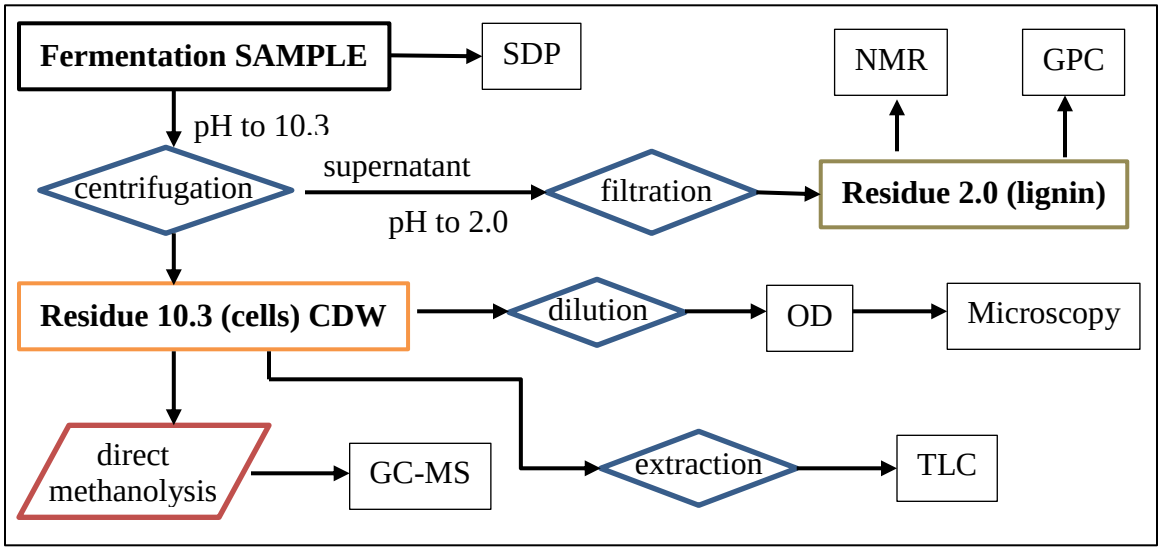

Figure 6.1. Sample preparations and analytical techniques used to monitor fermentation of lignin with oleaginous *Rhodococci*

6.3 Results and discussion

6.3.1 Substrate lignin properties

6.3.1.1 Loblolly pine and EOL properties

Growth and lipid accumulation on multiple lignin sources were evaluated, accordingly, first, all of these substrates were subject to structural and polymerization analysis by NMR and GPC, respectively. Furthermore, EOL was obtained from extracted loblolly pine (*Pinus taeda*) that had the chemical composition as detailed in Table 6.4, which is in good agreement with literature data summarized in Tables 2.2 and 2.12. The Klason (acid insoluble) lignin content of the extracted and the extracted then pretreated wood were compared to specify the amount of lignin loss as well. This number was 8.1 ± 0.5 % based on total wood weight (unextracted, ODW), as an average of 4 separate pretreatments, and 95 ± 2 % of this loss was recovered as EOL. This lignin yield is only 42 % compared to the original paper describing the pretreatment method. It has to be noted though, that the authors in the mentioned paper used mountain pine beetle killed lodgepole pine (*Pinus contorta*), moreover their experimental setup included a specific digester optimized for this pretreatment, not a regular Parr reactor [39].

Table 6.4. The chemical composition of loblolly pine used in the experimental work presented

Based on unextracted oven dried pine wood [%]					
Extractives	**Ash**				
3.38	**0.35**				
Sugars	Arabinose	Galactose	Glucose	Xylose	Mannose
64.26	0.85	2.24	44.63	5.81	10.73
Sum lignin	Klason	Acid-soluble			
31.33	29.84	1.49			

The freeze dried EOL, with less than 3 % moisture content that was used for further experiments, was insoluble in water at pH 7, consequently, ultrasonication treatments were applied combined with hydrogen-peroxide bleaching to obtain water soluble lignin *us*-EOL. This process was optimized for multiple parameters, such as ultrasonication amplitude and residence time, consistency of lignin solution (while pH was held constant at 12), H_2O_2 load and final temperature (Appendix A). Table A.A.1 contains the GPC results, showing that repeatedly 5 min ultrasonication at 40 % amplitude and 2 % consistency with 1 % H_2O_2 charge was the optimal treatment. Optimal not just because of complete lignin solubility after pH was decreased to 7, but also because it used the lower peroxide load. Similar results were obtained by peroxide bleaching alone, however, it took 24 h to reach complete solubility at neutral pH. Moreover, it was observed that ultrasonication increases M_w from ~2700 to ~3400 g/mol (GPC results), and this effect was observed to be more enhanced in case cavitation occurred (>4000 g/mol). The fact that ultrasonication combined with peroxide bleaching simultaneously increase M_w and solubility must be due to structural changes in lignin. Accordingly, ^{13}C and ^{31}P experiments were conducted to evaluate these structural changes as shown on Figure 6.2 and in Table 6.5. It is noteworthy that above GPC results are in good agreement with literature results for EOL as shown in Table 2.11.

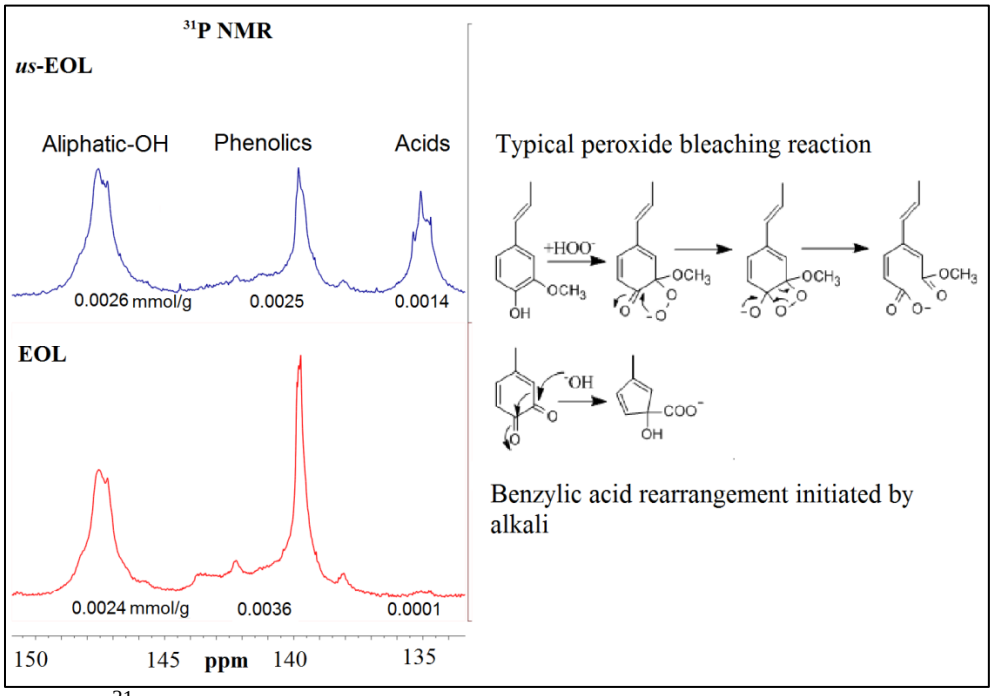

Figure 6.2. ^{31}P NMR results, shown as mmol functionality per g sample, indicate the loss of phenolics and the gain in acids. These results indicate typical peroxide bleaching reactions, as shown on the right hand-side, as well as quinone benzylic acid rearrangements initiated by alkali [105, 106].

Table 6.5. Comparing ^{13}C NMR analysis results of EOL with literature values, as well as with ultrasonicated samples

Carbon NMR		**functionality/aromatic ring**		
δ [ppm]	**Assignment**	**EOL [115]**	**EOL**	**us-EOL**
180.5-170.0	C=O in unconjugated C(O)OH	0.3	0.2	0.6
168.0-162.5	C=O in conjugated C(O)OH	0.1	0.1	0.3
154.0-140.0	C_3, C_4, C-O in aromatic ethers and phenols	2.1	2.1	2.1
140.0-127.0	C_1, Aromatic C–C bond	1.6	1.5	1.6
127.0-124.5	C_5, Aromatic C–C bond	0.5	0.3	0.3
124.5-117.0	C_6, Aromatic C–H bond	0.7	0.9	0.9
117.0-114.0	C_5, Aromatic C–H bond	0.6	0.5	0.5
114.0-105.0	C_2, Aromatic C–H bond	0.7	0.8	0.8
90.0-58.0	Aliphatic C–O	1.3	1.1	1.7
58.0-54.0	Methoxyl OCH_3	0.9	1.0	0.9

The NMR results described above strongly imply that ultrasonication enhances the efficiency of peroxide bleaching and lignin will have, in some cases 14 times, more carboxylic groups then before this treatment. This significant increase in acidic-groups also indicates that the number of possibly charged groups increases after ultrasonication/peroxide bleaching treatment, enabling solubility. ^{13}C NMR results (Table 6.5) also show an approximately 50 % increase in aliphatic ethers and alcohols, suggesting the increase in lignin inter-unit linkages, considering that ^{31}P NMR only shows an 8 % increase in aliphatic hydroxyls (Figure 6.2), and GPC data implied M_w increase. Sugar analysis on EOL showed that there is a 1.43 % sugar content in his type of lignin, composed of 67 % glucose, 22 % galactose and 11 % arabinose respectively. In summary, EOL properties show good agreement with the literature and it can be concluded that us-EOL samples gain solubility through the increase of acidic groups; however, ultrasonication also increases aliphatic ether (lignin inter-unit) linkages, resulting in higher M_w.

6.3.1.2 Kraft lignin properties

Kraft lignin was purified from black liquor (BL) by the acidification, followed by filtration and purification, including the step to eliminate traces of dioxane (Chapter 3). BL in this case was obtained from Cedar Sprigs (US), unlike the BL used in Chapter 4 that was originally from a Swedish softwood mill (Chapter 3). Kraft is a currently abundant and inexpensive lignin resource (Chapter 2); however, similarly to EOL it is not soluble in neutral media. Consequently, multiple different treatments were employed to enhance its solubility, namely: ultrasonication combined with peroxide bleaching, O_2-

delignification, and a uniquely developed method that uses pH decrease to separate lower M_w lignin at pH 4.5 (Chapter 3, Appendix C). Ultrasonication was conducted using the same conditions that were optimized for the EOL treatment, while typical O_2-delignification conditions were set according to literature values [114, 291-294] (Chapter 3). The third, unique method employed after Kraft lignin purification from BL, applied constantly decreasing pH and filtration (Chapter 3, Appendix C) to separate a low M_w lignin part that the cells can adapt to, before inoculation into media containing the "original" Kraft lignin. GPC results on the purified Kraft, low M_w Kraft and O_2-Kraft were 4800, 2600 and 4000 g/mol weight average molecular weights (M_w) respectively, illustrating that O_2-delignification decreases M_w as well. Both low M_w and O_2-Kraft were soluble in neutral media, while the originally purified Kraft (GP Containerboard) had an Mw in good agreement with the literature (Table 2.11). In case of low M_w Kraft separation the changes in total hydroxyl contents were followed by ^{31}P NMR, showing that low M_w Kraft contains 19.5 % more hydroxyl groups than the original Kraft lignin. The most significant increase was observed in phenolic hydroxyl content that reached 25.2 %. Detailed comparison of Kraft resources, such as present Kraft resource (Cedar Springs), the lignin used in Chapter 4 (Swedish softwood mill), separated low M_w Kraft, as well as previous literature data [42], was based on ^{13}C NMR experiments as summarized in Table 6.6.

Table 6.6. Comparison of Kraft lignin structure with previous literature data and the separated low M_w Kraft; n.p.- non published

Carbon NMR		mol % (ratio to all integrals)			
δ Region [ppm]	**Assignment**	**Kraft [42]**	**Kraft [9]**	**Kraft**	**Kraft low M_w**
215.0-162.5	Carbonyl C=O	1.6	n.p.	6.9	9.2
155.0-140.0	Aromatic C-O	27.3	22.5	15.7	16.3
140.0-123.0	Aromatic C-C	25.8	28.6	18.2	16.6
123.0-106.0	Aromatic C-H	26.4	24.7	18.6	15.2
90.0-58.0	Aliphatic C-O	5.8	8.3	13.0	15.1
58.0-54.0	Methoxyl	12.9	11.8	7.4	7.1
49.0-0.0	Aliphatic	0.3	4.1	20.2	20.6

Table 6.6 shows that the lignin used in present work (Chapter 6) is completely different from Kraft lignin used before, either in this work (Chapter 4) or in the literature. Aliphatic, carbonyl and aliphatic C-O contents are significantly higher than literature values compared to aromatic signals (Table 6.6). This difference is especially conspicuous for aliphatic carbon that represents 20 % of the spectrum, an almost 10 times increase compared to previous (Chapter 4) and literature results [9, 42]. This Kraft lignin was purified exactly the same way as all other Kraft lignin before, accordingly, the difference has to be in the BL. The high aliphatic and carboxylic content together with the decrease in aromatic peaks (Table 6) suggest that the extra signals are due to extractives [96].

Extractives in pine are composed of resin and fatty acids as detailed in Chapter 2 (Sections 2.3.5.1-2), and their average concentrations are listed in Table 2.13. There is very limited information available on these diterpenoic acids (DA) and fatty acids (FA) in the literature, especially NMR data [181-186]. In case of lignin 2D NMR analysis, mostly HSQC, a few other papers show the peaks in the aliphatic region, but don't analyze them in detail, only mentioning extractives in general [96]. However, there is some information on reduced (e.g. dihydroconiferyl, same structure as 1-propyl-alcohol) lignin side-chains

[96, 102]. Combining all the literature information, a collection of chemical shift pairs were created by excel, using all data-pairs found for DA, FA and lignin related aliphatics (LRA, alkyl side-chains, Appendix C). Then chemical shift pairs from Kraft and EOL lignin HSQC experiments (used in this work) were collected in excel as well (Appendix C). The resulting two datasets were plotted together in an overlay format, to enable predictions for "unidentified" lignin peaks. The overlapping lignin-extractive peaks were then collected in new HSQC database tables for not just the aliphatic region, but also for the aromatic, olefinic and aliphatic ether ranges (Appendix C). Figure 6.3 briefly demonstrates how these new HSQC tables from Appendix C were used in peak identification, showing the aliphatic region of Kraft lignin as an example. In summary, according to qualitative HSQC analysis, Kraft lignin's aliphatics were identified as diterpenoic (DA) and fatty acids (FA), as well as some unidentified lignin related aliphatics (LRA).

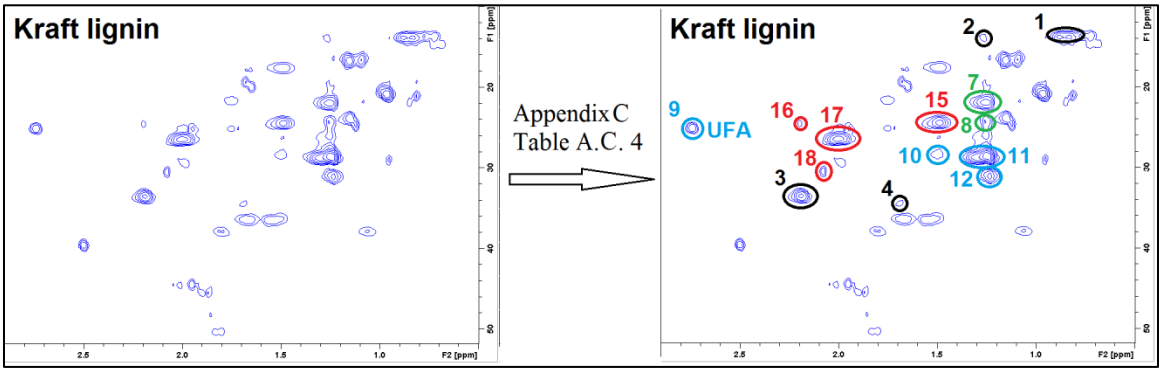

Figure 6.3. The use of Appendix C tables for the identification of HSQC peaks, as illustrated by Kraft lignin's aliphatic region (exact peak identification is detailed in Section 6.3.3.4)

Kraft lignin also contains 2.68 % carbohydrates, composed of 56.5 % glucose, 26.0 % arabinose and 17.5 % galactose, that is in agreement with the literature [96, 102].

In summary, Kraft lignin used in this chapter differs from the lignin used in Chapter 4, conclusively due to different BL sources (possibly originating from seasonal and other variances in biomass, Chapter 2). These differences are not visible on sugar (2.68 %) and M_w (4800 g/mol GPC) information, only on NMR structural data, showing that this Kraft lignin has a high, approximately 20 %, extractives content. These extractives were qualitatively identified by HSQC NMR to be diterpenoic (DA) and fatty acids (FA) as well as other lignin related aliphatics (LRA). Low M_w (2600 g/mol) also contains these extractives in similar amounts, Table 6.6.

6.3.2 Results from shake-flask and bench-top scale fermentations

6.3.2.1 EOL fermentations

Both Rhodococcus opacus DSM 1069 and PD630 were grown on EOL as a sole carbon and energy source in minimal media. EOL is not soluble so sterilization was conducted by pH increase (12.0) sterile filtration and pH reset with sterile acid (Chapter 3). Subsequently, shake flasks with 0.3 w/V% lignin media were inoculated, from fresh, full media grown and washed cells (Chapter 3). Cell growth was monitored by SDP and CDW measurements, as shown on Figure 6.4. *R. opacus* PD630 wasn't growing well enough to obtain sufficient cell material for CDW measurements, however, by day 7 its colony forming unit (CFU) numbers increased approximately 24 times compared to day 3, and over 300 times compared to the inoculation amount.

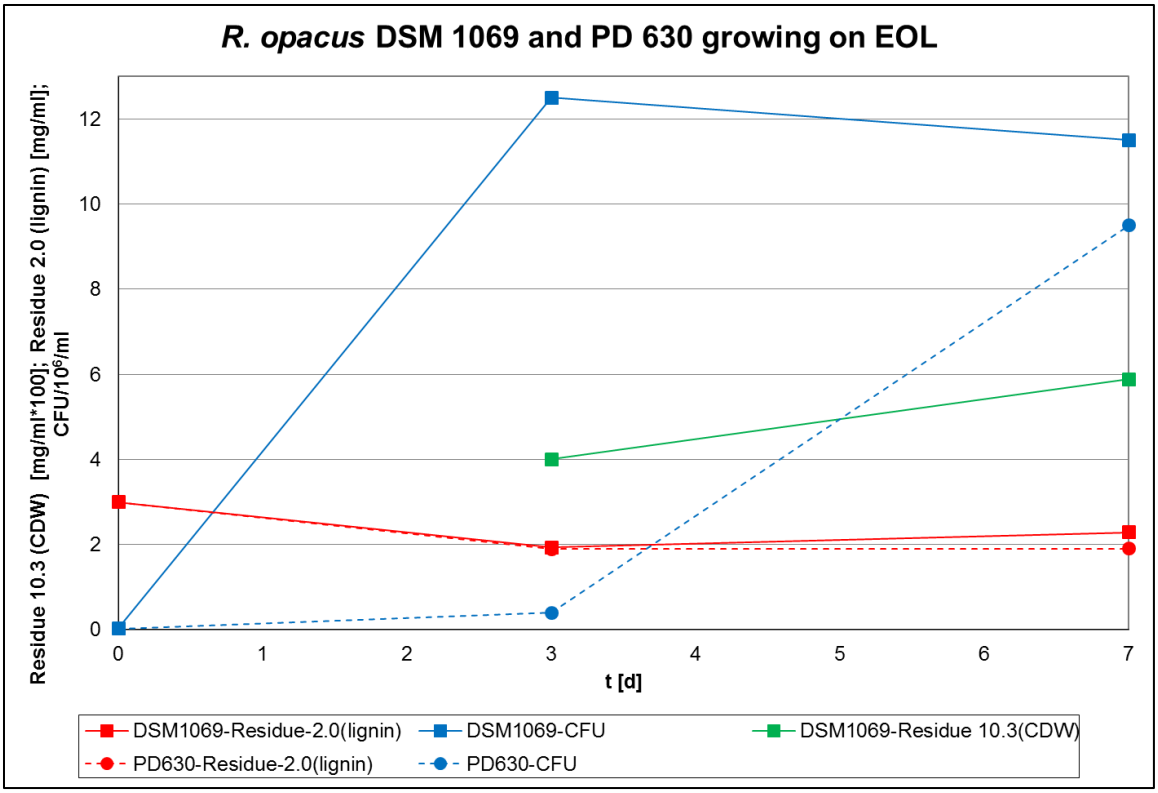

Figure 6.4. Growth of PD630 and DSM 1069 cell lines on EOL as a sole carbon source

The total loss of lignin as measured by Residue-2.0 quantity (Chapter 3) by day 7 was 0.7 mg/ml (Figure 6.1), meaning that the starting lignin concentration decreased by approximately 23 %, in case of DSM1069, and 1.1 mg/ml for PD630. Figure 6.5 shows the pictures taken on freeze dried Residue-10.3's (cells) obtained after 3 and 7 days. There's a significant color change from light brown (day 3) to light pink (1 week), latter being the original color of DSM 1069 cells if they grow on minimal media with glucose, 4-hydroxybenzoic acid or vanillic acid (Chapter 5). These observations made it clear, that cells cannot be completely separated from lignin with this method. It is also noteworthy though (the color change suggests), that lignin was "more" attached to the cells in the early stage of the fermentation, and then the microbes later "released it". Furthermore,

SDP measurements showed no contamination; accordingly, there's a possibility that the color change is due to the cell-bonded lignin.

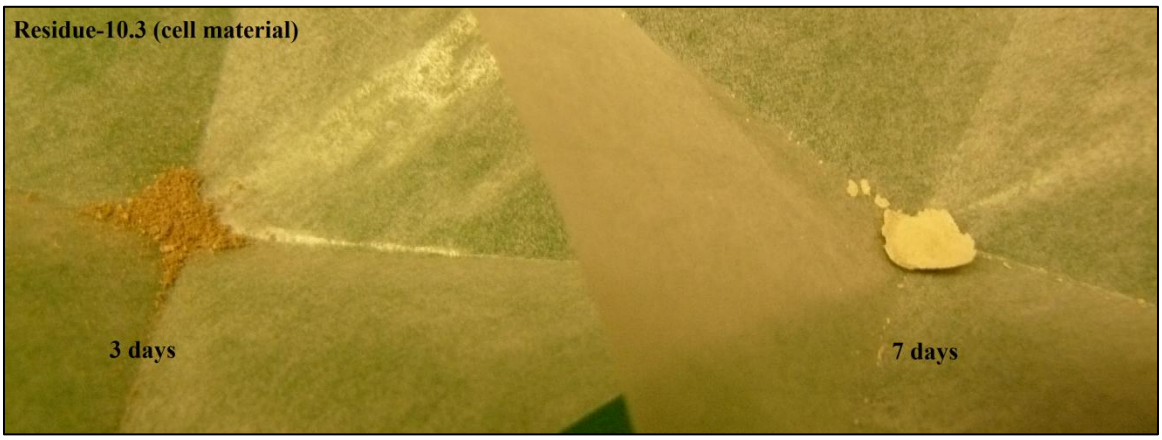

Figure 6.5. Residue-10.3 (cell material) separated from the fermentation broth after 3 and 7 days

DSM 1069 cell line produced enough CDW in the form of Residue-10.3 by the end of the fermentation (1 week) to apply direct methanolysis and analyze the obtained fatty acid methyl esters with GC-MS. The results showed that the cells contained 0.66 % fatty acids, composed of 51 % stearate and 49 % palmitate. Accordingly, yield calculations show that cell specific yield was Y_{cell} = 0.084 g/g EOL, while lipid specific yield was $Y_{lipid} = 5.6 \cdot 10^{-4}$ g/g EOL. These numbers are really small, compared to yields on lignin model compounds for example (Chapter 5), however, all this growth and lipid production was solely supported by EOL. This is also supported by the amount of lignin loss, overall 23 % (DSM 1069 and 36 % PD630), that is 21.87 % more than the sugar content of EOL.

GPC measurements on DSM 1069 modified EOL showed that the original 2700 g/mol M_w increased to 3500 then 3800 g/mol over 3 and 7 days respectively. (Conversely, hardly growing PD630 decreased M_w to approximately 2500 g/mol in 7 days.) Implying that DSM 1069 cells struggled with lignin (EOL) degradation and only

the lower M_w fractions had been digested, leaving high M_w EOL behind. ^{13}C NMR experiments were also conducted to visualize changes in EOL structure, due to modifications by DSM 1069, Figure 6.6. The only trends on Figure 6.6 show a 1.4 % increase in aromatic ethers/phenols and an approximately 1.5 % decrease in aliphatic ethers/alcohols. These changes suggest the breakdown of aliphatic ether lignin inter-unit linkages, leaving more recalcitrant, e.g. 4-O-5 bonds, revealed.

In summary, EOL is not an efficient growth substrate compared to model compounds for example, however, it supports the hypothesis that lignin can be converted into lipids, so far though, only at a really low specific productivity.

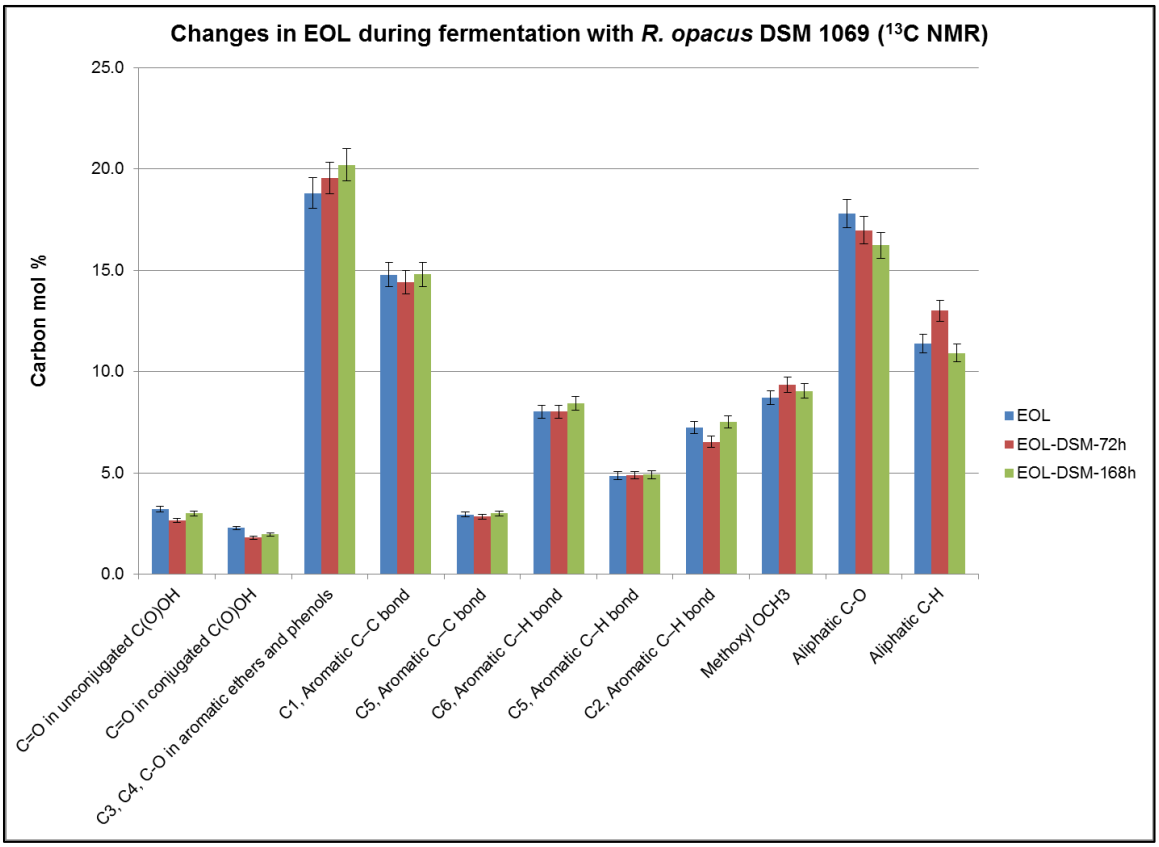

Figure 6.6. Structural changes in EOL during the growth of DSM 1069

6.3.2.2 us-EOL fermentation

The previous section concluded that *R. opacus* PD630 was not an efficient EOL degrader, concomitantly in this section, working with *us*-EOL, only DSM 1069 was utilized. Section 6.3.1.1 concluded that ultrasonication increases M_w through aliphatic ether bond, that reflect lignin inter-unit linkages, while acid goups are also increasing and to the expense of free phenolics. One of the great advantages of *us*-EOL is that it is readily sterilizable via sterile filtration. Consequently, freshly grown (~10 h) cells from full media, after washing, were inoculated into a shake flask containing *us*-EOL in 0.5 w/V% consistency. OD was monitored on a daily basis, while samplings were completed after 1, 7, 8 and 9 days. The starting pH was 7.20, and the cells were growing poorly after the first day of significant growth, as shown on Figure 6.7. Work with model compounds has shown that while growing on 4-HBA and vanillic acid, the cells, environment became slightly caustic (pH ~8.5) that didn't interfere with growth, on the contrary it seemed to be beneficial. Consequently, after 5 days of no significant change in present case the pH was artificially adjusted to 8.45 with sterile 1 M NaOH.

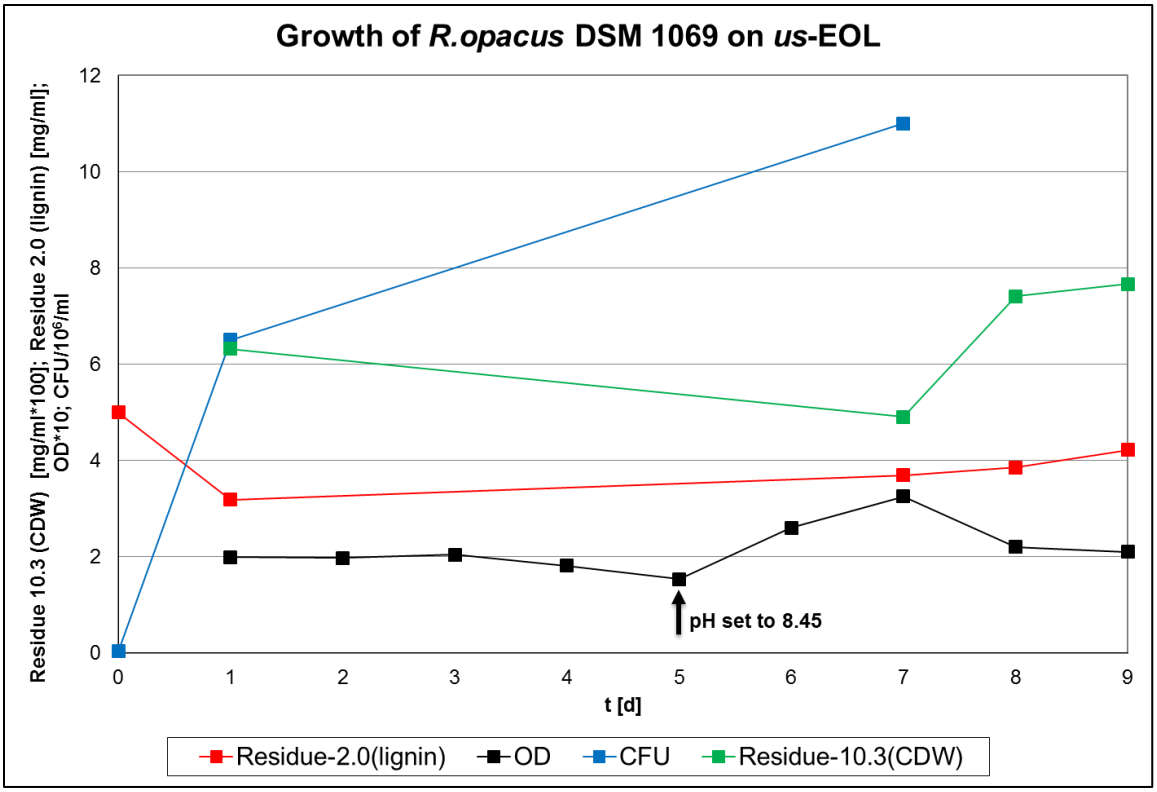

Figure 6.7. Growth of *R. opacus* DSM 1069 on us-EOL as a sole carbon source

Cell growth (Residue-10.3) in the first 24 h was really significant (Figure 6.7), CDW increased from virtually zero to 0.063 mg/ml, while CFU/ml increased 210 times compared to the inoculation number. This initial momentum abated though by the second day of fermentation, and didn't take up again until pH was adjusted after the measurements on the 5th day, then a second wave of growth was visible. Lignin (Residue-2.0) loss was approximately 0.8 mg/ml (total *us*-EOL loss, Table 6.7), from which some approximate yields/productivities were calculated, as shown in Table 6.7.

Table 6.7. Cell, lipid yields and volumetric productivities based on *us*-EOL as a sole carbon source

Productivities	**1 day**	**7 day**	**8 day**	**9 day**
Y_{cell} [g/g us-EOL]	0.079	0.061	0.093	0.096
Y_{lipid} [g/g us-EOL]	-	-	-	0.004
dc_{cell}/dt [mg/ml·day]	0.079	0.009	0.012	0.011

Specific productivity values are only 10-15 % of respective results when lignin model compounds or glucose were used (Chapter 5); moreover after day 7, Y_{cell} is only 72.6 % of the same value when pure EOL was used (Section 6.3.2.1). However, by day 9 in us-EOL fermentation CDW was high enough to do transesterification followed by GC-MS, to determine the FA content and composition of the grown DSM 1069 cells. These results showed that while growing on us-EOL cells accumulate 4.08 % FAs (based on CDW) that are composed of 40.2 % palmitic, 9.9 % hexadecenoic, 9.8 % heptadecenoic, 22.7 % stearic and 17.4 % oleic acids.

Changes in lignin structure (Residue-2.0) during fermentation were followed by ^{13}C NMR, as shown on Figure 6.8, as well as GPC. Latter experiments showed that the original 3400 g/mol weight average molecular weight (M_w) of *us*-EOL first decreased to ~3200 g/mol after 24 h, then increased to 3900 g/mol after 1 week of fermentation and stayed the same till the 9^{th} day.

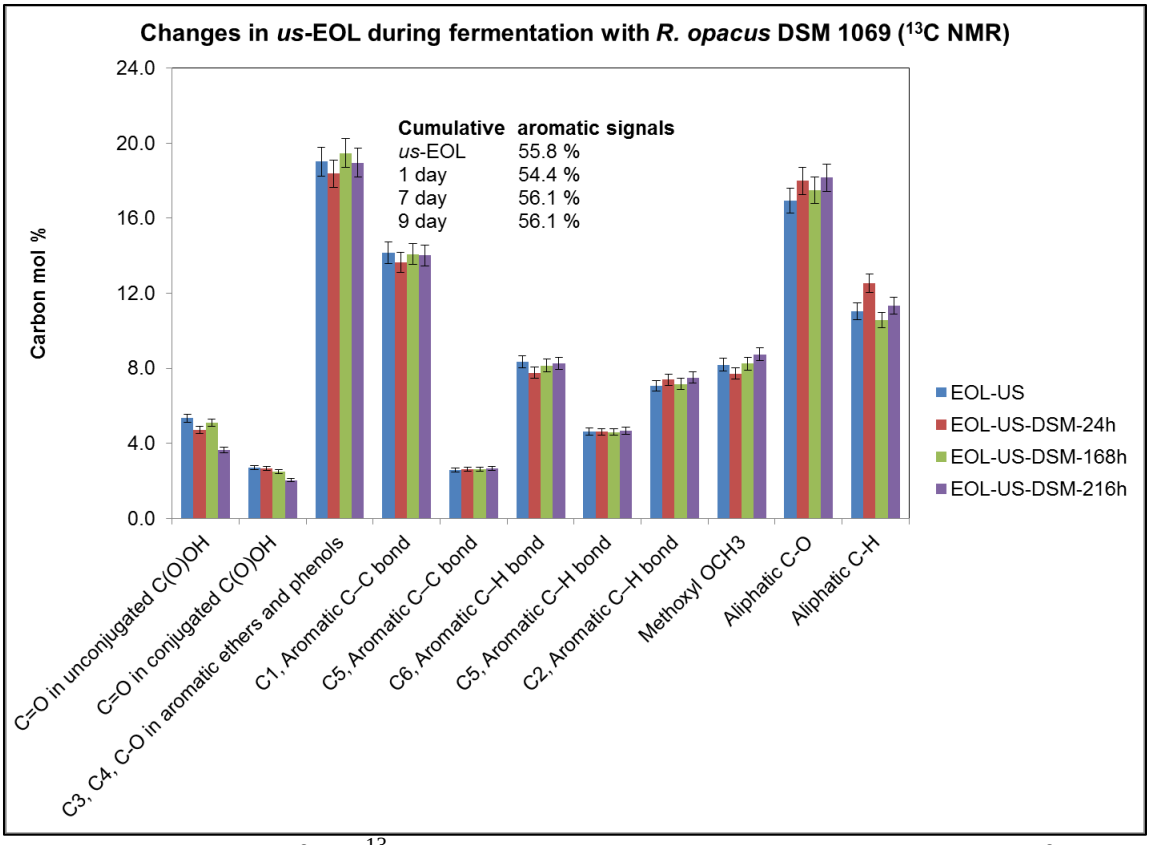

Figure 6.8. Results from ^{13}C NMR experiments obtained on microbially modified *us*-EOL samples

^{13}C NMR results (Figure 6.8) resonate with GPC results, although not many changes can be observed, some of them are significant. By day one of fermentation the cumulative aromatic signal decreases (Figure 6.8) while the aliphatic C-H signal increases with 6.0 % compared to *us*-EOL. Furthermore, carboxylic unconjugated and conjugated signals are decreasing by 32.0 and 24.7 % respectively by day 9, while methoxyl and aliphatic ether/alcohol signals are increasing by 6.7 and 7.3 % respectively. These observations together with GPC results imply that DSM 1069 probably breaks some of the lignin down in the early (first 24 h) stage of the fermentation, while also digesting the more oxidized (carboxylic) lignin monomers and oligomers. This process slows down as the cells face the more polymerized lignin, however, after day 5 when pH is adjusted to 8.45 (Figure

6.7), the aromatic degradation can resume to some extent, possibly due to the more alkaline condition. At the end of the fermentation the more polymerized, recalcitrant lignin is left behind.

In summary, *us*-EOL can support the growth of *R. opacus* DSM 1069, as a sole carbon source, as well as induce lipid accumulation to the extent of 4.08 % based on CDW. Lignin loss is 16.0 %, while us-EOL's sugar content is only 1.43 %, supporting the observation that the extracted FA's are indeed originate from lignin and not sugars. Both EOL sources are poor substrates though, compared to lignin model compounds suggesting that these *R. opacus* species are not primarily lignin degraders, however, more equipped for aromatic oligomer and monomer break down.

6.3.2.3 O_2-Kraft fermentations

The first type of Kraft lignin tested was the neutral media soluble O_2-Kraft, and fermentations were initiated with both R. opacus strains (Table 6.2). Moreover, using the experience from the previous section (6.2.3.2) 2 shake flasks were started with both strains, one with a media pH set to 7.2 and another set to 8.5. Following observations proved though that initial pH set to 8.5 was not enhancing growth, on the contrary, cells didn't gain weight. O_2-Kraft proved to be a really recalcitrant substrate in general, even at pH 7.2 the bacteria couldn't grow sufficient enough for CDW measurements. SDP measurements showed that DSM 1069 cell numbers increased by only 20 times throughout the 9 day fermentation, while in contrast PD630 numbers increased over 300 times during the first week. SDP had shown no contaminations. Substrate, O_2-Kraft (Residue-2.0) loss was, 47 % and 43 % for DSM 1069 and PD 630 respectively. Although there was no sufficient cell weight increase to analyze growth, lignins were

separated (Residue-2.0) to analyze molecular weight changes by GPC, as shown in Table 6.8. Results indicate that there was a really considerable increase in M_w's during fermentation in case of both cell lines. This phenomenon has not been observed with any other substrates, only O_2-Kraft, however, it supports poor growth of cells during fermentation. Lignin with molecular weight as high as represented in Table 6.8 must be recalcitrant to bacterial digestion. It is also noteworthy that these high M_w lignins stayed in solution in neutral media constantly, there were no precipitation observed.

Table 6.8. Increase in M_w of O_2-Kraft during microbial growth

Lignin sample	M_w	M_n	PD (M_w/M_n)
Kraft	4,800	1,300	3.7
O_2-Kraft	4,000	900	4.4
O_2-Kraft-DSM1069-7day	132,000	1,000	132.0
O_2-Kraft-DSM1069-9day	214,000	1,100	194.5
O_2-Kraft-PD630-7day	166,000	1,100	150.9
O_2-Kraft-PD630-9day	223,000	1,200	185.8

6.3.2.4 Kraft fermentations

Multiple different types of Kraft lignin were tested in fermentation experiments, however, the cell growth was either very poor (e.g. Section 6.3.2.3) or not visible at all. Consequently, a new strategy was implemented including low M_w Kraft, separated by acidification to pH 4.5 and filtration (Chapter 3 and 6, Sections 6.2.2 and 6.3.1.2, properties in Table 6.6). This low M_w Kraft was used as an adaptation substrate, based on the assumption that lower M_w lignin must be easier to utilize, as had been observed with EOL supported growth (EOL ~2700 g/mol; Kraft ~4800 g/mol). Accordingly, a fermentation experiment series were designed to test this theory. The last two rows of Table 6.2 indicate this series of experiments while Figure 6.9 details them (flowchart).

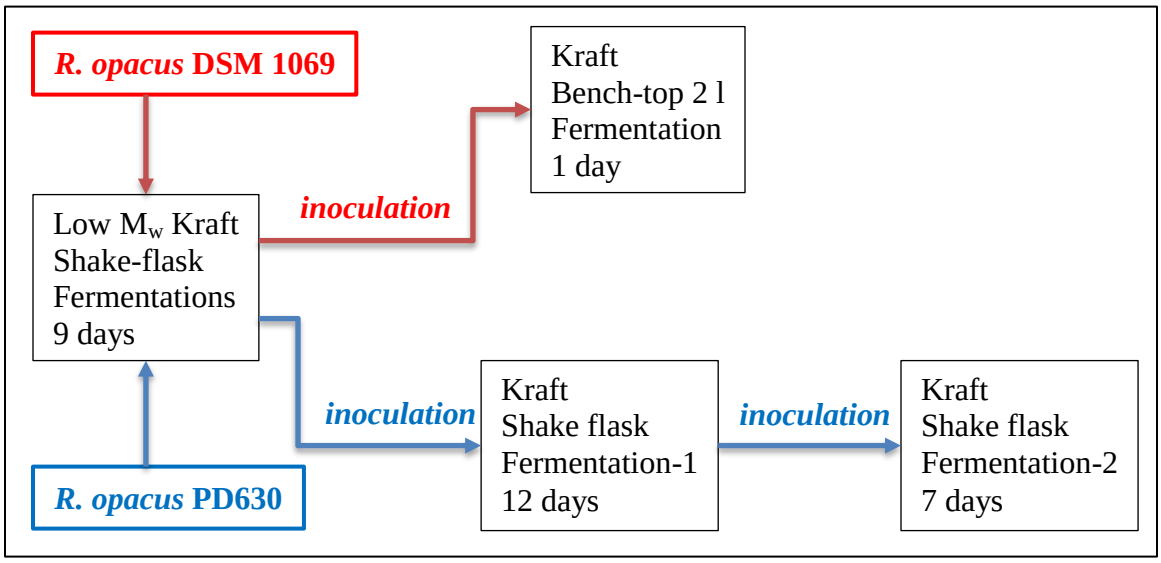

Figure 6.9. Flowchart of Kraft fermentations with *R. opacus* strains

6.3.2.4.1 Low M_w Kraft bioconversion

Both cell lines were inoculated and grown on low M_w Kraft to test their adaptation abilities (Figure 6.9), and if successful use them as starting cultures in "original" (high M_w) Kraft fermentations. The bacteria first struggled, however, by day 2 and 6, both DSM 1069 and PD630 were successfully adapted. Meaning that their colony forming units (CFU/ml) increased by one magnitude at least, and their cell dry weights reached 0.085-0.090 mg/ml by day 7. It has to be noted that between day 2 and 3 the colonies on SDP plates lost their coloration, however, the color returned after day 4. Furthermore these colorless cells were also inoculated into full media, where coloration has returned within 24 h. Residue-10.3 (lignin) was separated after 9 days, when cells were inoculated into Kraft fermentations, and residual lignin was analyzed by ^{13}C and HSQC NMR as shown on Figures 6.10 and 6.11 respectively.

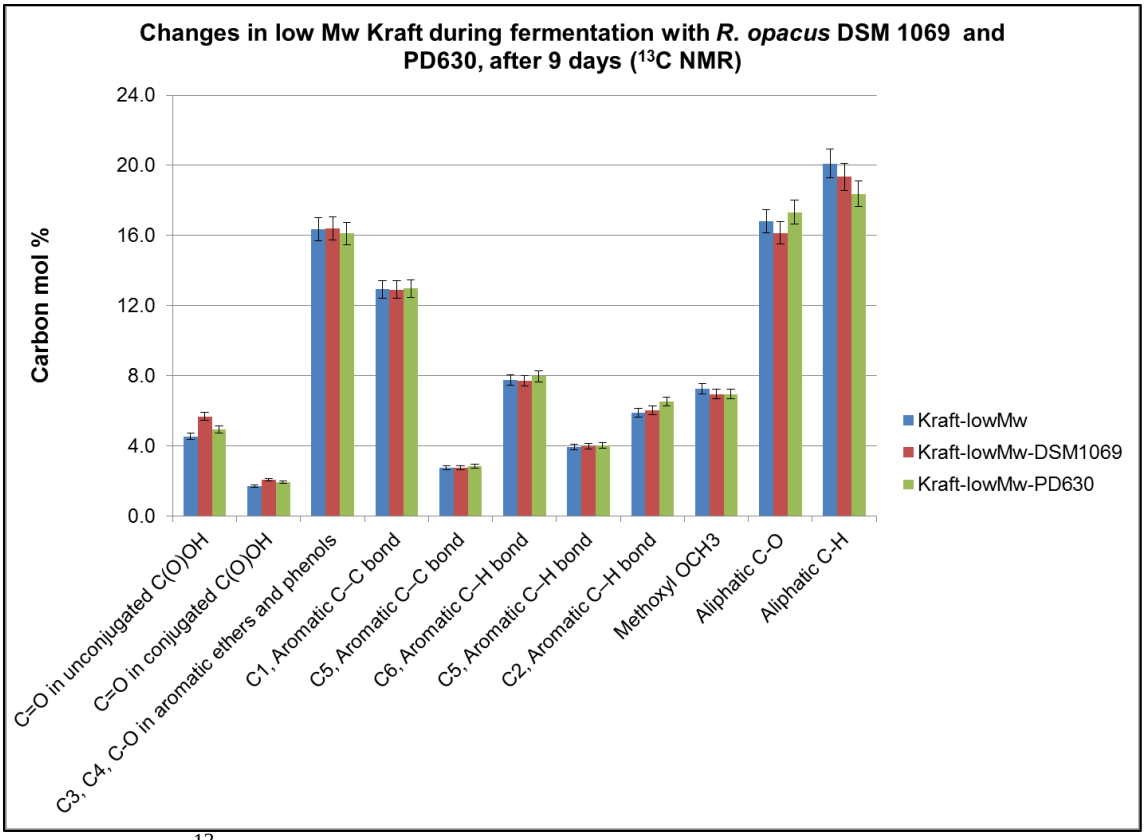

Figure 6.10. ^{13}C NMR results for low M_w Kraft fermentations

^{13}C NMR results indicate some differences, namely: 4-9 % decrease in aliphatics and a more significant 10-20 % increase in carboxylic acids. It is also visible on Figure 6.10, that PD630 and DSM 1069 had different effects on aliphatic ethers and alcohols (lignin inter-unit linkages), -4 and +3 % respectively. HSQC NMR shows the disappearance of diterpenoic acids (DA) and fatty acids (FA) mostly, as well as some yet unidentified lignin related aliphatics (LRA) on Figure 6.11 (Appendix D), from left to right. While it also shows the appearance of two new peaks, a DA (1) [181, 185] and a lignin related aliphatic alcohol namely the γ-OH in erythro β-O-4 linkages [96, 101, 102, 177].

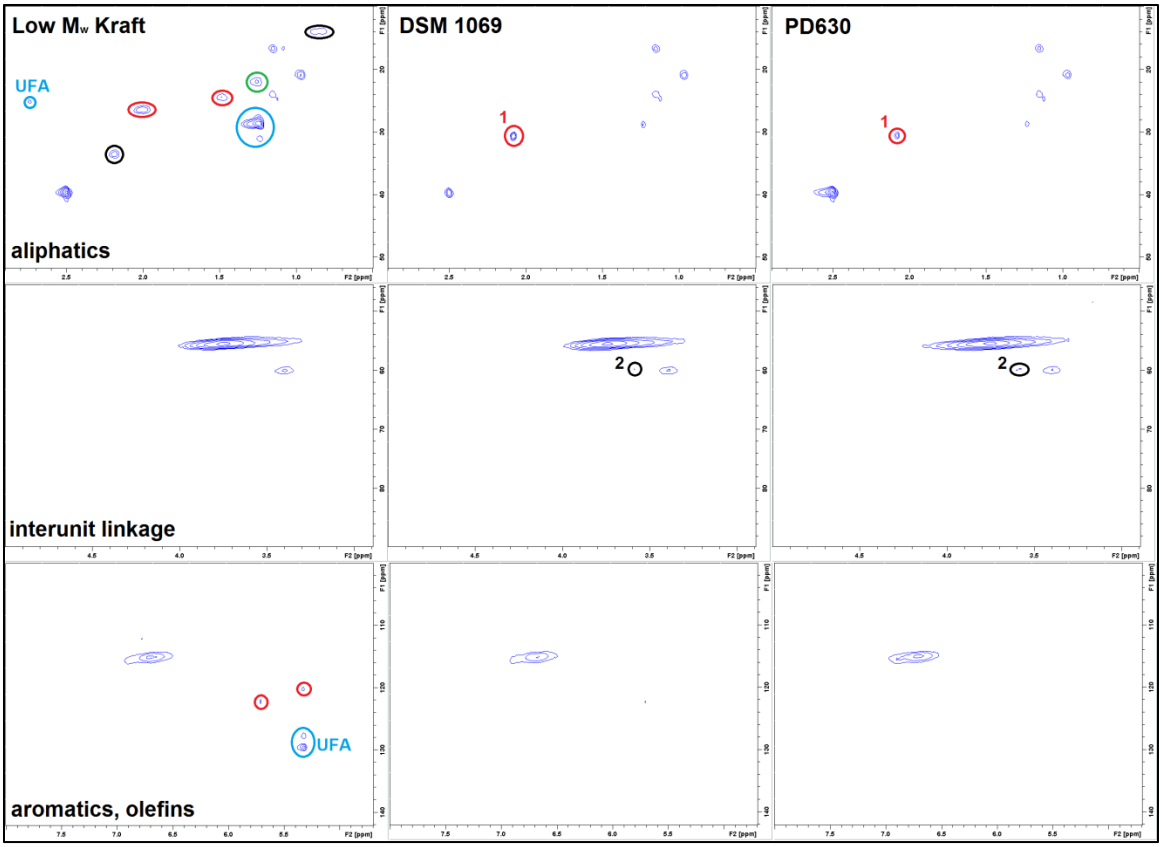

Figure 6.11. HSQC of changing low M_w Kraft as cells grow on it, including all three regions, where assignments were made according to Appendix D tables. Only changing peaks are assigned, diterpenoic acids (DA) with red, fatty acids (FA) with light blue, including unsaturated UFAs. Lignin related aliphatics (LRA) with black and FA-DA overlapping regions with green. DA-(1) and LRA-(2) are novel peaks showing up during fermentations.

In summary, when growing on low M_w Kraft lignin both strains (DSM 1069 and PD630) adapted slowly, however, after adaptation by the end of the first week, enough cellular material was collected for inoculation into larger scale fermentations. NMR data on microbially modified lignin showed that mostly FA and DA peaks disappeared as well as some yet unidentified lignin related aliphatics (LRA). Some new peaks showed up on HSQC NMR as well, for example the γ-OH in erythro β-O-4 linkages. Growth on this substrate was really challenging, colonies even lost their coloration for a short period, and even though it was regained, both in full media, and after 2 more days on low M_w Kraft

itself, more proof was called for that there's no other contaminating cell line. Accordingly, after sampling some cells were separated, washed and stained [263], and examined under light microscope, Figure 6.12 (method on Figure 6.1). Bacteria showed "healthy" (usual) shape and size under light microscope, an accordance with pictures from literature [256, 272].

Figure 6.12. *R. opacus* DSM 1069 cells growing on low M_w Kraft lignin, red bar shows 100 µm

6.3.2.4.2 R. opacus PD630 converting Kraft lignin

After growing on low M_w Kraft PD630 cells were separated, washed and inoculated into new media containing the original (high M_w) Kraft lignin, Figure 6.9, bottom row, and while Fermentation-1 served as further adaptation, Fermentation-2 was closely monitored for changes in both Residue-10.3 (cell material) and Residue-2.0 (lignin). In Fermentation-2 (Figure 6.9, bottom right hand-side) the total Residue-2.0 (lignin) loss was approximately 31.4 % by the end of the 7 day fermentation, while cell

number and weight increase, by day 2, were 640 and 17 times more than the inoculation values, as shown on Figure 6.13.

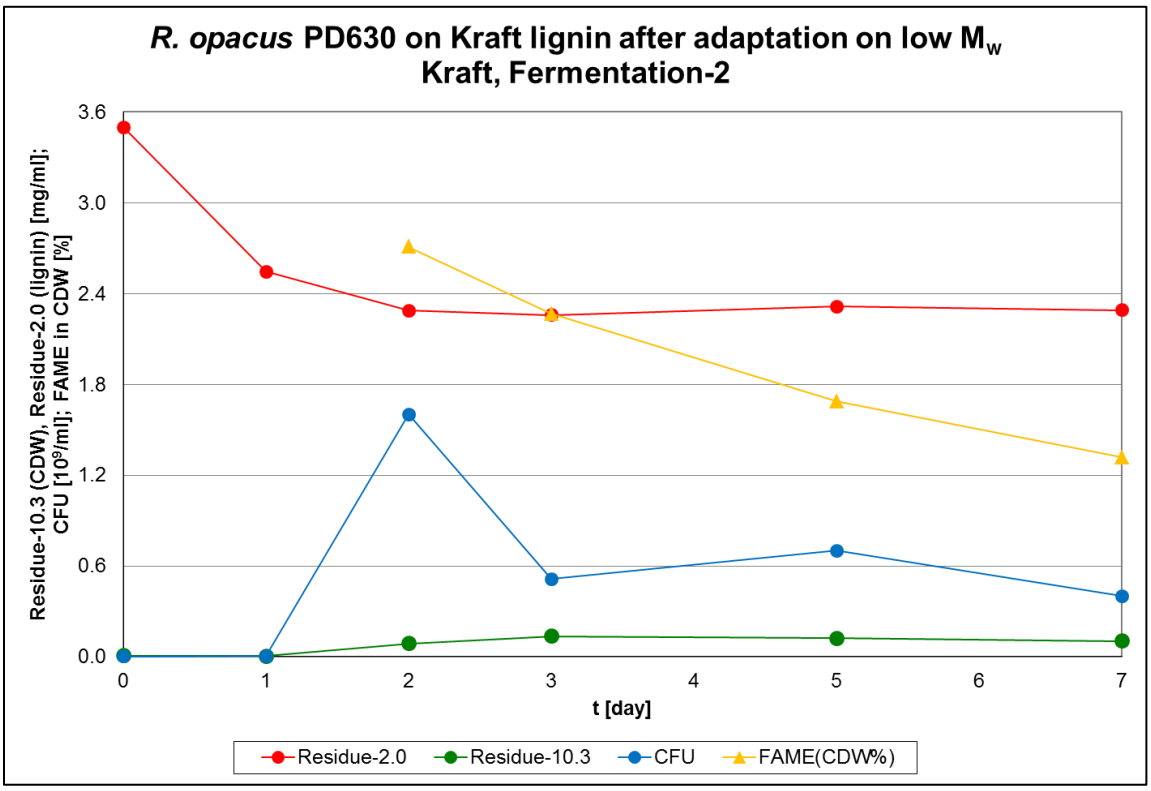

Figure 6.13. Lignin loss (Residue-2.0), bacterial growth (CFU and Residue-10.3) and fatty acid accumulation (FAME) during Fermentaion-2 on Kraft lignin with PD630

The growth of PD630 on Kraft was sufficient enough to isolate cell material for transesterification and FAME measurement by GC-MS. Latter value was translated as total accumulated FA, and it is illustrated on Figure 6.13, while their composition is listed in Table 6.9. FA composition changes in the cells constantly, however, a trend can be observed as fermentation proceeds, namely, the relative amount of unsaturated FA will decrease, while saturated FA increases (Table 6.9). Diterpenoic acid methyl esters (DAME) were also observed with GC-MS, however, without proper standards their

amounts had not been determined. Qualitatively though, Me-abietate, Me-dehydro-abietate and EPATME (Appendix D) were identified, as illustrated on Figure 6.14, together with FA types observed. The presence of these extractives in Kraft lignin were shown earlier (Section 6.3.1.2), accordingly, cell or lipid productivities calculated on lignin would be misleading. Instead, ^{13}C, ^{31}P and HSQC NMR experiments were conducted to follow changes in Residue-2.0 (Kraft lignin, including extractives), that can be an indicator to what materials were the cells (PD630) consuming and to what extent.

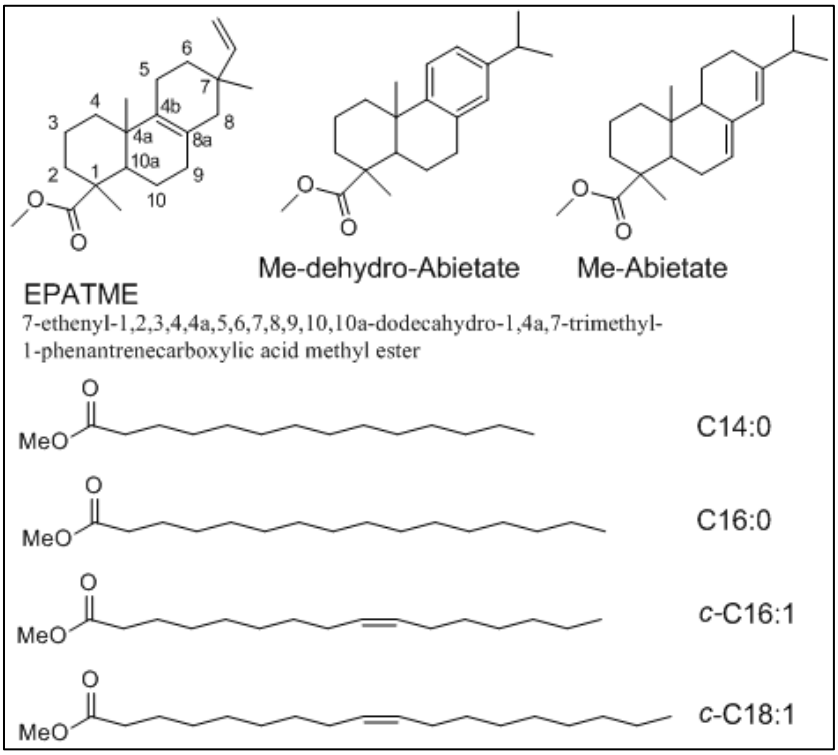

Figure 6.14. DAME and FAME found in cell material after growing on Kraft lignin; C14:0- Me-myristate; C16:0- Me-palmitate; c-C16:1- Me-palmitoleate and c-C18:1- Me-oleate

Table 6.9. FA content and composition of PD630 growing on Kraft, based on FAME composition after whole cell methanolysis

t [day]	Total FAME [CDW%]	FAME composition [% of total FAME]			
		C14:0	*c*-C16:1	C16:0	*c*-C18:1
2	**2.71**	8.4	21.5	44.6	25.5
3	**2.27**	11.6	13.9	49.5	25.0
5	**1.69**	15.7	12.5	50.3	21.6
7	**1.32**	19.8	13.6	50.1	16.5

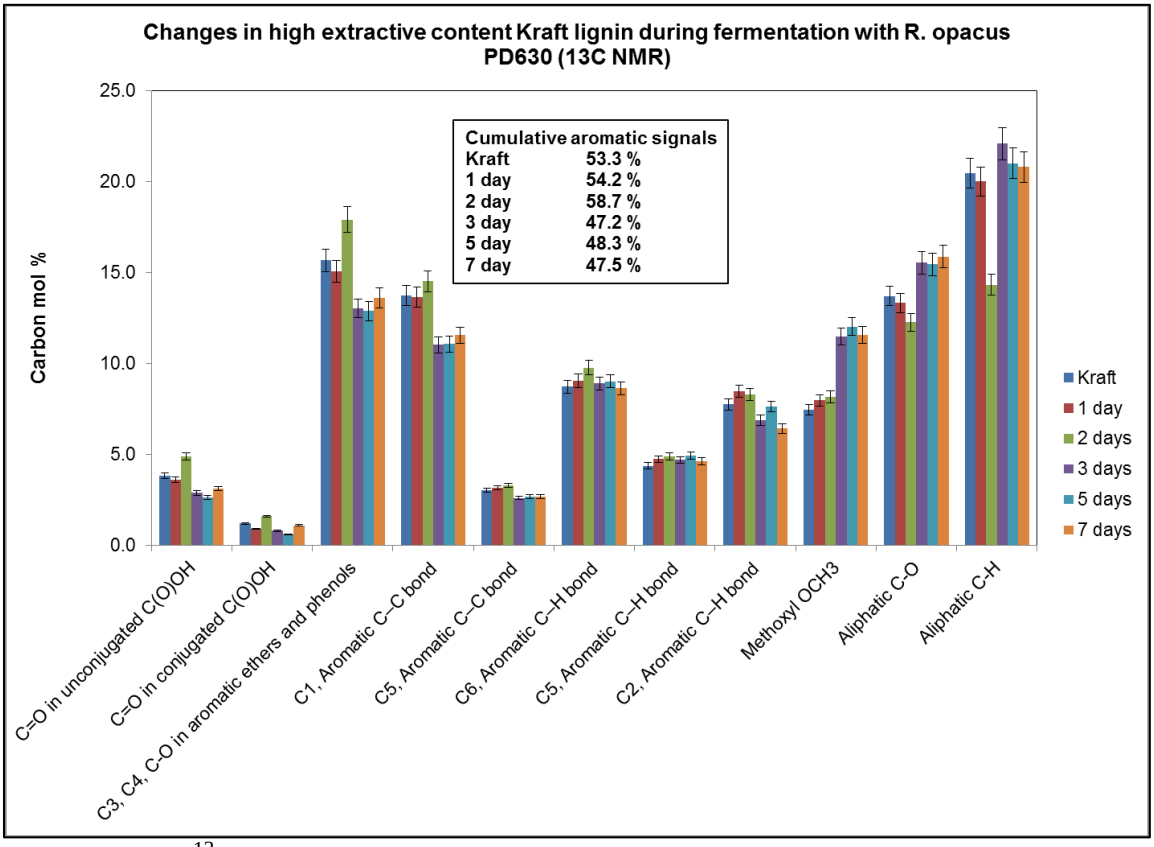

Figure 6.15. ^{13}C NMR comparison of functionality distribution changes as Fermentation-2 on Kraft lignin with R.opacus PD630 strain proceeds

Table 6.10. GPC results of Residue-2.0 (high extractive content lignin) during Fermentation-2 of Kraft lignin with PD630 strain

t [day]	M_w [g/mol]	M_n [g/mol]	PD
Kraft (0)	4800	850	5.6
1	2700	500	5.4
2	4300	700	6.1
3	4300	700	6.1
5	3600	650	5.5
7	3600	700	5.1

^{13}C NMR experiments (Figure 6.15) on Residue-2.0, representing high extractive content Kraft lignin after fermentation steps, show significant differences in composition (carbon distribution among functionalities) as Fermentation-2 proceeds. Looking at molar mass distribution (GPC) data (Table 6.10) and carbon distribution changes (^{13}C NMR, Figure 6.15) together with cell growth and FA loss information (Figure 6.13, Table 6.9) facilitates the understanding of the mentioned differences, especially if the data is dissected into three stages. These stages are based on elapsed fermentation time, as follows: 1) the first two days; 2) from day 2 to day 3; and 3) from day 3 till the end of the experiment on day 7.

In stage 1) of the fermentation, until the end of the second day, there is an average 30 % increase in carboxylic groups and a 14 % increase in aromatic C-O bonds suggesting the oxidation of lignin (Figure 6.15). Conversely, there's an 11 % decrease in aliphatic C-O, representing lignin inter-unit linkages and suggesting the depolymerization of lignin (Figure 6.15), this latter observation is also supported by M_w data (Table 6.10). Furthermore, there's a 30 % loss of aliphatic signal, implying that PD630 is consuming the extractives (Figure 6.15), e.g. DA and FA (Figure 6.14). These latter decreases in aliphatic C-H and C-O signals explain the 10 % relative increase in the cumulative aromatic signal in comparison to the total carbon signal (Figure 6.15). The changes in this fermentation stage suggest that cells grow, and accumulate lipids on extractives (Figures 6.13 and 6.15), while oxidizing and depolymerizing lignin (Figure 6.15 and Table 6.10).

Stage 2) between day 2 and 3, shows the most conspicuous changes in almost all functionalities. Carboxylic carbon signals decrease by 40 and 50 %, unconjugated and

conjugated acids respectively (Figure 6.15). Also aromatic C-O (on carbons C-3 and C-4) signal drops by 19 %, suggesting the degradation of lignin aromatics by PD630 that were oxidized in the previous stage (Figure 6.15). Aromatic C_1-C bond signal decreases by 7 %, while the cumulative aromatic signal by 20 %, supporting lignin degradation by cells (Figure 6.15). There is a 40 % increase in methoxyl groups (Figure 6.15) that the cells need to remove from lignin monomers, to form archetypal dioxygenase substrates (Chapter 2, Section 2.5.3, Figure 2.33), before further breakdown of aromatics [219, 236]. It has recently been shown that *R. jostii* RHA1 utilizes vanillin dehydrogenase and vanillate-O-demethylase to form protocatechuate (PCA) from vanillin (Figure 2.28, Section 2.5.2.2) while formaldehyde is released [219, 236]. The possibility that a similar enzyme pair is utilized in *R. opacus* PD630 is possible in theory, suggesting that demethoxylated lignin monomers are taken up by these cells, while methoxylated lignin monomers are enriched in the residual Kraft polymer (Residue-2.0), increasing the methoxyl signal on the ^{13}C NMR spectrum. This theoretical possibility is further supported by model compound experimental (Chapter 5) results, which showed PD630 forming PCA from vanillic acid in the supernatant (extracellularly) before uptaking it (HPLC and ^{1}H-NMR results in Chapter 5). Continuing the line of increasing functionalities in stage 2), are the aliphatic C-O (27 %) and C-H (54 %) signals, this relative rise in signal intensity arise because of the loss in aromatic signals (Figure 6.15). It is also noteworthy, that FA content in cells only decrease from day 2 (Figure 6.13), possibly meaning two things; 1, cellular lipids were only accumulated while utilizing extractives and aliphatics from Kraft; and 2, these lipids are now used as chemical energy

to support the degradation of aromatics. Former possibility resonates with conclusions withdrawn from Stage 1) results, while the latter lipid loss is visualized on Figure 6.13.

Stage 3) represents the last 4 days of Fermentation-2 with PD630 and it resembles Stage 1). After digesting the lower M_w, oxidized part of Kraft-lignin in Stage 2), depolymerization reactions need to commence again to reduce M_w, and GPC results show a 16 % decrease for Stage 3) (Table 6.10). Aliphatic signal also drops by 6 %, while the cumulative aromatic carbon signal increases by 2 % that is mostly due to the 5 % gain in aromatic C-O (Figure 6.15). Suggesting the digestion of aliphatics by PD630, that results in the simultaneous increase in the aromatic signal, moreover the further oxidation of lignin (Figure 6.15). Latter observation is supported by the increase in carboxyl groups, especially in case of conjugated acids (35 %), adding to the resemblance of Stage 3) to Stage 1). This latter observation also suggests that lignin side-chains ("propanoids", such as α-keto-phenylpropanoid, Figure 2.26) are degraded through an oxidative pathway, probably similar to fatty acid β-oxidation, as implied in Section 2.5.2.1 (β-O-4, degradation, Figure 2.26), to obtain vanillic acid [219, 222, 233]. HSQC analysis, as detailed below, supports this possibility.

2D NMR, such as HSQC has a better resolution in separating chemical shifts of functionalities then proton or ^{13}C NMR, however, it is only a qualitative measurement, due to reasons detailed in Section 2.4.3.1.2 [96, 101, 176, 177]. In case of high extractive content Kraft lignin, used in present work, HSQC proved to be a remarkable tool (e.g. analysis of low Mw Kraft, Section 6.3.2.4.1), especially in case of the overcrowded aliphatic region. However, to use it effectively for the analysis of extractives (e.g. DA

and FA) next to lignin a database had to be created (Kraft lignin properties, Section 6.3.2.4.1) by combining existing literature data on both lignin [93-96, 101, 102, 140, 142, 143, 165, 175, 177, 178, 180] and extractive chemical shifts [181-186, 295, 296] (Appendix C). In this section Tables A.C.4-6 from Appendix C were used as guidelines when analyzing changes in Residue-2.0, representing high extract content Kraft lignin modified by *R. opacus* PD630 during Fermentation-2 (Table 6.2). Figures 6.16-18 are showing the changes in Kraft lignin's aliphatic, inter-unit linkage (side-chain) and aromatic/olefinic regions respectively, during this one week fermentation.

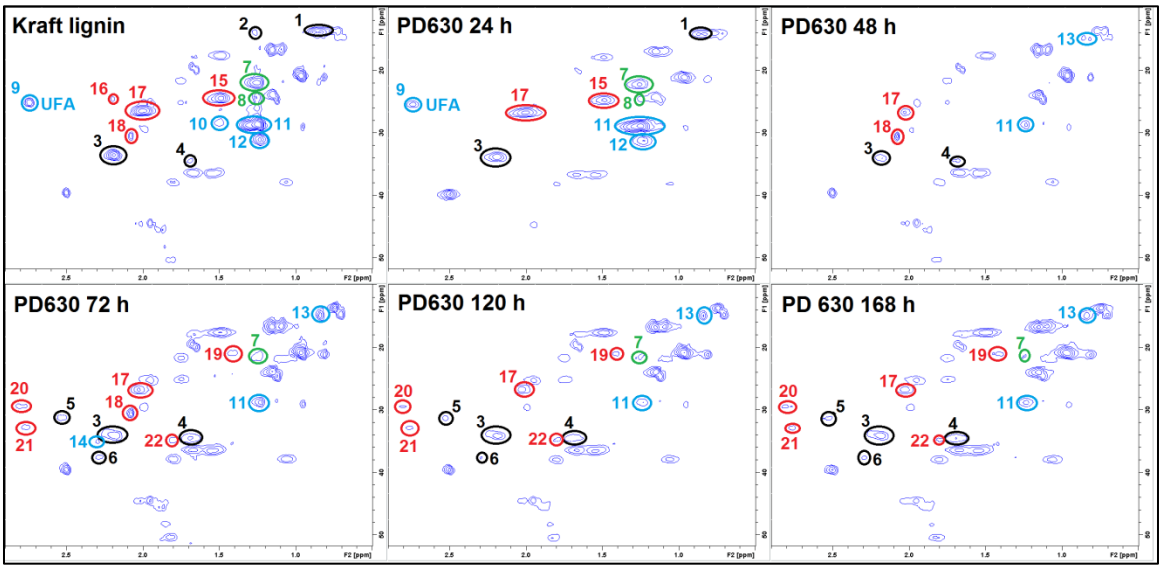

Figure 6.16. Changes in the aliphatic region of Kraft lignin (δ_H 0-3 ppm; δ_C 0-52 ppm); black, green, blue and red represent lignin related aliphatics (LRA), DA-FA overlap, FA and DA respectively. Numbered peaks showed qualitative changes during fermentation, accordingly they are listed in Table 6.11.

Table 6.11. Changes in the Kraft aliphatic region during Fermentation-2 with *R. opacus* PD630; UFA- unsaturated-FA

No.	δ_C/δ_H [ppm]	Region	Assignment/Change
1	13.8/0.7-0.8	LRA-(FA)	Disappears after 48 h
2	13.9/1.3	LRA	Disappears after 24 h
3	33.5/2.18		Significant decrease over the first 72 h
4	34.5/1/69		C_β in dihydroconferyl, disappear, then reappear
5	31.3/2.53		C_α in dihydroconferyl, appears after 72 h
6	37.6/2.29		Appear after 72 h
7	22.0/1.25	DA-FA	Significant decrease over the first 72 h
8	24.4/1.26		Disappears in 48 h
9	25.1/2.73	FA	UFA, Disappears in 24h
10	28.3/1.50		Disappears in 24h
11	28.6/1.25		Significant decrease over the first 72 h
12	31.1/1.24		Disappears in the first 72 h
13	14.8-9/0.7-8		Appears after 48 h
14	35.0/2.30		Appears at 72 h, disappears by 120 h
15	24.4/1.48	DA	Disappears in the first 48 h
16	24.6/2.20		Disappears by 24 h
17	25.2/1.95		Significant decrease in first 48 h
18	30.5/2.08		Disappear after 72 h
19	21.0/1.41		Appears after 72 h
20	29.4/2.81		Appears after 72 h
21	32.8/2.76		Appears after 72 h
22	34.7/1.79		Appears after 72 h

Briefly, the most conspicuous qualitative changes, during fermentation, in the aliphatic region are:

1. The decrease in both fatty acids (FA) and diterpenoic acids (DA) in the first 24-72 h, supporting the observations with ^{13}C NMR (Figure 6.15), and that PD630 utilizes these compounds more in the beginning.
2. Appearance of various, mostly, DA signals after 72 h, different from the ones that disappeared in the first 48 h. If the starting lignin or 24 h spectra are increased in intensity, these peaks are visible, meaning that their appearance after 72 h is due to the loss in other functionalities, and not the increase of these DA's. This supports ^{13}C NMR results (Figure 6.15), where the second

stage of the fermentation (from 2nd to 3rd day) showed a 20 % drop in aromatic signals.

HSQC of Kraft lignin side-chain region's changes during fermentation are illustrated on Figure 6.17, and peaks are listed in Table 6.12.

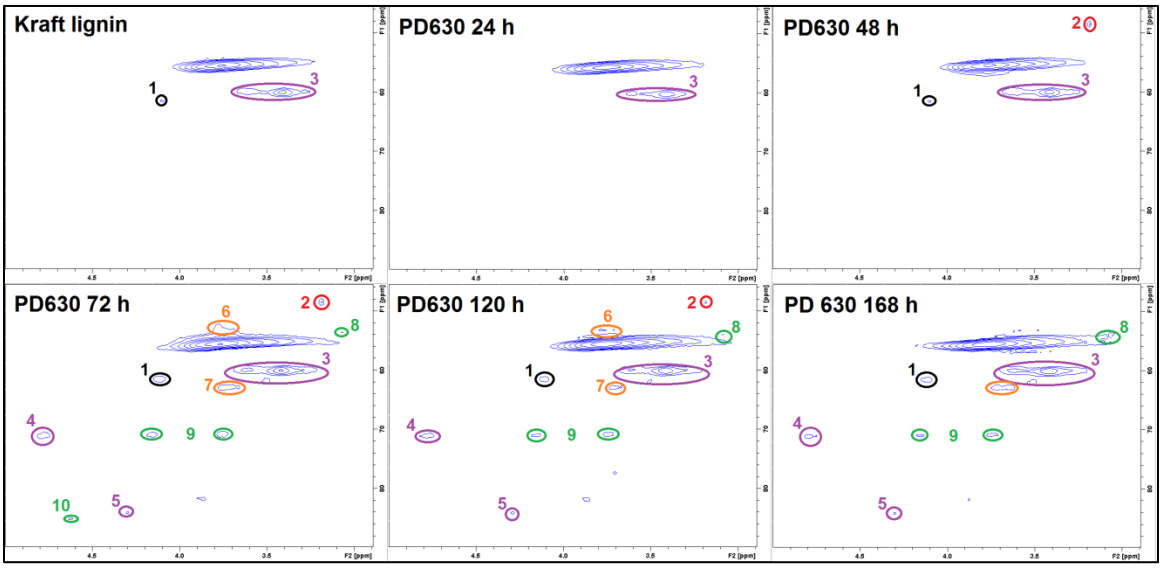

Figure 6.17. Changes in the side-chain region of Kraft lignin (δ_H 3-5 ppm; δ_C 45-90 ppm); black, red, green, orange and violet represent coniferyl-alcohol γ-OH, DA-methyl-ester, β-β, β-5 and β-O-4 linkages respectively. Numbered peaks showed qualitative changes during fermentation, accordingly they are listed in Table 6.12.

Table 6.12. Changes in the Kraft side-chain region during Fermentation-2 with *R. opacus* PD630

No.	δ_C/δ_H [ppm]	Linkage	Assignment/Change
1	62.5/4.11	n/a	C_γ/H_γ in coniferyl sidechain (Ar-CH=CH-$\underline{CH_2}$-OH)
2	53.0/3.8	n/a	DA-methyl-ester, appear 48 h, disappear 168 h
3	60-1/3.4-6	β-O-4	C_γ increase until 72 h, then no change
4	71.0/4.77		C_α appear at 72 h, then slight decrease
5	83.7/4.29		C_β appear at 72 h, then slight decrease
6	53.6/3.47	β-5	C_β appear at 72 h, then disappear by 168 h
7	62.7/3.70		C_γ appear at 72 h, then slight decrease
8	53.7/3.10	β-β	C_β appear at 72 h, then no change
9	71/3.8-4.2		C_γ appear at 72 h, then slight decrease
10	85.0/4.62		C_α appear at 72 h, then disappear by 120 h

Above results (Figure 6.17, Table 6.12) show a trend that fits all 3 major lignin inter-unit linkages, β-O-4, β-5 and β-β, namely, their signal become visible after 72 h of growth, then they fade until the end of the experiment. ^{13}C NMR results show a 20 % drop in aromatic signals between 48 and 72 h (Figure 6.15), while at the same time HSQC (Figure 6.17) spectra show an increase in three major inter-unit linkages. GPC on the other hand showed the same Mw for Kraft lignin (Residue-2.0) after both 48 and 72 h of fermentation (Table 6.10). These observations together suggest the (theoretical) possibility that while parts of lignin are depolymerizing and degrading, other parts are repolymerizing, and this repolymerization favors the formation of β-O-4, β-5 and β-β linkages.

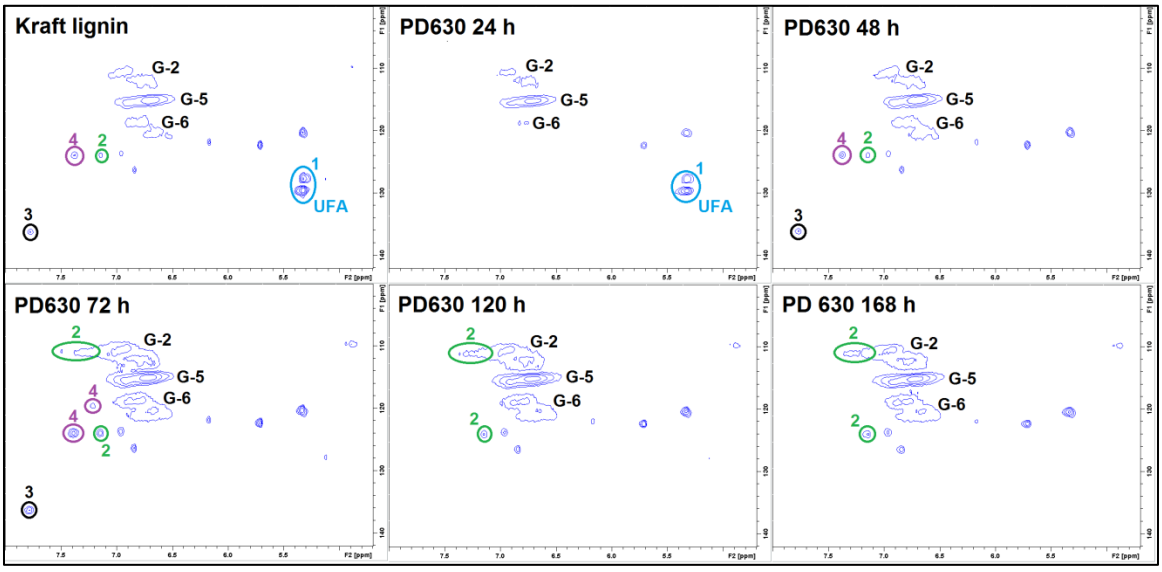

Figure 6.18. Changes in the aromatic/olefin region of Kraft lignin (δ_H 4-9 ppm; δ_C 100-160 ppm); light blue, green, violet and black represent UFA, C-2/H-2 and C-6/H-6 with conjugated C_α=O, C-6/H-6 with conjugated C_γ=O and unknown peaks respectively.

Changes in the aromatic/olefin part of Kraft lignin during fermentation are showed on Figure 6.18 that depicts the respective region of the HSQC spectra collected. Results show (Figure 6.18) that, just like in the aliphatic region UFA (1) will be the first to disappear, to be taken by the cells of *R. opacus* PD630. Guaiacyl-aromatics (G-2, G-5 and G-6) decrease by the end of the first day, then these signals increase till 72 h supporting GPC data (Table 6.10). It can also be observed that peaks 2, 3 and 4 are disappearing and reappearing repeatedly (2 is fluctuating as well, just not as conspicuously, Figure 6.18). Literature experimental data showed that peaks labeled (2) are C-2/H-2 and C-6/H-6 (110.9/7.29 and 123.9/7.15 ppm respectively [96, 177], Appendix C) cross-signals from aromatic rings that have a conjugated C_{α}=O. It has also been shown before that peaks labeled (4) are C-6/H-6 (119.4/7.21 and 123.9/7.38 ppm [96, 141, 177], Appendix C) cross-signals from aromatic rings that have conjugated C_{γ}=O substituents (peak 3 was not yet identified, however it fluctuates parallel to 4). These latter observations suggest the continuous formation and degradation of conjugated carbonyls, such as α-keto-phenylpropanoid or vanillic acid (Figure 2.26, Chapter 2, Section 2.5 [219]), that was also suggested as a possibility earlier, when analyzing Stages 1) and 3) in present fermentation, with ^{13}C NMR (Figure 6.15). In conclusion, both ^{13}C and HSQC NMR experiments seem to support the possibility that *R. opacus* PD630 has similar pathways for the breakdown of e.g. the β-O-4 linkage and subsequent phenylpropanoids, as other actinomycetes bacteria utilize (resembling β-oxidation, Figure 2.26 [219]).

6.3.2.4.3 Bench-top scale Kraft bioconversion with R. opacus DSM 1069

The last fermentation in the series of Kraft fermentations listed in Table 6.2, and detailed on Figure 6.9, was the bench-top scale (2 l) bioconversion of high extractive content Kraft lignin with *R. opacus* DSM 1069, that was previously adapted to this substrate on low M_w Kraft (Section 6.3.2.4.1). Table 6.13 summarizes all media and cellular changes that were measured when the fermentation was inoculated and 1 day later.

Table 6.13. Summary of results from high extractive content Kraft bioconversion with *R. opacus* DSM 1069 cell line in a bench-top bioreactor, after adaptation on low M_w Kraft; [a]Residue-10.3; [b]Residue-2.0; [c]FE- extractives as measured after Folch extraction; [d]g cells gained over g Kraft used

Time	**CDW[a]**	**Kraft[b]**	**NH_4^+**	**M_w**	**FE[c]**	**Y_{cell}**	**dc_{cell}/dt**	**dc_{lipid}/dt**
[h]		mg/ml		g/mol	CDW%	g/g[d]	g/l·h	
0	0.003	3.500	1.00	4800	-	-	-	-
24	0.248	2.448	0.20	5800	15.00	0.233	0.0102	0.0016

The values in Table 6.13 are closer to model compound fermentation results (Chapter 5), than to previous lignin experiments (Section 6.3). Accordingly, it can be concluded that the better aeration of the reactor and the preliminary adaptation proved successful. Folch-extraction (Chapter 3) on separated whole cell material (Residue-10.3), showed 15.00 % extractive content based on CDW, Table 6.13 [266]. After transesterification of the extractives [265], GC-MS results showed that next to methyl-palmitate and methyl-oleate methyl-abietate, methyl-dehydro-abietate and EPATME (Figure 6.14) compose the extractives, as illustrated on Figure 6.19. However, due to lack of proper standards the accurate ratios were not calculated. The extractives were also subjected to a TLC experiment, which concluded that the extractives contain only trace amounts of free FAs,

and that they're mostly composed of material(s) with a retardation factor (R_f) of 0.16. The standards used in the TLC experiments showed values that are widely accepted in the literature, for example 0.42 for TAGs [13, 264, 284]. The R_f of 0.16 was not found in the literature, accordingly (only as an educated guess), it is assumed that the extractives are mostly composed of the glycerol-esters of diterpenoic (DA) and fatty acids (FA), based on the research proving that *R. opacus* tends to incorporate different compounds (e.g. phenyldecane) into its reserve glycerol-esters, without modification [284]. In conclusion, without exact ratios, the cell extract composing DA and FA types are shown on Figure 6.19 (Chemical structures on Figure 6.14). It is also noteworthy, that just like in case of DSM 1069 growing on EOL as a sole carbon source (Figure 6.5), the extracted cell material (Residue-10.3) was light brown colored, instead of the light orange/pink color produced on full media, or model compounds, e.g. vanillic acid, Figure 6.19.

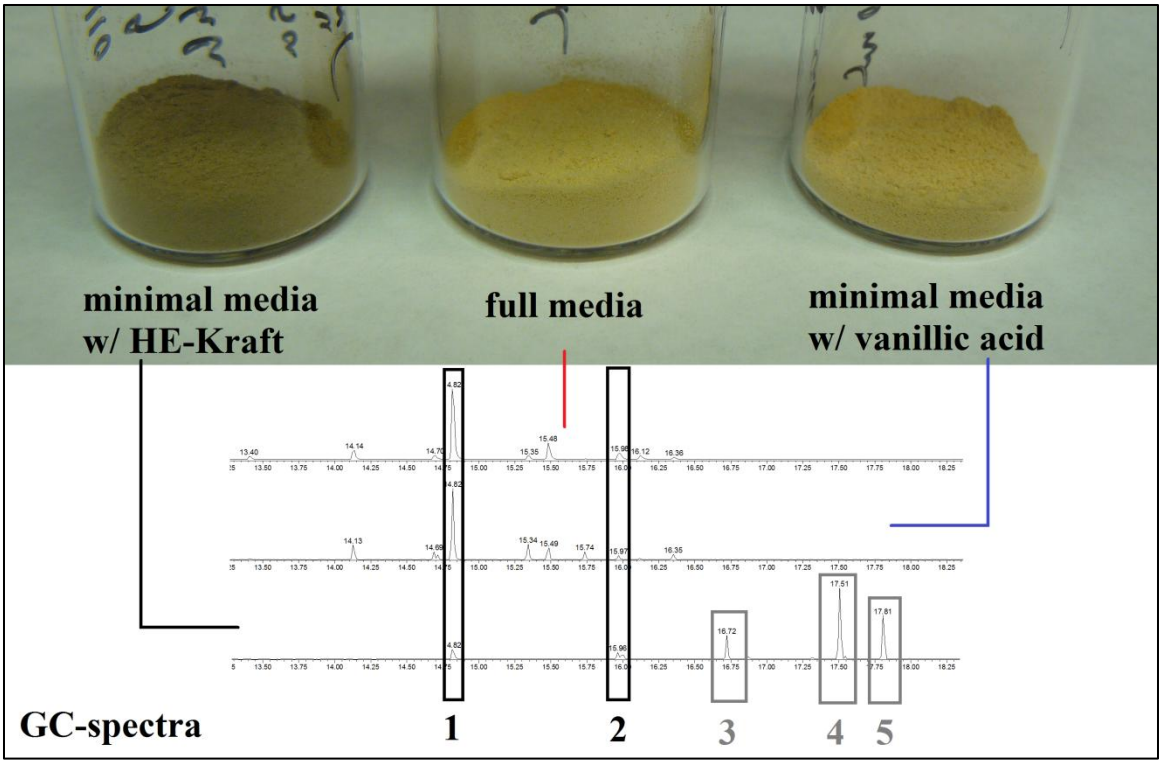

Figure 6.19. On the top showing Residue-10.3, separated and freeze-dried cells that had been grown on high extractive content (HE) Kraft lignin, full media and vanillic acid respectively. The lower part shows the GC spectra of the cell-extracts after transesterification; 1, Me-palmitate; 2, Me-oleate; 3, EPATME; 4, Me-dehydro-abietate and 5, Me-abietate; chemical structures are detailed on Figure 6.14.

Staining and light microscopy of the separated DSM 1069 cells after growing on high extract content Kraft was also conducted. Pictures showed normal growing cells (Figure 6.20), similarly to what has been seen when growing on low M_w Kraft lignin (Figure 6.12); and also, what is found in the literature [256, 272]. However, some unique formations were also seen on multiple occasions (Figure 6.20), and only when Kraft lignin was the carbon source. Plating experiments showed no contaminating microorganisms, accordingly, it has to be assumed that these unique shapes (Figure 6.20) are due to "changes" caused by the substrate Kraft lignin.

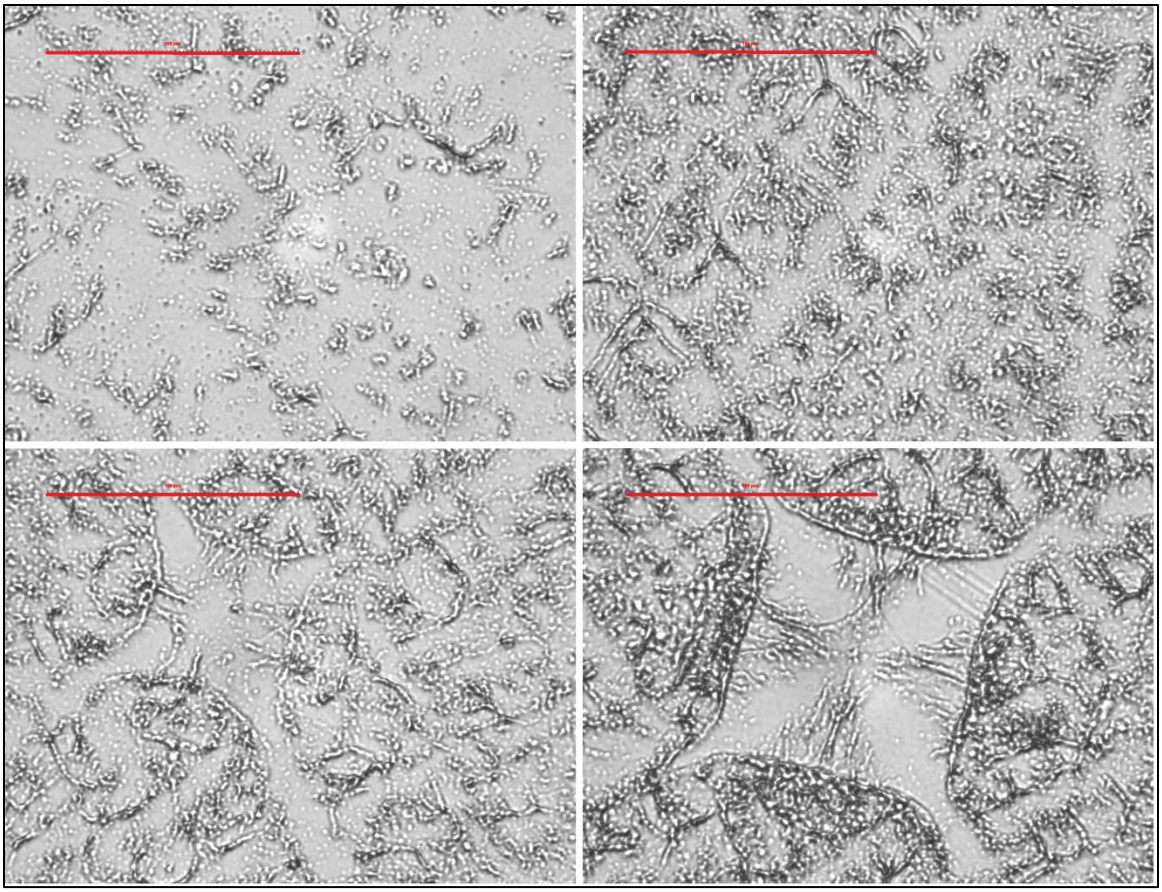

Figure 6.20. Top left picture showing "normal" growth of *R. opacus* DSM 1069 on Kraft lignin, as experienced previously with other substrates as well. Bottom right picture shows the unique shape formed while growing on Kraft lignin (the same substrate). These shapes were observed multiple times, while there was no sign of contamination by any other microbes. Top right and lower left pictures show what is assumed either the initiation and/or the degradation of these unique formations. Red bar equals 100 μm.

There's a 30 % loss in Residue 2.0 (lignin) as shown in Table 6.13, while Kraft's extractive content was maximally 20 % (Table 6.6), consequently parts of the lignin were converted. ^{13}C NMR result of the separated Kraft in present case is detailed in Table 6.14, together with the starting lignin. Results show relatively high (17 %) aliphatics content (Table 6.14), and considering the 30 % loss in substrate, this further supports the previous observation, that lignin had to be metabolized together with the extractives.

Table 6.14. ^{13}C NMR, comparison of functionality distribution of Kraft lignin before and after fermentation with *R. opacus* DSM 1069

Carbon NMR		functionality/aromatic ring	
∫ Region [ppm]	**Assignment**	**Kraft**	**DSM1069 24 h**
180.5-170.0	**C=O in unconjugated C(O)OH**	3.8	3.1
168.0-162.5	**C=O in conjugated C(O)OH**	1.2	0.7
154.0-140.0	**C_3, C_4, C-O in aromatic ethers and phenols**	15.7	18.4
140.0-127.0	**C_1, Aromatic C–C bond**	13.7	14.2
127.0-124.5	**C_5, Aromatic C–C bond**	3.0	3.3
124.5-117.0	**C_6, Aromatic C–H bond**	8.7	9.1
117.0-114.0	**C_5, Aromatic C–H bond**	4.4	4.9
114.0-105.0	**C_2, Aromatic C–H bond**	7.8	7.2
90-58, 54-52	**Aliphatic C-O**	13.7	13.1
58.0-54.0	**Methoxyl OCH_3**	7.5	8.9
52-44, 36-10	**Aliphatic C-H**	20.5	17.2
154.0-105.0	**Aromatic cumulative**	53.3	57.2

6.4 Conclusions

In conclusion, both *R. opacus* strains were capable of growing on lignin with various results in lipid accumulation, as summarized in Table 6.15. However, serious adaptation efforts were needed in case of high extractive content Kraft lignin as a sole carbon source. These adaptation efforts proved to be successful techniques, and their application for EOL might enhance specific lipid productivities on that substrate as well.

When *R. opacus* PD630 was grown on high extractive content Kraft lignin, after adaptation experiments, the detailed examination of changes in the substrate (Residue-2.0) suggested degradation patterns. In brief, first lignin depolyerization (GPC) was observed together with oxidation, while lignin related extractives were consumed. Then in the second step, aromatic degradation occurred, possibly to the extent of energy stored from growth on the extractives. This step indicated some possible similarities with lignin

degradation pathways proposed in the literature, such as β-O-4 degradation (especially steps after the break of the ether linkage) and vanillic acid demethylation [219, 222, 236]. In the third step the residual, higher M_w lignin was further degraded, resembling the first step as investigated by ^{13}C and HSQC NMR techniques.

Noteworthy observations were made when O_2 delignified Kraft lignin was used as a substrate, namely, its large increase in M_w during fermentation. Furthermore, unique cell formations were observed when *R. opacus* DSM 1069 cell line was grown on Kraft lignin.

Table 6.15. Summary of lignin fermentations with *Rhodococci* showing reserve compound (extractive) formation after transesterification to methanol, and respective extractive compositions; FAME-fatty acid methyl ester; DAME-Diterpenoic acid methyl ester; C14:0-myristate; C16:0-palmitate; C16:1-palmitoleate; C17:1-heptadecenoate; C18:0-stearate; C18:1-oleate

Lignin type	***R. opacus* sp.**	**Fermentation time [day]**	**Extractive [CDW%]**	**Extractive composition**	**Notes**
EOL	DSM 1069	7	0.66, FAME	51 % C18:0 49 % C16:0	Growth on lignin only
us-EOL	DSM 1069	9	4.08, FAME	40.2 % C16:0 9.9 % C16:1 9.8 % C17:1 22.7 % C18:0 17.4 % C18:1	Growth on lignin only
Kraft	PD630	2	2.71 FAME, plus unknown DAME	8.4 % C14:0 21.5 % C16:1 44.6 % C16:0 25.5 % C18.1	Growth on lignin and extractives
Kraft	DSM 1069	1	15.00 FAME+DAME	FA+DA in unknown composition	Growth on lignin and extractives

Chapter 7

Overall conclusions

This work addressed the conversion of lignin to biofuels via two distinctively different routes. The first pathway examined the direct thermochemical conversion of LignoBoost lignin; a CO_2 precipitated novel Kraft lignin type, obtained from black liquor. First however, Chapter 4, this new substrate was analyzed to evaluate its structural properties that enable it to precipitate from BL and further properties that will determine CO_2 precipitated lignin's future applications. As a result it has been shown, that in the CO_2 precipitation process, the entering BL separates into fraction P (precipitate) which is enriched in lignin and into fraction F (filtrate) which is enriched in salts and also contains some sugars and short chain acids (qualitative NMR data). It is noteworthy, that when the lower final pH had been applied (9.5) in CO_2 precipitation, it resulted in a better lignin separation. GPC data obtained on the purified P phase showed that the fraction is enriched in the ~3000 g/mol -low degree of polymerization (DP) - and in the 200-300 g/mol monomer regions. Quantitative NMR data showed that F contains almost two times the amount of carboxylic and phenolic groups, possibly causing its better solubility in water. Low DP together with low quantities of oxygen containing functional groups made both P 9.5 and P 10.5 viable starting feed-stocks for future biofuel (or biomaterial) productions.

After determining its structure the purified CO2 precipitated Kraft lignins (P9.5 and 10.5) were subjected to pyrolysis at 500 °C (previously optimized condition) together with acid precipitated (pH 3) Kraft lignin (APBL), to compare bio-oil formation properties, Chapter 4. These lignins contain only small amounts of α-O- and β-O-ether

linkages due to degradation by pulping chemicals. In accordance the major lignin inter-unit linkages are β-5, 5-5 and other minimally represented bonds e.g. β-1 as shown in the literature and present work. According to literature, during pyrolysis the remaining ether linkages will be the first to degrade, starting as low as 250 °C if phenolic groups are present as well, together with aliphatic hydroxyl, carboxyl and aromatic-methoxyl groups. Guaiacyl hydroxyls, aldehydes, toluols and styrenes are the primary cleavage products, while p-hydroxy-phenols, catechols and cresols are products of further decomposition as confirmed by NMR spectroscopy in present study. Proposed β-5 degradation is also indicated by ^{31}P NMR, producing β-5 and methyl-guaiacol products. It is noteworthy, that different sources which proceed through multiple pathways can result in a similar product mixture (e.g. aldehydes can be products of α-O-4, β-O-4 and β-1 cleavages as well). Considering this issue, NMR results have to be used only to support theoretical reaction routes, however, they proved to be great tools in pyrolysis product analysis as well.

Pyrolysis oil yields from CO_2 precipitated lignins exceeded APBL oil yield with over 30 % and ^{13}C, ^{1}H and ^{31}P NMR experiments showed the following differences. Oils from CO_2 precipitated lignins have more aliphatic compounds and this effect is significant with P10.5 (close to 30 %). These aliphatics are methyl and ethyl substituents on aromatic compounds such as phenol or anisole. It was also observed that CO_2 precipitated lignin pyrolysis oils will have more catechols and *p*-hydroxy phenols, while APBL based oils will be richer in guaiacols indicating that rearrangement reactions are more readily occurring in former lignins during pyrolysis. Furthermore, differences between CO_2 precipitated lignin and pyrolysis oil β-5 and 4-O-5 phenol contents are

more significant (increase 4-5 times) than in respective APBL materials (gain ~20 %). This was attributed to the higher precipitation pH applied in former cases which could selectively precipitate lignin fragments that pyrolyze easier. All these results support the applicability of CO_2 precipitated black liquor lignins for pyrolysis (high yields), as well as the utilization of the obtained oils as liquid biofuels, due to their low molecular weights and advantageous changes in composition, such as increased aliphatic and low oxygen contents.

The second route of lignin to biofuel conversion that has been investigated was the biological multistep conversion of EOL and high extractive content Kraft lignin to lipids, which can be further transesterified into biodiesel, in a separate step. The microorganisms that have been used in this study were *Rhodococcus opacus* PD630 and DSM 1069 Gram positive bacteria (from the actinomycetes group). These organisms had been successfully grown on lignin related compounds, and it had been proven that they are oleaginous, however the two traits have never been exploited simultaneously. Accordingly, first this theory was tested with lignin model compounds, such as vanillic acid in Chapter 5. Both strains were grown on 4-hydroxybenzoic acid (4-HBA) and vanillic acids (VanA) as lignin model compounds to evaluate lipid accumulation under nitrogen limiting conditions. Adaptation experiments showed that both strains can successfully grow on both substrates at multiple different concentrations, and that they can accumulate close to 20 % of their own weight in lipids in nitrogen limited shake flask fermentations. Lipid accumulation in DSM 1069 showed no nitrogen source dependence, on the other hand both strains showed pH dependence; growing faster at higher pH. This pH dependence might be due to multiple different effects, such as better conditions for

substrate conversion, membrane transport or other metabolic regulatory issues. Substrate consumption and fatty acid compositions were highly carbon source and strain dependent; however, both strains first accumulated lipids, which were then utilized to increase cell number. PD630 in some instances had higher unsaturated fatty acid ratios, close to 50 %, that might be beneficial in biodiesel applications, due to lower melting points. Furthermore, PD630 showed high palmitatic and *cis*-oleic acid accumulation in all cases, while DSM 1069 fatty acid distribution allowed for more variation, especially growing on glucose at low pH. Separate lipid extraction showed that simultaneous extraction and transesterification considerably underestimated total lipid contents, however, the application of other more reliable methods requires larger scale fermentations. TLC showed that neutral (TAG) lipids contribute most significantly (largest, almost only spot on TLC plate) to the total lipid content.

After successful growth and lipid accumulation experiments, the same cell lines were tested with EOL and Kraft lignins, with results showing, Chapter 6, that both *R. opacus* strains were capable of growing on lignin with various results in lipid accumulation. However, serious adaptation efforts were needed, especially in case of high extractive content Kraft lignin as a sole carbon source. These adaptation efforts proved to be successful techniques, and their application for EOL might enhance specific lipid productivities on that substrate as well. When *R. opacus* PD630 was grown on high extractive content Kraft lignin, after adaptation experiments, the detailed examination of changes in the substrate lignin suggested degradation patterns. In brief, first lignin depolyerization (GPC) was observed together with oxidation, while lignin related extractives were consumed. Then in the second step, aromatic degradation occurred,

possibly to the extent of energy stored from growth on the extractives. This step indicated some similarities with literature proposed lignin degradation pathways, such as β-O-4 degradation and vanillic acid demethylation. In the third step the residual, higher M_w lignin was further degraded, resembling the first step as investigated by ^{13}C and HSQC NMR techniques. Maximal extractive accumulation was 15 % in case of DSM 1069 growing on Kraft lignin, in a bench-top bioreactor, after adaptation on low M_w Kraft. However, the highest pure lipid yield, 4.08 % CDW, was obtained on *us*-EOL with DSM 1069, furthermore in this case the lipid accumulation could only happen on lignin as a sole substrate. Noteworthy observations were also made when O_2 delignified Kraft lignin was used as a substrate, namely, its large increase in M_w during fermentation. Furthermore, unique cell formations were observed when *R. opacus* DSM 1069 cell line was grown on Kraft lignin.

Overall, both direct and multistep lignin conversion routes have proven successful, however, refinement is needed in both cases. Pyrolysis oils that were obtained had 30-35 % yield based on lignin that can be even further improved. While bacteria did not consumed the lignin source fully, a considerable preference towards aliphatics was observed, however, in some cases that had been presented lignin was used as a sole carbon source for lipid accumulation, proving the hypothesis of present work.

Chapter 8

Recommendations for future work

Direct pyrolytic conversion of lignin has proven less capital intensive yet high yielding, including the case when the method was applied on CO_2 precipitated Kraft lignin. Pursuing further improvements to this method has a high possible payoff, based on the increased interest in commercializing the CO_2 precipitation process. In fact, one of the largest pulp and paper mill machinery manufacturing companies has already licensed the process, and the finalized precipitation units will soon go on sale. Consequently, any innovation, such as catalytic pyrolysis, that can improve the value of this specific lignin source can soon prove useful.

Bioconversion of lignin on the other hand, is in an absolutely basic stage, bacterial degradation had only been recently proven, not mentioning bioconversion to lipids that to this date has been unheard of. Present work proves the possibility of this metabolic route, and some recommendations can already be made:

- Adaptation experiments on lower molecular weight lignin substrates can prove crucial, before high M_w experiments. Bacteria are not excellent degraders, however once they adapt, they grow fast, and accumulate useful compounds, such as lipids.
- Aeration is of high importance, possibly because most of the lignin degradation enzymes use O_2 to break down inter-unit linkages or the aromatic ring itself. The same is true to iron, a myriad of the enzymes in the process utilize iron as a cofactor. Consequently, optimizing aeration and iron content in the media should enhance the process.

- The use of extracellular lignin active enzymes, such as laccase or different peroxidases might also prove successful. Bacterial enzymes are by far not as efficient as fungal ones.
- H lignin (p-coumaryl-alcohol) containing substrates can prove efficient for growth and lipid accumulation, based on model compound results (4-HBA, best substrate, better than glucose in some cases). Accordingly, switch-grass lignin is a highly recommended substrate for lignin to lipid bioconversion with *Rhodococci*.
- Present research showed fast lignin degradation after adaptation, and in case good aeration was involved. Concomitantly, it can be interesting to look into fundamental enzymatic processes and their genetic regulation via advanced proteomics, genomics.
- The peculiar cell growth, observed by light microscope when cells were grown on Kraft lignin can also prove to be an interesting area, considering that *Rhodococci* are not motile. Accordingly, there is a possibility that these structures show some kind of cellular attachment to lignin to enable constant contact and facilitate degradation.
- Finally, O_2 delignified Kraft lignin was highly polymerized in a short time by these microbes, illustrating a possibility to obtain valuable, high M_w lignin through this process.

APPENDIX A

LIGNIN ULTRASONICATION

Table A.A.1 details the experiments that were tested to optimize ultrasonication conditions for EOL, including M_w molecular weights obtained. Treatment B was chosen, because of lowest temperature and residence time; and not because of low M_w, because this latter property always increased during ultrasonication.

Table A.A.1. Ultrasonication optimalization experiment set; cc- solids consistency; ampl- amplitude of ultrasonicator head tip at 500 W

Sample	Tested method	M_w [g/mol]
1-2	EOL controls	2.6E+03
3	Ultrasonicated EOL, 45 °C, 10 min, 40% ampl, 2% cc, pH 12	3.3E+03
5	Ultrasonicated EOL, 32 °C, 5 min, 40% ampl, 2% cc, pH 12, 1% H2O2, 0.2 l/min air	3.9E+03
6	Ultrasonicated EOL, 39 °C, 10 min, 30% ampl, 2% cc, pH 12, 0.2% H2O2	3.5E+03
7	Ultrasonicated EOL, 47 °C, 5 min, 40% ampl, 2% cc, pH 12, 1% H2O2	3.6E+03
B	Ultrasonicated EOL, RT waterbath, 5 min, 40% ampl, 2% cc, pH 12, 1% H2O2	3.4E+03
C	EOL, RT 24 h, no Ultrasonication, 2% cc, pH 12, 1% H2O2	3.1E+03
D	EOL, 40 °C waterbath 1 h, RT 23 h, no Ultrasonication, 2% cc, pH 12, 1% H2O2	3.3E+03

APPENDIX B

SEPARATION OF LOW MOLECULAR WEIGHT LIGNIN

Low molecular weight Kraft lignin, was separated from Kraft lignin by pH change, and it is referred to as **Low M_w Kraft**. Briefly:

a. Kraft lignin was dissolved in dist. water at pH 12.0 then pH was decreased accurately till 4.5 and the precipitated higher molecular weight part was separated by filtration (fine sintered glass funnel). FIRST SEPARATION.

b. The filtrate pH was then adjusted to 3.0 and in the SECOND SEPARATION step **Low M_w Kraft** was filtered from solution.

c. pH 4.5 was designated as a good separation point by previous Kraft separation experiments at multiple pH's as shown on Figure A.B.1

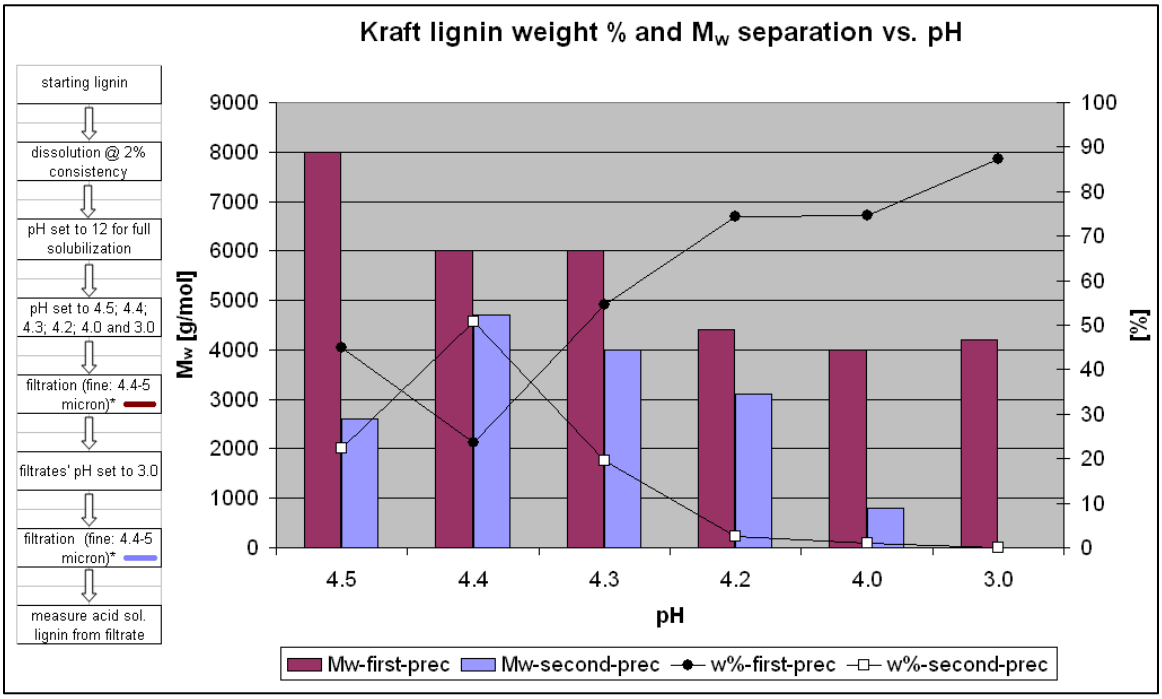

Figure A.B.1 Separation of Kraft lignin by lowering pH and filtration in two steps. Procedure steps on the left, separation results on right. Weight average molecular weights M_w are represented with red (first precipitate) and **light blue** (second, **Low M_w** precipitate) columns (left Y axis). Weight percent of each precipitate compared to starting weight are shown with black and white dots (right Y axis). Weight percent's don't add up to be 100 because of filtration losses and presence of acid soluble lignin (measured but not shown).

APPENDIX C

HSQC ANALYSIS

The aliphatic region of Kraft (obtained from GP Containerboard LLC, black liquor, and used in Chapter 6) lignin HSQC NMR is highly populated with peaks. However, these peaks are mostly unidentified at this point, and literature is limited in this area [48, 93-96, 101, 102, 140-145, 159, 162, 165, 174-180], even including proton [9, 10, 42, 146-148, 151, 153-159] and ^{13}C NMR papers [9, 10, 42, 115, 141, 143-151, 153, 158-167]. With the use of all aliphatic information from model compound and pyrolysis ^{1}H and ^{13}C papers (listed above), two charts can be generated. The first one, Figure A.C.1, illustrates the dissection of the HSQC plane (with the aliphatic region for Kraft lignin as an example) according to literature values, while the second figure (A.C.2) depicts only the distance from the aromatic ring for the given carbon/proton pair. Figure A.C.2 was created using excel to "re-plot" NMR data, by visualizing C/H pair chemical shift data on an excel chart and reversing the axes, this way the manually created figure resembles the NMR plot.

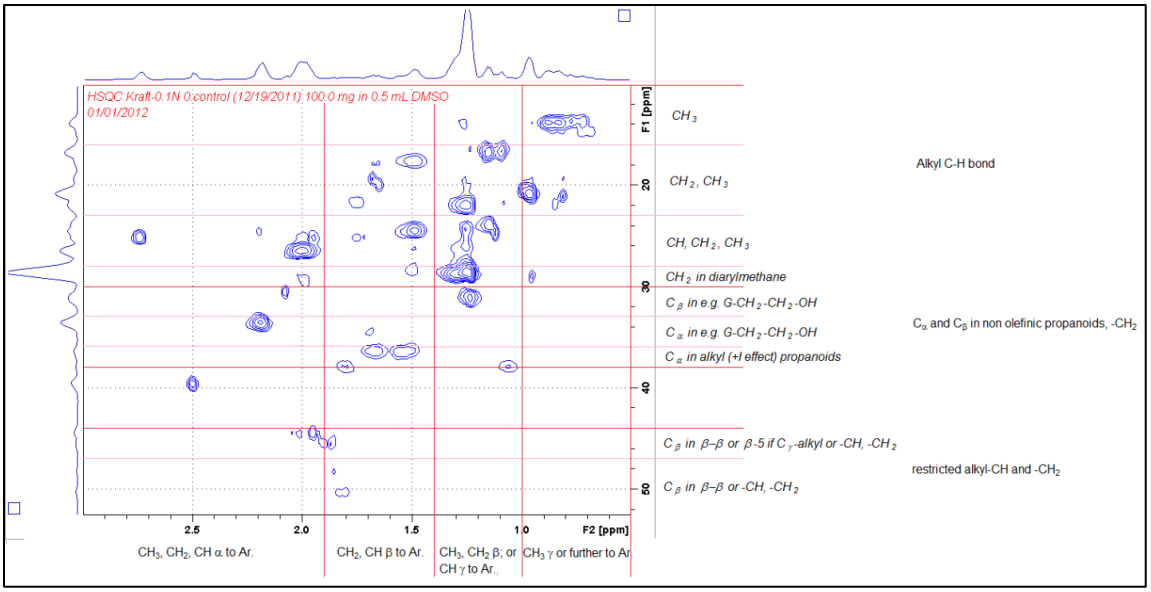

Figure A.C.1. Dissection of HSQC spectrum of the aliphatic region of Kraft lignin by integration regions used in the literature.

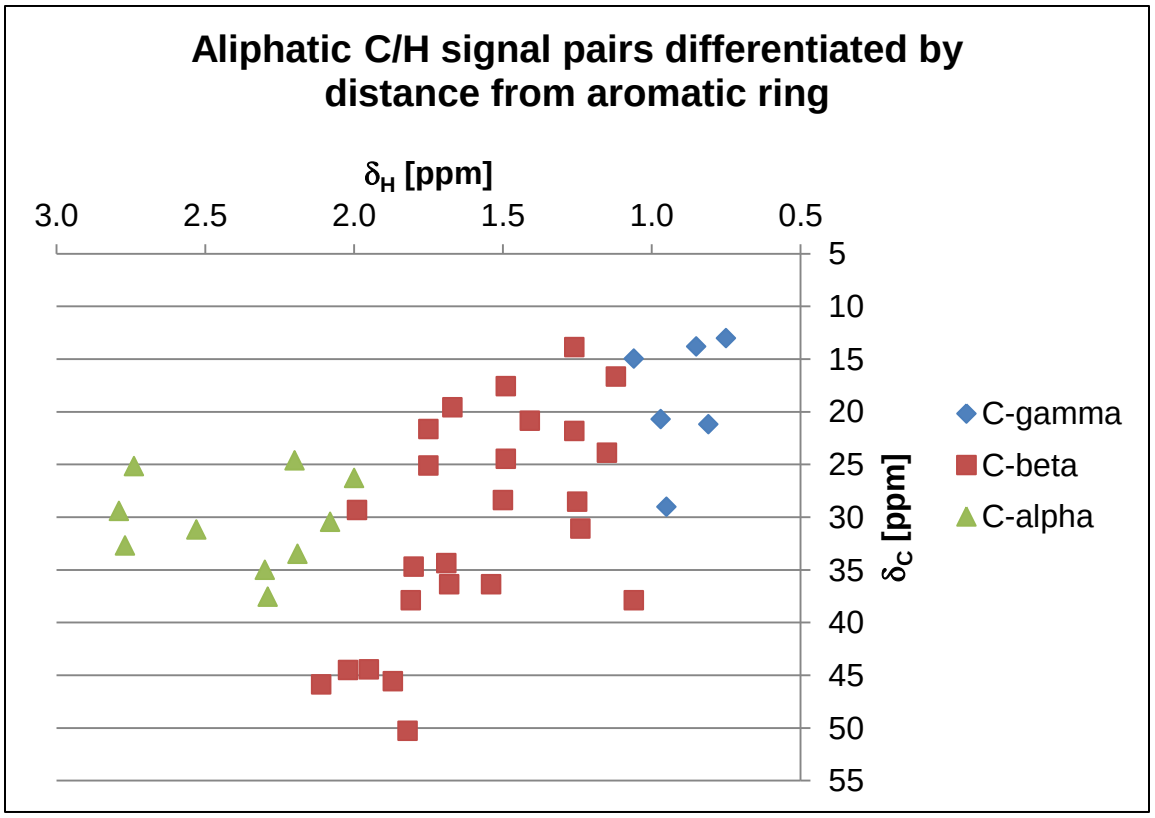

Figure A.C.2. Separation of C/H chemical shift pairs by their distance from the aromatic ring, in the "re-plotted" spectra of the aliphatic region of Kraft lignin.

Although Figures A.C.1-2 facilitates the identification of changes in lignin structure during fermentation, when the resulting cellular material was purified and further extracted to analyze lipid content the extracts showed the presence of diterpenoic acids. Pine contains these extractives in percentages shown in Table 2.13 in Chapter 2, together with fatty acids. As detailed in Chapter 3, when purifying Kraft lignin from BL, an extensive pentane extraction step was conducted. Against latter effort some of these extractives stayed with Kraft lignin and the cells utilized them. To analyze the amount of extractives present, qualitatively by HSQC, first the regional distribution of their signal needed to be defined. Literature data is limited on diterpenoid (in present case acids and methyl esters) NMR chemical shifts, however, with the use of the few papers found, together with data from the SDBS (Structural Database for Organic Compounds) [181-186] sources, most of the peaks could be identified (using also lignin and fatty acid-FA HSQC NMR data [48, 93-96, 101, 102, 140-145, 159, 162, 165, 174-180]). As shown in Chapter 2, section 2.3.5, pine contains diterpenoids and FAs, and for some of these compounds ^{13}C and proton NMR chemical shifts were found [181-186, 295, 296]. Another compound, EPATME: 7-ethenyl-1,2,3,4,4a,5,6,7,8,9,10,10a-dodecahydro-1,4a,7-trimethyl-1-phenantrenecarboxylic acid methyl ester, was identified by GC-MS from cell extracts, after growing on Kraft. It is not present in pine (Chapter 2), however, lignin goes through the Kraft pulping process before extraction from BL, and these procedures can possibly modify some of the present diterpenoids into EPATME. Using the above information and the C/H chemical shift pairs from all the Kraft and EOL lignin experiments that had been obtained during this work, overlay charts were created, as shown on Figures A.C.3-8. Subsequently, overlay data from these figures and lignin

HSQC NMR literature information were combined to create detailed Tables (A.C.1-3) that include all peaks found in all lignin types (EOL, ultrasonicated EOL, Kraft and low M_w Kraft), and their literature based assignments. These tables were used to create "high-definition re-plots" of NMR spectra, as shown on Figure A.C.9 (as an example for the aliphatic region), that enabled the detailed analysis of HSQC spectra. Although in some instances, e.g. dehydro-coniferyl groups (Figures A.C.9 and A.C.10), peaks separate well, on other occasions (e.g. multiple FA and diterpenoid peaks, Figures A.C.9 and A.C.10) they overlap. For this reason the tables were reorganized according to regions that represent the same chemical features or compounds (Tables A.C.4-6), and also HSQC-excel re-plots were simplified using the new tables (Figures A.C.10-12). All the tables are included here, to enable the use of chemical shift assignments for well separated peaks, identified by multiple literature resources, as well as general or overlapping regions. Briefly, all the above tables and figures are used in Chapter 6 for the HSQC analysis of lignin.

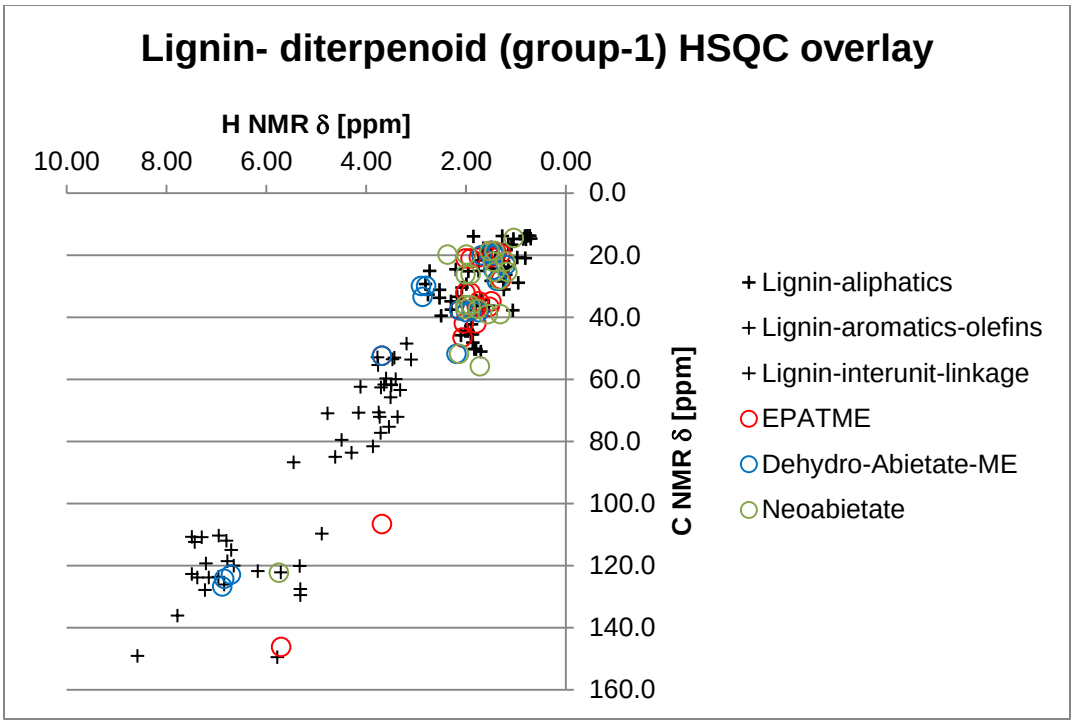

Figure A.C.3. Overlay of re-plotted HSQC lignin data (obtained in this work, showed with black crosses) with diterpenoid literature data. The diterpenoids were separated to 3 groups to facilitate analysis after visualization.

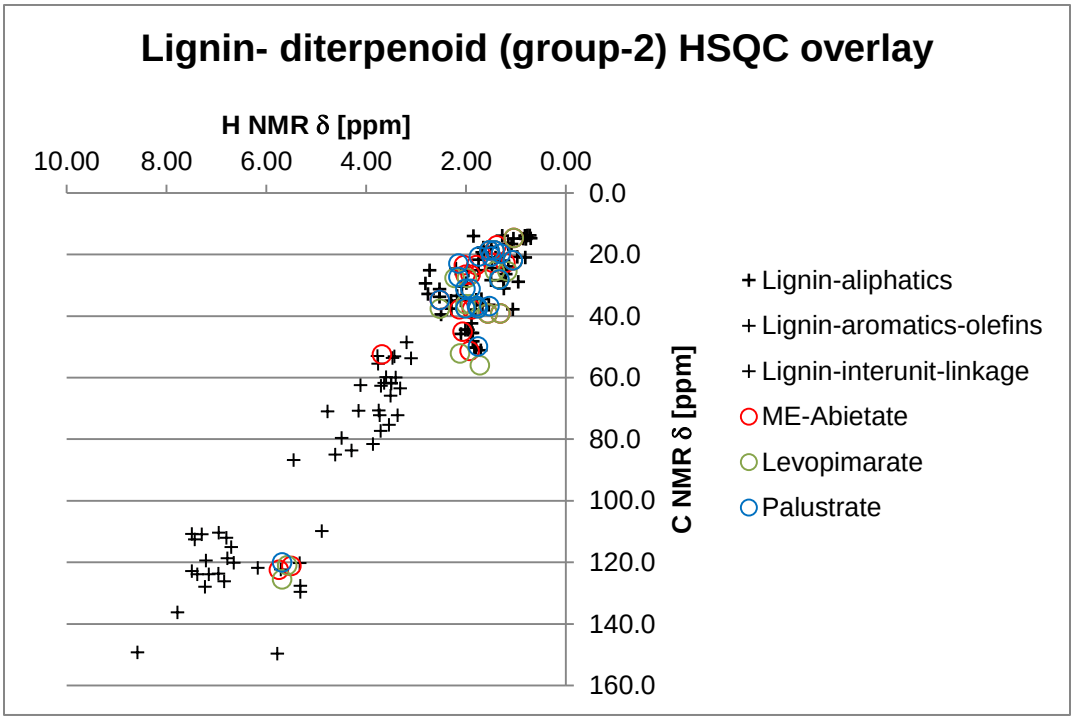

Figure A.C.4. Overlay of re-plotted HSQC lignin data (obtained in this work, showed with black crosses) with diterpenoid literature data.

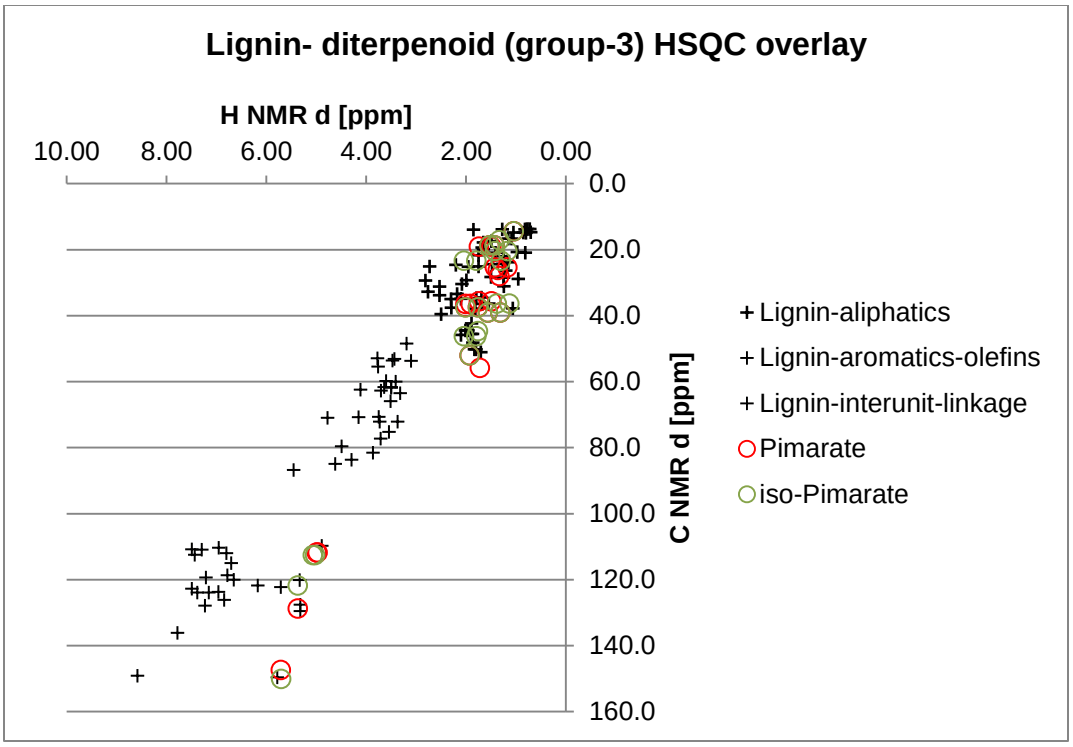

Figure A.C.5. Overlay of re-plotted HSQC lignin data (obtained in this work, showed with black crosses) with diterpenoid literature data.

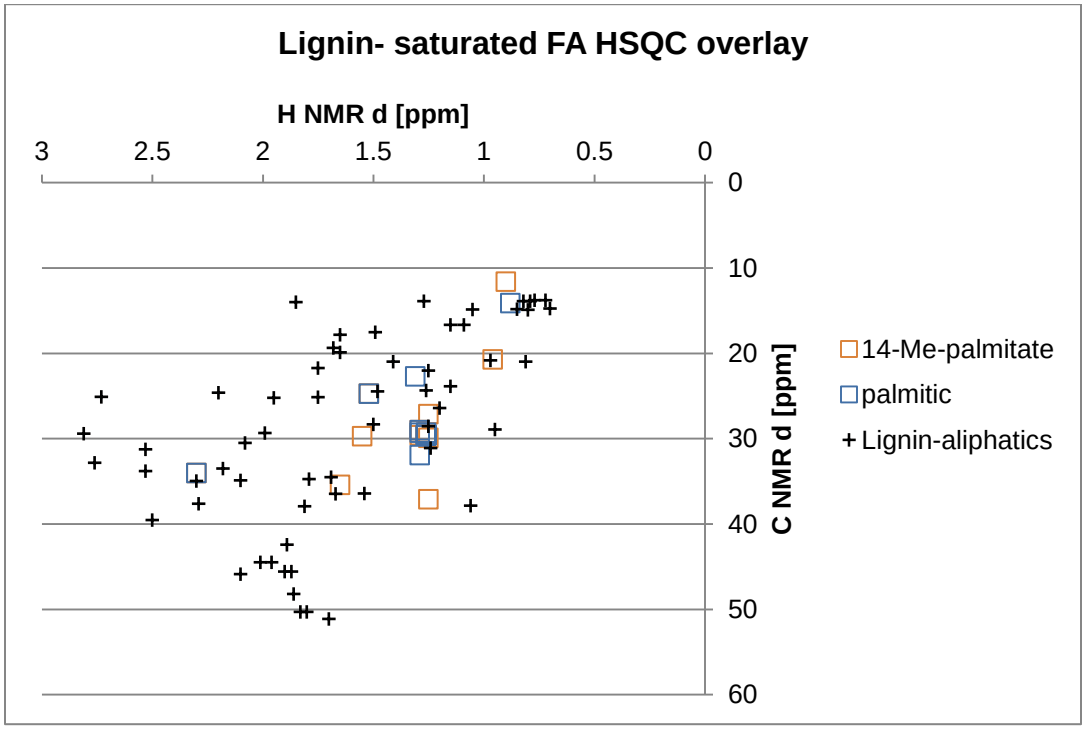

Figure A.C.6. Overlay of re-plotted HSQC lignin data (obtained in this work, showed with black crosses) with FA literature data.

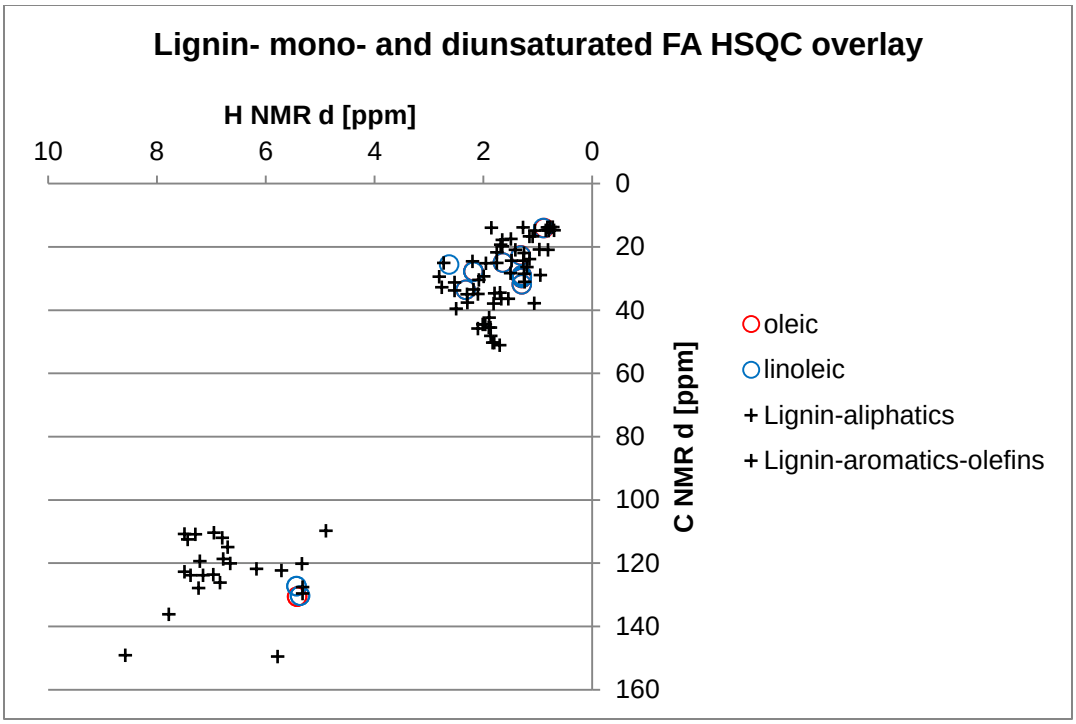

Figure A.C.7. Overlay of re-plotted HSQC lignin data (obtained in this work, showed with black crosses) with FA literature data.

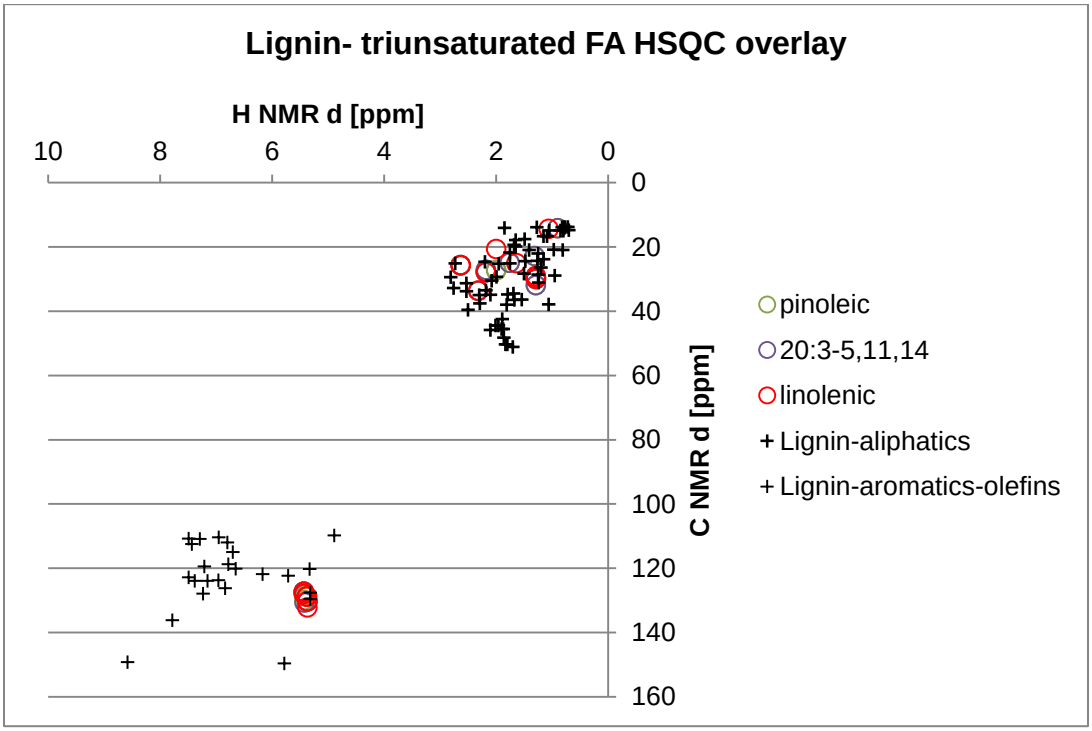

Figure A.C.8. Overlay of re-plotted HSQC lignin data (obtained in this work, showed with black crosses) with FA literature data.

Table A.C.1. Aliphatic peaks in (a) all EOL and (b) Kraft lignin types analyzed by HSQC in present work, orange letters represent peaks found in both lignin types; blue, only EOL; and black, only Kraft. (c) Peaks seen in lignin HSQC literature, but cited as unknown by authors.

Aliphatic sidechains					
#	δ_C	δ_H	EOL[a]	Kraft[b]	Peak assignment
1	13.8	0.72		+	(C_γ), or Ar-O-CH_2-$\underline{CH_3}$
2	13.8	0.77		+	
5	13.9	1.27		+	(C_β or C_γ), or Ar-O-CH_2-$\underline{CH_3}$
6	14.0	1.85		+	(C_α)
11	16.7	1.09		+	(C_β or C_γ), unknown[c]
12	16.7	1.15		+	
17	20.8	0.97		+	(C_γ)
19	21.0	0.81		+	(C_γ)
32	28.9	0.95		+	(C_γ)
37	31.3	2.53	+	+	(C_α), Ar-$\underline{CH_2}$-CH_2-CH_2-OH
39	33.5	2.18		+	(C_α)
41	34.5	1.69	+	+	(C_β), Ar-CH_2-$\underline{CH_2}$-CH_2-OH
47	37.6	2.29		+	(C_β)
51	42.4	1.89		+	(C_β), secoisolariciresinol
56	45.9	2.10	+		(C_β)
7	14.8	0.70		+	(C_γ), FA aliphatic "chain-ends" (C16-C18)
8	14.8	0.85		+	
9	14.9	0.80		+	
10	14.9	1.05	+		(C_β or C_γ), FA aliphatic "chain-ends" (C16-C18), linolenic
26	25.1	2.73		+	(C_α), Unsaturated FA
30	28.3	1.50		+	(C_β), FA
31	28.6	1.25	+	+	(C_β), FA
36	31.1	1.24		+	(C_β), FA
44	35.0	2.30		+	(C_β), FA
13	17.5	1.49		+	(C_β), Diterpenoic acids and their methyl esters (DA, DAME)
14	17.8	1.65		+	
15	19.4	1.68		+	
16	19.9	1.65		+	
18	21.0	1.41		+	(C_β), DA, DAME
20	21.7	1.75		+	(C_β), DA, DAME
22	23.9	1.15		+	(C_β or C_γ), DA, DAME
24	24.4	1.48		+	(C_β or C_γ), DA, DAME
25	24.6	2.20		+	(C_α), DA, DAME
28	25.2	1.95		+	(C_α), DA, DAME
29	26.4	1.20		+	(C_β), DA, DAME
34	29.4	2.81		+	(C_α), DA, DAME, dehydro-abietic acid
35	30.5	2.08		+	(C_α or C_β), DA, DAME, EPATMA, palustric acid
38	32.8	2.76		+	(C_α), DA, DAME, dehydro-abietic acid
42	34.7	1.79		+	(C_α or C_β), DA, DAME
43	34.9	2.10		+	
3	13.9	0.79		+	(C_γ), or Ar-O-CH_2-$\underline{CH_3}$, FA aliphatic "chain-ends" (C16-C18)
4	13.9	0.82		+	
21	22.0	1.25		+	(C_β), DA, DAME, and fatty acids (FA)
23	24.4	1.26		+	(C_β), DA, DAME, and FA
27	25.1	1.75		+	(C_β), β-methyl w/ α-OH, DA, DAME
33	29.3	1.99		+	(C_β), Ar-CH_2-$\underline{CH_2}$-COOH, or DA, DAME
40	33.8	2.53		+	(C_α), secoisolariciresinol, palustric acid
45	36.4	1.54		+	(C_β), DA, DAME, unknown[c]
46	36.4	1.67		+	
48	37.8	1.06		+	(C_β), DA, DAME, isopimaric acid, unknown[c]
49	37.9	1.81		+	(C_α or C_β), DA, DAME
50	39.5	2.50		+	(C_α or C_β), DA, DAME, levopimarate
52	44.5	1.96		+	(C_α or C_β), DA, DAME
53	44.5	2.01		+	
54	45.6	1.87		+	
55	45.6	1.90		+	
57	48.2	1.86		+	
58	50.3	1.80		+	
59	50.3	1.83		+	
60	51.1	1.70		+	

Table A.C.2. Interunit-linkage peaks in (a) all EOL and (b) Kraft lignin types analyzed by HSQC in present work, orange letters represent peaks found in both lignin types; blue, only EOL; and black, only Kraft.

Interunit-linkage-region					
#	δ_C	δ_H	EOL[a]	Kraft[b]	Peak assignment
61	48.5	3.19		+	(C_β)
62	53.0	3.77		+	(C_α) in α-6, -OMe in DAME
63	53.1	3.43	+		(C_β) in β-5
64	53.6	3.47		+	(C_β) in β-5
65	53.7	3.10		+	(C_β) in β-β
66	55.5	3.76	+	+	methoxyl
67	59.8	3.60	+	+	(C_γ) in β-O-4 (erythro), dihydroconiferyl
68	60.0	3.41	+	+	(C_γ) in β-O-4 (threo)
69	61.7	3.50	+	+	(C_γ) in β-O-4
70	61.7	3.64	+	+	
71	61.9	3.50		+	
72	62.5	4.11		+	(C_γ) in coniferyl
73	62.7	3.70	+	+	(C_γ) in β-5
74	63.5	3.32	+	+	LCC (C_5/H_5 in β-D-xylopiranoside)
75	65.9	3.51		+	
76	70.7	3.75	+	+	(C_γ) in β–β
77	70.8	4.15	+	+	
78	71.0	4.77	+	+	(C_α) in β-O-4
79	72.2	3.37	+	+	LCC (C_3/H_3 in β-D-xylopiranoside)
80	72.2	3.73	+	+	(C_γ) in β–β
81	75.3	3.54		+	LCC (C_4/H_4 in β-D-xylopiranoside)
82	77.3	3.71	+	+	Undefined
83	79.6	4.49	+	+	(C_α) Ar-O-$\underline{CH_2}$-CH_3, or α-O-4-O-LCC (on β-O-4 lignin)
84	81.6	3.86		+	Undefined
85	83.7	4.29	+	+	(C_β) in β-O-4
86	85.0	4.62	+	+	(C_α) in β–β
87	86.8	5.45	+		(C_α) in β-5

Table A.C.3. Aromatic and olefinic peaks in (a) all EOL and (b) Kraft lignin types analyzed by HSQC in present work, orange letters represent peaks found in both lignin types; blue, only EOL; and black, only Kraft.

Aromatic-olefinic-region					
#	δ_C	δ_H	EOL[a]	Kraft[b]	Peak assignment
87	109.8	4.89		+	DA, iso-pimaric and pimaric acids
88	110.4	6.95	+	+	(C_2) in G
89	110.8	7.49		+	(C_2) in conjugated G-C_α=O
90	110.9	7.29	+	+	(C_2) in conjugated FA-C_α=O
91	112.0	6.80	+	+	(C_2) in G
92	112.5	7.43	+	+	(C_2) in conjugated C_γ=O (cinnamyl)
93	115.0	6.70	+	+	(C_5) in G
94	118.7	6.78	+	+	(C_6) in G
95	119.4	7.21		+	(C_6) in conjugated C_γ=O (cinnamyl), or in 5-5
96	120.1	6.65	+	+	(C_6) in G
97	120.2	5.33		+	DA, iso-pimaric acid
98	121.8	6.17		+	(C_6) undefined
99	122.3	5.71		+	DA, multiple compounds
100	122.8	7.49	+	+	(C_6) in conjugated G-C_α=O, or in 5-5
101	123.7	6.96		+	DA, dehydroabietate
102	123.9	7.15		+	(C_6) in conjugated FA-C_α=O
103	123.9	7.38		+	(C_6) in conjugated C_γ=O (COOH), or in 5-5
104	126.2	6.84		+	(C_β) in cinnamyl aldehyde, or DA, dehydroabietate
105	127.6	5.32		+	Unsaturated FA
106	127.9	7.23		+	($C_{2/6}$) in conjugated C_γ=O (pCA, FA)-γ-ester-β-O-4
107	129.6	5.32		+	Unsaturated FA
108	136.2	7.78		+	(C_α) in conjugated C_γ-OOH
109	149.2	8.58		+	
110	149.6	5.78		+	DA, iso-pimaric and pimaric acids

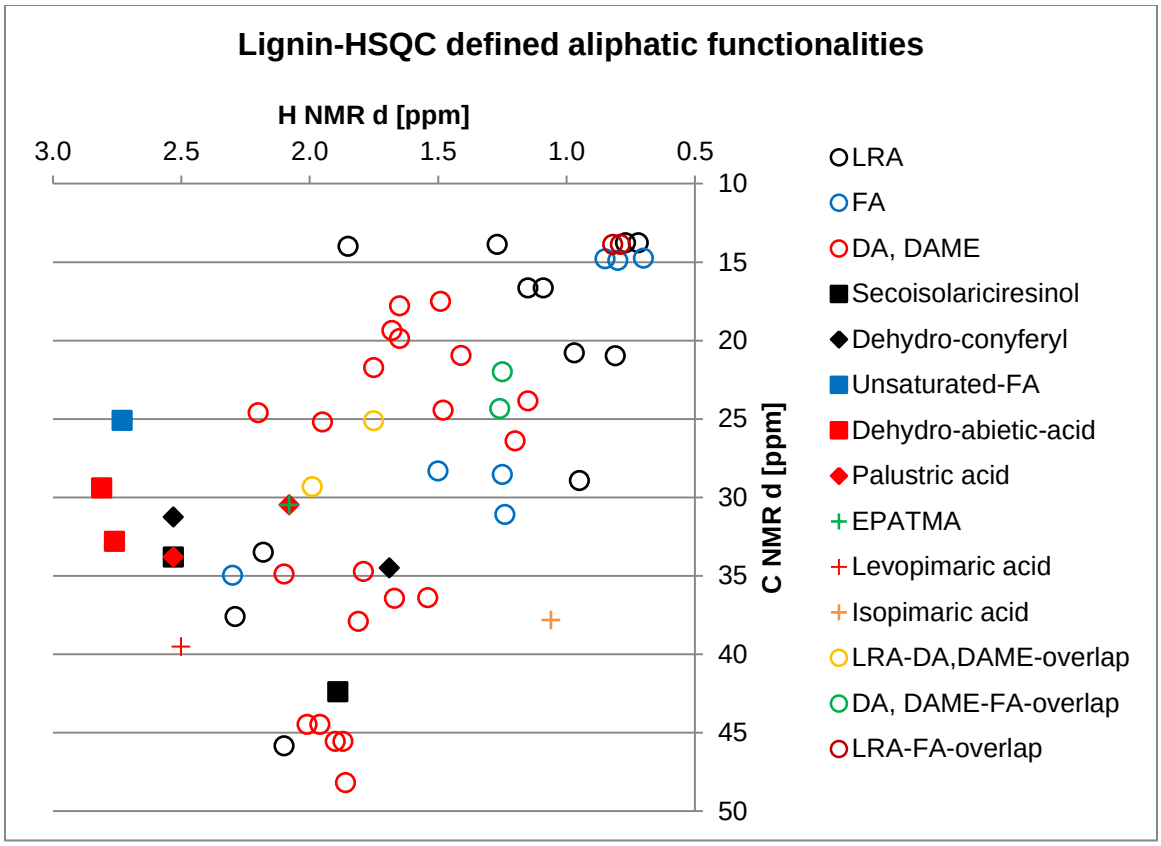

Figure A.C.9. Chemical shift assignments for aliphatic lignin peaks based on literature data collected from both extractive and lignin HSQC papers.

Table A.C.4. Functionalities found in lignin HSQC aliphatic region.

Aliphatic sidechains					
Region	δ_C	δ_H	EOL[a]	Kraft[b]	Peak assignment
1	13.8	0.72		+	Lignin-related aliphatic (LRA) peaks
	13.8	0.77		+	
	13.9	1.27		+	
	14.0	1.85		+	
	14.9	1.05	+		
	16.7	1.09		+	
	16.7	1.15		+	
	20.8	0.97		+	
	21.0	0.81		+	
	28.9	0.95		+	
	31.3	2.53	+	+	Ar-$\underline{CH_2}$-CH_2-CH_2-OH
	33.5	2.18		+	LRA
	34.5	1.69	+	+	Ar-CH_2-$\underline{CH_2}$-CH_2-OH
	37.6	2.29		+	LRA
	42.4	1.89		+	
	45.9	2.10	+		
2	14.8	0.70		+	Fatty acids (FA)
	14.8	0.85		+	
	14.9	0.80		+	
	25.1	2.73		+	Unsaturated FA
	28.3	1.50		+	Fatty acids (FA)
	28.6	1.25	+	+	
	31.1	1.24		+	
	35.0	2.30		+	
3	17.5	1.49		+	Diterpenoic acids and their methyl esters (DA, DAME)
	17.8	1.65		+	
	19.4	1.68		+	
	19.9	1.65		+	
	21.0	1.41		+	
	21.7	1.75		+	
	23.9	1.15		+	
	24.4	1.48		+	
	24.6	2.20		+	
	25.2	1.95		+	
	26.4	1.20		+	
	29.4	2.81		+	
	30.5	2.08		+	
	32.8	2.76		+	
	34.7	1.79		+	
	34.9	2.10		+	
	25.1	1.75		+	
	29.3	1.99		+	
	33.8	2.53		+	
	36.4	1.54		+	
	36.4	1.67		+	
	37.8	1.06		+	
	37.9	1.81		+	
	39.5	2.50		+	
4	13.9	0.79		+	LRA-FA-overlap
	13.9	0.82		+	
5	22.0	1.25		+	DA, DAME-FA-overlap
	24.4	1.26		+	
6	44.5	1.96		+	LRA-DAME-overlap
	44.5	2.01		+	
	45.6	1.87		+	
	45.6	1.90		+	
	48.2	1.86		+	
	50.3	1.80		+	
	50.3	1.83		+	
	51.1	1.70		+	

Table A.C.5. Functionalities found in lignin HSQC interunit-linkage region.

Interunit-linkage-region					
Region	**δ_C**	**δ_H**	**EOL[a]**	**Kraft[b]**	**Peak assignment**
Misc.	48.5	3.19		+	(C_β) alkyl
	53.0	3.77		+	(C_α) in α-6, -OMe in DAME
	55.5	3.76	+	+	methoxyl
	62.5	4.11		+	(C_γ) in coniferyl
	77.3	3.71	+	+	Undefined
	81.6	3.86		+	Undefined
β-O-4	59.8	3.60	+	+	(C_γ) in β-O-4 (erythro δ_H 3.6; threo 3.4), also dihydroconiferyl and α=O containing (β-O-4)
	60.0	3.41	+	+	
	61.7	3.50	+	+	
	61.7	3.64	+	+	
	61.9	3.50		+	
	71.0	4.77	+	+	(C_α) in β-O-4
	83.7	4.29	+	+	(C_β) in β-O-4
β-5	53.1	3.43	+		(C_β) in β-5
	53.6	3.47		+	
	62.7	3.70	+	+	(C_γ) in β-5
	86.8	5.45	+		(C_α) in β-5
β-β	53.7	3.10		+	(C_β) in β-β
	70.7	3.75	+	+	(C_γ) in β–β
	70.8	4.15	+	+	
	72.2	3.73	+	+	
	85.0	4.62	+	+	(C_α) in β–β
LCC	63.5	3.32	+	+	LCC (C_5/H_5 in β-D-xylopiranoside)
	65.9	3.51		+	
	72.2	3.37	+	+	LCC (C_3/H_3 in β-D-xylopiranoside)
	75.3	3.54		+	LCC (C_4/H_4 in β-D-xylopiranoside)
	79.6	4.49	+	+	(C_α) Ar-O-$\underline{CH_2}$-CH_3, or α-O-LCC (on β-O-4 lignin)

Table A.C.6. Functionalities found in lignin HSQC olefinic and aromatic regions.

Aromatic-olefinic-region					
Region	**δ_C**	**δ_H**	**EOL[a]**	**Kraft[b]**	**Peak assignment**
DA	109.8	4.89		+	DA, iso-pimaric and pimaric acids
	120.2	5.33		+	DA, iso-pimaric acid
	122.3	5.71		+	DA, multiple compounds
	123.7	6.96		+	DA, dehydroabietate
	149.6	5.78		+	DA, iso-pimaric and pimaric acids
UFA	127.6	5.32		+	Unsaturated FA
	129.6	5.32		+	Unsaturated FA
C_2	110.4	6.95	+	+	(C_2) in G
	110.8	7.49		+	(C_2) in conjugated G-C_α=O
	110.9	7.29	+	+	(C_2) in conjugated Ferul.-C_α=O
	112.0	6.80	+	+	(C_2) in G
	112.5	7.43	+	+	(C_2) in conjugated C_γ=O (cinnamyl)
C_5	115.0	6.70	+	+	(C_5) in G
C_6	118.7	6.78	+	+	(C_6) in G
	119.4	7.21		+	(C_6) in conjugated C_γ=O (cinnamyl), or in 5-5
	120.1	6.65	+	+	(C_6) in G
	122.8	7.49	+	+	(C_6) in conjugated G-C_α=O, or in 5-5
	123.9	7.15		+	(C_6) in conjugated Ferul.-C_α=O
	123.9	7.38		+	(C_6) in conjugated C_γ=O (COOH), or in 5-5
Misc.	121.8	6.17		+	(C_6) undefined
	126.2	6.84		+	(C_β) in cinnamyl aldehyde, or DA, dehydroabietate
	127.9	7.23		+	($C_{2/6}$) in conjugated C_γ=O (pCA, FA)-γ-ester-β-O-4
	136.2	7.78		+	Unidentified, close to (C_α) in conjugated C_γ-OOH
	149.2	8.58		+	

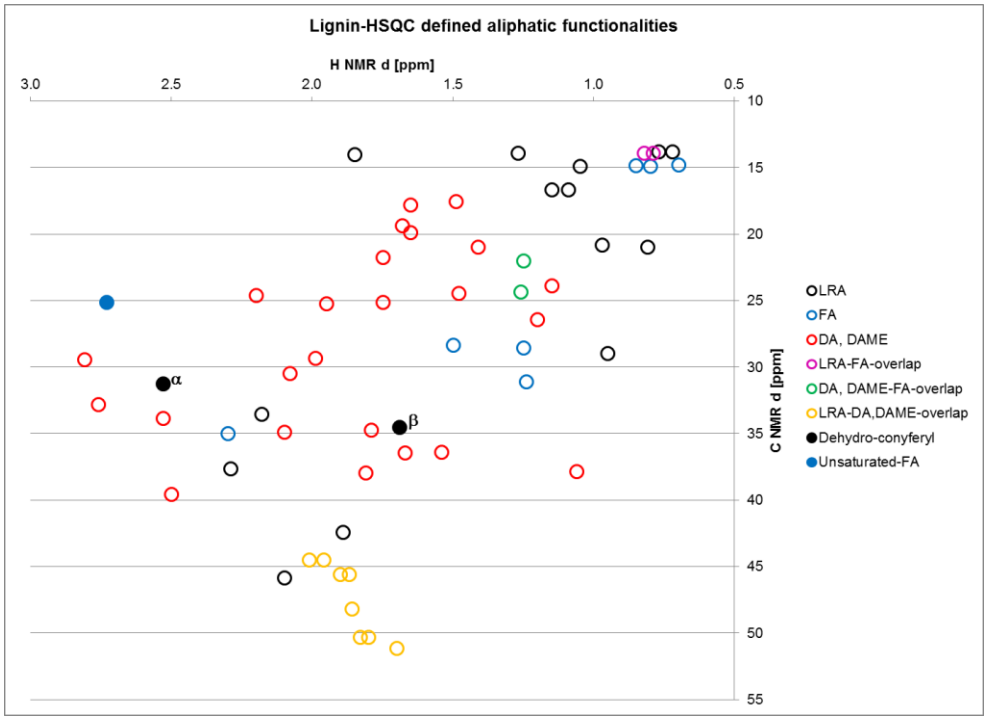

Figure A.C.10. Functionalities found in lignin HSQC aliphatic region.

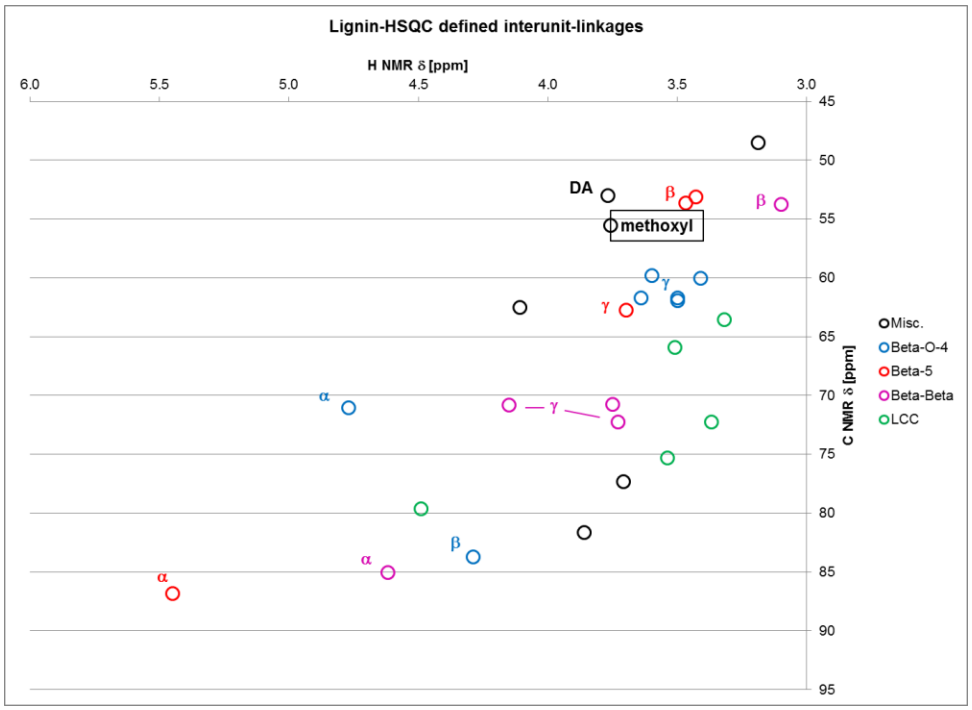

Figure A.C.11. Functionalities found in lignin HSQC interunit-linkage region.

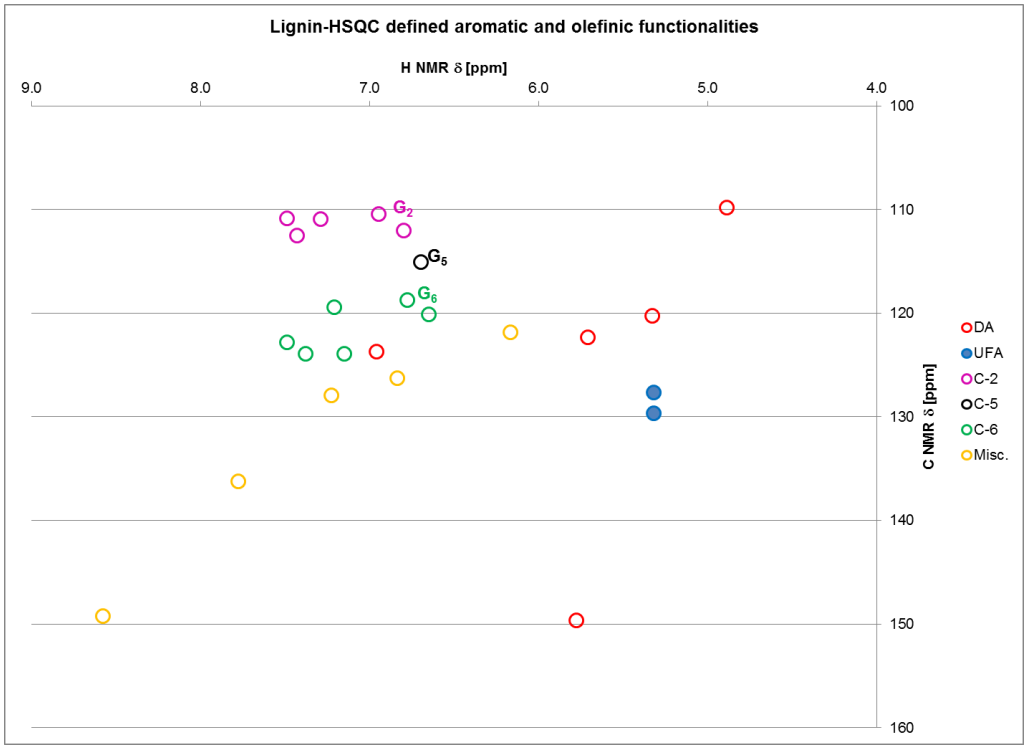

Figure A.C.12. Functionalities found in lignin HSQC olefinic and aromatic regions

APPENDIX D

COPYRIGHT PERMISSIONS

D.1 Permission from Green Chemistry

Dear Matyas

The Royal Society of Chemistry (RSC) hereby grants permission for the use of your paper(s) specified below in the printed and microfilm version of your thesis. You may also make available the PDF version of your paper(s) that the RSC sent to the corresponding author(s) of your paper(s) upon publication of the paper(s) in the following ways: in your thesis via any website that your university may have for the deposition of theses, via your university's Intranet or via your own personal website. We are however unable to grant you permission to include the PDF version of the paper(s) on its own in your institutional repository. The Royal Society of Chemistry is a signatory to the STM Guidelines on Permissions (available on request).
Please note that if the material specified below or any part of it appears with credit or acknowledgement to a third party then you must also secure permission from that third party before reproducing that material.

Please ensure that the thesis states the following:
Reproduced by permission of The Royal Society of Chemistry
and include a link to the paper on the Royal Society of Chemistry's website.

Please ensure that your co-authors are aware that you are including the paper in your thesis.

Regards

Gill Cockhead

Publishing Contracts & Copyright Executive
Gill Cockhead (Mrs), Publishing Contracts & Copyright Executive
Royal Society of Chemistry, Thomas Graham House
Science Park, Milton Road, Cambridge CB4 0WF, UK
Tel +44 (0) 1223 432134, Fax +44 (0) 1223 423623

D.2 Permission from Trends in Biotechnology

ELSEVIER LICENSE
TERMS AND CONDITIONS

Jul 23, 2012

This is a License Agreement between Matyas Kosa ("You") and Elsevier ("Elsevier") provided by Copyright Clearance Center ("CCC"). The license consists of your order details, the terms and conditions provided by Elsevier, and the payment terms and conditions.

All payments must be made in full to CCC. For payment instructions, please see information listed at the bottom of this form.

Supplier	Elsevier Limited The Boulevard,Langford Lane Kidlington,Oxford,OX5 1GB,UK
Registered Company Number	1982084
Customer name	Matyas Kosa
Customer address	500 10th street, NW Atlanta, GA 30332
License number	2954850842482
License date	Jul 23, 2012
Licensed content publisher	Elsevier
Licensed content publication	Trends in Biotechnology
Licensed content title	Lipids from heterotrophic microbes: advances in metabolism research
Licensed content author	Matyas Kosa,Arthur J. Ragauskas
Licensed content date	February 2011
Licensed content volume number	29
Licensed content issue number	2
Number of pages	9
Start Page	53
End Page	61
Type of Use	reuse in a thesis/dissertation
Intended publisher of new	other

work	
Portion	full article
Format	both print and electronic
Are you the author of this Elsevier article?	Yes
Will you be translating?	No
Order reference number	
Title of your thesis/dissertation	Direct and multistep conversion of lignin to biofuels
Expected completion date	Sep 2012
Estimated size (number of pages)	220
Elsevier VAT number	GB 494 6272 12
Permissions price	0.00 USD
VAT/Local Sales Tax	0.0 USD / 0.0 GBP
Total	0.00 USD
Terms and Conditions	

INTRODUCTION

1. The publisher for this copyrighted material is Elsevier. By clicking "accept" in connection with completing this licensing transaction, you agree that the following terms and conditions apply to this transaction (along with the Billing and Payment terms and conditions established by Copyright Clearance Center, Inc. ("CCC"), at the time that you opened your Rightslink account and that are available at any time at http://myaccount.copyright.com).

GENERAL TERMS

2. Elsevier hereby grants you permission to reproduce the aforementioned material subject to the terms and conditions indicated.

3. Acknowledgement: If any part of the material to be used (for example, figures) has appeared in our publication with credit or acknowledgement to another source, permission must also be sought from that source. If such permission is not obtained then that material may not be included in your publication/copies. Suitable acknowledgement to the source must be made, either as a footnote or in a reference list at the end of your publication, as follows:

“Reprinted from Publication title, Vol /edition number, Author(s), Title of article / title of chapter, Pages No., Copyright (Year), with permission from Elsevier [OR APPLICABLE SOCIETY COPYRIGHT OWNER].” Also Lancet special credit - “Reprinted from The Lancet, Vol. number, Author(s), Title of article, Pages No., Copyright (Year), with

permission from Elsevier."

4. Reproduction of this material is confined to the purpose and/or media for which permission is hereby given.

5. Altering/Modifying Material: Not Permitted. However figures and illustrations may be altered/adapted minimally to serve your work. Any other abbreviations, additions, deletions and/or any other alterations shall be made only with prior written authorization of Elsevier Ltd. (Please contact Elsevier at permissions@elsevier.com)

6. If the permission fee for the requested use of our material is waived in this instance, please be advised that your future requests for Elsevier materials may attract a fee.

7. Reservation of Rights: Publisher reserves all rights not specifically granted in the combination of (i) the license details provided by you and accepted in the course of this licensing transaction, (ii) these terms and conditions and (iii) CCC's Billing and Payment terms and conditions.

8. License Contingent Upon Payment: While you may exercise the rights licensed immediately upon issuance of the license at the end of the licensing process for the transaction, provided that you have disclosed complete and accurate details of your proposed use, no license is finally effective unless and until full payment is received from you (either by publisher or by CCC) as provided in CCC's Billing and Payment terms and conditions. If full payment is not received on a timely basis, then any license preliminarily granted shall be deemed automatically revoked and shall be void as if never granted. Further, in the event that you breach any of these terms and conditions or any of CCC's Billing and Payment terms and conditions, the license is automatically revoked and shall be void as if never granted. Use of materials as described in a revoked license, as well as any use of the materials beyond the scope of an unrevoked license, may constitute copyright infringement and publisher reserves the right to take any and all action to protect its copyright in the materials.

9. Warranties: Publisher makes no representations or warranties with respect to the licensed material.

10. Indemnity: You hereby indemnify and agree to hold harmless publisher and CCC, and their respective officers, directors, employees and agents, from and against any and all claims arising out of your use of the licensed material other than as specifically authorized pursuant to this license.

11. No Transfer of License: This license is personal to you and may not be sublicensed, assigned, or transferred by you to any other person without publisher's written permission.

12. No Amendment Except in Writing: This license may not be amended except in a writing signed by both parties (or, in the case of publisher, by CCC on publisher's behalf).

13. Objection to Contrary Terms: Publisher hereby objects to any terms contained in any purchase order, acknowledgment, check endorsement or other writing prepared by you, which terms are inconsistent with these terms and conditions or CCC's Billing and Payment terms and conditions. These terms and conditions, together with CCC's Billing and Payment terms and conditions (which are incorporated herein), comprise the entire agreement between you and publisher (and CCC) concerning this licensing transaction. In the event of any conflict between your obligations established by these terms and conditions and those established by CCC's Billing and Payment terms and conditions, these terms and conditions shall control.

14. Revocation: Elsevier or Copyright Clearance Center may deny the permissions described in this License at their sole discretion, for any reason or no reason, with a full refund payable to you. Notice of such denial will be made using the contact information provided by you. Failure to receive such notice will not alter or invalidate the denial. In no event will Elsevier or Copyright Clearance Center be responsible or liable for any costs, expenses or damage incurred by you as a result of a denial of your permission request, other than a refund of the amount(s) paid by you to Elsevier and/or Copyright Clearance Center for denied permissions.

LIMITED LICENSE

The following terms and conditions apply only to specific license types:

15. **Translation**: This permission is granted for non-exclusive world **English** rights only unless your license was granted for translation rights. If you licensed translation rights you may only translate this content into the languages you requested. A professional translator must perform all translations and reproduce the content word for word preserving the integrity of the article. If this license is to re-use 1 or 2 figures then permission is granted for non-exclusive world rights in all languages.

16. **Website**: The following terms and conditions apply to electronic reserve and author websites:
Electronic reserve: If licensed material is to be posted to website, the web site is to be password-protected and made available only to bona fide students registered on a relevant course if:
This license was made in connection with a course,
This permission is granted for 1 year only. You may obtain a license for future website posting,
All content posted to the web site must maintain the copyright information line on the bottom of each image,
A hyper-text must be included to the Homepage of the journal from which you are licensing at http://www.sciencedirect.com/science/journal/xxxxx or the Elsevier homepage for books at http://www.elsevier.com, and
Central Storage: This license does not include permission for a scanned version of the material to be stored in a central repository such as that provided by Heron/XanEdu.

17. **Author website** for journals with the following additional clauses:

All content posted to the web site must maintain the copyright information line on the bottom of each image, and the permission granted is limited to the personal version of your paper. You are not allowed to download and post the published electronic version of your article (whether PDF or HTML, proof or final version), nor may you scan the printed edition to create an electronic version. A hyper-text must be included to the Homepage of the journal from which you are licensing at http://www.sciencedirect.com/science/journal/xxxxx. As part of our normal production process, you will receive an e-mail notice when your article appears on Elsevier's online service ScienceDirect (www.sciencedirect.com). That e-mail will include the article's Digital Object Identifier (DOI). This number provides the electronic link to the published article and should be included in the posting of your personal version. We ask that you wait until you receive this e-mail and have the DOI to do any posting.

Central Storage: This license does not include permission for a scanned version of the material to be stored in a central repository such as that provided by Heron/XanEdu.

18. **Author website** for books with the following additional clauses:
Authors are permitted to place a brief summary of their work online only.
A hyper-text must be included to the Elsevier homepage. All content posted to the web site must maintain the copyright information line on the bottom of each image. You are not allowed to download and post the published electronic version of your chapter, nor may you scan the printed edition to create an electronic version.

Central Storage: This license does not include permission for a scanned version of the material to be stored in a central repository such as that provided by Heron/XanEdu.

19. **Website** (regular and for author): A hyper-text must be included to the Homepage of the journal from which you are licensing at http://www.sciencedirect.com/science/journal/xxxxx. or for books to the Elsevier homepage at http://www.elsevier.com

20. **Thesis/Dissertation**: If your license is for use in a thesis/dissertation your thesis may be submitted to your institution in either print or electronic form. Should your thesis be published commercially, please reapply for permission. These requirements include permission for the Library and Archives of Canada to supply single copies, on demand, of the complete thesis and include permission for UMI to supply single copies, on demand, of the complete thesis. Should your thesis be published commercially, please reapply for permission.

21. **Other Conditions**:

v1.6

If you would like to pay for this license now, please remit this license along with your

payment made payable to "COPYRIGHT CLEARANCE CENTER" otherwise you will be invoiced within 48 hours of the license date. Payment should be in the form of a check or money order referencing your account number and this invoice number RLNK500823649.
Once you receive your invoice for this order, you may pay your invoice by credit card. Please follow instructions provided at that time.

Make Payment To:
Copyright Clearance Center
Dept 001
P.O. Box 843006
Boston, MA 02284-3006

For suggestions or comments regarding this order, contact RightsLink Customer Support: +1-877-622-5543 (toll free in the US) or +1-978-646-2777.

Gratis licenses (referencing $0 in the Total field) are free. Please retain this printable license for your reference. No payment is required.

D.3 Permissions from Applied Microbiology and Biotechnology

D.3.1 Permission for the review

SPRINGER LICENSE TERMS AND CONDITIONS

Jul 23, 2012

This is a License Agreement between Matyas Kosa ("You") and Springer ("Springer") provided by Copyright Clearance Center ("CCC"). The license consists of your order details, the terms and conditions provided by Springer, and the payment terms and conditions.

All payments must be made in full to CCC. For payment instructions, please see information listed at the bottom of this form.

License Number	2954850095577
License date	Jul 23, 2012
Licensed content publisher	Springer
Licensed content publication	Applied Microbiology and Biotechnology
Licensed content title	Challenges of the utilization of wood polymers: how can they be overcome?
Licensed content author	Yunqiao Pu
Licensed content date	Jan 1, 2011
Volume number	91
Issue number	6
Type of Use	Thesis/Dissertation
Portion	Full text
Number of copies	5
Author of this Springer article	Yes and you are a contributor of the new work
Order reference number	None
Title of your thesis / dissertation	Direct and multistep conversion of lignin to biofuels
Expected completion date	Sep 2012
Estimated size(pages)	220
Total	0.00 USD

Terms and Conditions

Introduction

The publisher for this copyrighted material is Springer Science + Business Media. By clicking "accept" in connection with completing this licensing transaction, you agree that the following terms and conditions apply to this transaction (along with the Billing and Payment terms and conditions established by Copyright Clearance Center, Inc. ("CCC"), at the time that you opened your Rightslink account and that are available at any time at http://myaccount.copyright.com).

Limited License

With reference to your request to reprint in your thesis material on which Springer Science and Business Media control the copyright, permission is granted, free of charge, for the use indicated in your enquiry.

Licenses are for one-time use only with a maximum distribution equal to the number that you identified in the licensing process.

This License includes use in an electronic form, provided its password protected or on the university's intranet or repository, including UMI (according to the definition at the Sherpa website: http://www.sherpa.ac.uk/romeo/). For any other electronic use, please contact Springer at (permissions.dordrecht@springer.com or permissions.heidelberg@springer.com).

The material can only be used for the purpose of defending your thesis, and with a maximum of 100 extra copies in paper.

Although Springer holds copyright to the material and is entitled to negotiate on rights, this license is only valid, provided permission is also obtained from the (co) author (address is given with the article/chapter) and provided it concerns original material which does not carry references to other sources (if material in question appears with credit to another source, authorization from that source is required as well).

Permission free of charge on this occasion does not prejudice any rights we might have to charge for reproduction of our copyrighted material in the future.

Altering/Modifying Material: Not Permitted

You may not alter or modify the material in any manner. Abbreviations, additions, deletions and/or any other alterations shall be made only with prior written authorization of the author(s) and/or Springer Science + Business Media. (Please contact Springer at (permissions.dordrecht@springer.com or permissions.heidelberg@springer.com)

Reservation of Rights

Springer Science + Business Media reserves all rights not specifically granted in the combination of (i) the license details provided by you and accepted in the course of this licensing transaction, (ii) these terms and conditions and (iii) CCC's Billing and Payment

terms and conditions.

Copyright Notice:Disclaimer
You must include the following copyright and permission notice in connection with any reproduction of the licensed material: "Springer and the original publisher /journal title, volume, year of publication, page, chapter/article title, name(s) of author(s), figure number(s), original copyright notice) is given to the publication in which the material was originally published, by adding; with kind permission from Springer Science and Business Media"

Warranties: None

Example 1: Springer Science + Business Media makes no representations or warranties with respect to the licensed material.

Example 2: Springer Science + Business Media makes no representations or warranties with respect to the licensed material and adopts on its own behalf the limitations and disclaimers established by CCC on its behalf in its Billing and Payment terms and conditions for this licensing transaction.

Indemnity
You hereby indemnify and agree to hold harmless Springer Science + Business Media and CCC, and their respective officers, directors, employees and agents, from and against any and all claims arising out of your use of the licensed material other than as specifically authorized pursuant to this license.

No Transfer of License
This license is personal to you and may not be sublicensed, assigned, or transferred by you to any other person without Springer Science + Business Media's written permission.

No Amendment Except in Writing
This license may not be amended except in a writing signed by both parties (or, in the case of Springer Science + Business Media, by CCC on Springer Science + Business Media's behalf).

Objection to Contrary Terms
Springer Science + Business Media hereby objects to any terms contained in any purchase order, acknowledgment, check endorsement or other writing prepared by you, which terms are inconsistent with these terms and conditions or CCC's Billing and Payment terms and conditions. These terms and conditions, together with CCC's Billing and Payment terms and conditions (which are incorporated herein), comprise the entire agreement between you and Springer Science + Business Media (and CCC) concerning this licensing transaction. In the event of any conflict between your obligations established by these terms and conditions and those established by CCC's Billing and

Payment terms and conditions, these terms and conditions shall control.

Jurisdiction
All disputes that may arise in connection with this present License, or the breach thereof, shall be settled exclusively by arbitration, to be held in The Netherlands, in accordance with Dutch law, and to be conducted under the Rules of the 'Netherlands Arbitrage Instituut' (Netherlands Institute of Arbitration).***OR:***

All disputes that may arise in connection with this present License, or the breach thereof, shall be settled exclusively by arbitration, to be held in the Federal Republic of Germany, in accordance with German law.

Other terms and conditions:

v1.3

If you would like to pay for this license now, please remit this license along with your payment made payable to "COPYRIGHT CLEARANCE CENTER" otherwise you will be invoiced within 48 hours of the license date. Payment should be in the form of a check or money order referencing your account number and this invoice number RLNK500823632.
Once you receive your invoice for this order, you may pay your invoice by credit card. Please follow instructions provided at that time.

Make Payment To:
Copyright Clearance Center
Dept 001
P.O. Box 843006
Boston, MA 02284-3006

For suggestions or comments regarding this order, contact RightsLink Customer Support: +1-877-622-5543 (toll free in the US) or +1-978-646-2777.

Gratis licenses (referencing $0 in the Total field) are free. Please retain this printable license for your reference. No payment is required.

D.3.2 Permission for the original paper

SPRINGER LICENSE
TERMS AND CONDITIONS

Jul 23, 2012

This is a License Agreement between Matyas Kosa ("You") and Springer ("Springer") provided by Copyright Clearance Center ("CCC"). The license consists of your order details, the terms and conditions provided by Springer, and the payment terms and conditions.

All payments must be made in full to CCC. For payment instructions, please see information listed at the bottom of this form.

License Number	2954850267065
License date	Jul 23, 2012
Licensed content publisher	Springer
Licensed content publication	Applied Microbiology and Biotechnology
Licensed content title	Bioconversion of lignin model compounds with oleaginous *Rhodococci*
Licensed content author	Matyas Kosa
Licensed content date	Jan 1, 2011
Volume number	93
Issue number	2
Type of Use	Thesis/Dissertation
Portion	Full text
Number of copies	5
Author of this Springer article	Yes and you are a contributor of the new work
Order reference number	
Title of your thesis / dissertation	Direct and multistep conversion of lignin to biofuels
Expected completion date	Sep 2012
Estimated size(pages)	220
Total	0.00 USD
Terms and Conditions	

Introduction
The publisher for this copyrighted material is Springer Science + Business Media. By

clicking "accept" in connection with completing this licensing transaction, you agree that the following terms and conditions apply to this transaction (along with the Billing and Payment terms and conditions established by Copyright Clearance Center, Inc. ("CCC"), at the time that you opened your Rightslink account and that are available at any time at http://myaccount.copyright.com).

Limited License
With reference to your request to reprint in your thesis material on which Springer Science and Business Media control the copyright, permission is granted, free of charge, for the use indicated in your enquiry.

Licenses are for one-time use only with a maximum distribution equal to the number that you identified in the licensing process.

This License includes use in an electronic form, provided its password protected or on the university's intranet or repository, including UMI (according to the definition at the Sherpa website: http://www.sherpa.ac.uk/romeo/). For any other electronic use, please contact Springer at (permissions.dordrecht@springer.com or permissions.heidelberg@springer.com).

The material can only be used for the purpose of defending your thesis, and with a maximum of 100 extra copies in paper.

Although Springer holds copyright to the material and is entitled to negotiate on rights, this license is only valid, provided permission is also obtained from the (co) author (address is given with the article/chapter) and provided it concerns original material which does not carry references to other sources (if material in question appears with credit to another source, authorization from that source is required as well).

Permission free of charge on this occasion does not prejudice any rights we might have to charge for reproduction of our copyrighted material in the future.

Altering/Modifying Material: Not Permitted
You may not alter or modify the material in any manner. Abbreviations, additions, deletions and/or any other alterations shall be made only with prior written authorization of the author(s) and/or Springer Science + Business Media. (Please contact Springer at (permissions.dordrecht@springer.com or permissions.heidelberg@springer.com)

Reservation of Rights
Springer Science + Business Media reserves all rights not specifically granted in the combination of (i) the license details provided by you and accepted in the course of this licensing transaction, (ii) these terms and conditions and (iii) CCC's Billing and Payment terms and conditions.

Copyright Notice:Disclaimer
You must include the following copyright and permission notice in connection with any

reproduction of the licensed material: "Springer and the original publisher /journal title, volume, year of publication, page, chapter/article title, name(s) of author(s), figure number(s), original copyright notice) is given to the publication in which the material was originally published, by adding; with kind permission from Springer Science and Business Media"

Warranties: None

Example 1: Springer Science + Business Media makes no representations or warranties with respect to the licensed material.

Example 2: Springer Science + Business Media makes no representations or warranties with respect to the licensed material and adopts on its own behalf the limitations and disclaimers established by CCC on its behalf in its Billing and Payment terms and conditions for this licensing transaction.

Indemnity
You hereby indemnify and agree to hold harmless Springer Science + Business Media and CCC, and their respective officers, directors, employees and agents, from and against any and all claims arising out of your use of the licensed material other than as specifically authorized pursuant to this license.

No Transfer of License
This license is personal to you and may not be sublicensed, assigned, or transferred by you to any other person without Springer Science + Business Media's written permission.

No Amendment Except in Writing
This license may not be amended except in a writing signed by both parties (or, in the case of Springer Science + Business Media, by CCC on Springer Science + Business Media's behalf).

Objection to Contrary Terms
Springer Science + Business Media hereby objects to any terms contained in any purchase order, acknowledgment, check endorsement or other writing prepared by you, which terms are inconsistent with these terms and conditions or CCC's Billing and Payment terms and conditions. These terms and conditions, together with CCC's Billing and Payment terms and conditions (which are incorporated herein), comprise the entire agreement between you and Springer Science + Business Media (and CCC) concerning this licensing transaction. In the event of any conflict between your obligations established by these terms and conditions and those established by CCC's Billing and Payment terms and conditions, these terms and conditions shall control.

Jurisdiction
All disputes that may arise in connection with this present License, or the breach thereof, shall be settled exclusively by arbitration, to be held in The Netherlands, in accordance with Dutch law, and to be conducted under the Rules of the 'Netherlands Arbitrage Instituut'

(Netherlands Institute of Arbitration).***OR:***

All disputes that may arise in connection with this present License, or the breach thereof, shall be settled exclusively by arbitration, to be held in the Federal Republic of Germany, in accordance with German law.

Other terms and conditions:

v1.3

If you would like to pay for this license now, please remit this license along with your payment made payable to "COPYRIGHT CLEARANCE CENTER" otherwise you will be invoiced within 48 hours of the license date. Payment should be in the form of a check or money order referencing your account number and this invoice number RLNK500823635.
Once you receive your invoice for this order, you may pay your invoice by credit card. Please follow instructions provided at that time.

Make Payment To:
Copyright Clearance Center
Dept 001
P.O. Box 843006
Boston, MA 02284-3006

For suggestions or comments regarding this order, contact RightsLink Customer Support: +1-877-622-5543 (toll free in the US) or +1-978-646-2777.

Gratis licenses (referencing $0 in the Total field) are free. Please retain this printable license for your reference. No payment is required.

D.4 Permission from Biofuels (Future Science)

Dear Dr Kosa,

Thank you for your email.

Please find attached a copy of the permission grant for your records.

Sample Citations:

Reproduced from Biofuels, November 2010, Vol. 1, No. 6, Pages 839-845 with permission of Future Science Ltd

Adapted from Biofuels, November 2010, Vol. 1, No. 6, Pages 839-845 with permission of Future Science Ltd

Any further queries please do not hesitate to contact me.

Many thanks,
Javonne

Javonne Molloy
Administrative Assistant
Future Science Group
Unitec House
2 Albert Place
Finchley Central
London
N3 1QB
Tel: +44 (0)20 8371 6080
Fax: +44 (0)20 8371 6089
Email: j.molloy@futuremedicine.com
Website: www.future-science-group.com

Future Medicine Ltd, Unitec House, 2 Albert Place, London, N3 1QB, UK (registered in England & Wales, No: 4059017); VAT No: GB 833 0029 67
P Please consider the environment before printing this email.

FUTURE SCIENCE

Permission to use Future Science Ltd copyright material

Request from:

- Contact name: ..... Matyas Kosa
- Publisher/company name:
- Address: .....
- Telephone/e-mail: Matyas.Kosa@gatech.edu

Request details:

- Request to use the following content: Author - Full Article - Biofuels, November 2010, Vol. 1, No. 6, Pages 839-845
- In the following publication: Thesis
- In what media (print/electronic/print & electronic): Print
- In the following languages: All

We, Future Science Ltd, grant permission to reuse the material specified above within the publication specified above.

Notes and conditions:

1. This permission is granted free of charge, for one-time use only.
2. Future Science Ltd grant the publisher non-exclusive world rights to publish the content in the publication/website specified above.
3. Future Science Ltd retains copyright ownership of the content.
4. Permission is granted on a one-time basis only. Separate permission is required for any further use or edition.
5. The publisher will make due acknowledgement of the original publication wherever they republish the content: citing the author, content title, publication name and Future Science Ltd as the original publisher.
6. The publisher will not amend, abridge, or otherwise change the content without authorization from Future Science Ltd.
7. Permission does not include any copyrighted material from other sources that may be incorporated within the content.
8. Failure to comply with the conditions above will result in immediate revocation of the permission here granted.

Date: 24/07/2012.....

Future Science Ltd, Unitec House, 2 Albert Place, London, N3 1QB, UK
T: +44 (0)20 8371 6080 **F:** +44 (0) 20 8371 6099 **E:** info@future-science.com
www.future-science.com

REFERENCES

1. Doherty, W.O.S., P. Mousavioun, and C.M. Fellows, *Value-adding to cellulosic ethanol: Lignin polymers.* Industrial Crops and Products, 2011. **33**(2): p. 259-276.

2. Pu, Y., et al., *Challenges of the utilization of wood polymers: how can they be overcome?* Applied Microbiology and Biotechnology, 2011. **91**(6): p. 1525-1536.

3. Pu, Y., et al., *The new forestry biofuels sector.* Biofuels, Bioproducts and Biorefining, 2008. **2**(1): p. 58-73.

4. Ragauskas, A.J., et al., *The Path Forward for Biofuels and Biomaterials.* Science, 2006. **311**(5760): p. 484-489.

5. Zakzeski, J., et al., *The Catalytic Valorization of Lignin for the Production of Renewable Chemicals.* Chemical Reviews, 2010. **110**(6): p. 3552-3599.

6. David, K. and A.J. Ragauskas, *Switchgrass as an energy crop for biofuel production: A review of its ligno-cellulosic chemical properties.* Energy & Environmental Science, 2010. **3**(9): p. 1182-1190.

7. DOE, *U. S. Billion-Ton update.* 2011.

8. Kerr, R.A., *Do We Have the Energy for the Next Transition?* Science, 2010. **329**(5993): p. 780-781.

9. Kosa, M., et al., *Pyrolysis oils from CO2 precipitated Kraft lignin.* Green Chemistry, 2011. **13**(11): p. 3196-3202.

10. Nagy, M., et al., *Characterization of CO2 precipitated Kraft lignin to promote its utilization.* Green Chemistry, 2010. **12**(1): p. 31-34.

11. Harwood, C.S. and R.E. Parales, *THE β-KETOADIPATE PATHWAY AND THE BIOLOGY OF SELF-IDENTITY.* Annual Review of Microbiology, 1996. **50**(1): p. 553-590.

12. Warhurst, A.M. and C.A. Fewson, *Biotransformations Catalyzed by the Genus Rhodococcus.* Critical Reviews in Biotechnology, 1994. **14**(1): p. 29-73.

13. Alvarez, H.A. and A.S. Steinbüchel, *Triacylglycerols in prokaryotic microorganisms.* Applied Microbiology and Biotechnology, 2002. **60**(4): p. 367-376.

14. Ratledge, C. and J.P. Wynn, *The biochemistry and molecular biology of lipid accumulation in oleaginous microorganisms,* in *Advances in Applied Microbiology*. 2002, Academic Press. p. 1-51.

15. Kosa, M. and A.J. Ragauskas, *Lipids from heterotrophic microbes: advances in metabolism research.* Trends in Biotechnology, 2011. **29**(2): p. 53-61.

16. Beer, C., et al., *Terrestrial Gross Carbon Dioxide Uptake: Global Distribution and Covariation with Climate.* Science, 2010. **329**(5993): p. 834-838.

17. Graham-Rowe, D., *Agriculture: Beyond food versus fuel.* Nature, 2011. **474**(7352): p. S6-S8.

18. Robbins, M., *Policy: Fuelling politics.* Nature, 2011. **474**(7352): p. S22-S24.

19. Dillon, M.E., G. Wang, and R.B. Huey, *Global metabolic impacts of recent climate warming.* Nature, 2010. **467**(7316): p. 704-706.

20. Reich, P.B., *The Carbon Dioxide Exchange.* Science, 2010. **329**(5993): p. 774-775.

21. Fairley, P., *Introduction: Next generation biofuels.* Nature, 2011. **474**(7352): p. S2-S5.

22. Somerville, C., et al., *Feedstocks for Lignocellulosic Biofuels.* Science, 2010. **329**(5993): p. 790-792.

23. Service, R.F., *Is There a Road Ahead for Cellulosic Ethanol?* Science, 2010. **329**(5993): p. 784-785.

24. Cho, A., *Energy's Tricky Tradeoffs.* Science, 2010. **329**(5993): p. 786-787.

25. Kintisch, E., *Out of Site.* Science, 2010. **329**(5993): p. 788-789.

26. Roeb, M. and H. Müller-Steinhagen, *Concentrating on Solar Electricity and Fuels.* Science, 2010. **329**(5993): p. 773-774.

27. Gilbert, N., *Local benefits: The seeds of an economy.* Nature, 2011. **474**(7352): p. S18-S19.

28. Baum, R.M., *Climate Schizoprenia.* C&EN, 2011. **89**(36): p. 5.

29. Stephen, J.D., W.E. Mabee, and J.N. Saddler, *Biomass logistics as a determinant of second-generation biofuel facility scale, location and technology selection.* Biofuels, Bioproducts and Biorefining, 2010. **4**(5): p. 503-518.

30. Alvira, P., et al., *Pretreatment technologies for an efficient bioethanol production process based on enzymatic hydrolysis: A review.* Bioresource Technology, 2010. **101**(13): p. 4851-4861.

31. Banerjee, S., et al., *Commercializing lignocellulosic bioethanol: technology bottlenecks and possible remedies.* Biofuels, Bioproducts and Biorefining, 2010. **4**(1): p. 77-93.

32. Yang, B., et al., *Enzymatic hydrolysis of cellulosic biomass.* Biofuels, 2011. **2**(4): p. 421-450.

33. Richard, T.L., *Challenges in Scaling Up Biofuels Infrastructure.* Science, 2010. **329**(5993): p. 793-796.

34. Chisti, Y., *Biodiesel from microalgae beats bioethanol.* Trends in Biotechnology, 2008. **26**(3): p. 126-131.

35. Dumitriu, S., *Polysaccharides: Structural Diversity and Functional Versatility, Second Edition*. 2004: Taylor & Francis.

36. Ragauskas, A.J. *Chemical composition of wood*.

37. DOE. *Theoretical ethanol yield calculator*. 2012; Available from: http://www1.eere.energy.gov/biomass/ethanol_yield_calculator.html.

38. M. A. Elsayed, R.M., N. D. Mortimer, *Carbon and energy balances for a range of biofuels options.* 2003.

39. Pan, X., et al., *Pretreatment of Lodgepole Pine Killed by Mountain Pine Beetle Using the Ethanol Organosolv Process: Fractionation and Process Optimization.* Industrial & Engineering Chemistry Research, 2007. **46**(8): p. 2609-2617.

40. Bourne, J.K., *Biofuels.* National Geographic, 2007.

41. Balat, M., *An Overview of the Properties and Applications of Biomass Pyrolysis Oils.* Energy Sources Part A: Recovery, Utilization & Environmental Effects, 2011. **33**(7): p. 674-689.

42. Ben, H. and A.J. Ragauskas, *NMR Characterization of Pyrolysis Oils from Kraft Lignin.* Energy & Fuels, 2011. **25**(5): p. 2322-2332.

43. Czernik, S. and A.V. Bridgwater, *Overview of Applications of Biomass Fast Pyrolysis Oil.* Energy & Fuels, 2004. **18**(2): p. 590-598.

44. Demirbas, A. and G. Arin, *An Overview of Biomass Pyrolysis.* Energy Sources, 2002. **24**(5): p. 471-482.

45. Pandey, M.P. and C.S. Kim, *Lignin Depolymerization and Conversion: A Review of Thermochemical Methods.* Chemical Engineering & Technology, 2011. **34**(1): p. 29-41.

46. David, K., et al., *31P-NMR analysis of bio-oils obtained from the pyrolysis of biomass.* Biofuels, 2010. **1**(6): p. 839-845.

47. Ben, H. and A.J. Ragauskas, *Pyrolysis of Kraft Lignin with Additives.* Energy & Fuels, 2011. **25**(10): p. 4662-4668.

48. Ben, H. and A.J. Ragauskas, *Heteronuclear Single-Quantum Correlation–Nuclear Magnetic Resonance (HSQC–NMR) Fingerprint Analysis of Pyrolysis Oils.* Energy & Fuels, 2011. **25**(12): p. 5791-5801.

49. Briker, Y., et al., *Diesel Fuel Analysis by GC−FIMS: Aromatics, n-Paraffins, and Isoparaffins.* Energy & Fuels, 2000. **15**(1): p. 23-37.

50. Demirbas, A., *Biorefineries: Current activities and future developments.* Energy Conversion and Management, 2009. **50**(11): p. 2782-2801.

51. Knothe, G., *Dependence of biodiesel fuel properties on the structure of fatty acid alkyl esters.* Fuel Processing Technology, 2005. **86**(10): p. 1059-1070.

52. Mohan, D., C.U. Pittman, and P.H. Steele, *Pyrolysis of Wood/Biomass for Bio-oil: A Critical Review.* Energy & Fuels, 2006. **20**(3): p. 848-889.

53. Uthoff, S., D. Bröker, and A. Steinbüchel, *Current state and perspectives of producing biodiesel-like compounds by biotechnology.* Microbial Biotechnology, 2009. **2**(5): p. 551-565.

54. Nagy, M., *Biofuels from lignin and novel biodiesel analysis*, in *Department of Chemistry and Biochemistry*2009, Georgia Institute of Technology: Georgia Institute of Technology.

55. Knothe, G., *Analyzing biodiesel: standards and other methods.* Journal of the American Oil Chemists' Society, 2006. **83**(10): p. 823-833.

56. Shea, S.B., *Biodiesel Revs Up Its Applications.* 2011.

57. DOE, A. *Biodiesel Production and Distribution*. 2012; Available from: http://www.afdc.energy.gov/afdc/fuels/biodiesel_production.html.

58. Röttig, A., et al., *Fatty acid alkyl esters: perspectives for production of alternative biofuels.* Applied Microbiology and Biotechnology, 2010. **85**(6): p. 1713-1733.

59. Knothe, G., *"Designer" Biodiesel: Optimizing Fatty Ester Composition to Improve Fuel Properties†.* Energy & Fuels, 2008. **22**(2): p. 1358-1364.

60. Knothe, G., *Improving biodiesel fuel properties by modifying fatty ester composition.* Energy & Environmental Science, 2009. **2**(7): p. 759-766.

61. Nagy, M., et al., *Phosphitylation and quantitative 31P NMR analysis of partially substituted biodiesel glycerols.* Fuel, 2009. **88**(9): p. 1793-1797.

62. Nagy, M.t., M. Foston, and A.J. Ragauskas, *Rapid Quantitative Analytical Tool for Characterizing the Preparation of Biodiesel†.* The Journal of Physical Chemistry A, 2009. **114**(11): p. 3883-3887.

63. Kosa, M. and A.J. Ragauskas, *Bioconversion of lignin model compounds with oleaginous Rhodococci.* Applied Microbiology and Biotechnology, 2012. **93**(2): p. 891-900.

64. NREL, *Biomass Terms and Definitions Glossary.* 2012.

65. Rowell R M, P.R., Han J S, Rowell J S, Tshabalala M A, *Cell wall chemistry*. Handbook of Wood Chemistry and Wood Composites, ed. R.R. M. 2000: CRC Press, Boca Ranton.

66. Haygreen J G, B.J.L., *Composition and structure of wood cells*. Forest Products and Wood Science. 1996: Iowa State University Press, Ames.

67. Sticklen, M.B., *Plant genetic engineering for biofuel production: towards affordable cellulosic ethanol.* Nat Rev Genet, 2008. **9**(6): p. 433-443.

68. Mohnen D, B.-P.M., Somerville C *Cell wall polysaccharide synthesis*. Biomass recalcitrance: deconstruction the plant cell wall for bioenergy, ed. M.E. Himmel. 2008: Blackwell Publishing.

69. Boudet, A.M., et al., *Lignins and lignocellulosics: a better control of synthesis for new and improved uses.* Trends in Plant Science, 2003. **8**(12): p. 576-581.

70. Ding, S.Y. and M.E. Himmel, *The maize primary cell wall microfibril: A new model derived from direct visualization.* Journal of Agricultural and Food Chemistry, 2006. **54**(3): p. 597-606.

71. Hallac, B.B. and A.J. Ragauskas, *Analyzing cellulose degree of polymerization and its relevancy to cellulosic ethanol.* Biofuels, Bioproducts and Biorefining, 2011. **5**(2): p. 215-225.

72. Atalla, R.H. and D.L. Vanderhart, *NATIVE CELLULOSE - A COMPOSITE OF 2 DISTINCT CRYSTALLINE FORMS.* Science, 1984. **223**(4633): p. 283-285.

73. Ragauskas A J, N.M., Kim D H, Eckert C A, Hallett J P, Liotta C L, *From wood to fuels: integrating biofuels and pulp production.* Industrial Biotechnology, 2006. **2**: p. 55-65.

74. Nishiyama, Y., et al., *Crystal Structure and Hydrogen Bonding System in Cellulose Iα from Synchrotron X-ray and Neutron Fiber Diffraction.* Journal of the American Chemical Society, 2003. **125**(47): p. 14300-14306.

75. Sannigrahi, P., A.J. Ragauskas, and G.A. Tuskan, *Poplar as a feedstock for biofuels: A review of compositional characteristics.* Biofuels, Bioproducts and Biorefining, 2010. **4**(2): p. 209-226.

76. Larsson, P.T., K. Wickholm, and T. Iversen, *A CP/MAS13C NMR investigation of molecular ordering in celluloses.* Carbohydrate Research, 1997. **302**(1–2): p. 19-25.

77. Pu, Y., C. Ziemer, and A.J. Ragauskas, *CP/MAS 13C NMR analysis of cellulase treated bleached softwood kraft pulp.* Carbohydrate Research, 2006. **341**(5): p. 591-597.

78. Wickholm, K., P.T. Larsson, and T. Iversen, *Assignment of non-crystalline forms in cellulose I by CP/MAS 13C NMR spectroscopy.* Carbohydrate Research, 1998. **312**(3): p. 123-129.

79. Atalla R H, B.J.W., Matthews J F, Ding S Y, Himmel M E *Structures of plant cell wall celluloses*, in *Biomass recalcitrance: deconstruction the plant cell wall for bioenergy*, H.M. E, Editor. 2008, Blackwell Publishing. p. 188-212.

80. Willför, S., et al., *Polysaccharides in some industrially important softwood species.* Wood Science and Technology, 2005. **39**(4): p. 245-257.

81. Willför, S., et al., *Polysaccharides in some industrially important hardwood species.* Wood Science and Technology, 2005. **39**(8): p. 601-617.

82. Harris P J, S.B.A., *Chemistry and molecular organization of plant cell walls*, in *Biomass recalcitrance: deconstruction the plant cell wall for bioenergy*, M.E. Himmel, Editor. 2008, Blackwell Publishing. p. 61-93.

83. Boerjan, W., J. Ralph, and M. Baucher, *Lignin biosynthesis.* Annual Review of Plant Biology, 2003. **54**: p. 519-546.

84. Davin, L.B. and N.G. Lewis, *Lignin primary structures and dirigent sites.* Current Opinion in Biotechnology, 2005. **16**(4): p. 407-415.

85. Sangha, A.K., et al., *Radical Coupling Reactions in Lignin Synthesis: A Density Functional Theory Study.* The Journal of Physical Chemistry B, 2012. **116**(16): p. 4760-4768.

86. Stewart, J.J., et al., *The Effects on Lignin Structure of Overexpression of Ferulate 5-Hydroxylase in Hybrid Poplar.* Plant Physiology, 2009. **150**(2): p. 621-635.

87. Vanholme, R., et al., *Lignin engineering.* Current Opinion in Plant Biology, 2008. **11**(3): p. 278-285.

88. Chakar, F.S. and A.J. Ragauskas, *Review of current and future softwood kraft lignin process chemistry.* Industrial Crops and Products, 2004. **20**(2): p. 131-141.

89. Karhunen, P., et al., *DIBENZODIOXOCINS - A NOVEL TYPE OF LINKAGE IN SOFTWOOD LIGNINS.* Tetrahedron Letters, 1995. **36**(1): p. 169-170.

90. Kukkola, E.M., et al., *The dibenzodioxocin lignin substructure is abundant in the inner part of the secondary wall in Norway spruce and silver birch xylem.* Planta, 2004. **218**(3): p. 497-500.

91. Zhang, L.M., et al., *NMR studies on the occurrence of spirodienone structures in lignins.* Journal of Wood Chemistry and Technology, 2006. **26**(1): p. 65-79.

92. Hallac, B.B., *Fundamental understanding of the biochemical conversion of Buddleja davidii to fermentable sugars*, in *Department of Chemistry and Biochemistry*2011, Georgia Institute of Technology: Atlanta, GA.

93. Balakshin, M., et al., *Quantification of lignin–carbohydrate linkages with high-resolution NMR spectroscopy.* Planta, 2011. **233**(6): p. 1097-1110.

94. Yuan, T.-Q., et al., *Characterization of Lignin Structures and Lignin–Carbohydrate Complex (LCC) Linkages by Quantitative 13C and 2D HSQC NMR Spectroscopy.* Journal of Agricultural and Food Chemistry, 2011. **59**(19): p. 10604-10614.

95. Balakshin, M.Y., E.A. Capanema, and H.-m. Chang, *MWL fraction with a high concentration of lignin-carbohydrate linkages: Isolation and 2D NMR spectroscopic analysis.* Holzforschung, 2007. **61**(1): p. 1-7.

96. Balakshin, M.Y., et al., *Elucidation of the structures of residual and dissolved pine kraft lignins using an HMQC NMR technique.* Journal of Agricultural and Food Chemistry, 2003. **51**(21): p. 6116-6127.

97. Ernst L Back, L.H.A., *Pitch control, wood resin and deresination*. 2000, Atlanta: Tappi press.

98. Tsuchiya, Y., et al., *Inorganic elements in typical Japanese trees for woody biomass fuel.* Journal of Wood Science, 2010. **56**(1): p. 53-63.

99. Sjostrom, E., *Wood Chemistry. Fundamentals and Applications*. 1993: Academic press.

100. Sjöström, E. and R. Alén, *Analytical Methods in Wood Chemistry, Pulping, and Papermaking*. 1998: Springer.

101. Capanema Ewellyn, A., et al., *Structural Analysis of Residual and Technical Lignins by 1H-13C Correlation 2D NMR-Spectroscopy*, in *Holzforschung*2001. p. 302.

102. Liitiä, T.M., et al., *Analysis of Technical Lignins by Two- and Three-Dimensional NMR Spectroscopy.* Journal of Agricultural and Food Chemistry, 2003. **51**(8): p. 2136-2143.

103. Guomei Peng, J.C.R., *An improved method for analyzing resin acid in wood, pulp, process water, and effluent samples.* Tappi Journal, 2000. **82**(12): p. 1-7.

104. Vikström, F., B. Holmbom, and A. Hamunen, *Sterols and Triterpenyl alcohols in common pulpwoods and black liquor soaps.* European Journal of Wood and Wood Products, 2005. **63**(4): p. 303-308.

105. Gierer, J., *Chemistry of delignification.* Wood Science and Technology, 1985. **19**(4): p. 289-312.

106. Gierer, J., *Chemistry of delignification.* Wood Science and Technology, 1986. **20**(1): p. 1-33.

107. Moosavifar, A., P. Sedin, and H. Theliander, *Viscosity and boiling point elevation of black liquor: Consequences when lignin is extracted from the black liquor.* Nordic Pulp & Paper Research Journal, 2006. **21**(2): p. 180-187.

108. Ohman, F. and H. Theliander, *Washing lignin precipitated from kraft black liquor.* Paperi Ja Puu-Paper and Timber, 2006. **88**(5): p. 287-292.

109. Ohman, F., H. Wallmo, and H. Theliander, *A novel method for washing lignin precipitated from kraft black liquor - Laboratory trials.* Nordic Pulp & Paper Research Journal, 2007. **22**(1): p. 9-16.

110. Ohman, F., H. Wallmo, and H. Theliander, *Precipitation and filtration of lignin from black liquor of different origin.* Nordic Pulp & Paper Research Journal, 2007. **22**(2): p. 188-193.

111. Olsson, M.R., E. Axelsson, and T. Berntsson, *Exporting lignin or power from heat-integrated kraft pulp mills: A techno-economic comparison using model mills.* Nordic Pulp & Paper Research Journal, 2006. **21**(4): p. 476-484.

112. Wallmo, H., T. Richards, and H. Theliander, *Lignin precipitation from kraft black liquors: kinetics and carbon dioxide absorption.* Paperi Ja Puu-Paper and Timber, 2007. **89**(7): p. 436-442.

113. Wising, L., et al., *Consequences of lignin precipitation in the pulp and paper industry.* Tappi Journal, 2006. **5**(1): p. 3-8.

114. Yang, R., et al., *Oxygen Degradation and Spectroscopic Characterization of Hardwood Kraft Lignin.* Industrial & Engineering Chemistry Research, 2002. **41**(24): p. 5941-5948.

115. Sannigrahi, P., A.J. Ragauskas, and S.J. Miller, *Lignin Structural Modifications Resulting from Ethanol Organosolv Treatment of Loblolly Pine.* Energy & Fuels, 2009. **24**(1): p. 683-689.

116. Froass, P.M., A.J. Ragauskas, and J.-e. Jiang, *Chemical Structure of Residual Lignin from Kraft Pulp.* Journal of Wood Chemistry and Technology, 1996. **16**(4): p. 347-365.

117. Wallmo, H., *Lignin Extraction from Black Liquor, Precipitation, filtration and washing*, in *Forest Products and Chemicla Engineering, Department of Chemical and Biological Engineering*2008, Chalmers University of Technology: Goteborg, Sweden.

118. Alen, R., F. Sjostrom, and P. Vaskikari, *CARBON-DIOXIDE PRECIPITATION OF LIGNIN FROM ALKALINE PULPING LIQUORS.* Cellulose Chemistry and Technology, 1985. **19**(5): p. 537-541.

119. Laaksometsa, C., et al., *Energy savings combined with lignin extraction for production increase: case study at a eucalyptus mill in Portugal.* Clean Technologies and Environmental Policy, 2009. **11**(1): p. 77-82.

120. Luotfi, H., B. Blackwell, and V. Uloth, *Lignin recovery from black liquor: preliminary process design.* Tappi Journal, 1991. **74**: p. 203-210.

121. Moosavifar, A., *Lignin Extraction from Black Liquor, Properties of the Liquors and Sulphur Content in the Lignin*, in *Forest Products and Chemicla Engineering, Department of Chemical and Biological Engineering*2008, Chalmers University of Technology: Goteborg, Sweden.

122. Moosavifar, A., et al., *Modification of precipitated kraft lignin through the addition of calcium - reduction of SO2 emission.* Nordic Pulp & Paper Research Journal, 2006. **21**(4): p. 493-495.

123. Ohman, F. and H. Theliander, *Filtration properties of lignin precipitated from black liquor.* Tappi Journal, 2007. **6**(7): p. 3-9.

124. Ohman, F., et al., *Method for separating lignin from black liquor*, W.I.P. Organization, Editor 2006: Sweden.

125. Tomani, P., *THE LIGNOBOOST PROCESS.* Cellulose Chemistry and Technology, 2010. **44**(1-3): p. 53-58.

126. Metso. *LignoBoost-commercial scale*. 2011; Available from: http://www.metso.com/pulpandpaper/MPwArticles.nsf/WebWID/WTB-100225-2256F-51E3F?OpenDocument.

127. Lynd, L.R., et al., *Consolidated bioprocessing of cellulosic biomass: an update.* Current Opinion in Biotechnology, 2005. **16**(5): p. 577-583.

128. Den Haan, R., et al., *Functional expression of cellobiohydrolases in Saccharomyces cerevisiae towards one-step conversion of cellulose to ethanol.* Enzyme and Microbial Technology, 2007. **40**(5): p. 1291-1299.

129. Den Haan, R., et al., *Hydrolysis and fermentation of amorphous cellulose by recombinant Saccharomyces cerevisiae.* Metabolic Engineering, 2007. **9**(1): p. 87-94.

130. Galbe, M. and G. Zacchi, *Pretreatment of Lignocellulosic Materials for Efficient Bioethanol Production*
Biofuels, L. Olsson, Editor. 2007, Springer Berlin / Heidelberg. p. 41-65.

131. Ishizawa, C.I., et al., *Porosity and Its Effect on the Digestibility of Dilute Sulfuric Acid Pretreated Corn Stover*. Journal of Agricultural and Food Chemistry, 2007. **55**(7): p. 2575-2581.

132. Jeoh, T., et al., *Cellulase digestibility of pretreated biomass is limited by cellulose accessibility*. Biotechnology and Bioengineering, 2007. **98**(1): p. 112-122.

133. Zhu, J.Y., X. Pan, and R.S. Zalesny, Jr., *Pretreatment of woody biomass for biofuel production: energy efficiency, technologies, and recalcitrance.* Applied Microbiology and Biotechnology, 2010. **87**(3): p. 847-857.

134. Sannigrahi, P., S.J. Miller, and A.J. Ragauskas, *Effects of organosolv pretreatment and enzymatic hydrolysis on cellulose structure and crystallinity in Loblolly pine.* Carbohydrate Research, 2010. **345**(7): p. 965-970.

135. McDonough, T.J., *The Chemistry of Organosolv Delignification*, in *TAPPI Solvent Pulping Seminar*1992, TAPPI, IPST: Boston, Massachusetts. p. 1-17.

136. Gullichsen, J., et al., *Chemical pulping*. 1999: Fapet Oy.

137. Pulp Properties Committee of the Process and Product Quality Division, T., *Kappa number of pulp*, 1993.

138. A., S., et al., *Determination of Structural Carbohydrates and Lignin in Biomass*, 2008, NREL: Golden, CO.

139. Kaar, W.E. and D.L. Brink, *Simplified Analysis of Acid Soluble Lignin.* Journal of Wood Chemistry and Technology, 1991. **11**(4): p. 465-477.

140. del Río, J.C., et al., *Structural Characterization of the Lignin from Jute (Corchorus capsularis) Fibers.* Journal of Agricultural and Food Chemistry, 2009. **57**(21): p. 10271-10281.

141. Li, M.-F., et al., *Characterizaion of extracted lignin of bamboo (Neosinocalamus affinis) pretreated with sodium hydroxide/urea solution at low temperature.* Bioresources, 2010. **5**(3): p. 1762-1778.

142. Rencoret, J., et al., *Isolation and structural characterization of the milled-wood lignin from Paulownia fortunei wood.* Industrial Crops and Products, 2009. **30**(1): p. 137-143.

143. Villaverde, J.J., et al., *Native Lignin Structure of Miscanthus x giganteus and Its Changes during Acetic and Formic Acid Fractionation.* Journal of Agricultural and Food Chemistry, 2009. **57**(14): p. 6262-6270.

144. Yuan, T.-Q., et al., *Isolation and physico-chemical characterization of lignins from ultrasound irradiated fast-growing poplar wood.* Bioresources, 2011. **6**(1): p. 414-433.

145. Capanema, E.A., M.Y. Balakshin, and J.F. Kadla, *A comprehensive approach for quantitative lignin characterization by NMR spectroscopy.* Journal of Agricultural and Food Chemistry, 2004. **52**(7): p. 1850-1860.

146. Chen, C.-L. and D. Robert, *Characterization of lignin by 1H and 13C NMR spectroscopy*, in *Methods in Enzymology*, S.T.K. Willis A. Wood, Editor. 1988, Academic Press. p. 137-174.

147. Froass, P.M., A.J. Ragauskas, and J. Jiang, *Chemical structure of residual lignin from kraft pulp.* Journal of Wood Chemistry and Technology, 1996. **16**(4): p. 347-365.

148. Froass, P.M., A.J. Ragauskas, and J.E. Jiang, *NMR Studies Part 3: Analysis of Lignins from Modern Kraft Pulping Technologies.* Holzforschung, 1998. **52**(4): p. 385-390.

149. Holtman, K.M., et al., *Quantitative C-13 NMR characterization of milled wood lignins isolated by different milling techniques.* Journal of Wood Chemistry and Technology, 2006. **26**(1): p. 21-34.

150. Kringstad, K.P. and R. Morck, *C-13-NMR SPECTRA OF KRAFT LIGNINS.* Holzforschung, 1983. **37**(5): p. 237-244.

151. Runge, T.M. and A.J. Ragauskas, *NMR Analysis of Oxidative Alkaline Extraction Stage Lignins.* Holzforschung, 1999. **53**(6): p. 623-631.

152. Pu, Y., S. Cao, and A.J. Ragauskas, *Application of quantitative 31P NMR in biomass lignin and biofuel precursors characterization.* Energy & Environmental Science, 2011. **4**(9): p. 3154-3166.

153. Mullen, C.A., G.D. Strahan, and A.A. Boateng, *Characterization of Various Fast-Pyrolysis Bio-Oils by NMR Spectroscopy.* Energy & Fuels, 2009. **23**: p. 2707-2718.

154. Nagy, M., et al., *Catalytic hydrogenolysis of ethanol organosolv lignin.* Holzforschung, 2009. **63**(5): p. 513-520.

155. Olukcu, N., et al., *Liquefaction of beypazari oil shale by pyrolysis.* Journal of Analytical and Applied Pyrolysis, 2002. **64**(1): p. 29-41.

156. Onen, A., et al., *ESTIMATION OF THE AVERAGE STRUCTURAL PARAMETERS FROM ASPHALTITES AND OIL SHALES-PYROLYSIS PRODUCTS BY H-1 AND C-13 NMR-SPECTROSCOPY.* Fuel Processing Technology, 1992. **32**(3): p. 151-158.

157. Ozbay, N., et al., *Comparative analysis of pyrolysis oils and its subfractions under different atmospheric conditions.* Fuel Processing Technology, 2006. **87**(11): p. 1013-1019.

158. Ralph, S., L. Landucci, and J. Ralph, *NMR Database of Lignin and Cell Wall Model Compounds*, 2004, USDA Agriculture Research Service.

159. Silverstein, R.M., F.X. Webster, and D.J. Kiemle, *Spectrometric identification of organic compounds*. 2005: John Wiley & Sons.

160. Gellerstedt, G. and D. Robert, *Quantitative 13C NMR analyis of Kraft lignins.* Acta Chemica Scandinavica, 1987. **B 41**: p. 541-545.

161. Baptista, C., D. Robert, and A.P. Duarte, *Relationship between lignin structure and delignification degree in Pinus pinaster kraft pulps.* Bioresource Technology, 2008. **99**(7): p. 2349-2356.

162. Berlin, A., et al., *Inhibition of cellulase, xylanase and β-glucosidase activities by softwood lignin preparations.* Journal of Biotechnology, 2006. **125**(2): p. 198-209.

163. DeSisto, W.J., et al., *Fast Pyrolysis of Pine Sawdust in a Fluidized-Bed Reactor.* Energy & Fuels, 2010. **24**: p. 2642-2651.

164. Gellerstedt, G., et al., *Chemical Structures Present in Biofuel Obtained from Lignin.* Energy & Fuels, 2008. **22**(6): p. 4240-4244.

165. Pu, Y., et al., *NMR Characterization of C3H and HCT Down-Regulated Alfalfa Lignin.* Bioenergy Research, 2009. **2**(4): p. 198-208.

166. Qi-Cheng, W., et al., *13C-NMR Data of Three Important Diterpenes Isolated from Euphorbia Species.* Molecules, 2009. **14**(11): p. 4454-4475.

167. Sannigrahi, P., et al., *Pseudo-lignin and pretreatment chemistry.* Energy & Environmental Science, 2011. **4**(4): p. 1306-1310.

168. Hatzakis, E. and P. Dais, *Determination of Water Content in Olive Oil by 31P NMR Spectroscopy.* Journal of Agricultural and Food Chemistry, 2008. **56**(6): p. 1866-1872.

169. Jiang, Z.H., D.S. Argyropoulos, and A. Granata, *CORRELATION-ANALYSIS OF P-31 NMR CHEMICAL-SHIFTS WITH SUBSTITUENT EFFECTS OF PHENOLS.* Magnetic Resonance in Chemistry, 1995. **33**(5): p. 375-382.

170. Wroblewski, A.E., et al., *P-31 NMR SPECTROSCOPIC ANALYSIS OF COAL PYROLYSIS CONDENSATES AND EXTRACTS FOR HETEROATOM FUNCTIONALITIES POSSESSING LABILE HYDROGEN.* Energy & Fuels, 1988. **2**(6): p. 765-774.

171. Wroblewski, A.E., K. Reinartz, and J.G. Verkade, *Moisture determination of Argonne Premium coal extracts by phosphorus-31 NMR spectroscopy.* Energy & Fuels, 1991. **5**(6): p. 786-791.

172. Zawadzki, M. and A. Ragauskas, *N-Hydroxy Compounds as New Internal Standards for the 31P-NMR Determination of Lignin Hydroxy Functional Groups,* in *Holzforschung*2001. p. 283.

173. Kosa, M. and A.J. Ragauskas, *Phosphitylation and 31P NMR Analysis Chemical shifts (ppm) of model compounds Relevant to Lignin/Pyrolysis Oils/Coal Related Aliphatic/Phenoxy/Carboxylic Acids*, 2010, IPST.

174. Heikkinen, S., et al., *Quantitative 2D HSQC (Q-HSQC) via Suppression of J-Dependence of Polarization Transfer in NMR Spectroscopy: Application to Wood Lignin.* Journal of the American Chemical Society, 2003. **125**(14): p. 4362-4367.

175. Zhang, L. and G. Gellerstedt, *Quantitative 2D HSQC NMR determination of polymer structures by selecting suitable internal standard references.* Magnetic Resonance in Chemistry, 2007. **45**(1): p. 37-45.

176. Sette, M., R. Wechselberger, and C. Crestini, *Elucidation of Lignin Structure by Quantitative 2D NMR.* Chemistry – A European Journal, 2011. **17**(34): p. 9529-9535.

177. Kim, H. and J. Ralph, *Solution-state 2D NMR of ball-milled plant cell wall gels in DMSO-d6/pyridine-d5.* Organic & Biomolecular Chemistry, 2010. **8**(3): p. 576-591.

178. Rencoret, J., et al., *HSQC-NMR analysis of lignin in woody (Eucalyptus globulus and Picea abies) and non-woody (Agave sisalana) ball-milled plant materials at the gel state 10th EWLP, Stockholm, Sweden, August 25–28, 2008,* in *Holzforschung*2009. p. 691.

179. Capanema, E.A., M.Y. Balakshin, and J.F. Kadla, *Quantitative Characterization of a Hardwood Milled Wood Lignin by Nuclear Magnetic Resonance Spectroscopy.* Journal of Agricultural and Food Chemistry, 2005. **53**(25): p. 9639-9649.

180. Hu, G., et al., *Structural Characterization of Switchgrass Lignin after Ethanol Organosolv Pretreatment.* Energy & Fuels, 2011. **26**(1): p. 740-745.

181. Carvalho, M.G.d., et al., *Diterpenes from pinus taeda.* Phytochemistry, 1998. **49**(4): p. 1101-1105.

182. Pacheco, A.G., et al., *13C-NMR Data of Diterpenes Isolated from Aristolochia Species.* Molecules, 2009. **14**(3): p. 1245-1262.

183. Topcu, G. and A. Ulubelen, *Structure elucidation of organic compounds from natural sources using 1D and 2D NMR techniques.* Journal of Molecular Structure, 2007. **834–836**(0): p. 57-73.

184. Wu, Q.-C., et al., *13C-NMR Data of Three Important Diterpenes Isolated from Euphorbia Species.* Molecules, 2009. **14**(11): p. 4454-4475.

185. Yamaji, T. *Structural Database for Organic Compounds (SDBS)*. Available from: http://riodb01.ibase.aist.go.jp/sdbs/cgi-bin/cre_index.cgi?lang=eng.

186. Zdero, C., F. Bohlmann, and R.M. King, *Diterpenes and norditerpenes from the Aristeguetia group.* Phytochemistry, 1991. **30**(9): p. 2991-3000.

187. Balat, M., et al., *Main routes for the thermo-conversion of biomass into fuels and chemicals. Part 2: Gasification systems.* Energy Conversion and Management, 2009. **50**(12): p. 3158-3168.

188. Zinoviev, S., et al., *Next-Generation Biofuels: Survey of Emerging Technologies and Sustainability Issues.* Chemsuschem, 2010. **3**(10): p. 1106-1133.

189. Vispute, T.P., et al., *Renewable Chemical Commodity Feedstocks from Integrated Catalytic Processing of Pyrolysis Oils.* Science, 2010. **330**(6008): p. 1222-1227.

190. Babu, B.V., *Biomass pyrolysis: a state-of-the-art review.* Biofuels, Bioproducts and Biorefining, 2008. **2**(5): p. 393-414.

191. Balat, M., *Mechanisms of Thermochemical Biomass Conversion Processes. Part 1: Reactions of Pyrolysis.* Energy Sources, Part A: Recovery, Utilization, and Environmental Effects, 2008. **30**(7): p. 620-635.

192. Balat, M., et al., *Main routes for the thermo-conversion of biomass into fuels and chemicals. Part 1: Pyrolysis systems.* Energy Conversion and Management, 2009. **50**(12): p. 3147-3157.

193. Van de Velden, M., et al., *Fundamentals, kinetics and endothermicity of the biomass pyrolysis reaction.* Renewable Energy, 2010. **35**(1): p. 232-242.

194. Fatih Demirbas, M., *Biorefineries for biofuel upgrading: A critical review.* Applied Energy, 2009. **86, Supplement 1**(0): p. S151-S161.

195. Mettler, M.S., et al., *Revealing pyrolysis chemistry for biofuels production: Conversion of cellulose to furans and small oxygenates.* Energy & Environmental Science, 2012. **5**(1): p. 5414-5424.

196. Zhang, X., et al., *Formation Mechanism of Levoglucosan and Formaldehyde during Cellulose Pyrolysis.* Energy & Fuels, 2011. **25**(8): p. 3739-3746.

197. Lin, Y.-C., et al., *Kinetics and Mechanism of Cellulose Pyrolysis.* The Journal of Physical Chemistry C, 2009. **113**(46): p. 20097-20107.

198. Mettler, M.S., et al., *Pyrolytic conversion of cellulose to fuels: levoglucosan deoxygenation via elimination and cyclization within molten biomass.* Energy & Environmental Science, 2012. **5**(7): p. 7864-7868.

199. Shen, D.K. and S. Gu, *The mechanism for thermal decomposition of cellulose and its main products.* Bioresource Technology, 2009. **100**(24): p. 6496-6504.

200. Zhang, X., W. Yang, and W. Blasiak, *Thermal decomposition mechanism of levoglucosan during cellulose pyrolysis.* Journal of Analytical and Applied Pyrolysis, 2012. **96**(0): p. 110-119.

201. Zhang, X., W. Yang, and W. Blasiak, *Kinetics of levoglucosan and formaldehyde formation during cellulose pyrolysis process.* Fuel, 2012. **96**(0): p. 383-391.

202. Jiang, G., D.J. Nowakowski, and A.V. Bridgwater, *Effect of the Temperature on the Composition of Lignin Pyrolysis Products.* Energy & Fuels, 2010. **24**: p. 4470-4475.

203. Bahng, M.-K., et al., *Current technologies for analysis of biomass thermochemical processing: A review.* Analytica Chimica Acta, 2009. **651**(2): p. 117-138.

204. Britt, P.F., et al., *Flash vacuum pyrolysis of methoxy-substituted lignin model compounds.* Journal of Organic Chemistry, 2000. **65**(5): p. 1376-1389.

205. Britt, P.F., A.C. Buchanan, and E.A. Malcolm, *Impact of restricted mass transport on pyrolysis pathways for aryl ether containing lignin model compounds.* Energy & Fuels, 2000. **14**(6): p. 1314-1322.

206. Britt, P.F., M.K. Kidder, and A.C. Buchanan, III, *Oxygen substituent effects in the pyrolysis of phenethyl phenyl ethers.* Energy & Fuels, 2007. **21**(6): p. 3102-3108.

207. Caballero, J.A., et al., *FLASH PYROLYSIS OF KLASON LIGNIN IN A PYROPROBE-1000.* Journal of Analytical and Applied Pyrolysis, 1993. **27**(2): p. 221-244.

208. Jegers, H.E. and M.T. Klein, *PRIMARY AND SECONDARY LIGNIN PYROLYSIS REACTION PATHWAYS.* Industrial & Engineering Chemistry Process Design and Development, 1985. **24**(1): p. 173-183.

209. Kawamoto, H., S. Horigoshi, and S. Saka, *Pyrolysis reactions of various lignin model dimers.* Journal of Wood Science, 2007. **53**(2): p. 168-174.

210. Kawamoto, H., T. Nakamura, and S. Saka, *Pyrolytic cleavage mechanisms of lignin-ether linkages: A study on p-substituted dimers and trimers.* Holzforschung, 2008. **62**(1): p. 50-56.

211. Kawamoto, H., M. Ryoritani, and S. Saka, *Different pyrolytic cleavage mechanisms of beta-ether bond depending on the side-chain structure of lignin dimers.* Journal of Analytical and Applied Pyrolysis, 2008. **81**(1): p. 88-94.

212. Kawamoto, H. and S. Saka, *Role of side-chain hydroxyl groups in pyrolytic reaction of phenolic beta-ether type of lignin dimer.* Journal of Wood Chemistry and Technology, 2007. **27**(2): p. 113-120.

213. Klein, M.T. and P.S. Virk, *MODEL PATHWAYS IN LIGNIN THERMOLYSIS .1. PHENETHYL PHENYL ETHER.* Industrial & Engineering Chemistry Fundamentals, 1983. **22**(1): p. 35-45.

214. Kuroda, K. and A. Nakagawa-izumi, *Analytical pyrolysis of lignin: Products stemming from beta-5 substructures.* Organic Geochemistry, 2006. **37**(6): p. 665-673.

215. McDermott, J.B., M.T. Klein, and J.R. Obst, *CHEMICAL MODELING IN THE DEDUCTION OF PROCESS CONCEPTS - A PROPOSED NOVEL PROCESS FOR LIGNIN LIQUEFACTION.* Industrial & Engineering Chemistry Process Design and Development, 1986. **25**(4): p. 885-889.

216. Nakamura, T., H. Kawamoto, and S. Saka, *Pyrolysis behavior of Japanese cedar wood lignin studied with various model dimers.* Journal of Analytical and Applied Pyrolysis, 2008. **81**(2): p. 173-182.

217. Singh, R., et al., *Distal Heme Pocket Residues of B-type Dye-decolorizing Peroxidase: Arginine but not Aspartate is Essential for Peroxidase Activity.* Journal of Biological Chemistry, 2012. **287**(13): p. 10623-10630.

218. Widsten, P. and A. Kandelbauer, *Laccase applications in the forest products industry: A review.* Enzyme and Microbial Technology, 2008. **42**(4): p. 293-307.

219. Bugg, T.D.H., et al., *Pathways for degradation of lignin in bacteria and fungi.* Natural Product Reports, 2011. **28**(12): p. 1883-1896.

220. Bugg, T.D.H., et al., *The emerging role for bacteria in lignin degradation and bio-product formation.* Current Opinion in Biotechnology, 2011. **22**(3): p. 394-400.

221. Fuchs, G., M. Boll, and J. Heider, *Microbial degradation of aromatic compounds — from one strategy to four.* Nat Rev Micro, 2011. **9**(11): p. 803-816.

222. Masai, E., Y. Katayama, and M. Fukuda, *Genetic and Biochemical Investigations on Bacterial Catabolic Pathways for Lignin-Derived Aromatic Compounds.* Bioscience, Biotechnology, and Biochemistry, 2007. **71**(1): p. 1-15.

223. Kalscheuer, R., T. Stoelting, and A. Steinbuechel, *Microdiesel: Escherichia coli engineered for fuel production.* Microbiology-Sgm, 2006. **152**: p. 2529-2536.

224. Steen, E.J., et al., *Microbial production of fatty-acid-derived fuels and chemicals from plant biomass.* Nature, 2010. **463**(7280): p. 559-U182.

225. Baldrian, P., *Fungal laccases – occurrence and properties.* FEMS Microbiology Reviews, 2006. **30**(2): p. 215-242.

226. Hammel, K.E. and D. Cullen, *Role of fungal peroxidases in biological ligninolysis.* Current Opinion in Plant Biology, 2008. **11**(3): p. 349-355.

227. Hofrichter, M., *Review: lignin conversion by manganese peroxidase (MnP).* Enzyme and Microbial Technology, 2002. **30**(4): p. 454-466.

228. Martínez, A., et al., *Biodegradation of lignocellulosics: microbial, chemical, and enzymatic aspects of the fungal attack of lignin.* International Microbiology, 2005. **8**: p. 195-204.

229. Garavaglia, S., et al., *The Structure of Rigidoporus lignosus Laccase Containing a Full Complement of Copper Ions, Reveals an Asymmetrical Arrangement for the T3 Copper Pair.* Journal of Molecular Biology, 2004. **342**(5): p. 1519-1531.

230. Kallio, J.P., et al., *Structure–Function Studies of a Melanocarpus albomyces Laccase Suggest a Pathway for Oxidation of Phenolic Compounds.* Journal of Molecular Biology, 2009. **392**(4): p. 895-909.

231. Morozova, O.V., et al., *"Blue" laccases.* Biochemistry. Biokhimiia, 2007. **72**(10): p. 1136-1150.

232. Quintanar, L., et al., *Shall We Dance? How A Multicopper Oxidase Chooses Its Electron Transfer Partner.* Accounts of Chemical Research, 2007. **40**(6): p. 445-452.

233. Ahmad, M., et al., *Development of novel assays for lignin degradation: comparative analysis of bacterial and fungal lignin degraders.* Molecular BioSystems, 2010. **6**(5): p. 815-821.

234. Ahmad, M., et al., *Identification of DypB from Rhodococcus jostii RHA1 as a Lignin Peroxidase.* Biochemistry, 2011. **50**(23): p. 5096-5107.

235. Brunel, F. and J. Davison, *Cloning and sequencing of Pseudomonas genes encoding vanillate demethylase.* Journal of Bacteriology, 1988. **170**(10): p. 4924-4930.

236. Chen, H.-P., et al., *Vanillin Catabolism in Rhodococcus jostii RHA1.* Applied and Environmental Microbiology, 2012. **78**(2): p. 586-588.

237. Priefert, H., J. Rabenhorst, and A. Steinbüchel, *Molecular characterization of genes of Pseudomonas sp. strain HR199 involved in bioconversion of vanillin to protocatechuate.* Journal of Bacteriology, 1997. **179**(8): p. 2595-607.

238. Wackett, L.P., *Mechanism and applications of Rieske non-heme iron dioxygenases.* Enzyme and Microbial Technology, 2002. **31**(5): p. 577-587.

239. Mutti, F.G., *Alkene Cleavage Catalysed by Heme and Nonheme Enzymes: Reaction Mechanisms and Biocatalytic Applications.* Bioinorganic Chemistry and Applications, 2012. **2012**: p. 13.

240. Bains, J., et al., *A Product Analog Bound Form of 3-Oxoadipate-enol-Lactonase (PcaD) Reveals a Multifunctional Role for the Divergent Cap Domain.* Journal of Molecular Biology, 2011. **406**(5): p. 649-658.

241. Chari, R.V.J., et al., *ABSOLUTE STEREOCHEMICAL COURSE OF MUCONOLACTONE DELTA-ISOMERASE AND OF 4-CARBOXYMUCONOLACTONE DECARBOXYLASE - A H-1-NMR RICOCHET ANALYSIS.* Journal of the American Chemical Society, 1987. **109**(18): p. 5520-5521.

242. Eulberg, D., et al., *Characterization of a protocatechuate catabolic gene cluster from Rhodococcus opacus 1CP: Evidence for a merged enzyme with 4-carboxymuconolactone-decarboxylating and 3-oxoadipate enol-lactone-hydrolyzing activity.* Journal of Bacteriology, 1998. **180**(5): p. 1072-1081.

243. Halak, S., et al., *Structure and function of the 3-carboxy-cis,cis-muconate lactonizing enzyme from the protocatechuate degradative pathway of Agrobacterium radiobacter S2.* Febs Journal, 2006. **273**(22): p. 5169-5182.

244. Lipscomb, J.D. and A.M. Orville, *MECHANISTIC ASPECTS OF DIHYDROXYBENZOATE DIOXYGENASES.* Metal Ions in Biological Systems, 1992. **28**: p. 243-298.

245. Vaillancourt, F.H., J.T. Bolin, and L.D. Eltis, *The Ins and Outs of Ring-Cleaving Dioxygenases.* Critical Reviews in Biochemistry and Molecular Biology, 2006. **41**(4): p. 241-267.

246. Valley, M.P., et al., *Roles of the equatorial tyrosyl iron ligand of protocatechuate 3,4-dioxygenase in catalysis.* Biochemistry, 2005. **44**(33): p. 11024-11039.

247. Yang, J., et al., *Crystal structure of 3-carboxy-cis,cis-muconate lactonizing enzyme from Pseudomonas putida, a fumarase class II type cycloisomerase: Enzyme evolution in parallel pathways.* Biochemistry, 2004. **43**(32): p. 10424-10434.

248. Vetting, M.W., et al., *Structure of Acinetobacter strain ADP1 protocatechuate 3,4-dioxygenase at 2.2 angstrom resolution: Implications for the mechanism of an intradiol dioxygenase*. Biochemistry, 2000. **39**(27): p. 7943-7955.

249. Parke, D., R.B. Meagher, and L.N. Ornston, *Relations among enzymes of the β-ketoadipate pathway. III. Properties of crystalline γ-carboxymuconolactone decarboxylase from Pseudomonas putida.* Biochemistry, 1973. **12**(18): p. 3537-3542.

250. Athenstaedt, K. and G. Daum, *The life cycle of neutral lipids: synthesis, storage and degradation.* Cellular and Molecular Life Sciences, 2006. **63**(12): p. 1355-1369.

251. Schujman, G.E. and D. de Mendoza, *Transcriptional control of membrane lipid synthesis in bacteria.* Current Opinion in Microbiology, 2005. **8**(2): p. 149-153.

252. Schujman, G.E. and D. de Mendoza, *Regulation of type II fatty acid synthase in Gram-positive bacteria.* Current Opinion in Microbiology, 2008. **11**(2): p. 148-152.

253. White, S.W., et al., *The structural biology of type II fatty acid biosynthesis*, in *Annual Review of Biochemistry*. 2005. p. 791-831.

254. Zhang, Y.-M. and C.O. Rock, *Transcriptional regulation in bacterial membrane lipid synthesis.* Journal of Lipid Research, 2009. **50**(Supplement): p. S115-S119.

255. Waeltermann, M., T. Stoeveken, and A. Steinbuechel, *Key enzymes for biosynthesis of neutral lipid storage compounds in prokaryotes: Properties, function and occurrence of wax ester synthases/acyl-CoA : diacylglycerol acyltransferases.* Biochimie, 2007. **89**(2): p. 230-242.

256. Waltermann, M., et al., *Mechanism of lipid-body formation in prokaryotes: how bacteria fatten up.* Molecular Microbiology, 2005. **55**(3): p. 750-763.

257. Gouda, M.K., S.H. Omar, and L.M. Aouad, *Single cell oil production by Gordonia sp DG using agro-industrial wastes.* World Journal of Microbiology & Biotechnology, 2008. **24**(9): p. 1703-1711.

258. Lu, X., H. Vora, and C. Khosla, *Overproduction of free fatty acids in E. coli: Implications for biodiesel production.* Metabolic Engineering, 2008. **10**(6): p. 333-339.

259. Alvarez, A.F., et al., *Cloning and characterization of a gene involved in triacylglycerol blosynthesis and identification of additional homologous genes in the oleaginous bacterium Rhodococcus opacus PD630.* Microbiology-Sgm, 2008. **154**: p. 2327-2335.

260. Kalscheuer, R., M. Arenskotter, and A. Steinbuchel, *Establishment of a gene transfer system for Rhodococcus opacus PD630 based on electroporation and its application for recombinant biosynthesis of poly(3-hydroxyalkanoic acids).* Applied Microbiology and Biotechnology, 1999. **52**(4): p. 508-515.

261. Eggeling, L. and H. Sahm, *DEGRADATION OF CONIFERYL ALCOHOL AND OTHER LIGNIN-RELATED AROMATIC-COMPOUNDS BY NOCARDIA SP DSM-1069.* Archives of Microbiology, 1980. **126**(2): p. 141-148.

262. Schlegel, H.G., H. Kaltwasser, and G. Gottschalk, *EIN SUBMERSVERFAHREN ZUR KULTUR WASSERSTOFFOXYDIERENDER BAKTERIEN - WACHSTUMSPHYSIOLOGISCHE UNTERSUCHUNGEN.* Archiv Fur Mikrobiologie, 1961. **38**(3): p. 209-&.

263. Burdon, K.L., *Fatty Material in Bacteria and Fungi Revealed by Staining Dried, Fixed Slide Preparations.* Journal of Bacteriology, 1946. **52**(6): p. 665-678.

264. Alvarez, H.M., R. Kalscheuer, and A. Steinbuchel, *Accumulation of storage lipids in species of Rhodococcus and Nocardia and effect of inhibitors and polyethylene glycol.* Fett-Lipid, 1997. **99**(7): p. 239-246.

265. Brandl, H., et al., *PSEUDOMONAS-OLEOVORANS AS A SOURCE OF POLY(BETA-HYDROXYALKANOATES) FOR POTENTIAL APPLICATIONS AS BIODEGRADABLE POLYESTERS.* Applied and Environmental Microbiology, 1988. **54**(8): p. 1977-1982.

266. Harris, S.P., et al., *Identification of Rhodococcus equi lipids recognized by host cytotoxic T lymphocytes.* Microbiology-Sgm, 2010. **156**: p. 1836-1847.

267. Baumberger, S., et al., *Molar mass determination of lignins by size-exclusion chromatography: towards standardisation of the method.* Holzforschung, 2007. **61**(4): p. 459-468.

268. Zhang, K., et al., *Sulfur content of gasoline and diesel fuels in northern China.* Energy Policy, 2010. **38**(6): p. 2934-2940.

269. Cordero, T., et al., *Improved solid fuels from co-pyrolysis of a high-sulphur content coal and different lignocellulosic wastes.* Fuel, 2004. **83**(11-12): p. 1585-1590.

270. Singh, P., et al., *Biopulping of lignocellulosic material using different fungal species: a review.* Reviews in Environmental Science and Bio-Technology, 2010. **9**(2): p. 141-151.

271. Alvarez, H.M. and A. Steinbuchel, *Triacylglycerols in prokaryotic microorganisms.* Applied Microbiology and Biotechnology, 2002. **60**(4): p. 367-376.

272. Alvarez, H.M., et al., *Formation of intracytoplasmic lipid inclusions by Rhodococcus opacus strain PD630.* Archives of Microbiology, 1996. **165**(6): p. 377-386.

273. Kadakol, J.C. and C.M. Kamanavalli, *Biodegradation of Eugenol by Bacillus Cereus Strain PN24.* E-Journal of Chemistry, 2010. **7**(S1): p. S474-S480.

274. Brinkrolf, K., I. Brune, and A. Tauch, *Transcriptional regulation of catabolic pathways for aromatic compounds in Corynebacterium glutamicum.* Genetics and Molecular Research, 2006. **5**(4): p. 773-789.

275. Zhao, K.X., et al., *PcaO Positively Regulates pcaHG of the beta-Ketoadipate Pathway in Corynebacterium glutamicum.* Journal of Bacteriology, 2010. **192**(6): p. 1565-1572.

276. Kim, S.J., et al., *Genomic analysis of polycyclic aromatic hydrocarbon degradation in Mycobacterium vanbaalenii PYR-1.* Biodegradation, 2008. **19**(6): p. 859-881.

277. Patrauchan, M.A., et al., *Catabolism of benzoate and phthalate in Rhodococcus sp strain RHA1: Redundancies and convergence.* Journal of Bacteriology, 2005. **187**(12): p. 4050-4063.

278. Davis, J.R. and J.K. Sello, *Regulation of genes in Streptomyces bacteria required for catabolism of lignin-derived aromatic compounds.* Applied Microbiology and Biotechnology, 2010. **86**(3): p. 921-929.

279. Bleichrodt, F.S., R. Fischer, and U.C. Gerischer, *The beta-ketoadipate pathway of Acinetobacter baylyi undergoes carbon catabolite repression, cross-regulation and vertical regulation, and is affected by Crc.* Microbiology-Sgm, 2010. **156**: p. 1313-1322.

280. Parke, D., *Acquisition, reorganization, and merger of genes: Novel management of the beta-ketoadipate pathway in Agrobacterium tumefaciens.* Fems Microbiology Letters, 1997. **146**(1): p. 3-12.

281. Jimenez, J.I., et al., *Genomic analysis of the aromatic catabolic pathways from Pseudomonas putida KT2440.* Environmental Microbiology, 2002. **4**(12): p. 824-841.

282. Santala, S., et al., *Improved Triacylglycerol Production in Acinetobacter baylyi ADP1 by Metabolic Engineering.* Microbial Cell Factories, 2011. **10**.

283. Arabolaza, A., et al., *Multiple pathways for triacylglycerol biosynthesis in Streptomyces coelicolor.* Applied and Environmental Microbiology, 2008. **74**(9): p. 2573-2582.

284. Alvarez, H.M., et al., *Identification of phenyldecanoic acid as a constituent of triacylglycerols and wax ester produced by Rhodococcus opacus PD630.* Microbiology-Sgm, 2002. **148**: p. 1407-1412.

285. Alvarez, H.M., R. Kalscheuer, and A. Steinbuchel, *Accumulation and mobilization of storage lipids by Rhodococcus opacus PD630 and Rhodococcus ruber NCIMB 40126.* Applied Microbiology and Biotechnology, 2000. **54**(2): p. 218-223.

286. Nichols, N.N. and C.S. Harwood, *PcaK, a high-affinity permease for the aromatic compounds 4-hydroxybenzoate and protocatechuate from Pseudomonas putida.* Journal of Bacteriology, 1997. **179**(16): p. 5056-5061.

287. Carrapiso, A.I. and C. Garcia, *Development in lipid analysis: Some new extraction techniques and in situ transesterification.* Lipids, 2000. **35**(11): p. 1167-1177.

288. Voss, I. and A. Steinbuchel, *High cell density cultivation of Rhodococcus opacus for lipid production at a pilot-plant scale.* Applied Microbiology and Biotechnology, 2001. **55**(5): p. 547-555.

289. Kurosawa, K., et al., *High-cell-density batch fermentation of Rhodococcus opacus PD630 using a high glucose concentration for triacylglycerol production.* Journal of Biotechnology, 2010. **147**(3-4): p. 212-218.

290. Sannigrahi, P., Y. Pu, and A. Ragauskas, *Cellulosic biorefineries-unleashing lignin opportunities.* Current Opinion in Environmental Sustainability, 2010. **2**(5-6): p. 383-393.

291. Lucia, L.A., A.J. Ragauskas, and F.S. Chakar, *Comparative Evaluation of Oxygen Delignification Processes for Low- and High-Lignin-Content Softwood Kraft Pulps.* Industrial & Engineering Chemistry Research, 2002. **41**(21): p. 5171-5180.

292. Moe Størker, T. and J. Ragauskas Arthur, *Oxygen Delignification of High-Yield Kraft Pulp. Part I: Structural Properties of Residual Lignins*, in *Holzforschung*1999. p. 416.

293. Yang, R., et al., *Oxygen Delignification Chemistry and Its Impact on Pulp Fibers.* Journal of Wood Chemistry and Technology, 2003. **23**(1): p. 13-29.

294. Zhang, D., et al., *Elucidating carboxylic acid profiles for extended oxygen delignification of high-kappa softwood kraft pulps*, in *Holzforschung*2006. p. 123.

295. Skakovskii, E., et al., *NMR analysis of oils from pine nuts (<i>Pinus sibirica) and seeds of common pine (<i>Pinus silvestris L.).* Journal of Applied Spectroscopy, 2007. **74**(4): p. 584-588.

296. Spyros, A. and D. Anglos, *Study of Aging in Oil Paintings by 1D and 2D NMR Spectroscopy.* Analytical Chemistry, 2004. **76**(17): p. 4929-4936.